Janus Particles at Interfaces

DISSERTATION

zur Erlangung des akademischen Grades eines
Doktors der Naturwissenschaften (Dr. rer. nat.)
an der Bayreuther Graduiertenschule für Mathematik und
Naturwissenschaften der Universität Bayreuth
vorgelegt von

Thomas Max Ruhland
Geboren in Selb

Bayreuth, 2012

Die vorliegende Arbeit wurde in der Zeit von August 2009 bis Dezember 2012 in Bayreuth am Lehrstuhl Makromolekulare Chemie II unter Betreuung von Herrn Prof. Dr. Axel H.E. Müller angefertigt.

Vollständiger Abdruck der von der Bayreuther Graduiertenschule für Mathematik und Naturwissenschaften der Universität Bayreuth genehmigten Dissertation zur Erlangung des akademischen Grades eines Doktors der Naturwissenschaften (Dr. rer. nat.).

Dissertation eingereicht am: 9.01.2013

Zulassung durch die Promotionskommission: 13.02.2013

Wissenschaftliches Kolloquium: 25.04.2013

Amtierender Direktor der Graduiertenschule: Prof. Dr. Franz X. Schmid

Prüfungsausschuss:

Prof. Dr. Axel H. E. Müller (Erstgutachter)
Prof. Dr. Thomas Hellweg (Zweitgutachter)
Prof. Dr. Birgit Weber (Vorsitz)
Prof. Dr. Stephan Förster

Life isn´t about waiting for the storm to pass…..

…..It`s about learning to *dance in the rain!*

"*Unknown*"

To my family

Table of Contents

Summary **1**

Zusammenfassung **4**

Glossary **7**

Chapter 1 - Introduction **11**

1. Anisotropic Particles with patchy, multicompartment and Janus Architecture 11
2. Janus Particles 13
   2.1 Synthetic Strategies 14
      2.1.1 Self-Assembly Method 16
         2.1.1.1 Self-Assembly in Solution 16
         2.1.1.2 Self-Assembly in Bulk 19
      2.1.2. Desymmetrization of Particles 24
         2.1.2.1 Liquid-Liquid Pickering Emulsions 26
         2.1.2.2 Polymer and Wax based Pickering Emulsions 27
   2.2 Properties and Applications 30
   2.3 Conclusion and Outlook 34
3. Aim of the Thesis 35
4. References 36

Chapter 2 – Overview of the Thesis **41**

2.1 Janus Cylinders at Liquid-Liquid Interfaces 43

2.2 Influence of Janus Particle Shape on their Interfacial Behavior at Liquid-Liquid Interfaces 47

2.3 Superparamagnetic and fluorescent thermo-responsive Core-Shell-Corona hybrid Nanogels with a protective Silica Shell 52

2.4 Magnetic Core-Shell Nanoparticles as Carriers for Olefin Dimerization Catalysts 57

2.5 Nanoscale hybrid Silica/Polymer Janus Particles with a double-responsive Hemicorona 62

2.6 References 67

2.7 Individual Contributions to Joint Publications 67

Chapter 3..... 71

Janus Cylinder at Liquid-Liquid Interfaces

Chapter 4..... 93

Influence of Janus Particle Shape on their Interfacial Behavior at Liquid-Liquid Interfaces

Chapter 5..... 117

Superparamagnetic and fluorescent thermo-responsive Core-Shell-Corona hybrid Nanogels with a protective Silica Shell

Chapter 6..... 145

Magnetic Core-Shell Nanoparticles as Carriers for Olefin Dimerization Catalysts

Chapter 7..... 165

Nanoscale hybrid Silica/Polymer Janus Particles with a double-responsive Hemicorona

List of Publications..... 193

Acknowledgements..... 195

Summary

This thesis describes the synthesis and the characterization of both polymeric and hybrid Janus particles of well-defined size, shape and functionality and their high potential for applications in colloidal and material science. In principal, Janus particles are compartmentalized colloids with two sides of different chemistry or polarity.

Soft Janus particles, based on polystyrene-*block*-polybutadiene-*block*-poly(methyl methacrylate) (SBM) triblock terpolymers, represent a fascinating group of polymeric materials, which open new ways in academia and industry. Since the size, shape and functionality of the particles directly influences their adsorption behavior at liquid-liquid interfaces, a completely new and fascinating class of surfactants for the nanostructuring of interfaces is created.

First, the adsorption behavior of Janus cylinders at liquid-liquid interfaces was studied using the pendant drop technique. The interfacial self-assembly of Janus cylinders has been investigated for the first time here. The interfacial tension decreases with increasing Janus cylinder length and concentration. From the time evolution of the interfacial tension the characteristics of early and late stages of the Janus cylinder adsorption were specified. A series of TEM images of the liquid-liquid interface taken during the cylinder adsorption confirm these observations. Janus cylinders behave differently at the interfaces as compared to the block terpolymer precursor SBM and to cylinders of comparable sizes with a polybutadiene core and a homogeneous polystyrene shell.

Understanding the effect of Janus particles at fluid interfaces is not the only criterion for an efficient industrial use. Even more important is to know in detail how far the particle size and architecture influence the adsorption process. To establish the effect of the Janus character together with the effect of particle shape on the interfacial activity and orientation of the Janus particles at an liquid-liquid interface, we present a combination of experimental and simulation data together with detailed studies elucidating the mechanisms governing the adsorption process of Janus spheres, Janus cylinders and Janus discs. These studies demonstrate that changes in the geometry of the particles strongly influence the stabilization of the liquid-liquid interface. As the shape changes from spheres to discs and cylinders, different adsorption kinetics, different packing behavior, different energy barriers and finally different equilibrium values for the interfacial tension can be found.

Another main point of this thesis was the synthesis of functional and/or stimuli-responsive hybrid core-shell-corona Janus particles based on inorganic colloids and the characterization of their unique properties and fascinating self-assembly behavior. The first step towards these Janus particles was to understand in detail the formation of core-shell-corona particles with a homogeneous corona, and then in a second step, to use our new knowledge to create hybrid core-shell-corona Janus particles with two polymers immobilized to the opposite sides of the core-shell particles on the basis of our particles.

In the following, we developed an easy and completely reproducible preparation and characterization of the solution behavior and functional properties of superparamagnetic and/or fluorescent, thermo-responsive inorganic/organic hybrid nanogels with an intermediate protective silica shell and a smart and interactive polymer layer. These well-defined and near monodisperse multifunctional nanogels were prepared via two consecutive encapsulation processes of superparamagnetic and/or fluorescent semiconductor nanocrystals with a silica layer and a crosslinked and responsive polymer poly(*N*-isopropylacrylamide) (PNIPAAm) corona. The precise adjustment of the conditions allows to achieve a reliable encapsulation and to either entrap several particles or single ones and to precisely tailor the thickness of the silica shell. Full functionality of the encapsulated nanocrystals is retained, but excellent wettability, biocompatibility, flexible surface chemistry, drastically increased chemical stability are implemented together with a thermo-responsive polymer corona. The flexible surface chemistry due to the silica intermediate offers a wide range of different functionalization and polymerization types (RAFT, ATRP, Free Radical Polymerization or Click Chemistry).

Furthermore, on the basis of our well-characterized core-shell particles we took advantage of the variable surface chemistry of the silica shell to combine the properties of the superparamagnetic core-shell nanoparticles with the catalytic character of nickel complexes in hybrid core-shell-corona nanoparticles forming heterogeneous nanocatalysts. In that way a heterogeneous catalyst was created for facile product separation in the catalytic conversion of olefins.

In the next level, an efficient and simple strategy for the large-scale synthesis of well-defined hybrid Janus particles with a silica core (<< 100 nm) and a stimuli-responsive PDMAEMA hemicorona was developed. The synthesis is based on a modified version of the Pickering emulsion technique in combination with surface-initiated atom transfer radical polymerization (ATRP) in a “grafting from” approach. First, 30 nm silica nanoparticles are immobilized at the interface of sub-micrometer sized droplets of poly(vinyl acetate). Since the nanoparticles are partially embedded, one hemisphere is protected. After the modification with an ATRP-

initiator and the detachment of the modified silica particles, PDMAEMA was grafted from one hemisphere via ATRP. The obtained Janus nanoparticles are well-defined in size and shape and show stimuli-responsive structural changes depending on pH and temperature. In a future step it will be possible to modify the still unmodified side with further stimuli-responsive polymers in order to create hybrid Janus particles with two different hemispheres. Most importantly, this synthetic approach is easily scalable and can be amended to furnish a wide range of nanoscale hybrid Janus particles below 100 nm in high quality.

Zusammenfassung

Die vorliegende Arbeit beschreibt die Synthese und Charakterisierung von polymeren und hybriden Janus-Partikeln wohl definierter Größe, Form und Funktionalität und deren Potential für Anwendungen in den Kolloid- und Materialwissenschaften. Janus-Partikel sind oberflächenkompartimentierte kolloidale Partikel, die gekennzeichnet sind durch unterschiedliche Funktionalität oder Polarität auf beiden Seiten der Partikel.

Organische Janus-Partikel aus dem Triblockterpolymer Polystyrol-*block*-Polybutadien-*block*-Polymethylmethacrylat bieten ganz neue, faszinierende Möglichkeiten in Wissenschaft und Industrie. Da das Verhalten von Janus-Partikeln an flüssig-flüssig Grenzflächen durch Größe, Form und Architektur der Janus-Partikel gezielt gesteuert werden kann, werden vollkommen neue Möglichkeiten für eine neue Klasse von Tensiden zur Nanostrukturierung von Grenzflächen geschaffen.

Das Adsorptionsverhalten von Janus-Partikeln an flüssig-flüssig-Grenzflächen wurde durch die Methode des hängenden Tropfens untersucht. Ausgehend von der Zeitabhängigkeit der Grenzflächenspannung ist es erstmals gelungen, die Charakteristika der ersten und der letzten Stufen im Adsorptionsprozess von Janus-Zylindern genauer zu spezifizieren, womit deren Selbstorganisationsverhalten an flüssig-flüssig Grenzflächen genauer aufgeklärt worden ist. Die Grenzflächenspannung nimmt mit zunehmender Zylinderlänge und Zylinderkonzentration ab. Dabei kann man verschiedene Adsorptionsstufen beobachten, die mit Hilfe von TEM-Aufnahmen sichtbar gemacht werden konnten. Die amphiphilen Janus-Zylinder besitzen eine signifikant höhere Grenzflächenaktivität im Vergleich zu homogenen Kern-Schale Zylindern mit einen Polybutadien-Kern und einer Schale aus Polystyrol und dem unversetzten Triblockterpolymer SBM, die beide direkte Vorstufen der Janus-Zylinder sind.

Eine weitere wichtige Voraussetzung für einen industriellen Einsatz von Janus-Partikeln ist es zu verstehen, welche Rolle Größe, Form und Architektur spielen. Dafür wurde in einer weiteren Versuchsreihe das zeitabhängige Absorptionsverhalten von drei verschiedenen Partikelarchitekturen (Kugeln, Zylinder und Scheiben) an flüssig-flüssig Grenzflächen untersucht, um anschließend zusammen mit Daten aus Simulationen Rückschlüsse auf das Adsorptionsverhalten und die Dynamik, aber auch auf die Lage der Partikel an der Grenzfläche ziehen zu können. Dabei konnte ganz klar gezeigt werden, dass die Partikelarchitektur den gesamten

Adsorptionspozesses der Partikel und deren Anordnung und Strukturierung an Grenzflächen signifikant beeinflusst.

Ein weiteres Augenmerk der Doktorarbeit lag auf der Darstellung von funktionalen und/ oder stimuli-responsiven hybriden Kern-Schale-Korona Janus-Partikeln, die auf anorganischen Kolloiden basieren, und der Aufklärung ihrer einzigartigen Selbstorganisationseigenschaften. Der erste Teilabschnitt bei der Synthese dieser Janus-Partikel war es, die Darstellung und Synthese von Kern-Schale-Korona Partikeln erstmals prinzipiell im Detail zu verstehen, um in den nächsten Schritten diese neuen Erkenntnisse für die Synthese von hybriden Janus-Partikel ausnutzen zu können.

Dies wurde realisiert mit der Synthese und ausführlichen Charakterisierung von hybriden Kern-Schale-Korona-Nanogelen (NP/SiO_2/PNIPAAm). Den besonderen Charme dieser Nanogele stellt die Kombination der funktionalen Eigenschaften von anorganischen Nanopartikeln (CdSe(ZnS), γ-Fe_2O_3) im Kern mit dem temperatur-responsiven Verhalten der Polymerkorona dar. Die Syntheseroute führt zu monodispersen hybriden Kern-Schale Partikeln, die dauerhafte magnetische und/oder luminiszente Eigenschaften zeigen, da der Kern durch eine Silica-Hülle geschützt ist, und gleichzeitig eine einheitliche Temperaturselektivität bedingt durch die PNIPAAm-Korona (Poly(*N*-isopropylacrylamid)-Korona) aufweisen. Die Größe der Silica-Hülle kann für unterschiedliche Anwendung gezielt gesteuert werden. Die Silica-Hülle dient aber nicht nur als Schutzfunktion für die anorganischen Kerne, sondern auch als synthetisch sehr variable Zwischenstufe, da die Oberflächenchemie der Silica-Partikel Möglichkeiten bietet viele unterschiedliche Polymerisationsmethoden von Click-Chemie über ATRP bis hin zu freier radikalischer Polymerisation anzuwenden.

Basierend auf dieser Variabilität wurde auf Kern-Schale-Partikel, bestehend aus einen superparamagnetischen Kern, eingebettet in eine wohl definierte Silica-Hülle (γ-Fe_2O_3/SiO_2-NPs), speziell funktionalisierte Nickel-Komplexe kovalent gebunden, für die Anwendung als heterogene Katalysatoren in der Olefin-Dimerization.

Im darauffolgendem Arbeitsschritt in Richtung von hybriden stimuli-responsiven Janus Partikeln, der Desymmetrisierung der Kerne-Schale-Partikel, d.h. Anlagerung von unterschiedlichen Polymerketten pro Hemisphäre, wurde eine auf der Pickering-Technik beruhende Methode entwickelt, 30 nm große Silica-Partikel an einer Polyvinylacetat-Latex zu immobilisieren. Nach der Modifikation der freien Seite der Silica-Partikel mit einem ATRP-Initiator und der Ablösung dieser Partikel von der Trägerlatex wird über einen „grafting-from"-Ansatz eine temperatur- und pH-abhängige PDMAEMA-Halbkorona kontrolliert-radikalisch polymeri-

siert. Es bilden sich wohl definierte hybride Janus-Partikel mit einer scharfen Grenzfläche zwischen der unmodifizierten Seite des Silica-Partikels und PDMAEMA-Halbkorona, die eine einheitliche und kontrollierbare temperatur- und pH-Responsivität zeigen. Die von uns entwickelte Methode der Desymmetrisierung bietet das erste Mal die Möglichkeit hybride Kern-Schale-Korona Janus-Partikel in einer Größenordnung unter 100 nm in großer Menge, aber gleichzeitig mit hoher Qualität herzustellen und ist für eine Vielzahl an verschiedenen Polymeren anwendbar.

Glossary

1D	one-dimensional
2D	two-dimensional
3D	three-dimensional
^{1}H-NMR	proton nuclear magnetic resonance
AFM	atomic force microscopy
ATRP	atom transfer radical polymerization
BuLi	butyl-lithium
Cryo-TEM	cryogenic transmission electron microscopy
Cryo-SEM	cryogenic scanning electron microscopy
CdSe	cadmium selenide
CdSe(ZnS)	cadmium selenide (zinc sulfide)
DLS	dynamic light scattering
DMAEMA	2-(dimethylamino)ethyl methacrylate
DMSO	dimethylsulfoxide
DP_n	number-average degree of polymerization
EDX	energy dispersive X-ray spectroscopy
γ -Fe_2O_3	iron oxide
g	gram
GPC	gel permeation chromatography
h	hour
HCl	hydrochloric acid
HF	hydrofluoric acid
HR-TEM	hight resolution transmission electron microscopy
H_20	water
γ	interfacial tension
JC	Janus cylinders
JD	Janus discs
JP	Janus particles
JS	Janus spheres
L	liter
lc	lamella-cylinder
ll	lamella-lamella
ls	lamella-sphere
Ludox TM-40	colloidal silica

mg	milligram
***m*-EOF**	*m*-poly(ethylethylene) - poly(ethylene oxide)-poly(perfluoropropylene oxide)
MHz	megahertz
mL	milliliter
Mn	number average molecular weight
Mw	weight average molecular weight
nm	nanometer
tBA	*tert*-butyl acrylate
NPs	nanoparticle(s)
OsO4	osmium tetroxide
P2VN-*b*-PAA	poly(2-vinyl naphthalene)-*b*- poly(acrylic acid)
PAA	poly(acrlyic acid)
PB	polybutadine
PDI	polydispersity Index (M_w/M_n)
PEO-*b*-PAA	poly(ethylene oxide)-*b*-poly(acrylic acid)
PEO-PB-PNIPAAm	poly(ethylene oxide)-*b*-poly(n-butylacrylate)-*b*-poly(N-isopropylacrylamide)
PEO-*b*-PPO	poly(ethylene oxide)-*b*-poly(propylene oxide)
PtBS–PB–PtBMA	Poly(*tert*-butoxystyrene)-*b*-poly(butadiene)-*b*-poly(*tert*-butyl methacrylate)
PDMAEMA	poly(2-(dimethylamino)ethyl methacrylate
PtBA-*b*-PCEMA-*b*-PSGMA	poly(*tert*-butyl acrylate)-*b*-poly(2-cinnamoyloxyethyl methacrylate)-*b*-poly(sucinnated glyceryl monomethacrylate)
PFO	perfluoroctane
PMMA	poly(methylmethacrylate)
PS	polystyrene
PSMA	poly(sodium methacrylate)
PS-*b*-PB-*b*-P*t*BA	poly(styrene)-*b*-poly(butadiene)-*b*-poly(*tert*-butyl acrylate)
PXRD	Powder x-ray diffractometry
***t*SBT**	poly(*tert*-butoxystyrene)-*b*-PB-*b*-poly(*tert*-butyl methacrylate
SBM	Polystyrene-*block*-polybutadiene-*block*-poly(methyl methacrylate)
SEM	scanning electron microscopy

SiO_2	silicon dioxide, silica
TEM	transmission electron microsopy
TGA	thermogravimetric analysis
THF	tetrahydrofuran
UV	ultraviolet

Chapter 1 – Introduction

1. Anisotropic Particles with patchy, multicompartment and Janus Architecture

Throughout the history, living organisms often served as sources of inspiration for the technological development of materials of all types since nature provides a multiplicity of the most diverse materials, architectures, systems and functions. Natural materials are characterized by hierarchical structures at scales ranging from nanometer to millimeters, which comprise all kinds of properties occurring at these diverse structural levels. Thus, a broad range of motifs for designing elegant micro- and nanoparticles with multiple functions can be found.[1] Nature as inspiring example and the demand for advanced functional materials with novel properties has led to a continually expanding, highly innovative and most promising research area called nanotechnology that covers not only chemistry, but also biology, physics and materials sciences. For the last twenty years, nanotechnology has been undergoing an incredible boom and is without any doubt one of the most important key technologies of the 21st century. It is a very interesting, complex, multifarious and versatile field, which contributes new impulses and answers to current problems in science and technology. In this context, scientific research has led to a much more sophisticated set of tools to control the size, shape, dispersity and surface chemistry of nanoparticles. Hence, the complexity of possible structures offers completely new ways to tailor particles for specific tasks. One of the most promising research topics is the bottom-up design of materials for which desired engineered building blocks are used to create new materials by their spontaneous self-assembly. Therefore, significant attention has been devoted to the preparation of various types of highly functional nano-scaled building blocks.

Not surprisingly, nanoparticles have been identified as one of the most promising building blocks for the formation of more complex structures. In fact, since today a wide variety of techniques have been developed to produce nanoparticles consisting of both inorganic materials and polymers, which can be further used for potential applications in almost all fields of industrial business. The real challenge for scientists is now to find new strategies to synthesize nanoparticles with desired properties. So far, most recipes lead to the preparation of particles with isotropic bulk and surface properties. While these nanoparticles are ideal

systems for the investigations of fundamental scientific aspects, for real applications a more advanced engineering is mandatory. Until now, the self-assembly of isotropic nanoparticles is quite well understood, but there are less possibilities in terms of achievable structures and resulting properties. Therefore, particles with an anisotropic structure are even more interesting, since not only their shape, but also their functionality can be controlled.

The past few years have seen an almost unbelievable revolution in materials science, especially in the preparation and design of nano- or micro-sized anisotropic particles such as patchy, multicompartment and Janus particles, which are intriguing building blocks of precisely defined size, shape and functionality. These particles have attracted much attention since they are offering an incredible playground and a versatile platform for the creation of new materials with new specific and predictable properties for special applications in science and industry due to their non-centrosymmetric features.

In 2010, O Reilly *et al.* classified in a review article the key features of all types of anisotropic particles and compared their structural properties as well as their preparation techniques.[2] With reference to a number of excellent reviews covering all types of anisotropic particles[3-9] they gave a highly sophisticated classification of patchy, multicompartment and Janus particles.

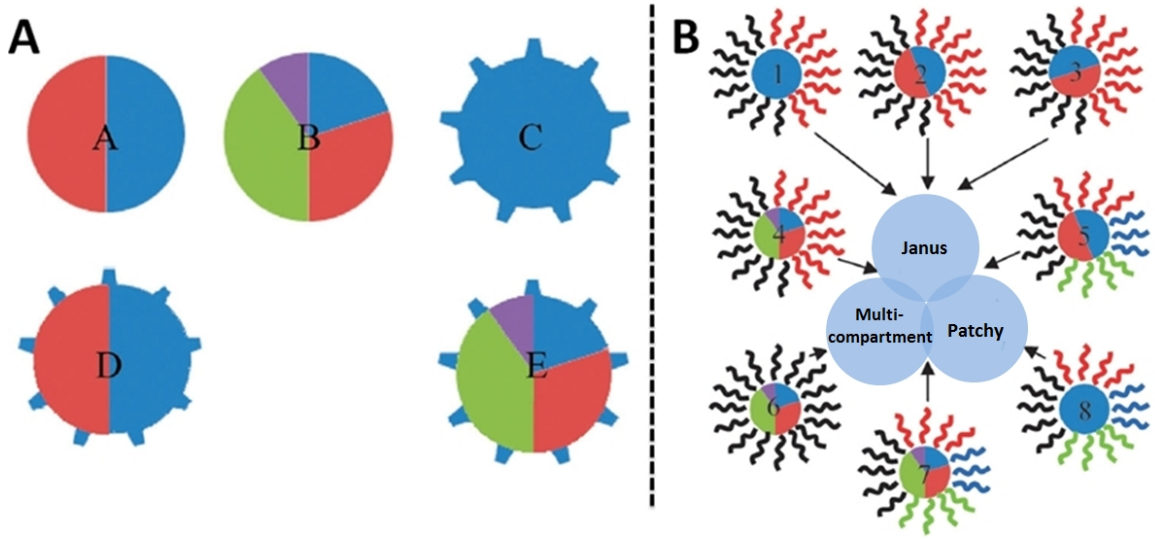

Figure 1-1. Schematic representation of anisotropic particles in A: (A) Janus particles, (B) multi- compartment particles, (C) patchy particles, (D) patchy Janus particles, (E) patchy multi-compartment particles. Illustration of structural similarities of all three types of anisotropic particles using the example of anisotropic micelles B: (1) Janus micelles, (2–3) Janus–Janus micelles, (4) Janus multicompartment micelles, (5) patchy Janus micelles, (6) multi-compartment micelles, (7) patchy multi-compartment micelles, (8) patchy micelles.[2]

Figure 1-1 shows a schematic representation of all anisotropic particles studied in recent years. Here, Janus particles (Figure 1-1 A-A), named after the double-faced Roman god, have equal phase-separated domains which can be located in the core or in the corona. Further, multicompartment particles (Figure 1-1 A-B) are colloidal structures with a multi-phasic anisotropic architecture in the core domain. Finally, particles with patches on the surface are called patchy particles (Figure 1-1 A-C). Additionally, Janus or multicompartment particles with patches on the surface can be called ‘‘patchy Janus particles’’ (Figure 1-1 A-D) or ‘‘patchy-multicompartment particles’’ (Figure 1-1 A-E), respectively.

Due to the fact that during the last years a lot of new and more complex morphologies have been investigated, the originally used nomenclature of the particles overlapped. Figure 1-1 B represents the overlapping of all definitions using the example of anisotropic micelles and illustrates the difficult situation to find a unique definition for every particle type due to the structural similarities.

2. Janus Particles

In his Nobel lecture 1991 De Gennes highlighted the term ‘‘Janus grains’’, pointing out that these particles have the unique advantage of densely self-assembling at liquid-liquid interfaces allowing material transport through the gaps between the solid amphiphilic particles.[10] After their introduction, Janus particles turned out to be a very encouraging group of nanoparticles for a lot of scientists. Thus, Janus particles, named after the double-faced Roman god, have come up as a new class of colloidal structures among micron- or nanosized particles. The terminology is based on the special architectural feature of having two sides or at least two surfaces with different chemistry or polarity. In general, Janus particles can be divided into three superordinate classes according to their architecture and dimensionality: spherical (3D), disc-like (2D) and cylindrical (1D) Janus particles (Figure 1-2).[8,11]

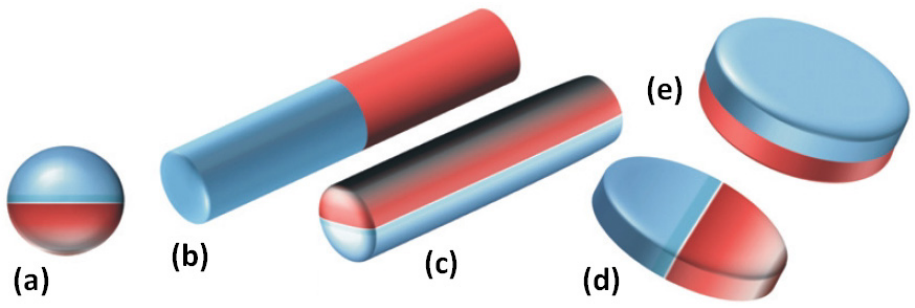

Figure 1-2. Overview of possible Janus particle architectures. (a) Sphere, (b + c) cylinders and (d + e) discs.[8]

Due to this special non-centrosymmetric property, the synthesis of Janus particles is very difficult. On the other side, the lack of centrosymmetry in Janus systems has led to the discovery of new properties as well as unusual aggregation behavior into superstructures. This chemical asymmetry creates very interesting properties and as a result a wide field of conceivable applications makes this research area an interdisciplinary field with researchers from different backgrounds contributing together. The number of publications on Janus particles increased almost exponentially in the last few years (Figure 1-3 A) and the trend is still continuing with extensive key aspects ranging from the synthesis to applications of Janus particles (Figure 1- 3 B).[12]

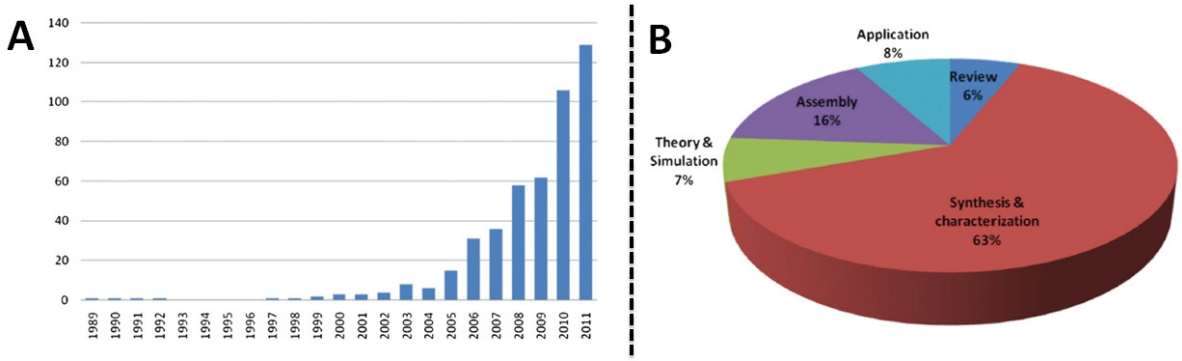

Figure 1-3. (A) Statistics of publications on Janus particles from 1989 to 2011. (B) Analysis of research topics based on the publications shown in (A).[12]

In the beginning, the synthetic access to Janus particles was limited to extremely small amounts, thus also limiting further studies. However, nowadays, new approaches have overcome those limitations and the generation of significant quantities is possible. Various groups have reported the successful preparation of different types of Janus particles with different shape, composition, chemistry, polarity, functionality and properties using various synthetic techniques. In the following, an overview of several synthetic procedures, self-assembly behavior and properties as well as applications is presented.

2.1 Synthetic Strategies

During the last decades a wide range of particles with different chemical properties have been developed and their complexity is increasing due to the variety of new techniques. Particles on every length scale, organic, inorganic or hybrids materials have been prepared with a lot of different shapes ranging from spherical, cylindrical, disc-like, snowman-, hamburger- to raspberry-like structures. Hence, for the fabrication of Janus particles several different synthetic procedures including microfluidic techniques[13,14], lithography[15], controlled phase

separation phenomena[16,17], template-directed self-assembly[8,18,19], controlled surface nucleation[20-22] or partial masking[23,24] have been developed. Further, Monte Carlo computer simulations were used to describe all kinds of Janus particles and their aggregation behavior.[25,26] Janus particles can be regarded as complicated colloidal particles with a lot of different synthesis techniques. But, in fact, all techniques are based on three superordinate categories: masking, phase separation and self-assembly (Figure 1-4).[3]

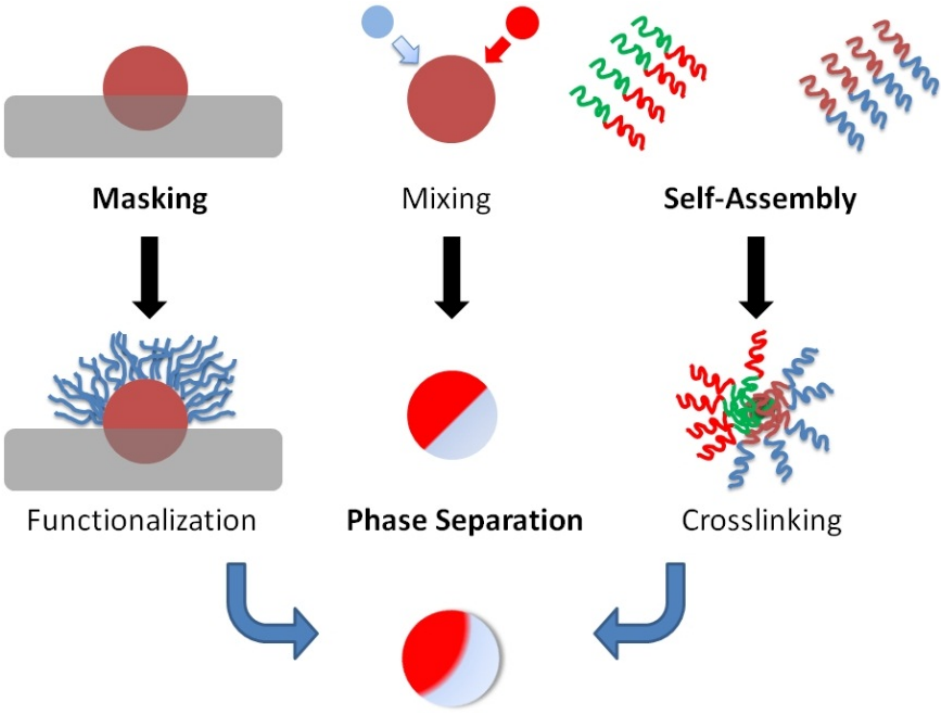

Figure 1-4. Illustration of the three main strategies for the synthesis of Janus particles: Masking, Phase Separation and Self-assembly.[3]

Recent review articles on this topic have been written from different perspectives: Some focus on the synthetic methods and/or the self-assembly behavior of polymeric Janus particles, some mainly discuss the fabrication methods and self-assembly of both polymeric and inorganic Janus particles, other concentrate on the design and fabrication of other anisotropic Janus particles (patchy or multicompartment Janus particles).[3-8,27]

Besides all different available procedures, the focus will be in the following on two of the three main preparation techniques in more detail because these two were mainly used for the synthesis of all Janus particles investigated in this thesis. First, as an example for the category self-assembly, the synthesis of Janus particles *via* the self-assembly of triblock terpolymers in bulk and solution is discussed and further, as a special form of masking, the Pickering emulsion method is described in detail later.

2.1.1 Self-Assembly Method

Block copolymer self-assembly is an elegant tool to create a wide variety of well-defined structures in bulk and in solution. In this context, living polymerization methods are a advantageous. They permit the preparation of block copolymers with well-defined architecture, composition and narrow molecular weight distribution.[28,29] Here, AB diblock copolymers or ABC triblock terpolymers are the most relevant polymers for the synthesis of polymeric Janus particles.

In the following sections self-assembly in solution as a kinetically controlled process and the thermodynamically controlled bulk self-assembly strategy will be discussed in more detail.

2.1.1.1 Self-Assembly in Solution

Historically, one of the first techniques to prepare Janus nanoparticles was the self-assembly of block copolymers in solution. This process is based on a complicated interplay of several factors such as enthalpy, entropy and the dynamics of self-assembly. The general principle can be summarized as a ‘‘freezing-in’’ of the middle block (B) by covalent or non-covalent crosslinking, while the mutually incompatible end blocks (A and C) point in different directions. The preparation begins in most cases with the synthesis of the copolymers in a common solvent, and upon change of solvent the self-assembly is induced. In case of diblock copolymers, two combinations can be chosen for the preparation of Janus particles. Either a combination of AB and BC diblock copolymers, in which the B segments are insoluble in a given solvent and serve as the micellar core or a mixture of AB and CD diblock copolymers, where B and C have an attractive interaction which forces the two polymers to co-assemble. In order to use ABC triblock terpolymers for the formation of Janus particles, the terpolymers need to have two outer soluble end blocks, A and C, and an inner insoluble block, B.

An elegant non-covalent co-assembly of two diblock copolymers was presented by Voets and co-workers.[30-32] Cheng *et al.* showed how to transform mixed shell micelles formed by a mixture of poly(ethylene oxide)-*b*-poly(acrylic acid) (PEO-*b*-PAA) and poly(2-vinyl naphthalene)-*b*-poly(acrylic acid) (P2VN-*b*-PAA) diblock copolymers into Janus micelles *via* a clever use of the different solubility characteristics of the blocks, as well as crosslinking reactions.[33] Wurm *et al.* presented the formation of Janus micelles after an olefin metathesis reaction of vinylether-initiated PEO-*b*-PPO diblock copolymers (poly(ethylene oxide)-*b*-poly(propylene oxide) with Grubbs first-generation catalyst. In water, the modified polyethers form Janus structures, in particular, uni-molecular micelles and ill-defined superstructures.

The latter structures transform into well-defined supermicelles after longer equilibration times (Figure 1-5 A).[34]

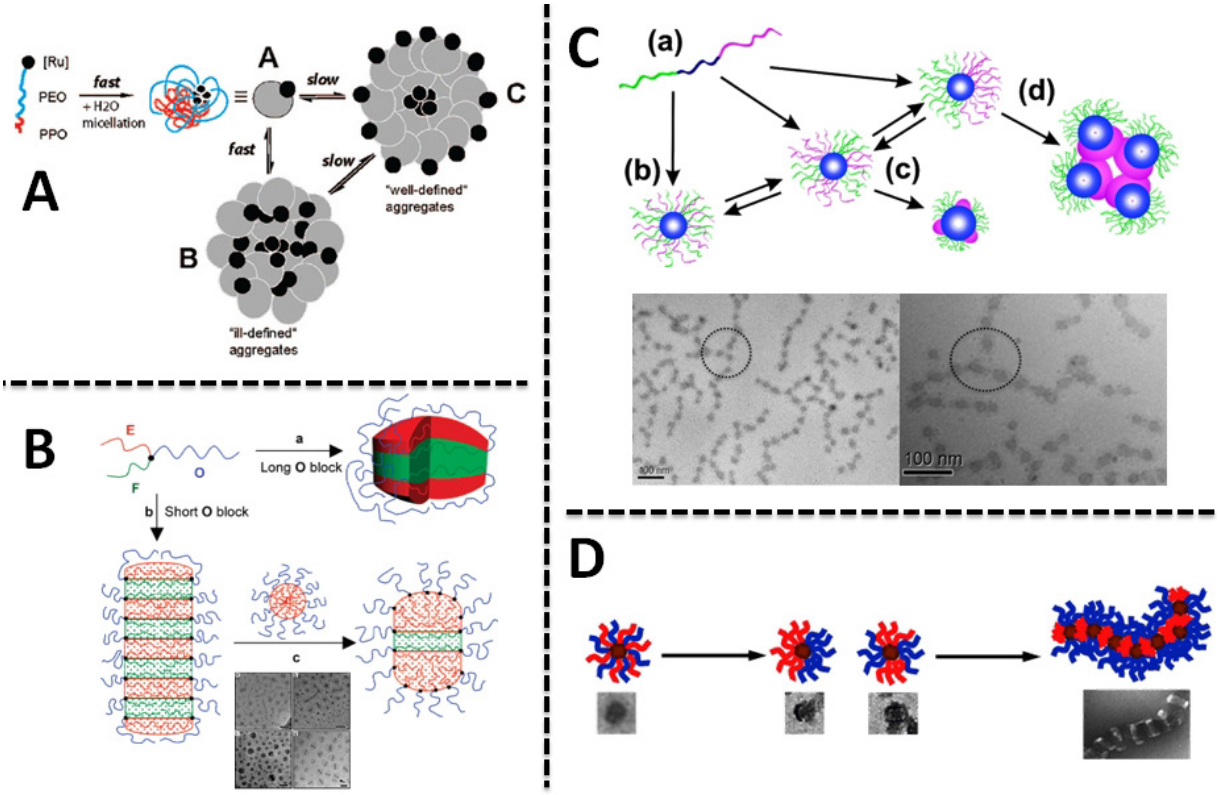

Figure 1-5. (A) Schematic drawing showing the formation of Janus-type micelles and their assembly into larger aggregates depending on equilibration time.[34] (B) Scheme of the mutlicompartment micelle formation from *i*-EOF star terpolymers and binary blends of *i*-EOF/ EO: (*a*) hamburger micelle from *i*-EOF with a very long PEO block; (*b*) segmented wormlike micelle from *i*-EOF with a short PEO block, (*c*) hamburger micelle from blends of *i*-EOF/EO.[37] (C) Schematic illustration of possible corona configuration for a triblock terpolymer consisting of a solvophopic middle block and representative cryo-TEM images.[39] (D) Preparation of multicompartment cylinders by directed stacking polymer micelles with compartmentalized corona.[38]

Lodge and Hillmyer studied the formation of multicompartment micelles by blending two micellar solutions of a star terpolymer containing different arms with an AB diblock copolymer.[35-37] The star terpolymer in Figure 1-5 B, consisting of *m*-poly(ethylethylene)-poly(ethylene oxide)-poly(perfluoropropylene oxide) (m-EOF) has a PEO middle block of various length and molecular weights. Aqueous solutions of these m-EOF star polymers form long cylindrical shaped micelles while the shape generally depends on the length of the PEO block. Furthermore, mixing the m-EOF star polymer micelles with a diblock copolymer based on PEO and poly(ethylethylene) new aggregates with a narrow size distribution are observed. Afterwards, annealing leads to the formation of "hamburger" micelles, which consist of a fluorocarbon disc surrounded by hydrocarbon "buns". Fang *et al.*[38] and also Walther *et al.*[39] showed similar structures for a poly(*tert*-butoxystyrene)-*b*-poly(butadiene)-*b*-poly(*tert*-butyl

methacrylate) in which the PB middle block was modified by fluoroalkyl groups in a post polymerization reaction and for a poly(ethylene oxide)-*b*-poly(n-butylacrylate)-*b*-poly(N-isopropylacrylamide) (PEO-PB-PNIPAAm) triblock terpolymer (Figure 1-5 C/D). An ABC linear triblock terpolymer poly(*tert*-butyl acrylate)-*b*-poly(2-cinnamoyloxyethyl methacrylate)-*b*-poly(sucinnated glyceryl monomethacrylate) (PtBA-*b*-PCEMA-*b*-PSGMA) was synthesized by Dupont *et al*.. Here, in a poor solvent for the middle block and in the presence of a diamine, which builds a complex with the C block and makes it insoluble, the terpolymer arranges into hamburger-like micellar aggregates and segmented cylinders *via* self-assembly.[40]

Recently, Gröschel *et al.* demonstrated a novel solution-based one-pot approach to prepare soft and nano-sized Janus particles with tunable structural and physical properties at very high volume yields by simple crosslinking of uniform compartments of spherical multicompartment micelles (Figure 1-6).

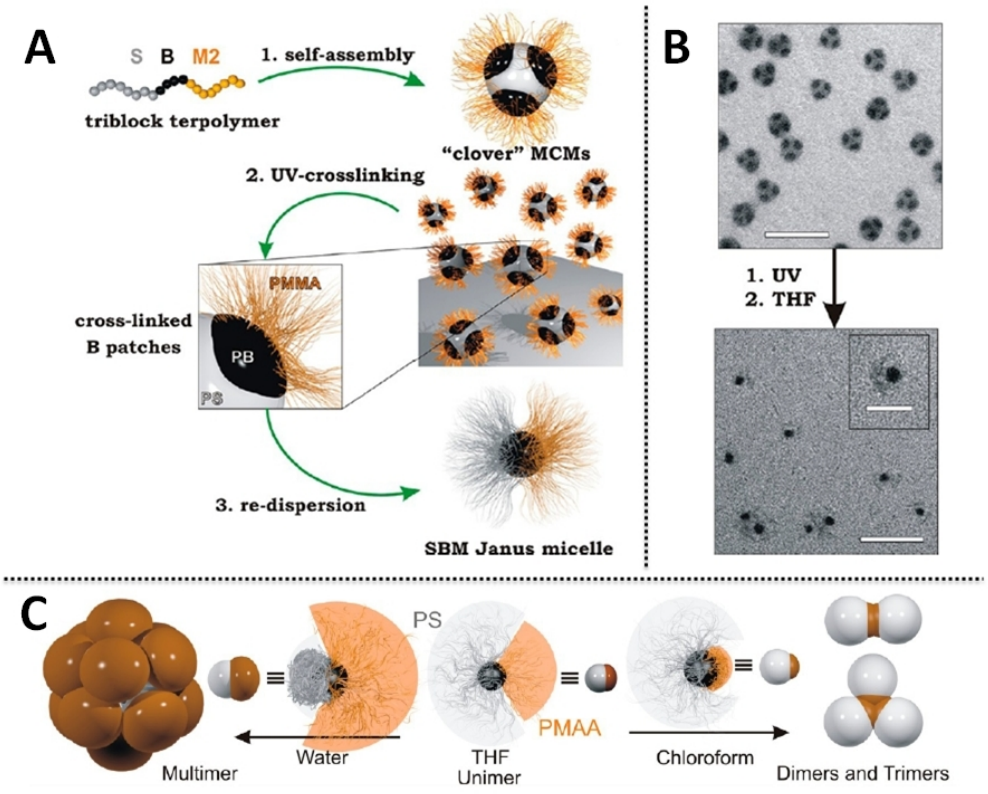

Figure 1-6. (A) Formation of Janus particles by a self-assembly process of multicompartment micelles, following subsequent cross-linking of the compartments and finally, redispersion in THF. (B) TEM images of "clover" multicompartment micelles and corresponding Janus particles. (OsO_4 staining: PS gray, PB black, and PMMA is not visible due to electron beam degradation) (Scale bars: 200 nm and 50 nm in the inset). (C) Schematic clustering of asymmetric JPs in dependence of the corona size in chloroform and water pH 10 (PS is gray and PB is black).[41]

These micelles are formed by the stepwise self-assembly of ABC triblock terpolymers. This approach can be used for a lot of different terpolymers.[41,42] Thereby, the C blocks serve as the stabilizing corona emanating from the B compartments, which reside on an A core. Crosslinking of the B compartments allows fixing this phase separated state and the dissolution of the resulting structure in a good solvent for all blocks breaks up the multicompartment micelles into single Janus particles. The particles now consist of a core of crosslinked B block and two phase separated hemispheres of A and C, whereas the core size of the Janus particles can be adjusted *via* the length of the triblock terpolymer middle block. A very interesting point is that the relative volumes of the corona hemispheres (Janus balance) can be controlled by adjusting the lengths of the outer blocks of the terpolymers.

The process gives access to very interesting features such as tunable core diameter and control over the Janus balance ranging from dominant A side over equal hemispheres to dominant C side. This straightforward approach can be extended to a wide range of triblock terpolymers with different block lengths and block chemistries and consequently the synthesis of a lot of different Janus particles with wide tunable physical properties is possible. For all investigated systems the self-assembly of asymmetric Janus particles in selective solvents for each hemispheres results in a concentration dependent cluster growth or a concentration independent persistence of unimers, dimers and trimers depending on the insolubility of the corona.

2.1.1.2 Self-Assembly in the Bulk

The self-assembly of block copolymer in bulk is a flexible strategy, which can be applied to many different polymer types. Here, the design of Janus particles based on block copolymers requires a good knowledge of the thermodynamics of polymer mixtures, as well as the effect of all parameters affecting the self-assembly (temperature, pH, etc.). Therefore, in the last years widespread research was done in this field of polymer science. Due to the incompatibility of different polymers, block copolymers exhibit microphase-segregated morphologies in the bulk. The thermodynamic description of the phase behavior of a polymer pair is given by the Flory-Huggins equation. The appearance of certain morphologies is not only determined by the Flory-Huggins interaction parameter between the blocks (χ_{AB}), but also by the volume fractions and the degree of polymerization. The phase diagrams of diblock copolymers are theoretically as well as experimentally well investigated.[43-47] Generally, several structural transitions can be observed by an increase of the volume fraction of one

block from zero to fifty volume percent, starting from a mixed system, *via* a spherical phase, a cylindrical phase, a gyroidal phase and finally ending up in a lamellar phase (Figure 1-7 A).

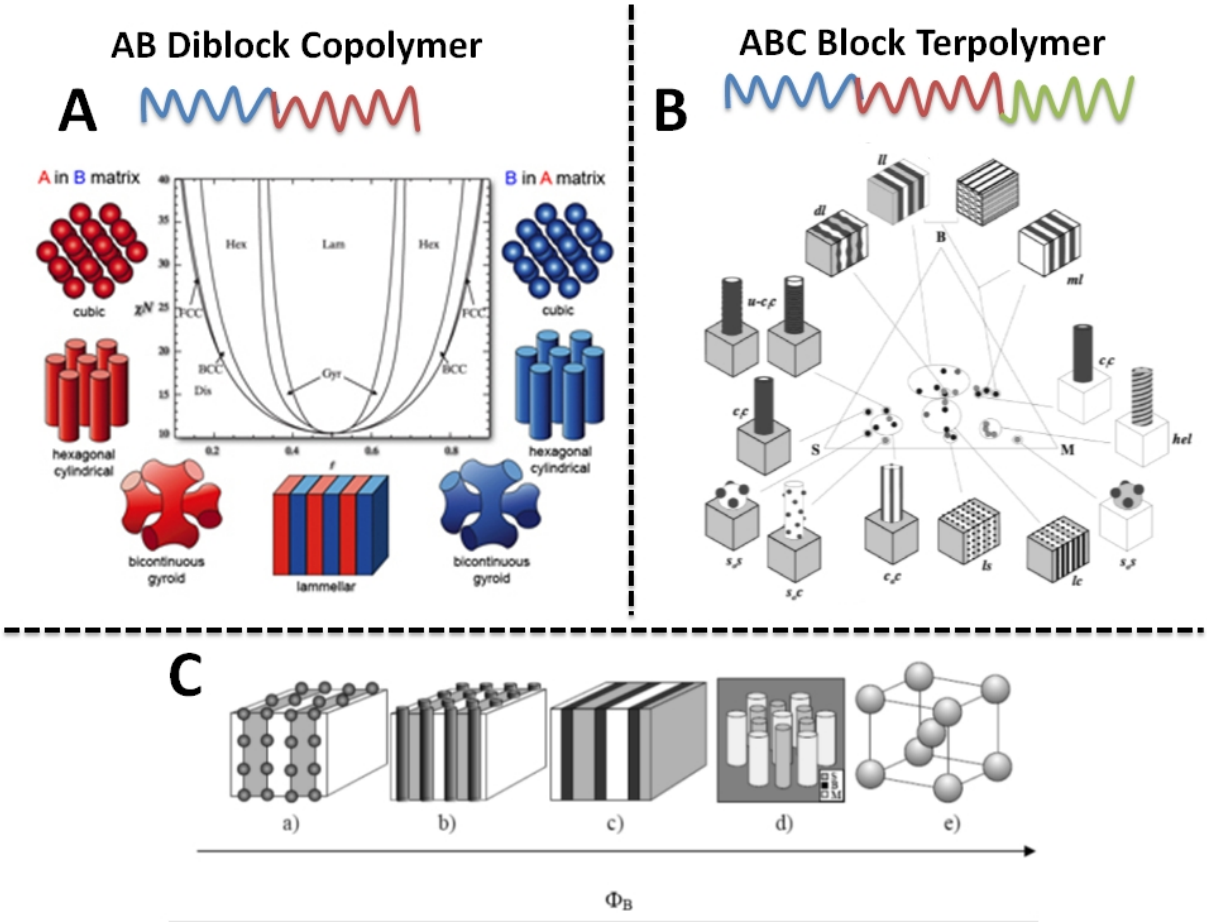

Figure 1-7. (A) Phase diagram for a diblock copolymer with according morphologies.[48] (B) Ternary phase diagram of SBM block terpolymers.[49] (C) SBM-morphologies for terpolymers with symmetric end blocks. The polybutadiene volume fraction increases from left to right. (a) ls = lamella sphere ($S_{45}B_6M_{49}$[225]), (b) lc = lamella cylinder ($S_{48}B_{17}M_{35}$[238]), (c) ll = lamella lamella ($S_{24}B_{38}M_{38}$[245]), (d) cylinders in PB-matrix ($S_{23}B_{57}M_{20}$[215]), (e) mixed sphere of PS and PMMA in PB-matrix ($S_{11}B_{84}M_5$[97]).[50]

However, upon introduction of a third block to the system, the situation becomes fairly more complicated due to the drastically increasing number of parameters and possible morphologies. Three Flory-Huggins interaction parameters exist, χ_{AB}, χ_{AC}, χ_{BC} and two independent volume fractions, Φ_A and Φ_B ($\Phi_C = 1 - \Phi_A - \Phi_B$). As a consequence predictions for stability of certain morphologies are difficult. Stadler *et al.* was an pioneer in the field of block terpolymers and developed a ternary phase diagram for poly(styrene)-*b*-poly(butadiene)-*b*-poly(methyl methacrylate) (SBM) triblock terpolymers (Figure 1-7 B).[51-56] The phase diagram of SBM triblock terpolymers and other triblock terpolymers comprises a multitude of phase-segregated structures on the nanometer scale. For the synthesis of Janus particles based on block terpolymer bulk structures, mainly morphologies of block

terpolymers with symmetric outer blocks have received attention. Morphological studies on the phase separation in ABC terpolymers consisting of three chemically different blocks were theoretically and experimentally done. It was found that even a minor variation in the volume fractions or a change in the interaction parameters between the different blocks results in a significant change of the microphase-segregated morphology. This is shown in Figure 1-7 B for the well investigated systems of the SBM block terpolymer. An increase of the inner PB fraction, while keeping the end blocks of PS and PMMA symmetric, leads to five different morphologies (Figure 1-7 C). Low fractions of PB lead to spherical domains of PB at the lamellar interface of PS and PMMA (lamella-sphere, *ls*), which are followed by PB cylinders (lamella-cylinder, *lc*) with a further increase of PB. A lamellar phase with alternating layers of PS, PB and PMMA (lamella-lamella, *ll*) can be achieved for SBM block terpolymers which have three similar volume fractions.

The first approaches for the preparation of Janus micelles utilizing bulk self-assembly of ABC block terpolymers were presented by two different groups. Ishizu *et al.*[57,58] was the first who introduced the technique of crosslinking a specific domain of a block copolymer. In this way, microspheres could be successfully prepared *via* crosslinking the hexagonal bulk structure of poly(styrene)-*b*-poly(vinylpyridine)-*b*-poly(*tert*-butyl acrylate) with 1,4-diiodobutane gas. Other experimental results were published by Müller's group in 2001, in which crosslinked Janus polymer particles were prepared by the self-assembly of SBM terpolymer synthesized *via* classical anionic polymerization. Here, different block ratios were used to obtain morphologies that allow the later crosslinking of the PB middle block poly(styrene)-*b*-poly(butadiene)-*b*-poly(methyl methacrylate) (PS-*b*-PB-*b*-PMMA).[59] They have also extended this synthetic approach for the synthesis of multicompartment micelles. Their pioneering work took advantage of the wide variety of complex morphologies with a high degree of spatial control that can be obtained spontaneously by the self-organization of the SBM terpolymer during film casting. This procedure is based on the chemical nature and molecular weights of the different blocks. A scheme of the general preparation strategy is shown in Figure 1-8. First, a film from a polymer solution is cast in a suitable solvent which leads to the formation of the desired morphology. Subsequently, the inner PB block, is crosslinked. After dissolution of the film by a suitable solvent, Janus crosslinked particles were recovered. Their shape depends on the morphology of the PB domain with two distinct faces consisting of PMMA and PS.

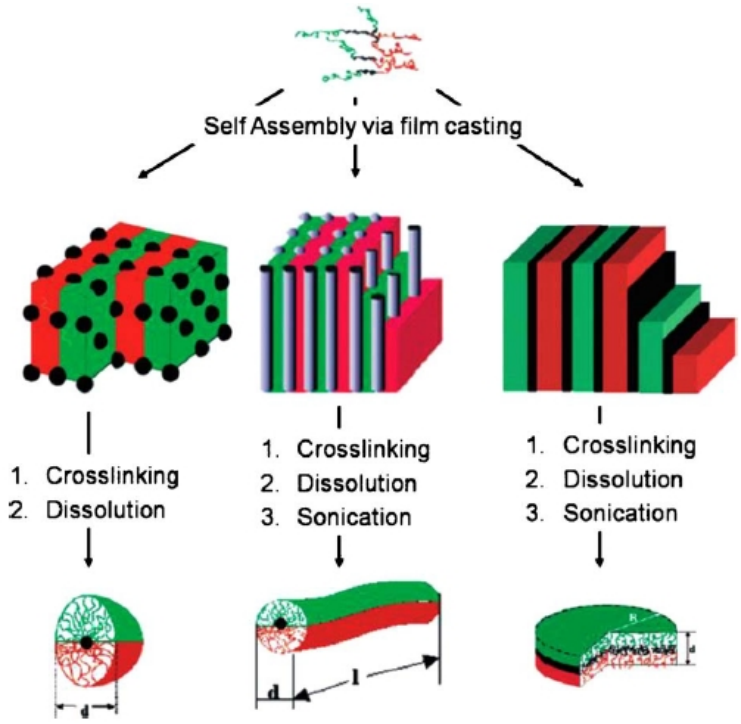

Figure 1-8. Overview of the pathway for the preparation of different Janus particles *via* selective crosslinking of microphase-segregated structures of block terpolymers.[8]

The shape of the inner block is retained after the crosslinking procedure as well as after dissolution of the polymer. Hence, the crosslinking define the shape of the actual Janus particle. One major advantage of this approach is the fact that the two-sided nature of the resulting Janus particle is predetermined in the respective morphology and therefore additional modification is normally not necessary. Generally, it was possible to vary the morphology of the Janus objects, ranging from spheres to cylinders to discs, by varying the block lengths of the ABC terpolymers. Further, the middle block of PB can be crosslinked *via* several techniques, such as vulcanization or the use of AIBN.[8,60]

Erhardt *et al.* reported the preparation of amphiphilic Janus spherical micelles, using the same strategy, but followed by alkaline hydrolysis of the PMMA ester groups, leading to negatively charge hydrophilic pH-sensitive and water-soluble poly(methacrylic acid) (PMAA) groups (Figure 1-9 A).[59,61] In a similar approach, Janus cylinders have been successfully be prepared by Liu *et al.*[62] and Walther *et al.*[63] using a lamella-cylinder (*lc*) morphology of a SBM terpolymer (Figure 1-9 B). To achieve soluble Janus particles, an additional sonification step was introduced in the process. Furthermore, Walther *et al.* showed that Janus discs, using a block terpolymer based on poly(styrene)-*b*-poly(butadiene)-*b*-poly(*tert*-butyl acrylate) (PS-*b*-PB-*b*-P*t*BA), can be synthesized with the same experimental procedure (Figure 1-9 C).[64,65]

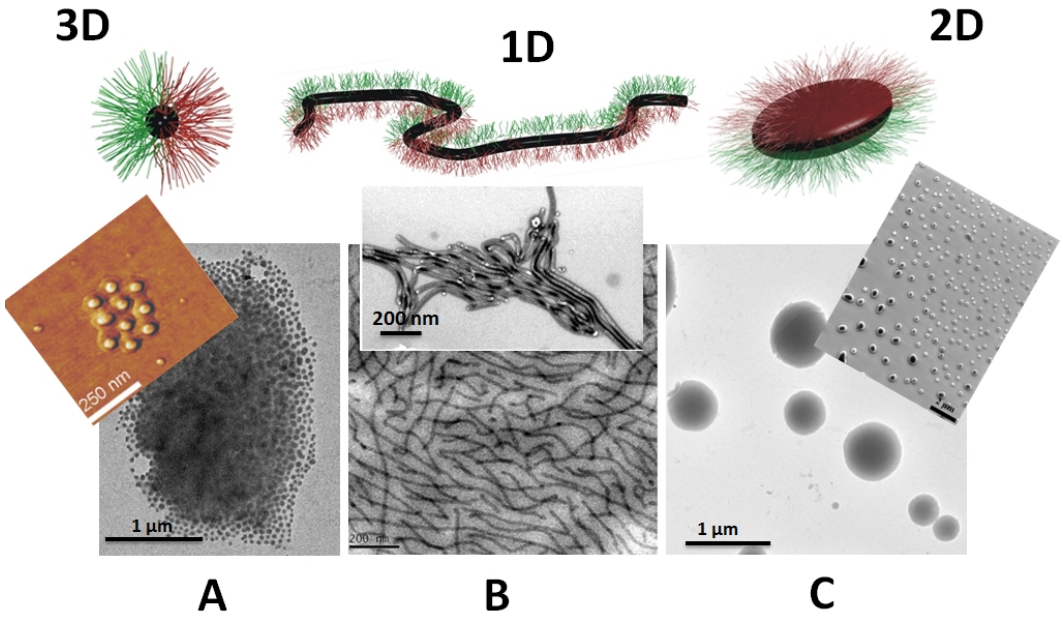

Figure 1-9. Overview of possible Janus particle architectures. (A) Sphere (**3D**), (B) cylinders (**1D**) and (C) discs (**2D**) with characteristic and representative TEM, SEM or AFM images for each particle architecture.

Wolf *et al.* created Janus ribbons from poly(*tert*-butoxystyrene)-*b*-PB-*b*-poly(*tert*-butyl methacrylate) (*t*SBT), *via* controlling the phase transitions *via* pretreatment and crosslinking conditions of the lamella-cylinder bulk morphology.[66] To increase the stability of the Janus sheets, other solvents were added (decane, etc.) which resulted in a better ability to swell the PB phase than the usually used acetonitrile. To prevent the complete dissolution of *t*SBT while still keeping decane as a good swelling agent for PB, a mixture of decane and acetonitrile was used in a certain ratio of 1:1. After a swelling time of 14 h in the steadily stirred decane/acetonitrile mixture, the tSBT was crosslinked with sulfur monochloride (S_2Cl_2). Janus ribbons could be formed by connecting the two Janus cylinders along their major axis *via* a thin PB layer (Figure 1-10).

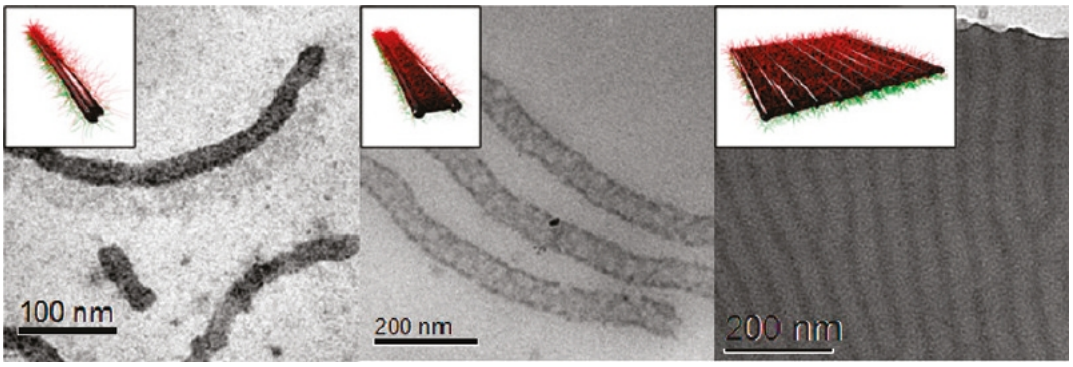

Figure 1-10. Janus cylinders, sheets and Janus ribbons by controlling the phase transitions *via* pretreatment and crosslinking conditions of the lamella-cylinder equilibrium bulk morphology of poly(*tert*-butoxystyrene)-*b*-polybutadiene-*b*-poly(*tert*-butyl methacrylate) (*tSBT*).[66]

The biggest advantage of the phase separation based strategy is that the whole process is not complicated. So it is possible to synthesize a large amount of Janus particles with different morphologies in the range of hundreds of nanometres to several micrometres. Thus, the bulk self-assembly process of ABC block terpolymers can be used for the synthesis of a great variety of Janus particles in gram scale.

2.1.2. Desymmetrization of Particles

A large number of preparation techniques for Janus particles use different alternatives of the masking technique. This means that asymmetric functionalization of nanoparticles is achieved *via* a selective protection of one part of an isotropic particle while the exposed surface area of the particle is chemically modified. The masking process is based on solid–liquid, liquid–liquid, liquid–gas or gas–solid interfaces, and as a consequence, it is ideal for fabrication of all polymeric, inorganic and polymeric–inorganic Janus particles due to its controllable size and morphology. The main challenge is to modify one hemisphere without altering the surface of the other one.

The first example was mentioned by De Gennes in 1991[10] and, in fact, it had been already reported by some of his colleagues before.[67-69] They described the elaboration process of amphiphilic glass microspheres (40–50 mm in diameter) and their behavior at water/oil interfaces. In recent literature the most common ways to break the symmetry of spherical particles can be categorized with respect to the used substrates used for the immobilization of the particles. Here, the particles are immobilized on hard substrates[70] (Figure 1-11 A), soft flat substrates, particles dispersion[71] (Figure 1-11 B) or in droplets, Pickering emulsions and air-water interface[72] (Figure 1-11 C). Therefore, masking is probably the most flexible of all techniques to prepare Janus nanoparticles. It is applicable to nearly any type of material and it offers the possibility to modify the surfaces of nanoparticles with a very wide variety of functional groups. However, they usually lead to Janus particles with a good homogeneity and large quantities for laboratory use, but an up-scaling of these processes to an industrial level is more difficult. An obvious up-scaling strategy for Janus particles is based on previously described techniques at interfaces, but trying to increase the size of the interface as much as possible. In order to exponentially increase the accessible interface area droplets, emulsions or suspensions are often used and are a good alternative to obtain larger quantities of Janus particles.

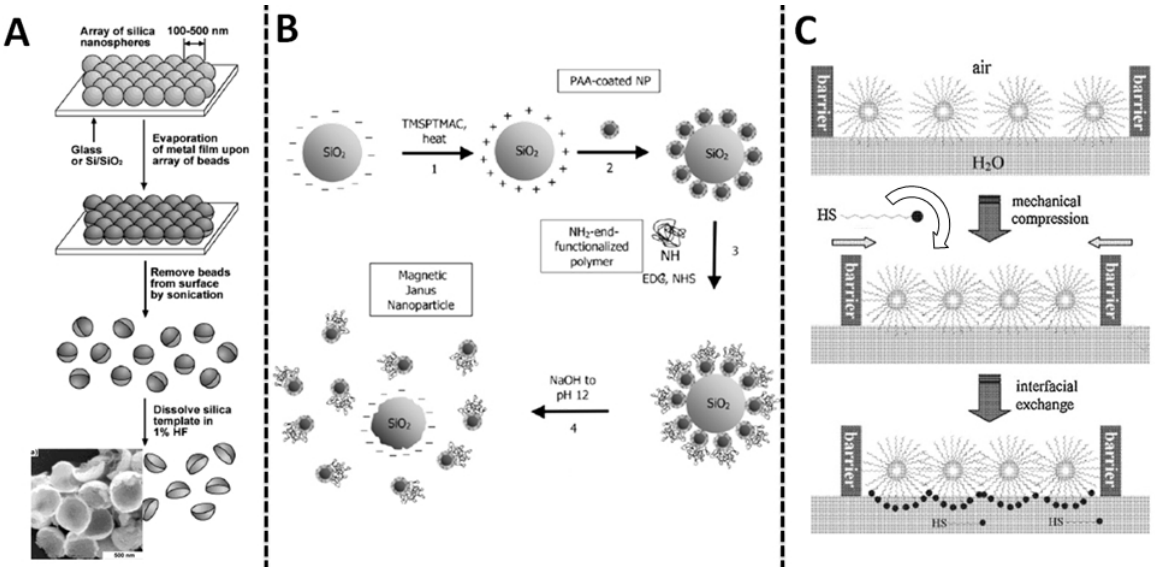

Figure 1-11. Schematic illustrations of different substrates for the masking technique. (A) Hard substrates: Scheme for the synthesis of metallic half-shells with a SEM image of 10 nm thick gold half shells (450 nm diameter).[66] (B) Particle dispersions: Schematic drawing of masking procedure for the asymmetric functionalization of PAA-coated magnetic nanoparticles.[67] (C) Water-Air interface: Illustration of the preparation pathway towards Janus particles based on the Langmuir-Blodgett technique.[68]

In the following section, the focus will be on the Pickering emulsion method and the differences between liquid-liquid Pickering emulsions and polymer or wax based Pickering emulsions will be described.

Pickering Emulsions

Despite all advances of the synthesis routes mentioned above, most applications require large amounts of Janus particles. But all these routes have problems with low efficiencies and are limited in respect to complexity and scale. A promising route towards a large number of complex anisotropic Janus colloids is the Pickering emulsion based method. Hereby, an emulsion stabilized by particles instead of surfactant molecules is called Pickering emulsion. Pickering emulsion assisted synthesis of Janus colloids is very interesting since it is adaptive for a lot of different particle sizes and compositions. One main advantage regarding to this method is the high yield of Janus particles. A stable emulsion is achieved when particles in the range of nanometer to micrometer are located at the interface between oil and water. In order to decrease the surface energies of emulsion interfaces, particles tend to adsorb strongly at these interfaces and stabilize the emulsion. Then, one hemisphere of a particle is located in oil phase while the other one is in aqueous phase, and after chemical modification amphiphilic Janus particles could be obtained.

2.1.2.1 Liquid–Liquid Pickering Emulsions

Particles adsorbed at a Pickering interface can be modified topo-selectively since one particle side is protected whereas the other side is free for any modifications. Generally, tailored modification of the area which should be functionalized is possible due to the fact that the particle embedding in the droplet depends either on the droplet polarity or on surface hydrophobicity of the particle.

One example are spherical metal NPs adsorbed at an oil-water emulsion interface in combination with the reduction of silver, resulting in the formation of bimetallic nanometer-sized Janus particles.[73] The concept of water accessible surface modification was adapted by Suzuki *et al.* to microgels for creating amidecarboxylic acid Janus microgels, which can be topo-selectively stained with gold NPs.[74] A relevant problem is that the rotation of the particles at the liquid-liquid interfaces affects the formation of Janus particles. Even if several publications report the non-rotation of spherical particles,[75] it is very important to find a versatile way to prevent rotation in order to generate well-defined Janus particles.

In this context, several methods have been reported for water in oil emulsions as well as oil in water emulsions.

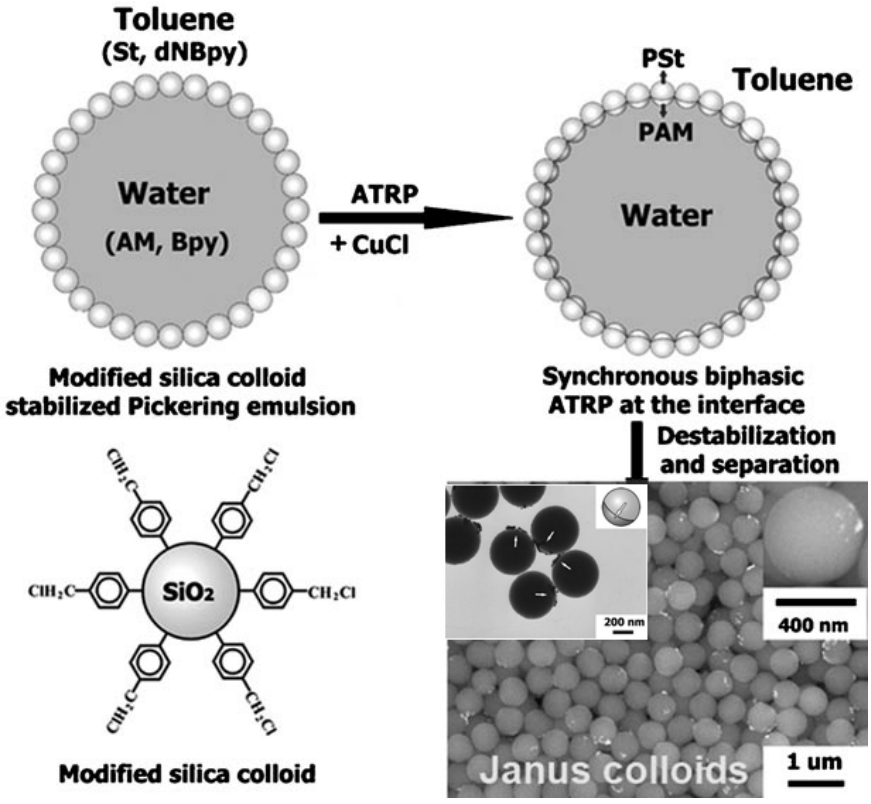

Figure 1-12. Synthesis of Janus colloids by biphasic grafting at a liquid-liquid Pickering emulsion interface.[76]

Recently, a method involving water in oil emulsions containing different monomers in both phases and modified sub-micrometer silica particles at the interfaces was reported. During the polymerization process of both monomers at the particle surfaces, their amphiphilic character changes, and thus, the rotation of the particles is prohibited (Figure 1-12).[76] In another report, using an oil in water emulsion Zhang *et al.* prepared amphiphilic Janus silica particles with hydrophobic polystyrene (PS) and hydrophilic poly(sodium methacrylate) (PSMA) brushes on two hemispheres by surface-initiated polymerization. The basic idea was that the polymerization occurs not only at the surface of the particles, but also in the whole emulsion. As a consequence the viscosity in the system is also increased, which restricts the rotation of the particles.[77]

2.1.2.2 Polymer and Wax based Pickering Emulsions

Another possibility to avoid rotation of the colloids at Pickering interfaces is to trap them directly before their modification. This can be achieved using an oil in water emulsion with droplets containing monomers or polymers which can be solidified through polymerization[78] or solvent evaporation.[79]

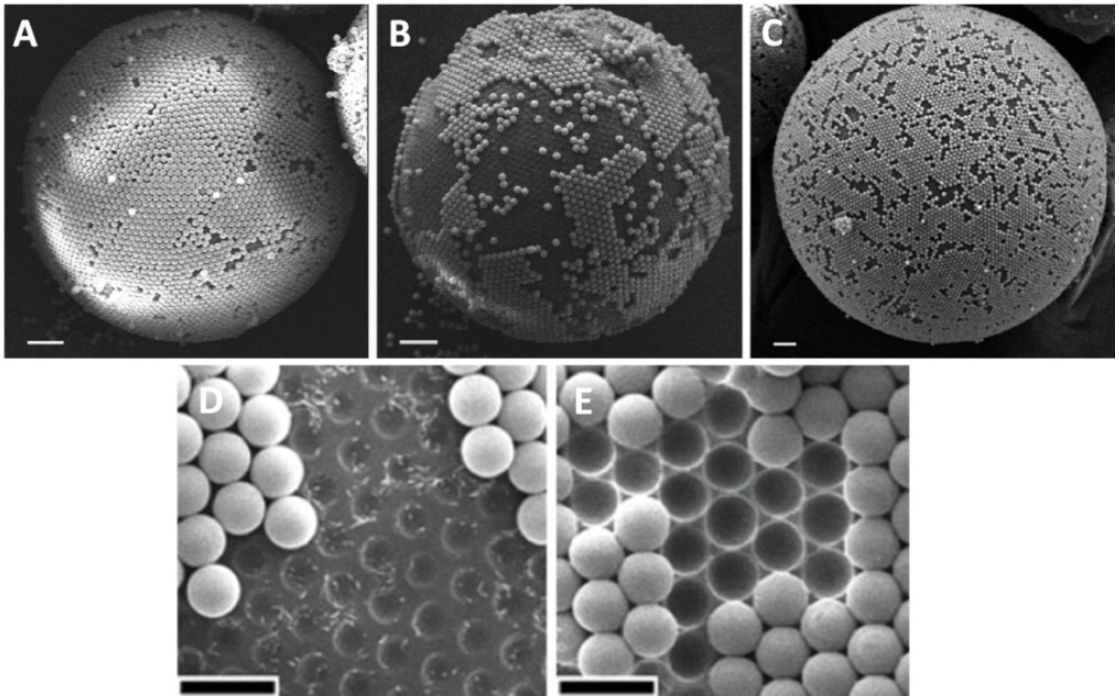

Figure 1-13. SEM images of colloidosomes: (A) before chemical modification; (B) modified to be hydrophobic using solvent-based method (C) modified to be hydrophobic *via* vapor-phase deposition (scale bar: 10µm).[83] (D+E) The used surfactants adsorb strongly on the silica particles and make the particle more hydrophobic, resulting in a deeper penetration depth in the oil phase and a changed contact angle. Particles with different Janus balance can be obtained *via* this method (scale bar: 5µm).[82]

A very elegant and inexpensive way of preparing gram-scale quantities of Janus particles was originally proposed by Granick and co-workers.[80-84] The particles are frozen at the interface between water and wax. Here, for example, silica nanoparticles are dispersed in a melted wax. The silica particles stabilize the emulsion covering the surface of the wax droplet. Upon lowering the temperature, the wax solidifies, while the silica nanoparticles are immobilized. Afterwards the silica particles can be chemically modified on their unprotected side (Figure 1-13). In this way they produced bipolar Janus particles and Janus particles with different charges on each side as a colloid analogue of a surfactant (Figure 1-13 A/B).[82,83] Using additional surfactants which can adsorb on the surface of the particles, leads to a control of the relative ratio of exposed and covered surface area, also called the "Janus balance" (Figure 1-13 D/E).[81,82] Within the same working group a solvent-free synthesis of these Janus particles was developed in detail taking advantage of the quick and efficient access of vapor to surfaces. At the liquid-liquid interface of emulsified molten wax and water, untreated silica particles adsorb and are frozen in place when the wax solidifies. The exposed surfaces of the immobilized particles are modified chemically by exposure to silane vapor and, in principle, subsequent dissolution of the wax opens up the inner particle surface for further chemical modification (Figure 1-13 C).[83]

On the basis of this method, Stamm *et al.* prepared stimuli-responsive bicomponent polymeric Janus particles *via* a sequential "grafting-from and grafting-to approach" (Figure 1-14 A).[85] Hence, Granick's experimental procedure was used for a lot of different studies to synthesize sub-micrometer sized polymer-laponite core-shell particles with anisotropic surface potentials,[86] and 100 nm silica JPs.[87] Etching of the unprotected silica part leads to original Janus particle morphologies (Figure 1-14 B).[88]

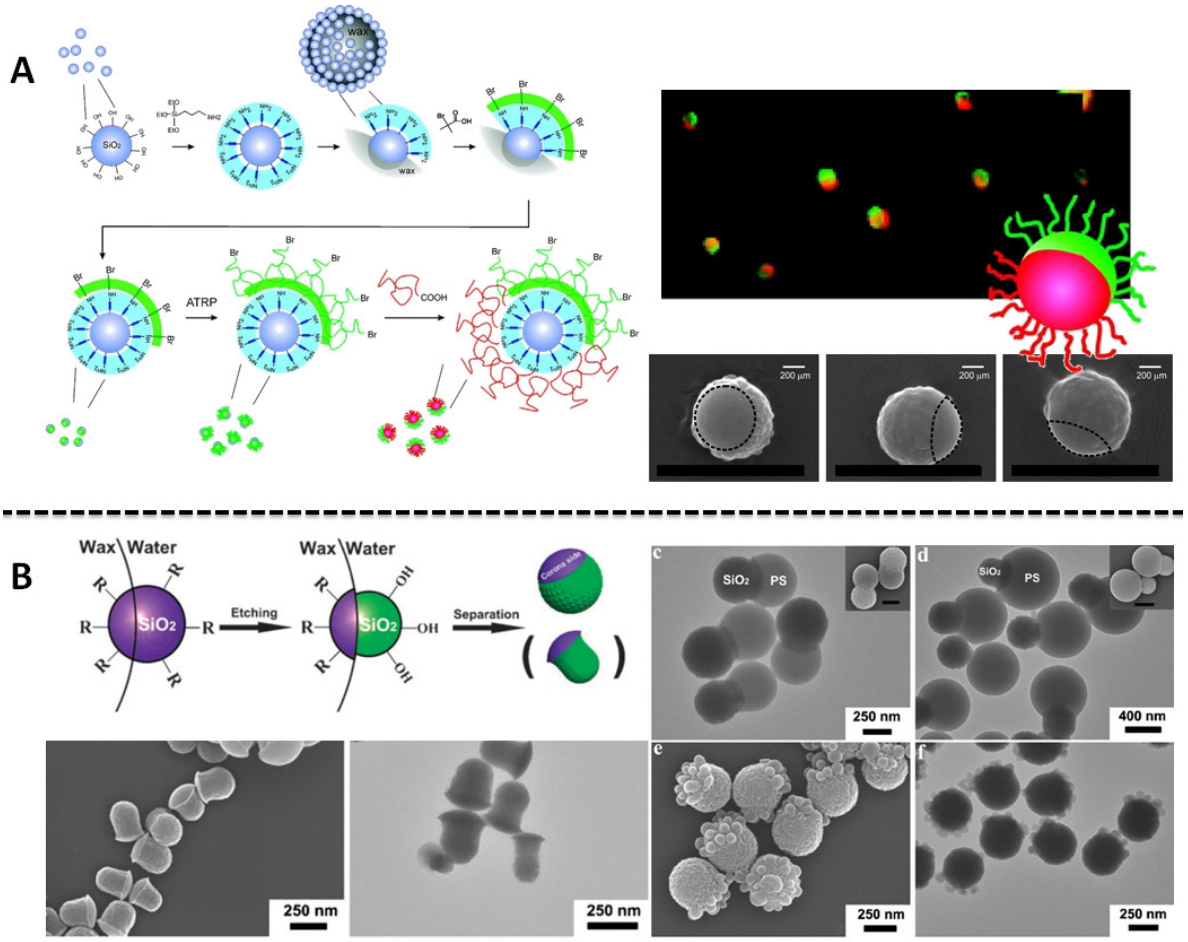

Figure 1-14. (A) Scheme of the synthesis of bicomponent Janus particles *via* "grafting from" and "grafting to" approaches.[85] (B) TEM and SEM of the mushroom-like Janus particles after a defined etching process (left side), of the Janus PS/SiO_2/PS dimers with increased PS fractions and of Janus PS/SiO_2 composite colloids with PS nano-flowers grown on the corona side.[88]

Kim *et al.* developed an interesting process which requires a photo-curable oil phase in an oil in water Pickering emulsion.[89,90] The particles are PS microbeads and the droplets contain the photo-curable polymer. The affinity between polymer and PS particles will direct the final shape from Janus particles to snowman-like anisotropic Janus particles. Other groups used this method as well to create a particularly interesting field of Janus colloidal particles which have asymmetric surface structures and specifically responding to external stimuli.[91,92] In a slightly different approach compared to the method proposed by Granick and co-workers, Paunov *et al.* assembled PS latex particles at a water/oil interface. The water contained gellan, which leads to a freezing in of the aqueous layer upon cooling. The organic layer was replaced with a PDMS layer in which the PS particles were immobilized after curing. Evaporation of gold onto the half-exposed PS latex particles results in the formation of PS Janus particles which are capped with gold.[24,93]

It is still a question whether rotation of the particles at the interface really affects the formation of Janus colloids. Many research articles are focused on rather large Pickering particles (>> 100 nm), which are of course easier to immobilize at interfaces. With respect to nanoscale Pickering particles, rotation should be avoided to obtain high-quality Janus nanoparticle. This topic will be discussed in detail in chapter 7. All in all, pioneering work on this research topic for this problem was done, for instance, by Landfester *et al.*[94] and Bon *et al.*[95-101] who worked with silica particles or clay platelets in the size of nano-scale Janus particles.

2.2 Properties and Applications

In recent years, Janus particles are the subject of intensive research. Since the challenges in the synthesis of Janus particles are nearly solved and additionally, theoretical predictions point to unique properties of Janus nanoparticles and possible applications of Janus particles come into focus of many scientists. There are several examples in literature which demonstrate the use of Janus particles in new materials with advanced properties. Here, the Janus particles exhibit several unique properties related to their asymmetric structure and/or their functionalization. Therefore, it is possible to change their amphiphilic, magnetic, catalytic, optical and electrical and surface active properties and, as a consequence, their self-assembly mechanisms, can be changed. So, Janus particles offer a versatile platform of applications ranging from material science to biology and catalysis. Besides, the use as building blocks for supramolecular hierarchal structures, Janus particles have already demonstrated a huge potential in a large number of different fields such as drug carriers, stabilizers in emulsion polymerizations and blends, surfactants, switchable devices, optical probes. Nevertheless, the most relevant property is their self-assembly behavior and their interfacial activity.

A first example for an interesting switchable device was shown by Nisisako *et al.*[102], who used the electrical anisotropy of Janus particles filled with white pigments in one hemisphere and black pigments in the other. In order to create a switchable display panel, a thin layer of these spheres was placed between two electrodes. After switching on an electric field, the particles orientate their black sides to the negative electrode and their white sides to the positive electrode. The orientation of the particles and thus the color of the display can be flipped simply by reversing the electrical field. With this method, very thin, robust and stable displays can be created. Further, Janus particles are used as efficient optical probes for

biological interactions or rheological measurements in confined space. In recent years, this concept has been brought forward by Behrend and coworkers who used Janus beads coated with metal on one side.[103-106] These so-called modulated optical nanoprobes reflect and transmit light or emit fluorescence anisotropically.

Also biological applications of Janus nanoparticles have been reported. For example, Lahann and co-workers tested the biocompatibility of Janus particles obtained by co-jetting of two liquid solutions containing immiscible polymers (Figure 1-15 A).[107-109]

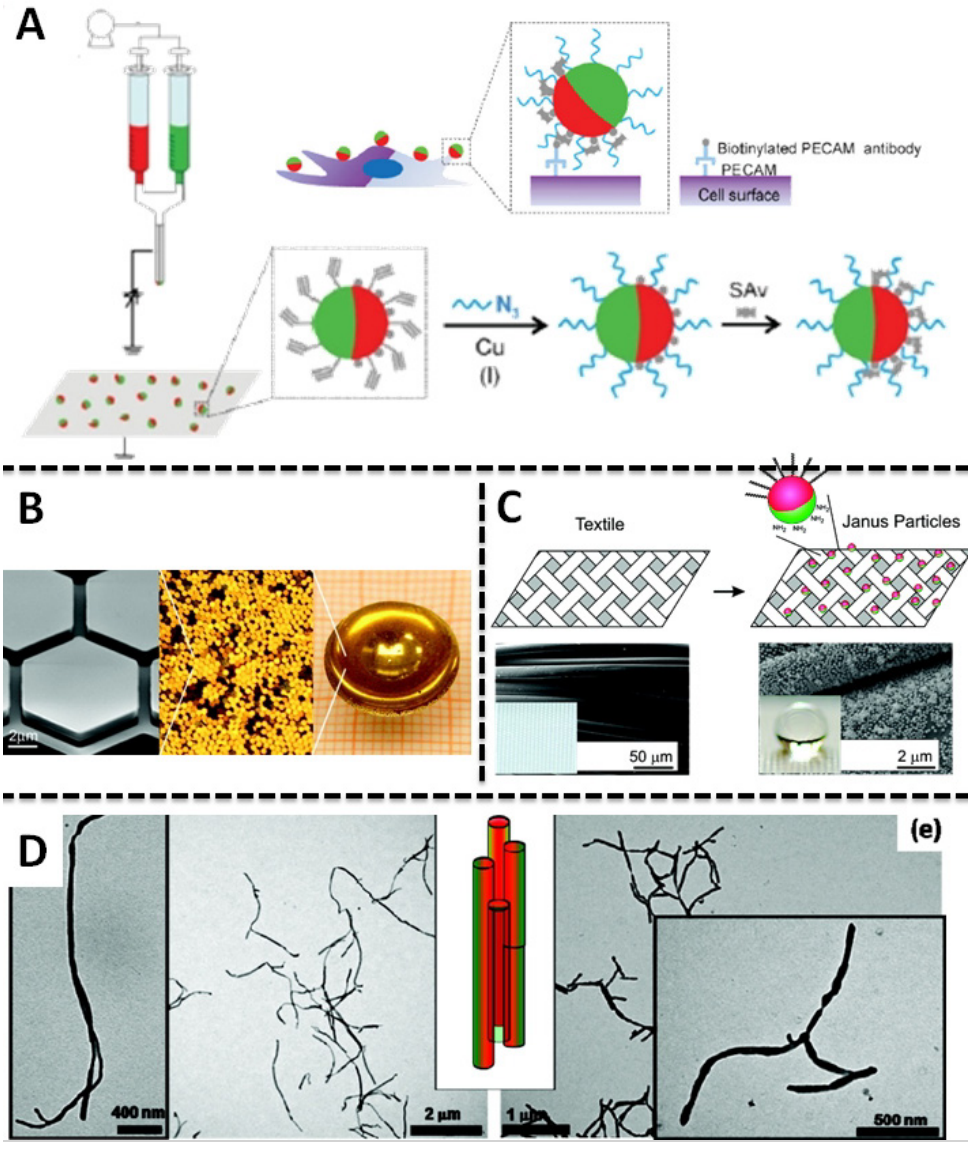

Figure 1-15. (A) Scheme for the binding of Janus particles fabricated *via* co-jetting of two polymer solutions to cells.[108] (B) Tunable, high-reflectivity optofluidic device based on self-assembly of anisotropically functionalized hexagonal micromirrors (Janus tiles) on the surface of an oil droplet to create a concave liquid mirror.[110] (C) Scheme of modification of a textile surface using amphiphilic Janus particles.[111] (D) TEM images obtained after deposition from a 0.5 g/L acetone solution of Janus cylinders onto TEM grids after 2.5 min and 30 min sonication. The scheme highlights the formed superstructures (PS (red) is hidden within the center of a fiber-like aggregate).[63]

Aizenberg et.al. has described a tunable, high-reflectivity optofluidic device based on self-assembly of Janus tiles (functionalized hexagonal micromirrors) on the surface of an oil droplet. Hereby, a concave liquid mirror could be formed (Figure 1-15 B).[110] Recently, Synytska *et al.* showed that water repellent nanofibers can be prepared by coating polyethylene terephtalate-based textile fibers with amphiphilic Janus nanoparticles. Here, the hydrophilic reactive side is bound to fibers whereas the hydrophobic face remains free to provide the water repellent behavior (Figure 1-15 C).[111] Besides this, experimental and theoretical studies of the self-propelled dynamic motions of a new genre of catalytic sphere Janus particles, which comprises a non-catalytic silica sphere connected to a catalytic platinum sphere, are reported for the first time by Valadares *et al.*.[112] Further, it has to be mentioned that the first example of controlled self-assembly of Janus nanoparticles into highly ordered superstructures was observed by Müller *et al.* and so controlled self-assembly for Janus spheres[59,61], Janus cylinders (Figure 1-15 D)[63] as well as Janus discs[64,65] using either "good" or "bad" solvents for each polymer block was possible. The controlled self-assembly of Janus particles have been reported by many other authors as well.[71,72,91,113]

The stabilization of emulsions and dispersions is very important for a lot of problems in daily life. For a lot of products, such as milk or cosmetics, an emulsifier of suitable type which prevents a phase separation between oil and water and stabilizes the mixtures is needed. In contrast to a particle with uniform wettability, the surface of Janus particles, as already mentioned, has two parts exhibiting different wettability, and therefore, these particles are perfect candidates to assemble at interfaces. From an industrial point of view, the surface activity of Janus particles is of fundamental interest. Hence, an amphiphilic particle that combines the typical Pickering effect of the particles and the amphiphilicity of a classical surfactant can be obtained.

At the beginning of the last century, Pickering and Ramsden discovered the stabilizing effect of particles in emulsions[114,115], followed by the theoretical description of this effect by Pieranski[116]. Since this time, nanoparticle adsorption at fluid interfaces has been studied from a fundamental point of view.[117-123]. Consequently, there is an enormous potential to assemble anisotropic particles as well as Janus particles or anisotropic Janus particles at fluid interfaces. By now, intensive work has been carried out to observe and understand the extraordinary high adsorption strength of Janus particles at fluid interfaces, caused by the decrease in interfacial energy and additional stabilization of the liquid-liquid interfaces. In the following, several theoretical and practical studies have been performed to investigate Janus particle behavior at

liquid-liquid interfaces after Binks and Fletcher's first calculations of interfacial adsorption capabilities of biphasic Janus spheres, which predicted an up to three fold stronger adsorption compared to particles of uniform wettability.[124] Further, Nonomura *et al.* published results of theoretical calculations about the influence of disc-shaped Janus beads on the oil/water interfacial tension.[125,126] These calculations demonstrated that the adsorption energy of Janus discs is several orders of magnitude higher than that of common surfactants. As a consequence, a considerable increase in surface activity is expected. These predictions render Janus structures an extremely interesting new class of future surfactants and for the nanostructuring of interfaces.

Glaser *et al.* showed that bimetallic Janus particles lead to a significant reduction of the oil/water interfacial tension compared to uniform metallic nanoparticles of similar size (iron oxide or gold) (Figure 1-16 A).[127] In the following, other groups also reported the stabilization of liquid-liquid interfaces.[90,128] In terms of real prototype applications, Walther *et al.* demonstrated a superior performance of Janus particles in case of surface activity[64] (Figure 1-16 B), nanostructuring of polymer blend systems[129] (Figure 1-16 C) and emulsion polymerization[130] (Figure 1-16 D).

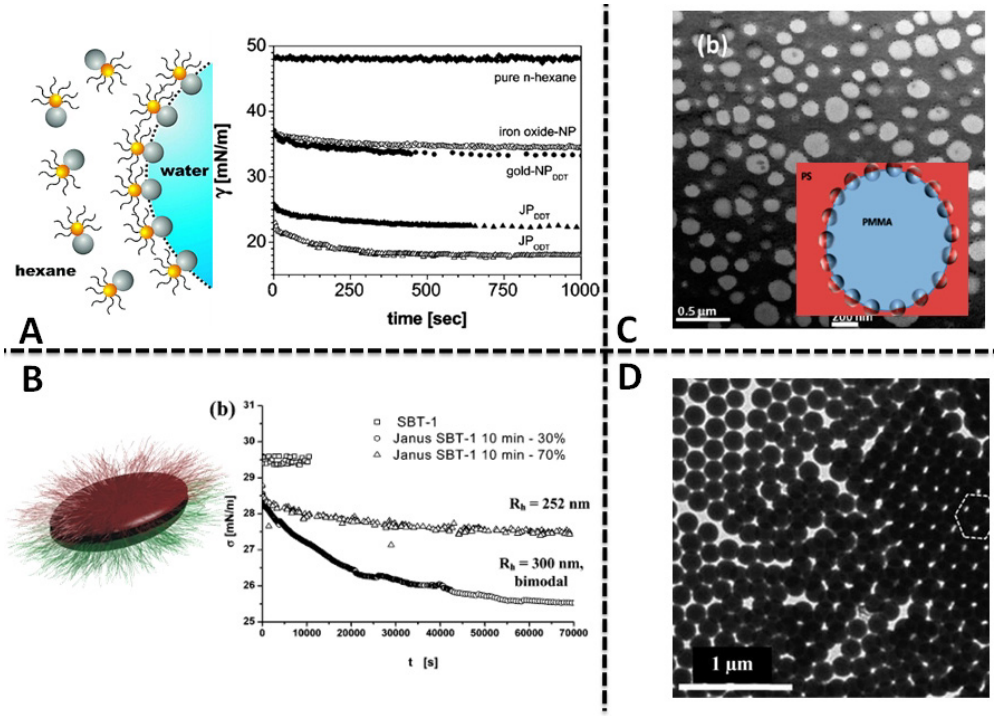

Figure 1-16. (A) Scheme of bimetallic Janus particles at the hexane/water interface (yellow: gold part with surfactant; gray: iron oxide) and the corresponding plot of the interfacial tension vs. time as measured by a pendant drop tensiometer.[127] (B) Schematic illustration of a single Janus disc and interfacial tension isotherms of solutions of Janus discs in cyclohexane at the cyclohexane/water interface (c = 1 mg/mL).[64] (C) TEM images obtained for 20 wt % Janus particles in a 60/40 PS/PMMA blend.[130] (D) TEM images of Latex PS Particle stabilized by a single Janus particles.[131]

Additional studies suggested that the geometry including size, aspect ratio, form and shape as well as the surface properties of Janus particles play a significant role for their surface activity, particle orientation and packing geometry (Figure 1-17 A/B).[131-133]

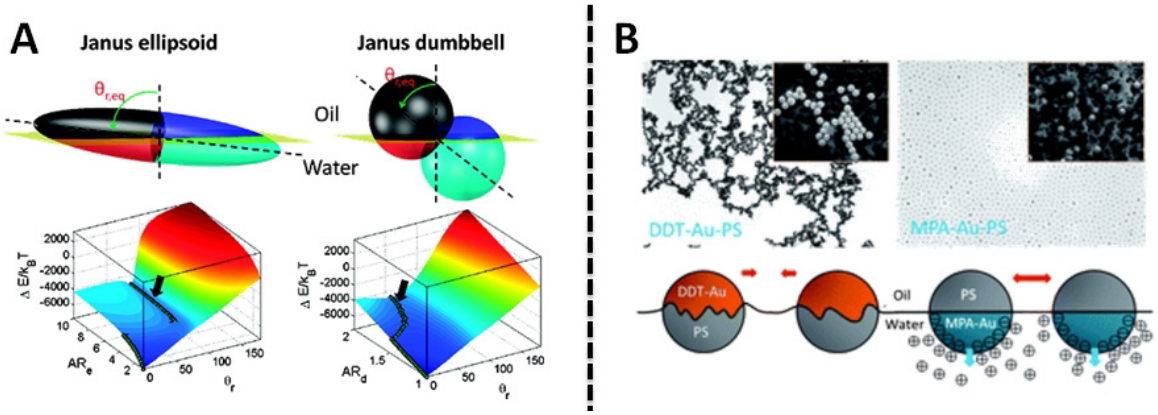

Figure 1-17. (A) Equilibrium orientation of nonspherical Janus particles (Janus ellipsoids and Janus dumbbells) at an oil/water interface with corresponding three-dimensional (3D) contour plot of attachment energy (ΔE) as a function of the aspect ratio and rotational angle (green symbolize the global energy minimum).[131] (B) Microstructures formed by DDT-Au-PS and MPA-Au-PS Janus particles at the oil–water interface and the proposed mechanism for the long-range repulsions between the Janus particles at the oil–water interface.[132]

Unfortunately, most of theoretical work was focused on the understanding of the behavior and the equilibrium orientation of spherical Janus particles at fluid-fluid interfaces. Understanding the effect of anisotropic Janus particles at fluid interfaces and the influence of particle shape will be highly important to find special design criteria for an efficient industrial use of Janus particles. The first two chapters of this thesis are focused on this issue.

In general, the combination of amphiphilicity combined with particle character and their strong adsorption and orientation at the interface makes Janus particles an attractive tool for the nanostructuring of blends, liquid-liquid interfaces or block copolymers[134].

2.3. Conclusion and Outlook

Janus particles represent a very unique class of particles which combine properties and functionalities of different materials in one single unit. Over the last years, enormous progress has been made in the preparation of well-defined Janus particles with a variety of highly sophisticated techniques due to an increasing interest in new and more complex particles in all scientific fields. Their fascinating properties, based on precisely controllable sizes, shapes and functionalities, turn Janus particles into promising candidates for a wide range of high-quality applications ranging from material science to biology. However, the major outstanding

challenge for the next years is still the development of smart strategies for the preparation of nano-sized Janus particles in large quantities.

3. Aim of the Thesis

The design and synthesis of Janus structures with controlled size, shape, and functionality is a fundamental and intense field of research. After being able to produce larger amounts of different types of polymeric Janus particles, the basic knowledge of their solution and interfacial behavior is very important to create new and more efficient materials.

The motivation of this work is, in general, the investigation of the effect of the biphasic Janus particles on their behavior at interfaces and thereby, in particular, the influence of particle size and architecture. Therefore, the focus of this thesis is the behavior of spherical, cylindrical and disc-like Janus particles at liquid-liquid interfaces. Until now, the importance of controlling the particle shape is not well understood. Thus, detailed systematic studies have to be performed to study the influence of size and form of polymeric Janus particles on their surface activity, their orientation and their self-assembly process at liquid-liquid interfaces.

Hybrid nanoparticles which combine relevant properties of different materials are fundamental components for multifunctional materials in future technologies. Therefore, inorganic/organic hybrids were investigated as Janus particles in addition to triblock terpolymer based ones. Here, special attention is given to the combination of the properties of inorganic nanoparticles with the stimuli-responsive behavior of polymers in hybrid nano-sized inorganic/organic core-shell-corona particles and the development of reliable experimental procedures in the preparation of inorganic/organic core-shell-corona hybrid Janus particles.

4. References

1. Sanchez, C.; Rozes, L.; Ribot, F.; Laberty-Robert, C.; Grosso, D.; Sassoye, C.; Boissiere, C.; Nicole, L., *C.R. Chim.* **2010**, 13, 3.
2. Du, J.; O'Reilly, R. K., *Chem. Soc. Rev.* **2011**, 40, 2402.
3. Lattuada, M.; Hatton, T. A., *Nano Today* **2011**, 6, 286.
4. Perro, A.; Reculusa, S.; Ravaine, S.; Bourgeat-Lami, E.; Duguet, E., *J. Mater. Chem.* **2005**, 15, 3745.
5. Loget, G.; Kuhn, A., *J. Mater. Chem.* **2012**, 22, 15457.
6. Hu, J.; Zhou, S.; Sun, Y.; Fang, X.; Wu, L., *Chem. Soc. Rev.* **2012**, 41, 4356.
7. Pawar, A. B.; Kretzschmar, I., *Macromol. Rapid Commun.* **2010**, 31, 150.
8. Walther, A.; Müller, A. H. E., *Soft Matter* **2008**, 4, 663.
9. Lee, K. J.; Yoon, J.; Lahann, J.*, J. Colloid Interface Sci.* **2011**, 16, 195.
10. de Gennes, P.-G., *Angew. Chem. Int. Ed.* **1992**, 31, 842.
11. Walther, A.; Müller, A. H. E., In: Janus particle synthesis, self-assembly and applications, Jiang, S.; Granick, S., Eds. The Royal Society of Chemistry: Cambridge, 2012; p 1.
12. Jiang, S.; Granick, S., In: Janus particle synthesis, self-assembly and applications, The Royal Society of Chemistry: 2012; p 5.
13. Roh, K. H.; Yoshida, M.; Lahann, J., *Materialwiss. Werkstofftech.* **2007**, 38, 1008.
14. Roh, K.-H.; Martin, D. C.; Lahann, J., *Nat. Mater.* **2005**, 4, 759.
15. Dendukuri, D.; Gu, S. S.; Pregibon, D. C.; Hatton, T. A.; Doyle, P. S., *Lab Chip* **2007**, 7, 818.
16. Vilain, C.; Goettmann, F.; Moores, A.; Le Floch, P.; Sanchez, C., *J. Mater. Chem.* **2007**, 17, 3509.
17. Gu, H.; Zheng, R.; Zhang, X.; Xu, B., *J. Am. Chem. Soc.* **2004**, 126, 5664.
18. Nagle, L.; Fitzmaurice, D., *Adv. Mater.* **2003**, 15, 933.
19. Yin, Y.; Lu, Y.; Xia, Y., *J. Am. Chem. Soc.* **2001**, 123, 771.
20. Gao, X.; Yu, L.; MacCuspie, R.; Matsui, H., *Adv. Mater.* **2005**, 17, 426.
21. Teranishi, T.; Inoue, Y.; Nakaya, M.; Oumi, Y.; Sano, T., *J. Am. Chem. Soc.* **2004**, 126, 9914.
22. Yu, H.; Chen, M.; Rice, P. M.; Wang, S. X.; White, R. L.; Sun, S., *Nano Lett.* **2005**, 5, 379.
23. Bao, Z.; Chen, L.; Weldon, M.; Chandross, E.; Cherniavskaya, O.; Dai, Y.; Tok, J. B. H., *Chem. Mater.* **2001**, 14, 24.
24. Paunov, V. N.; Cayre, O. J., *Adv. Mater.* **2004**, 16, 788.
25. Vanakaras, A. G., *Langmuir* **2005**, 22, 88.
26. Cheung, D. L.; Bon, S. A. F., *Soft Matter* **2009**, 5, 3969.
27. Glotzer, S. C.; Solomon, M. J., *Nat. Mater.* **2007**, 6, 557.
28. Hawker, C. J., *Acc. Chem. Res.* **1997**, 30, 373.
29. Braunecker, W. A.; Matyjaszewski, K., *Prog. Polym. Sci.* **2007**, 32, 93.
30. Voets, I. K.; de Keizer, A.; de Waard, P.; Frederik, P. M.; Bomans, P. H. H.; Schmalz, H.; Walther, A.; King, S. M.; Leermakers, F. A. M.; Cohen Stuart, M. A., *Angew. Chem. Int. Ed.* **2006**, 45, 6673.
31. Voets, I. K.; van der Burgh, S.; Farago, B.; Fokkink, R.; Kovacevic, D.; Hellweg, T.; de Keizer, A.; Cohen Stuart, M. A., Macromolecules **2007**, 40, 8476.
32. Voets, I. K.; Fokkink, R.; de Keizer, A.; May, R. P.; de Waard, P.; Cohen Stuart, M. A., *Langmuir* **2008**, 24, 12221.

33. Cheng, L.; Zhang, G.; Zhu, L.; Chen, D.; Jiang, M., *Angew. Chem. Int. Ed.* **2008**, 47, 10171.
34. Wurm, F.; König, H. M.; Hilf, S.; Kilbinger, A. F. M., *J. Am. Chem. Soc.* **2008**, 130, 5876.
35. Li, Z.; Kesselman, E.; Talmon, Y.; Hillmyer, M. A.; Lodge, T. P., *Science* **2004**, 306, 98.
36. Li, Z.; Hillmyer, M. A.; Lodge, T. P., *Macromolecules* **2004**, 37, 8933.
37. Li, Z.; Hillmyer, M. A.; Lodge, T. P., *Macromolecules* **2005**, 39, 765.
38. Fang, B.; Walther, A.; Wolf, A.; Xu, Y.; Yuan, J.; Müller, A. H. E., *Angew. Chem. Int. Ed.* **2009**, 48, 2877.
39. Walther, A.; Barner-Kowollik, C.; Müller, A. H. E., *Langmuir* **2010**, 26, 12237.
40. Dupont, J.; Liu, G., *Soft Matter* **2010**, 6, 3654.
41. Gröschel, A. H.; Walther, A.; Löbling, T. I.; Schmelz, J.; Hanisch, A.; Schmalz, H.; Müller, A. H. E., *J. Am. Chem. Soc.* **2012**, 134, 13850.
42. Gröschel, A. H.; Schacher, F. H.; Schmalz, H.; Borisov, O. V.; Zhulina, E. B.; Walther, A.; Müller, A. H. E., *Nat. Commun.* **2012**, 3, 710.
43. Aranda-Espinoza, H.; Bermudez, H.; Bates, F. S.; Discher, D. E., *Phys. Rev. Lett.* **2001**, 87, 208301.
44. Nonobe, T.; Tsuge, S.; Ohtani, H.; Kitayama, T.; Hatada, K., *Macromolecules* **1997**, 30, 4891.
45. Matsen, M. W.; Bates, F. S., *Macromolecules* **1996**, 29, 1091.
46. Matsen, M. W.; Bates, F. S., *J. Chem. Phys.* **1997**, 106, 2436.
47. Leibler, L., *Macromolecules* **1980**, 13, 1602.
48. Segalman, R. A., *Mater. Sci. Eng., R* **2005**, 48, 191.
49. Tschierske, C., *Annu. Rep. R. Soc. Chem. Sect. C. Phys. Chem.* **2001**, 97, 191.
50. Brinkmann, S., *PhD Thesis*, Mainz **1997**.
51. Breiner, U.; Krappe, U.; Stadler, R., *Macromol. Rapid Commun.* **1996**, 17, 567.
52. Breiner, U.; Krappe, U.; Thomas, E. L.; Stadler, R., *Macromolecules* **1998**, 31, 135.
53. Breiner, U.; Krappe, U.; Abetz, V.; Stadler, R., *Macromol. Chem. Phys.* **1997**, 198, 1051.
54. Yang, S.; Chen, J.-S.; Körner, H.; Breiner, T.; Ober, C. K.; Poliks, M. D., *Chem. Mater.* **1998**, 10, 1475.
55. Mannebach, G.; Bieringer, R.; Morschhäuser, R.; Stadler, R., *Makromol. Chem. Macromol. Symp.* **1998**, 132, 245.
56. Stadler, R.; Auschra, C.; Beckmann, J.; Krappe, U.; Voight-Martin, I.; Leibler, L., *Macromolecules* **1995**, 28, 3080.
57. Ishizu, K.; Fukutomi, T., *J. Polym. Sci., Part A: Polym. Chem.* **1989**, 27, 1259.
58. Ishizu, K.; Onen, A., *J. Polym. Sci., Part A: Polym. Chem.* **1989**, 27, 3721.
59. Erhardt, R.; Böker, A.; Zettl, H.; Kaya, H.; Pyckhout-Hintzen, W.; Krausch, G.; Abetz, V.; Müller, A. H. E., *Macromolecules* **2001**, 34, 1069.
60. Walther, A.; Göldel, A.; Müller, A. H. E., *Polymer* **2008**, 49, 3217.
61. Erhardt, R.; Zhang, M.; Böker, A.; Zettl, H.; Abetz, C.; Frederik, P.; Krausch, G.; Abetz, V.; Müller, A. H. E., *J. Am. Chem. Soc.* **2003**, 125, 3260.
62. Liu; Abetz, V.; Müller, A. H. E., *Macromolecules* **2003**, 36, 7894.
63. Walther, A.; Drechsler, M.; Rosenfeldt, S.; Harnau, L.; Ballauff, M.; Abetz, V.; Müller, A. H. E., *J. Am. Chem. Soc.* **2009**, 131, 4720.
64. Walther, A.; André, X.; Drechsler, M.; Abetz, V.; Müller, A. H. E., *J. Am. Chem. Soc.* **2007**, 129, 6187.
65. Walther, A.; Drechsler, M.; Müller, A. H. E., *Soft Matter* **2009**, 5, 385.

66. Wolf, A.; Walther, A.; Müller, A. H. E., *Macromolecules* **2011**, 44, 9221.
67. Cho, I.; Lee, K.-W., *J. Appl. Polym. Sci.* **1985**, 30, 1903.
68. Casagrande, C.; Fabre, P.; Raphaël, E.; Veyssié, M., *EPL* **1989**, 9, 251.
69. Ondarçuhu, T.; Fabre, P.; Raphaël, E.; Veyssié, M., *J. Phys. France* **1990**, 51, 1527.
70. Love, J. C.; Gates, B. D.; Wolfe, D. B.; Paul, K. E.; Whitesides, G. M., *Nano Lett.* **2002**, 2, 891.
71. Lattuada, M.; Hatton, T. A., *J. Am. Chem. Soc.* **2007**, 129, 12878.
72. Pradhan, S.; Xu, L.; Chen, S., *Adv. Funct. Mater.* **2007**, 17, 2385.
73. Gu, H.; Yang, Z.; Gao, J.; Chang, C. K.; Xu, B., *J. Am. Chem. Soc.* **2004**, 127, 34.
74. Suzuki, D.; Tsuji, S.; Kawaguchi, H., *J. Am. Chem. Soc.* **2007**, 129, 8088.
75. Li, D.; He, Y.; Wang, S., *J. Phys. Chem. C* **2009**, 113, 12927.
76. Liu, B.; Wei, W.; Qu, X.; Yang, Z., *Angew. Chem. Int. Ed.* **2008**, 47, 3973.
77. Zhang, J.; Jin, J.; Zhao, H., *Langmuir* **2009**, 25, 6431.
78. He, Y.; Li, K., *J. Colloid Interface Sci.* **2007**, 306, 296.
79. Zhang, J.; Wang, X.; Wu, D.; Liu, L.; Zhao, H., *Chem. Mater.* **2009**, 21, 4012.
80. Hong, L.; Jiang, S.; Granick, S., *Langmuir* **2006**, 22, 9495.
81. Jiang, S.; Granick, S., *J. Chem. Phys.* **2007**, 127, 161102.
82. Jiang, S.; Granick, S., *Langmuir* **2008**, 24, 2438.
83. Jiang, S.; Schultz, M. J.; Chen, Q.; Moore, J. S.; Granick, S., *Langmuir* **2008**, 24, 10073.
84. Jiang, S.; Chen, Q.; Tripathy, M.; Luijten, E.; Schweizer, K. S.; Granick, S., *Adv. Mater.* **2010**, 22, 1060.
85. Berger, S.; Synytska, A.; Ionov, L.; Eichhorn, K.-J.; Stamm, M., *Macromolecules* **2008**, 41, 9669.
86. Pardhy, N. P.; Budhlall, B. M., *Langmuir* **2010**, 26, 13130.
87. Perro, A.; Meunier, F.; Schmitt, V.; Ravaine, S., *Colloids Surf., A* **2009**, 332, 57.
88. Liu, B.; Zhang, C.; Liu, J.; Qu, X.; Yang, Z., *Chem. Commun.* **2009**, 3871.
89. Kim, S.-H.; Yi, G.-R.; Kim, K. H.; Yang, S.-M., *Langmuir* **2008**, 24, 2365.
90. Kim, S.-H.; Lee, S. Y.; Yang, S.-M., *Angew. Chem. Int. Ed.* **2010**, 49, 2535.
91. Nie, L.; Liu, S.; Shen, W.; Chen, D.; Jiang, M., *Angew. Chem. Int. Ed.* **2007**, 46, 6321.
92. Wang, B.; Li, B.; Zhao, B.; Li, C. Y., *J. Am. Chem. Soc.* **2008**, 130, 11594.
93. Paunov, V. N., *Langmuir* **2003**, 19, 7970.
94. Tiarks, F.; Landfester, K.; Antonietti, M., *Langmuir* **2001**, 17, 5775.
95. Cauvin, S.; Colver, P. J.; Bon, S. A. F., *Macromolecules* **2005**, 38, 7887.
96. Colver, P. J.; Chen, T.; Bon, S. A. F., *Makromol. Chem. Macromol. Symp.* **2006**, 245-246, 34.
97. Chen, T.; Colver, P. J.; Bon, S. A. F., *Adv. Mater.* **2007**, 19, 2286.
98. Colver, P. J.; Colard, C. A. L.; Bon, S. A. F., *J. Am. Chem. Soc.* **2008**, 130, 16850.
99. Fortuna, S.; Colard, C. A. L.; Troisi, A.; Bon, S. A. F., *Langmuir* **2009**, 25, 12399.
100. Colard, C. A. L.; Teixeira, R. F. A.; Bon, S. A. F., *Langmuir* **2010**, 26, 7915.
101. Teixeira, R. F. A.; McKenzie, H. S.; Boyd, A. A.; Bon, S. A. F., *Macromolecules* **2011**, 44, 7415.
102. Nisisako, T.; Torii, T.; Takahashi, T.; Takizawa, Y., *Adv. Mater.* **2006**, 18, 1152.
103. Behrend, C. J.; Anker, J. N.; Kopelman, R., *Appl. Phys. Lett.* **2004**, 84, 154.

104. Behrend, C. J.; Anker, J. N.; McNaughton, B. H.; Brasuel, M.; Philbert, M. A.; Kopelman, R., *J. Phys. Chem. B* **2004**, 108, 10408.

105. Anker, J.; Behrend, C.; Huang, H.; Kopelman, R., *Proceedings of the Fifth International Conference on Scientific and Clinical Apllications of Magnetic Carriers* **2005**, 293, 655.

106. Behrend, C. J.; Anker, J. N.; McNaughton, B. H.; Kopelman, R., *J. Magn. Magn. Mater.* **2005**, 293, 663.

107. Yoshida, M.; Roh, K.-H.; Lahann, J., *Biomaterials* **2007**, 28, 2446.

108. Yoshida, M.; Roh, K.-H.; Mandal, S.; Bhaskar, S.; Lim, D.; Nandivada, H.; Deng, X.; Lahann, J., *Adv. Mater.* **2009**, 21, 4920.

109. Bhaskar, S.; Gibson, C. T.; Yoshida, M.; Nandivada, H.; Deng, X.; Voelcker, N. H.; Lahann, J., *Small* **2011**, 7, 812.

110. Bucaro, M. A.; Kolodner, P. R.; Taylor, J. A.; Sidorenko, A.; Aizenberg, J.; Krupenkin, T. N., *Langmuir* **2008**, 25, 3876.

111. Synytska, A.; Khanum, R.; Ionov, L.; Cherif, C.; Bellmann, C., *Appl. Mater. Interfaces* **2011**, 3, 1216.

112. Valadares, L. F.; Tao, Y.-G.; Zacharia, N. S.; Kitaev, V.; Galembeck, F.; Kapral, R.; Ozin, G. A., *Small* **2010**, 6, 565.

113. Isojima, T.; Lattuada, M.; Vander Sande, J. B.; Hatton, T. A., *ACS Nano* **2008**, 2, 1799.

114. Pickering, S. U., *J. Chem. Soc. Trans.* **1907**, 91, 2001.

115. Ramsden, W., *Proc. R. Soc. London* **1903**, 72, 156.

116. Pieranski, P., *Phys. Rev. Lett.* **1980**, 45, 569.

117. Popp, N.; Kutuzov, S.; Böker, A.; Müller, A. H. E.; Schmidt, H.-W., In: *Complex Macromolecular Systems II*, Springer Berlin / Heidelberg: 2010; Vol. 228, p 39.

118. Niu, Z.; He, J.; Russell, T. P.; Wang, Q., *Angew. Chem. Int. Ed.* **2010**, 49, 10052.

119. Garbin, V.; Crocker, J. C.; Stebe, K. J., *J. Colloid Interface Sci.* **2012**, 387, 1.

120. Lewandowski, E. P.; Bernate, J. A.; Searson, P. C.; Stebe, K. J., *Langmuir* **2008**, 24, 9302.

121. Lewandowski, E. P.; Bernate, J. A.; Tseng, A.; Searson, P. C.; Stebe, K. J., *Soft Matter* **2009**, 5, 886.

122. Lewandowski, E. P.; Cavallaro, M.; Botto, L.; Bernate, J. C.; Garbin, V.; Stebe, K. J., *Langmuir* **2010**, 26, 15142.

123. Lin, Y.; Skaff, H.; Emrick, T.; Dinsmore, A. D.; Russell, T. P., *Science* **2003**, 299, 226.

124. Binks, B. P.; Fletcher, P. D. I., *Langmuir* **2001**, 17, 4708.

125. Nonomura, Y.; Komura, S.; Tsujii, K., *Langmuir* **2004**, 20, 11821.

126. Hirose, Y.; Komura, S.; Nonomura, Y., *J. Chem. Phys.* **2007**, 127, 054707.

127. Glaser, N.; Adams, D. J.; Böker, A.; Krausch, G., *Langmuir* **2006**, 22, 5227.

128. Zheng, Z.; Nottbohm, C. T.; Turchanin, A.; Muzik, H.; Beyer, A.; Heilemann, M.; Sauer, M.; Gölzhäuser, A., *Angew. Chem. Int. Ed.* **2010**, 49, 8493.

129. Walther, A.; Matussek, K.; Müller, A. H. E., *ACS Nano* **2008**, 2, 1167.

130. Walther, A.; Hoffmann, M.; Müller, A. H. E., *Angew. Chem. Int. Ed.* **2008**, 47, 711.

131. Park, B. J.; Lee, D., *ACS Nano* **2011**, 6, 782.

132. Park, B. J.; Brugarolas, T.; Lee, D., *Soft Matter* **2011**, 7, 6413.

133. Park, B. J.; Lee, D., *Soft Matter* **2012**, 8, 7690.

134. Yan, L.-T.; Popp, N.; Ghosh, S.-K.; Böker, A., *ACS Nano* **2010**, 4, 913.

Chapter 2 - Overview of the Thesis

This thesis consists of seven chapters, including five publications, which are presented in Chapters 3 to 7.

The design of Janus structures either of polymeric or hybrid nature with control of size, shape and functionality together with their self-assembly behavior at liquid-liquid interfaces is the common theme that connects the thesis. The research efforts were focused on (i) the general understanding of the self-assembly behavior of polymeric Janus particles at liquid-liquid interfaces and particularly, on the influence of their size and architecture on the adsorption kinetics. Further, research has been conducted on (ii) the combination of the properties of inorganic nanoparticles with the stimuli-responsive behavior of polymers in hybrid nano-sized inorganic/inorganic/organic core-shell-corona particles and (iii) the development and characterization of reliable experimental procedure in the synthesis of inorganic/inorganic/organic core-shell-corona hybrid Janus particles based on the knowledge obtained in the work with polymeric Janus structures and core-shell-corona particles.

For an efficient industrial use of Janus particles the understanding of the effect of Janus particles at fluid interfaces is very important. In the course of this work, we describe adsorption studies of moderately amphiphilic Janus cylinders made from a polystyrene-*block*-polybutadiene-*block*-poly(methyl methacrylate) triblock terpolymer at liquid-liquid interfaces. We deduce the effect of Janus cylinder length and the adsorption time from the structures formed at the interface and characterize the time-dependent evolution of the interfacial tension (**Chapter 3**). Until now, the importance of controlling the architecture of the particles is not well understood and therefore, motivated from the results obtained in chapter 3, systematic studies and simulations on the influence of spherical, cylindrical and disc-like Janus particles on adsorption process, adsorptions dynamics and the structures formed at the interface were performed (**Chapter 4**).

To increase the toolbox of Janus particles and to create Janus particles with even higher functionality, reliable experimental procedures to synthesize high-quality nano-sized Janus particles were developed. At first, an easy and completely reproducible preparation

and characterization of the solution behavior and functional properties of superparamagnetic and/or fluorescent, thermo-responsive inorganic/organic hybrid nanogels with an intermediate protective silica shell and a smart and interactive polymer layer is shown. These well-defined multifunctional nanogels were prepared *via* two consecutive encapsulation processes of superparamagnetic Fe_2O_3 nanoparticles (NPs) and/or fluorescent CdSe(ZnS) semiconductor nanocrystals with a silica layer and a crosslinked poly(*N*-isopropylacrylamide) (PNIPAAm) polymer corona (**Chapter 5**). Furthermore, the Fe_2O_3/SiO_2 core-shell nanoparticles were used as carrier systems for olefin dimerization catalysts for facile product separation in the catalytic conversion of olefins **(Chapter 6)**.

Finally, benefiting from the knowledge of the previous projects an efficient and simple strategy for the synthesis of well-defined hybrid Janus nanoparticles with a SiO_2 core and a stimuli-responsive PDMAEMA hemicorona was developed. This stategy takes advantage of a modified Pickering emulsion technique combined with a surface initiated "grafting from" atom transfer radical polymerization (ATRP) process (**Chapter 7**).

In the following, a summary of the key results obtained within this thesis is presented. A complete coverage of the experimental results and conclusions is presented in the respective chapters.

2.1 Janus Cylinders at Liquid-Liquid Interfaces

Colloidal objects in the range from nanometer to micrometer are one of the main building blocks for modern materials. Therefore, Janus structures have been the subject of intensive research due to their special architecture. The lack of centrosymmetry in Janus systems has led to the discovery of new properties as well as very interesting aggregation behavior into superstructures.[1,2] Until now, simulations and calculations demonstrated that the adsorption energy of Janus particles can be higher compared to classic surfactants by several orders of magnitude. As a consequence, a considerable increase in surface activity is expected. These predictions render Janus structures as an extremely interesting new class of future surfactants.[1,3]

In this chapter, adsorption studies of moderately amphiphilic Janus cylinders at liquid-liquid interfaces are presented. The focus was laid on the effect of the Janus cylinder length and the adsorption times on the resulting structures at the interface. This was characterized *via* TEM and time-dependent evolution measurements of the interfacial tension.

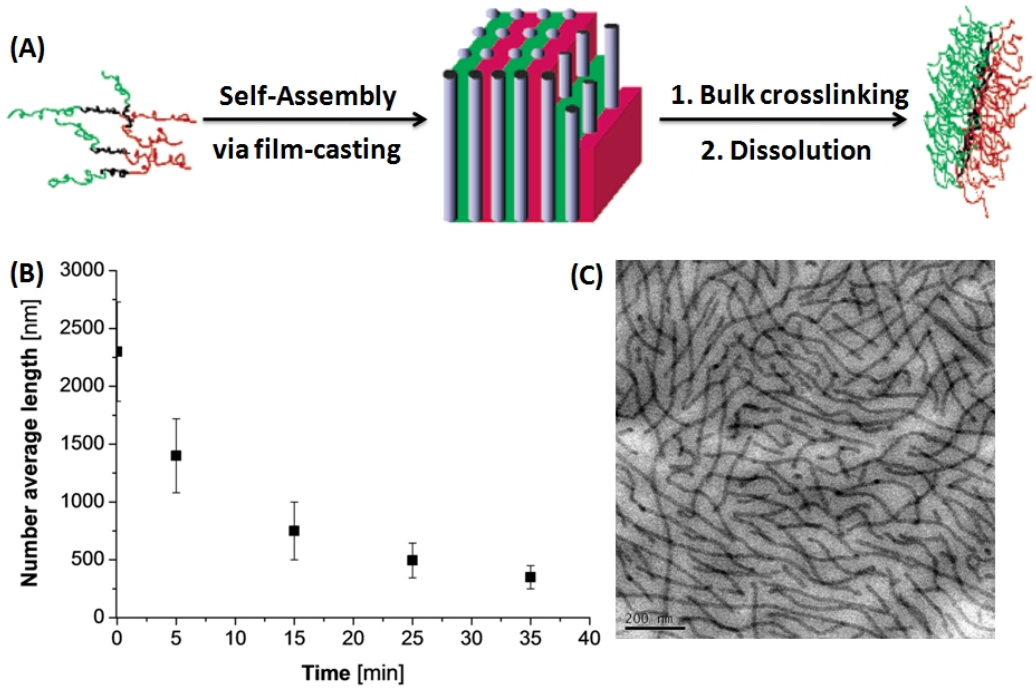

Figure 2-1. (A) Schematic synthesis of Janus cylinders. (B) Time dependence of the number-average length for different sonication times at 30% amplitude. Error bars represent the standard deviations of the length distribution. (C) Cryo-TEM image of Janus cylinder dispersion in THF with a number-average length of 2300 nm.

The synthetic pathway to obtain cylindrical Janus structures was based on a template-assisted synthesis, involving crosslinking of a microphase-segregated lamellar-cylinder morphology of a bulk film of a polystyrene-*b*-polybutadiene-*b*-poly(methyl methacrylate) ($S_{41}B_{14}M_{45}^{110}$), followed by sonication (Figure 2-1 A). This process resulted in the formation of core-crosslinked cylinders, possessing a PB core and two hemicylinders of PS and PMMA (Figure 2-1 C). It was possible to adjust the cylinder length *via* variation of the sonication time. A detailed look at the evolution of cylinder length with sonication time showed a rapid decay with increasing sonication time (Figure 2-1 B). Here, the length of the cylinders followed a non linear decay from 2300 nm to 350 nm with increasing sonication times from 0 to 35 minutes.

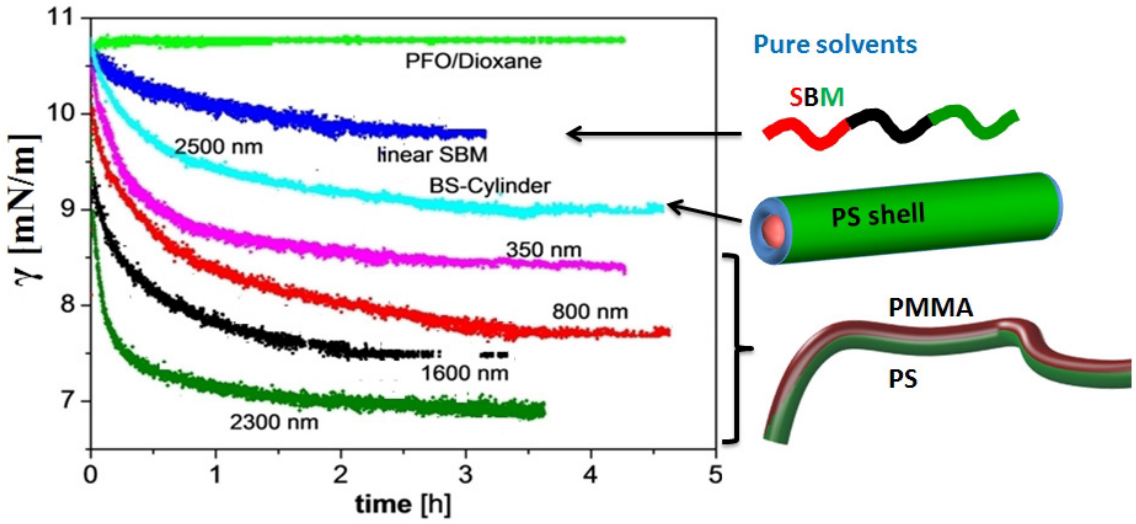

Figure 2-2. Influence of the Janus cylinder length on the interfacial tension. Interfacial tension isotherms of solutions of Janus cylinders in dioxane at the PFO/dioxane interface (c = 1 g/L). Interfacial tension isotherms for uncrosslinked SBM and homogeneous BS core-shell cylinders are included.

An elegant way for the determination of the influence of particles at liquid-liquid interfaces is to analyze the interfacial tension of a dispersion of the desired material *via* the pendant-drop method. From the time dependent measurements of the interfacial tension, it was possible to specify the characteristics of different stages of the adsorption process.

In Figure 2-2 the adsorption behavior of Janus cylinders with different lengths, uncrosslinked SBM and polystyrene-*b*-polybutadiene (BS) core-shell cylinders at a perfluorooctane (PFO)/dioxane interface was investigated. Due to their slightly amphiphilic character, the Janus cylinders demonstrated a significantly enhanced surface activity compared to cylindrical particles with a homogeneous PS corona (made from the diblock copolymer SB (polystyrene-*b*-polybutadiene)) or the block terpolymer precursor SBM. Therefore,

these particles are ideal systems for a new class of superior surfactant. A series of pendant drop tensiometer measurements for cylinders with number-average lengths of 2300 nm to 350 nm, dissolved in dioxane at a concentration of 1 g/L, is shown in Figure 2-3. The interfacial tension decreased with time and approached quasi-equilibrium after 3 h. At the beginning of the adsorption process, the interfacial tension decreased fast. Subsequently, the decrease slowed down, and finally, it approached a plateau, where the maximum coverage of the interface with cylinders was obtained. After reaching the plateau value, the Janus cylinders were located and arranged at the interface. An increase of the average length of the Janus cylinders led to an enhanced adsorption at the interface and the plateau value was reached earlier. The interfacial tension decreased with increasing Janus cylinder length and concentration.

For a better understanding of the structures formed at the interface and the adsorption mechanism, the absorption of 2300 nm Janus cylinder was investigated using pendant drop tensiometry (Figure 2-3). Simultaneously, TEM images of the particle assemblies at the interface were taken at the adsorption times indicated in the interfacial tension isotherms. In combination with the logarithmic representation of the interfacial tension (Figure 2-3 inset), the three different adsorption stages can be identified. At first, free diffusion to the interface occurred (I), followed by continuous adsorption of cylinders including an ordering and domain formation at the interface (II). Finally, additional packing led to a rearrangement of the domains and to the formation of a multilayer system (III). The cylinders showed a liquid crystalline like short-range correlation at the fluid interfaces.

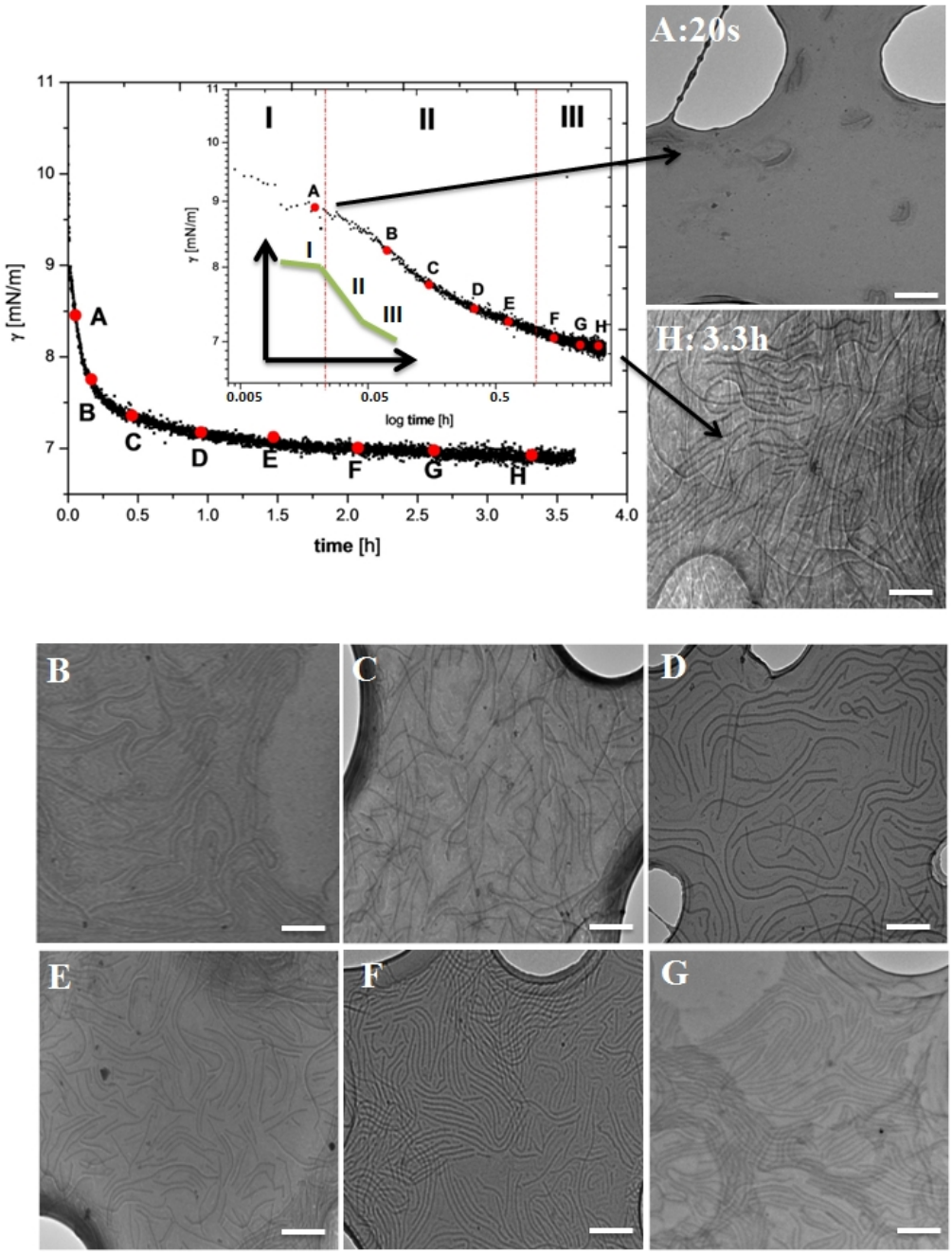

Figure 2-3. Left top: Adsorption curves in linear and logarithmic presentation. The red points **A-H** indicate: Series of TEM images (obtained from lacey grids) of 2300 nm Janus cylinders (1 g/L) adsorbing at the PFO/dioxane interface at different times as noted in the interfacial isotherms. (scale bars: 1 µm).

As a further result it was found that the adsorption behavior is independent of the solvent combination. This was confirmed by two different systems, PFO/Dioxane and PFO/DMSO, and the obtained relative change in interfacial tension showed similar characteristics. Hence, these results showed the high potential of Janus particles as a new class of superior surfactants and as a novel tool for the nanostructuring of interfaces.

2.2 Influence of Janus Particle Shape on their Interfacial Behavior at Liquid-Liquid Interfaces

Due to their non-centrosymmetric architecture Janus particles combine amphiphilicity similar to surfactants with the Pickering character that strongly holds solid particles at interfaces.[1] These combined properties are not accessible for their homogeneous analogues. Their superior affinity toward interfaces and their significantly enhanced reduction of interfacial tension as compared to particles with an isotopic chemical structure was already shown in the chapter before.[4,5,6] A very important point and main challenge is now to understand the effect of the Janus particle size and architecture on the adsorption behavior. This includes the characterization of the adsorption with respect to adsorption dynamics as well as on the particle orientation and particle self-assembly at the interface and in the end on the structures formed at the liquid-liquid interface.

The work in this chapter extends the results of the previous chapter and was focused on systematic study of the influence of the geometry of spherical, cylindrical and disc-like Janus particles on their surface activity and their orientation at a fluid-fluid interface.

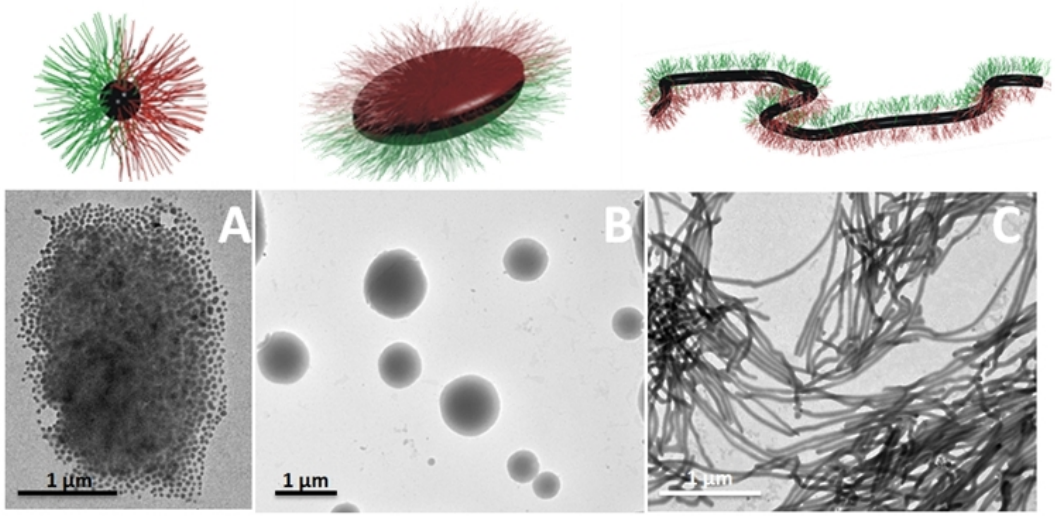

Figure 2-4. Representative TEM images of (A) Janus spheres, (B) Janus discs and (C) Janus cylinders with corresponding schemes of the particle architecture.

Three Janus particles with different architectures were used in pendant-drop tensiometer measurements to determine the influence of shape on the interfacial assembly process: Janus spheres, Janus cylinders and Janus discs. All these structures were made from SBM triblock terpolymers (Figure 2-4). The Janus spheres are monodisperse in size and shape

with a diameter of ca. 50 nm. A polydisperse length distribution was found for the Janus cylinders with the main peak at 2300 nm. The Janus discs show a bimodal size distribution with a fraction of relatively large discs (ca. 350 nm in diameter) and a fraction of smaller ones with a diameter of around 250 nm.

For all experiments the liquid-liquid interface of toluene and water was chosen as the basic system since it fulfills all criteria needed for a successful measurement of the changes in the interfacial tension for all three polymeric Janus structures (γ_0 = 34 mN/m). We first studied time-dependent measurements at the toluene/water interface for the Janus particles dissolved in toluene at a concentration of 1 g/L.

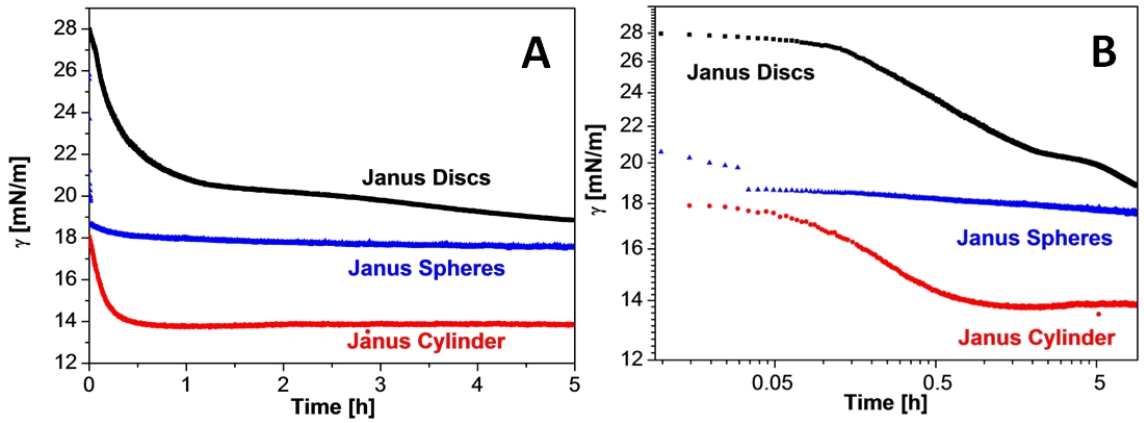

Figure 2-5. Influence of the Janus particle shape on the interfacial tension. (A) Interfacial tension isotherms of solutions of Janus particles in toluene (c = 1g/L) at a water/toluene interface. (B) Double-logarithmic representation of the data in (A).

Figure 2-5 presents plots of the dynamic surface tension in linear and double-logarithmic fashion. The interfacial tension decreased with time, approaching a quasi-equilibrium value. At a short time scale, the interfacial tension for all particles dropped rapidly because of instantaneous self-assembly of the particles at the interface, then the decrease in interfacial tension slowed down and once the droplet was mostly covered, the decrease in interfacial tension reached a quasi-equilibrium. It can be seen that the equilibrium γ_∞-value decreased significantly from discs to cylinders. So, a change in the architecture led to different adsorption dynamics at the interface. Here, the addition of Janus cylinders resulted in the maximum reduction in the equilibrium interfacial tension, while Janus spheres showed a moderately lower surface activity with an intermediate γ_∞-value and Janus discs provided the smallest amount of effective interfacial tension reduction. In the

case of Janus discs, in addition, we observed a more complex behavior since an additional plateau can be found due to additional repositioning processes.

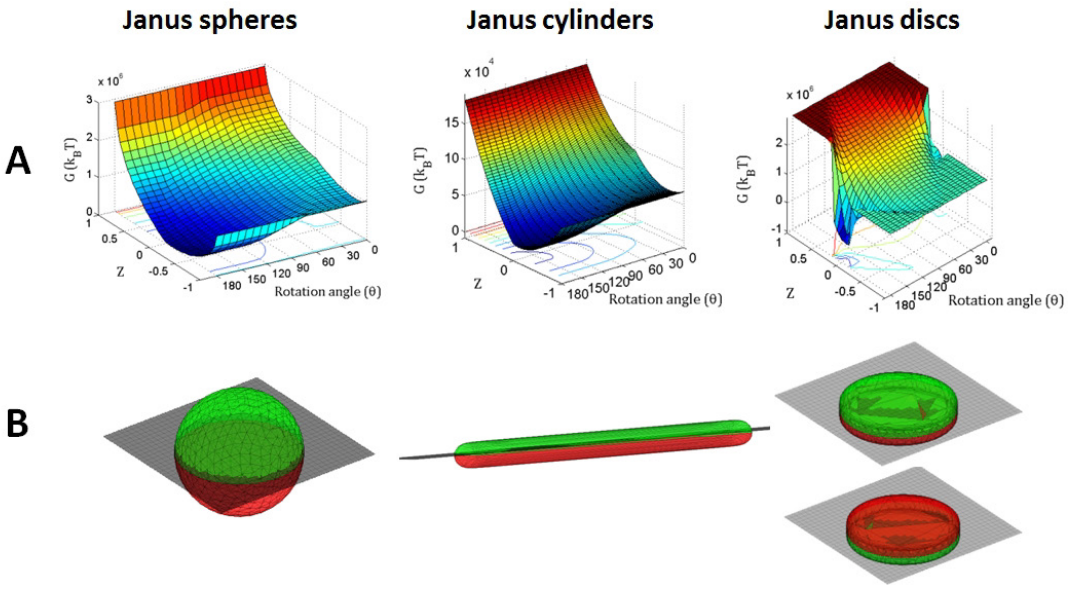

Figure 2-6. (A) Energy profiles for Janus spheres, Janus cylinders and Janus discs at toluene/water interface. **(B)** Shape dependent equilibrium position of Janus particles at toluene (bottom phase) and water (top phase) interface. PS is labeled red and PMMA is labeled green.

To obtain a better understanding of the adsorption process, simulations on the Janus particle orientation on the toluene/water interface were performed (Figure 2-6). Based on the energy profiles it can be seen that Janus particle adsorption is effectively irreversible (Figure 2-6 A). The simulations resulted in a global interfacial tension, which is a function of the packing of the particles and the energy calculated here. In principle, large particles offer strong adsorption towards the interface, preventing its removal. Thus, particles with a large cross-sectional area can be strongly adsorbed to the interface and so different energy barriers resulted for Janus spheres (5×10^4 kT), Janus cylinders (1×10^6 kT) and Janus discs (1.5×10^6 kT or 5×10^5 kT). Based on the calculated data, a favored orientation of polystyrene (PS) to the toluene phase and the poly(methyl methacrylate) (PMMA) side chains to the water phase for the Janus spheres and cylinders was found (Figure 2-6 B). Further, Janus discs seem to be a special case since two different energy minima can be found where both orientations of the discs are possible. The energy barrier for removal from the global minimum is ~1.5×10^6 kT whereas the energy barrier for removal of the second local energy minimum is 5×10^5 kT.

One reason for the different adsorption kinetics is the size of the Janus particles. Smaller sizes lead to higher diffusion coefficients and faster adsorption kinetics. A faster diffusion may also contribute to lower values of the quasi-equilibrium state as the further minimization in this stage is collision-controlled in contrast to diffusion control in the early stages. Nevertheless, the simulations pointed toward a complicated interplay between size and architecture. Now, based on the experimental data and these simulation results, it was possible to describe the fundamental aspects of Janus particle adsorption and kinetics at liquid-liquid interfaces (Figure 2-7). All in all, changes in the geometry directly influence the adsorption process, the interfacial behavior and lead to different structures formed at the interface during the different stages of the adsorption process.

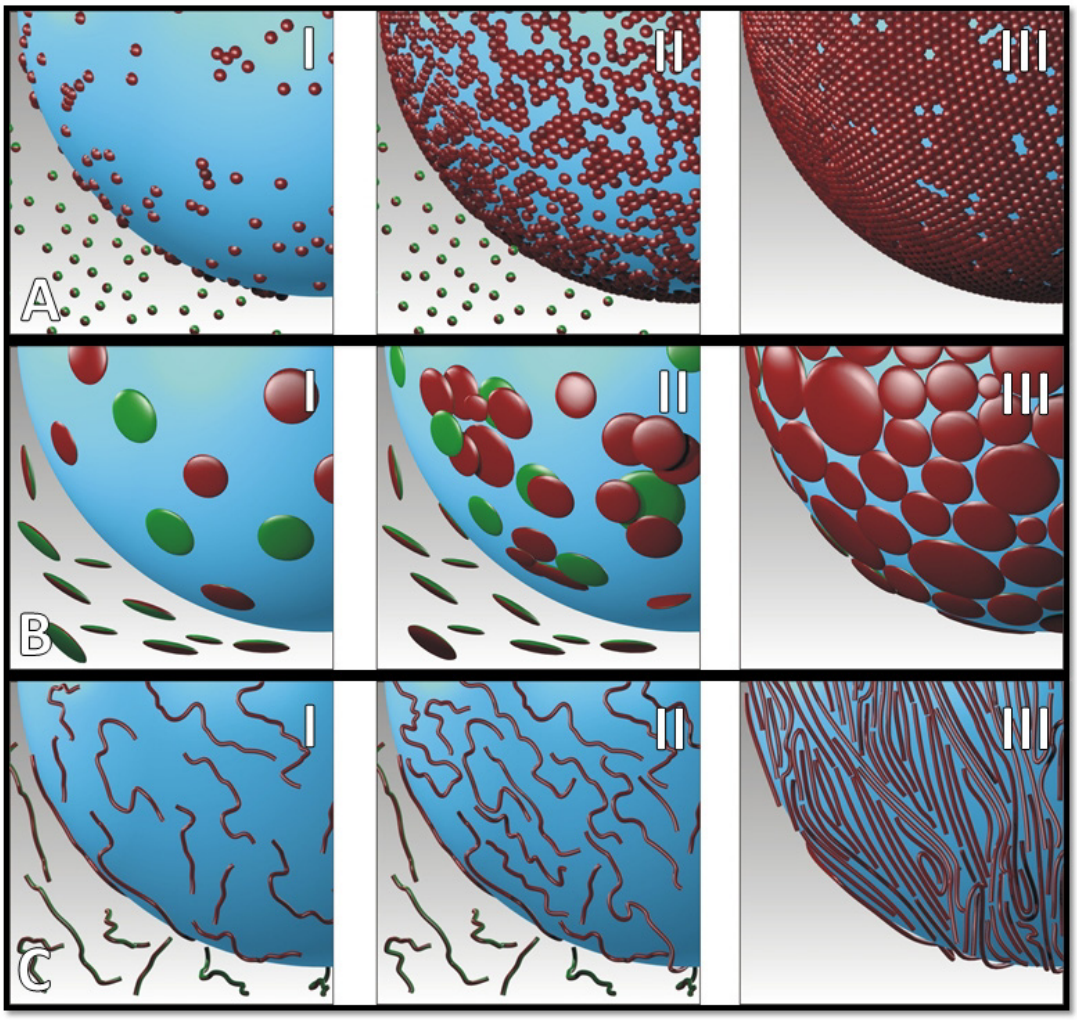

Figure 2-7. Schematic representation of the packing behavior of the Janus particles at the toluene/water interface during the adsorption process. The most typical adsorption stages pointed out for (A) Janus spheres, (B) Janus discs and (C) Janus cylinders. The Janus particles are simplified for a better illustration of their position at the liquid-liquid interface.

In conclusion, differences in the reduction of the interfacial tension can be attributed to enhanced adsorption of Janus particles at the oil-water interface under the strong influence of different architectures. Variation in shape directly influences the adsorption kinetics, the packing behavior and the energy barriers. Thus, the results provide important guidance to design Janus particles with special geometry and surface properties suitable for a lot of possible applications.

2.3 Superparamagnetic and fluorescent thermo-responsive Core–Shell–Corona hybrid Nanogels with a protective Silica Shell

Colloidal hybrid nanostructures can be used as components for multifunctional materials in future technologies, in which the most interesting functionalities of different material classes are combined in a single entity.[7,8]

Particular attention was paid to the combination of the properties of inorganic NPs with stimuli-responsive polymers in hybrid inorganic/inorganic/organic core-shell-corona particles. So, an easy and completely reproducible strategy for the preparation and characterization of the solution behavior and functional properties of superparamagnetic and/or fluorescent, thermo-responsive inorganic/organic hybrid nanogels with a γ-Fe_2O_3/SiO_2, $CdSe(ZnS)/SiO_2$ and γ-$Fe_2O_3/CdSe(ZnS)/SiO_2$ intermediate core-shell structure and a thermosensitive poly(*N*-isopropylacrylamide) (PNIPAAm) corona was developed.

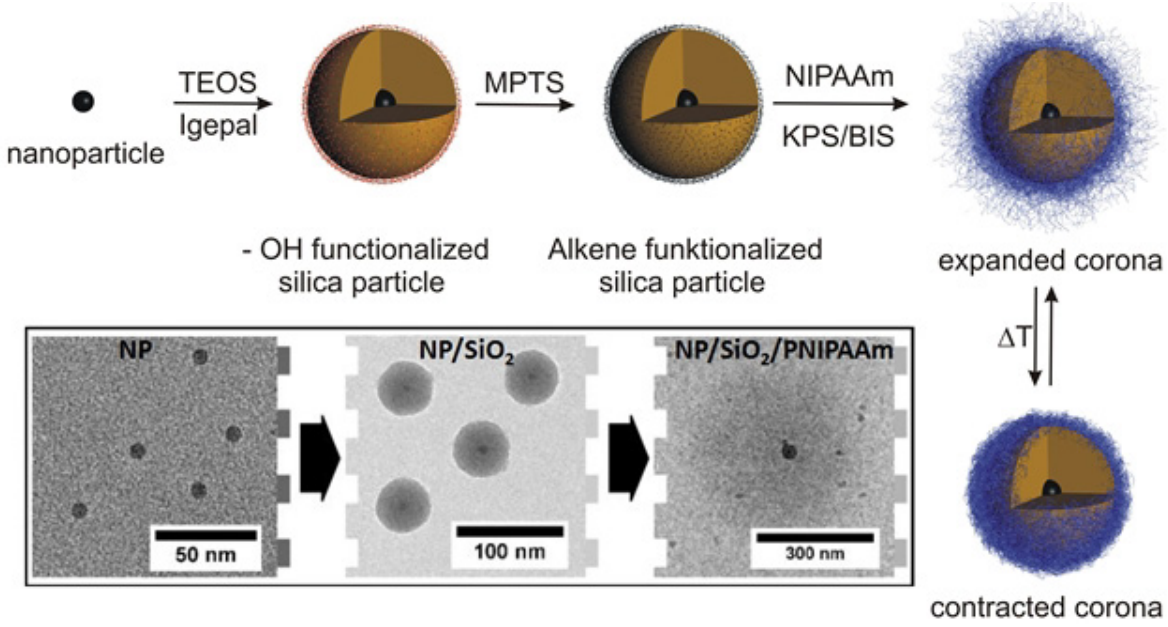

Figure 2-8. Schematic drawing of the synthesis of NP/SiO_2/PNIPAAm core-shell-corona hybrid nanogels and representative TEM images of CdSe(ZnS)-NPs, $CdSe(ZnS)/SiO_2$-NPs and $CdSe(ZnS)/SiO_2$/PNIPAAm nanogels.

These well-defined and nearly monodisperse multifunctional nanogels were prepared *via* two consecutive encapsulation processes of superparamagnetic and/or fluorescent semiconductor nanocrystals with a silica layer, further covered with a crosslinked and responsive polymer corona *via* a "grafting from/grafting onto" polymerization process. The syn-

thetic strategy towards monodisperse thermo-sensitive hybrid materials is schematically illustrated in Figure 2-8.

The main focus was to investigate the challenging experimental preparation conditions in detail and then, to transfer this encapsulation strategy to other hydrophobic nanoparticles and provide a platform technology for such core-shell-corona hybrids. With a precise adjustment of the conditions it was possible to achieve a reliable encapsulation and to either entrap several or single particles. The thickness of the SiO_2 shell can be controlled and the composition of the NPs within the silica particle can be manipulated according to the needs of a given application. The total diameter can be reliably varied between 20 nm to 60 nm for both types of NPs (CdSe(ZnS) and γ-Fe_2O_3) upon increasing the concentration of tetraethyl orthosilicate (TEOS) from 0.05 to 1 mmol (Figure 2-9). The intermediate silica shell was not only chosen as a synthetic intermediate and for an improvement of the biocompatibility, but also to impart the final nanocomposite particles with a beneficial barrier layer that also protects the nanocrystals against harmful chemicals degrading the functionality of the core nanocrystals.

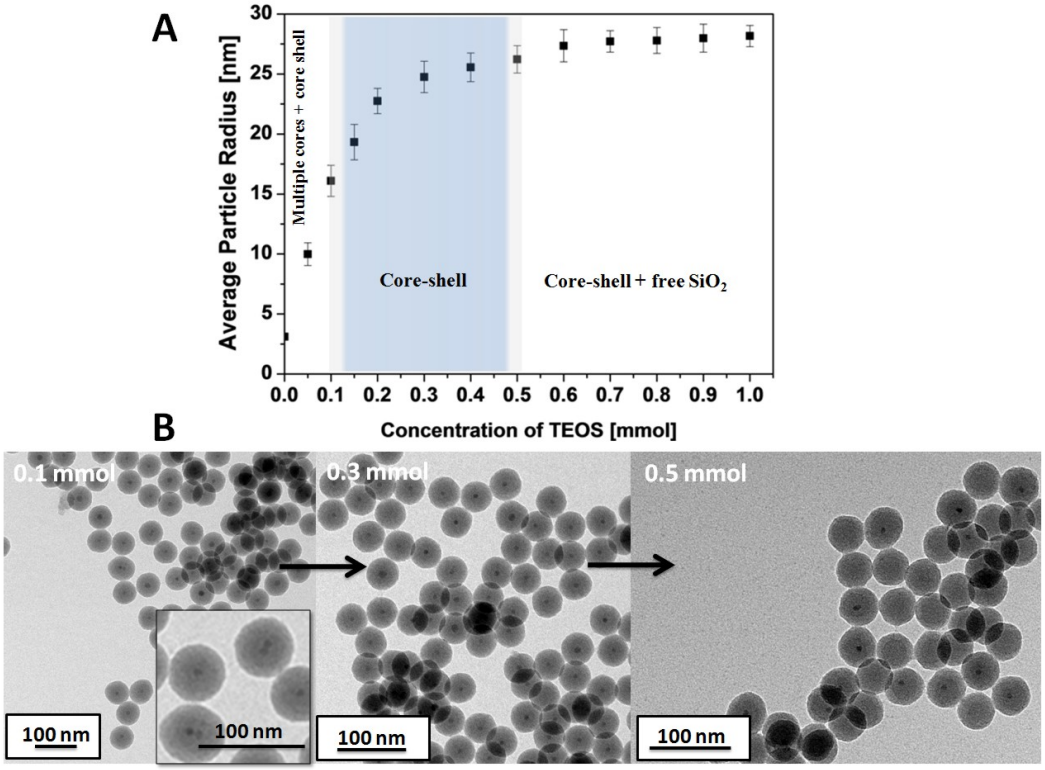

Figure 2-9. (A) Dependence of the particle radius and product homogeneity of CdSe(ZnS)/SiO_2 core-shell particles as a function of the TEOS concentration and constant NP concentration. (B) TEM images of CdSe(ZnS)/SiO_2 core shell particles prepared using different TEOS amounts.

The hydrodynamic radius distributions of all nanogels showed a consistent increase throughout the various steps and the obtained distribution functions were remarkably narrow pointing towards monodisperse and well-defined core-shell-corona particles (Figure 2-10).

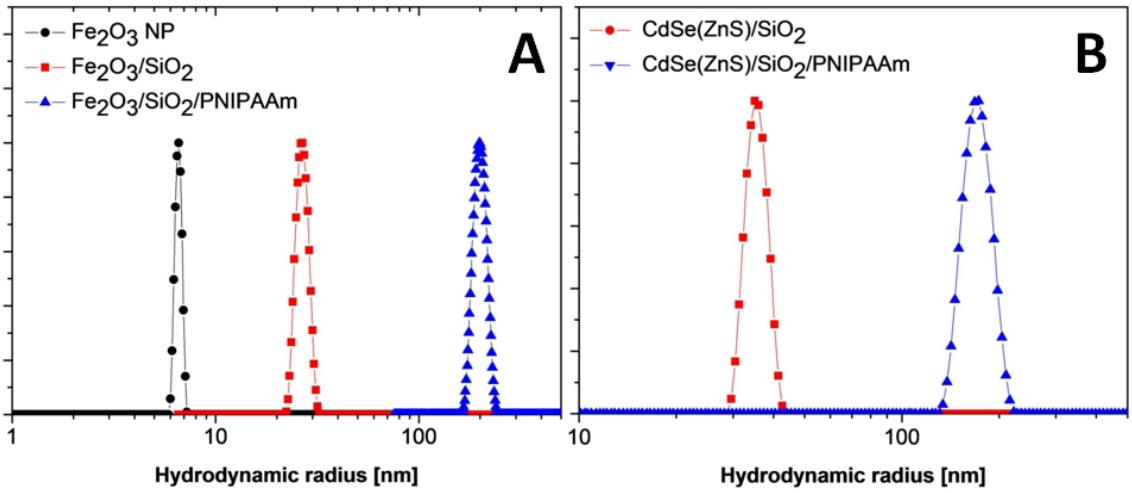

Figure 2-10. Intensity-weighted hydrodynamic radii distribution (DLS) of (A) γ-Fe_2O_3, γ-Fe_2O_3/SiO_2 and γ-Fe_2O_3/SiO_2/PNIPAAm and (B) CdSe(ZnS)/SiO_2 and CdSe(ZnS)/SiO_2/PNIPAAm hybrid nanoparticles at 10% cross-linking density and RT.

To confirm the structures of the materials, TEM and cryo-TEM measurements of the fluorescent CdSe(ZnS)/SiO_2/PNIPAAm hybrids were performed and are shown in Figure 2-11. All resulting hybrid core-shell-corona particle were very uniform in size and shape and exhibited a narrow size distribution (Figure 2-11 A). The radius of the core-shell-corona materials obtained *via* TEM was 110 ± 15 nm for both types of hybrid materials. This radius was lower than the dimensions determined by DLS, which measures the fully extended particle in solution, whereas the TEM values corresponded to sizes in dried state. Therefore, also cryo-TEM images were recorded. The micrographs of CdSe(ZnS)/SiO_2/PNIPAAm in Figure 2-11 B showed a fuzzy corona, highlighted by the encircled areas (Figure 2-11 B) and the greyscale analysis (Figure 2-11 C).

Nevertheless, the imaging data in combination with DLS data confirm the successful formation of the hybrid core-shell-corona nanogels and a successful immobilization of a PNIPAAm gel-like corona on the activated core-shell particles.

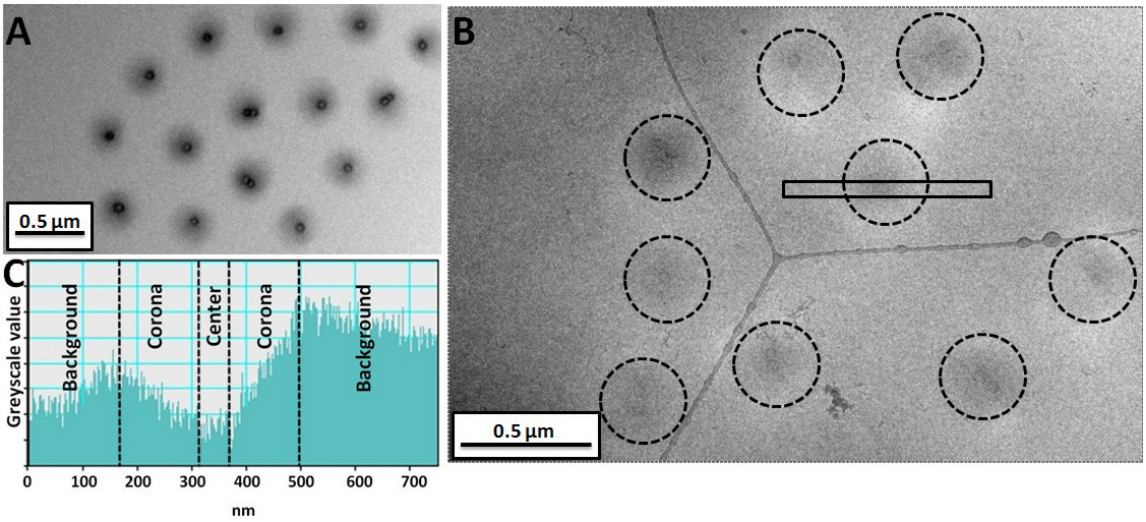

Figure 2-11. (A) TEM image and (B) cryo-TEM images of CdSe(ZnS)/SiO_2/PNIPAAm nanogels. (C) Greyscale analysis of the cross section indicated in micrograph B.

The hybrid core-shell-corona particles retained full functionality of the superparamagnetic and fluorescent core materials, which was investigated using a vibrating sample magnetometer and a fluorescence spectroscopy (Figure 2-12 A/B). Further, they combined it with the barrier properties and ease of chemical functionalization of the silica shell.

The thermo-responsive character was investigated by DLS (Figure 2-12 C). The samples exhibited a thermo-responsive volume phase-transition nearly at 33-34 °C, originating from the PNIPAAm corona around the core-shell particles. With an increase in temperature the dimensions of the hybrids decreased strongly and the shrinking and swelling process of the CdSe(ZnS)/SiO_2/PNIPAAm particles was fully reproducible as depicted in the inset of Figure 2-12 C. This behavior is comparable to spherical PNIPAAm micro/nanogels. But herein, the overall property profile was amplified by the presence of functional components inside the core.

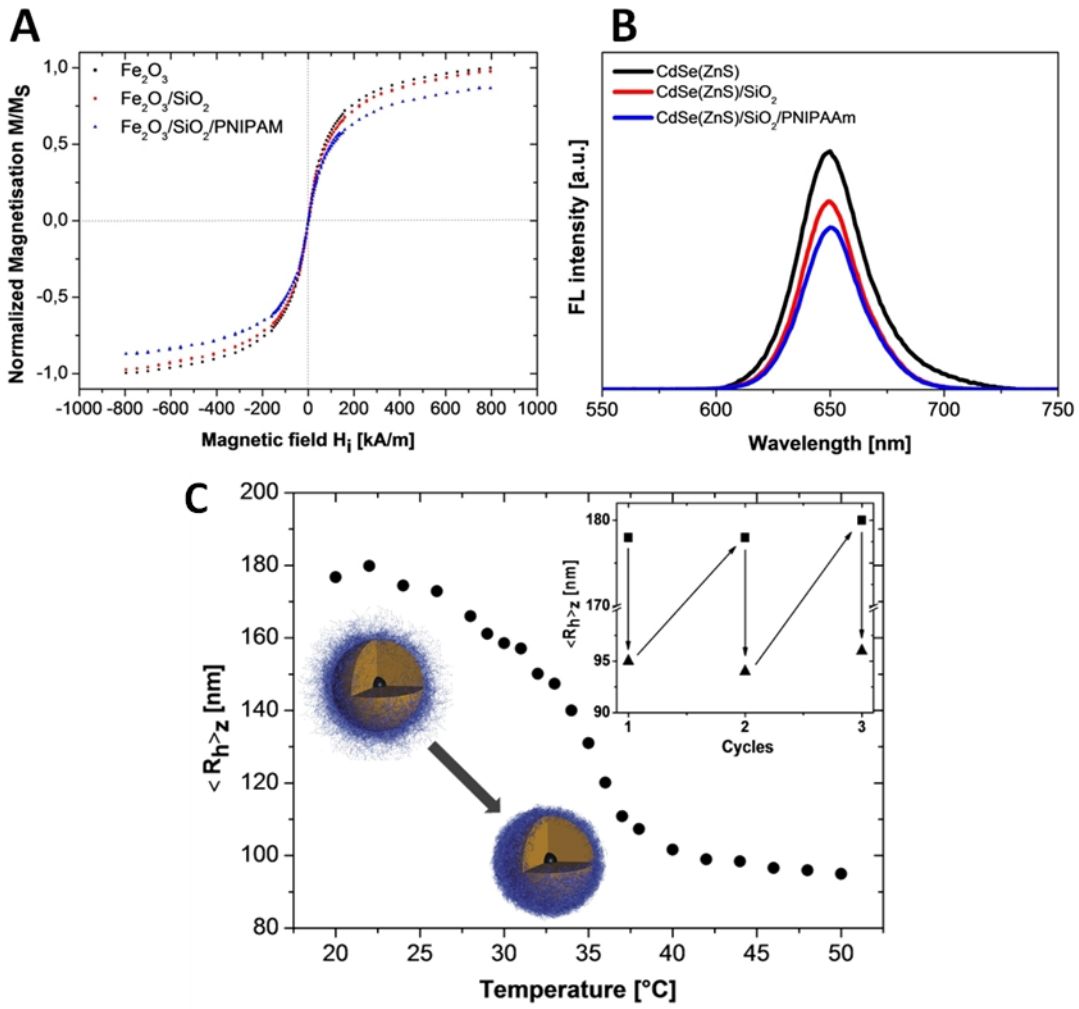

Figure 2-12. (A) Magnetic hysteresis curves of γ-Fe_2O_3 nanoparticles, γ-Fe_2O_3/SiO_2 core-shell particles and γ-Fe_2O_3/SiO_2/PNIPAAm hybrid material with a 10% crosslinking density at RT. (B) Fluorescence spectra for CdSe(ZnS), CdSe(ZnS)/SiO_2 and CdSe(ZnS)/SiO_2/PNIPAAm. (C) Dependence of the z-average hydrodynamic radius of CdSe(ZnS)/SiO_2/PNIPAAm nanogel particles upon temperature with a crosslinking density of 10%. The inset depicts the changes in the z-average hydrodynamic radius for various temperature cycles below and above the volume transition temperature, respectively.

The reported well-defined size-controlled core-shell particles have high potential as flexible carrier materials in a lot of applications and further, the multifunctional hybrid core-shell-corona nanogels could be applied to possible applications in cell and tissue imaging, delivery of acid-sensitive imaging probes and clinical diagnosis.

The aim of further studies is to use this new knowledge about the synthesis of core-shell-corona particles and their stimuli-responsive properties to create hybrid core-shell-corona Janus particles with two different polymers immobilized to the opposite sides of the core-shell particles on the basis of our particles.

2.4 Magnetic Core-Shell Nanoparticles as Carriers for Olefin Dimerization Catalysts

Nanotechnology is a multidisciplinary platform for target materials used in a wide field of applications. Magnetic hybrid core-shell-corona particles received a lot of attention in the field of catalysis because nanocatalysts with tunable size, shape and composition could be the answer for some current scientific and as well industrial problems such as the problematic separation of the catalysts and products and the re-use of the catalyst.

Herein, the main challenge was to combine the properties of the very well investigated magnetic core-shell nanoparticles (Fe_2O_3/SiO_2) with the catalytic character of certain complexes in hybrid core-shell-corona nanoparticles. The idea was to create a heterogeneous catalyst for a facile product separation for the catalytic conversion of olefins.

Following, the covalent connection of functionalized nickel complexes on magnetic core-shell hybrid particles γ-Fe_2O_3/SiO_2 is presented. Two completely different ways for the combination of the particle with these nickel complexes were carried out and from this perspective a series of catalysts for two ways of linkage with the core-shell support material was designed (Scheme 2-1).

Scheme 2-1. Nickel complexes used for the preparation of the heterogeneous nanocatalysts.

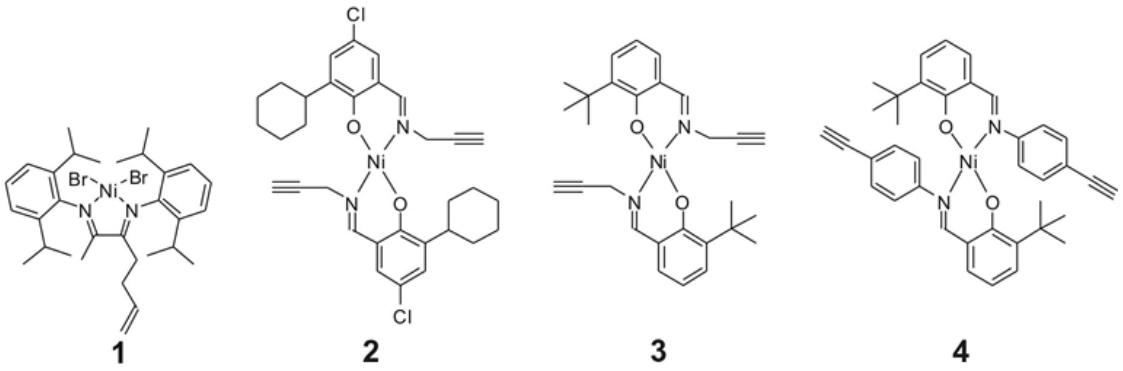

The first synthetic strategy (Scheme 2-2) involved a precursor consisting of an ω-alkenyl diimine moiety coordinated to nickel(II)bromide (Scheme 2-1 **1**) and a silane, which reacted with silica based core-shell particles. After the silane-ene reaction the complex combined with a triethoxysilane group was coupled directly to the support material (Scheme 2-2).

Scheme 2-2. Synthetic procedure 1: (A) Hydrosilylation reaction of the diimine nickel complex and triethoxysilane. (B) Route of heterogenization for complex **1**.

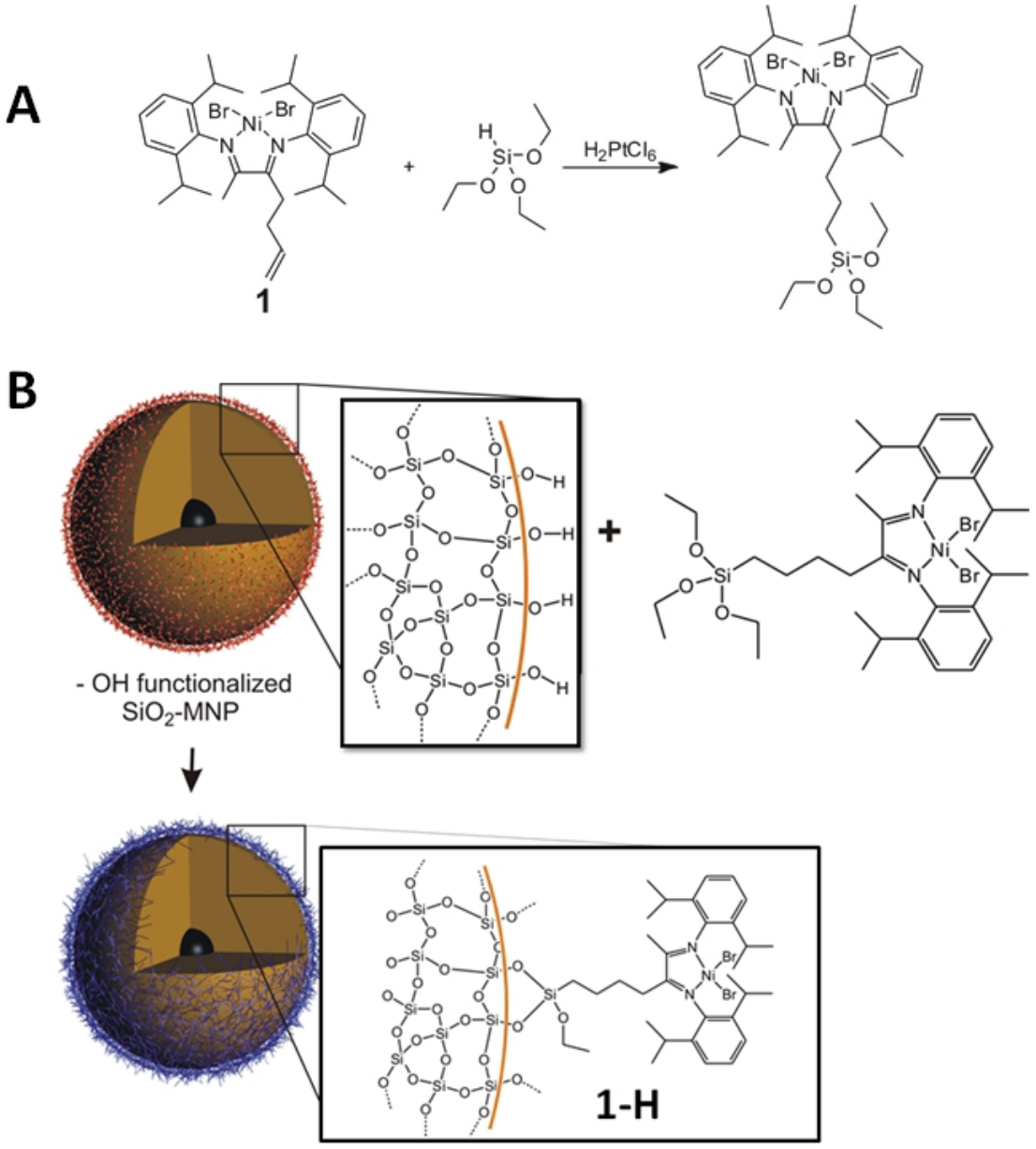

The new formed nanocatalysts showed a certain surface roughness compard to pristine γ-Fe_2O_3/SiO_2 nanoparticles. The surface of the particles with attached complexes was distinctly coarser than the blank γ-Fe_2O_3/SiO_2 nanoparticles (Figure 2-13 A). This indicated that a thin layer of supported catalyst covered the silica particles. Energy dispersive x-ray diffraction (EDX) was used to identify the chemical composition at the surface and of the particles (Figure 2-13 B). The EDX spectrum featured the typical peaks of the iron core and the silicon (shell) and oxygen (core and shell).These results were in good agreement with the proposed structure and the conclusion drawn from the TEM images.

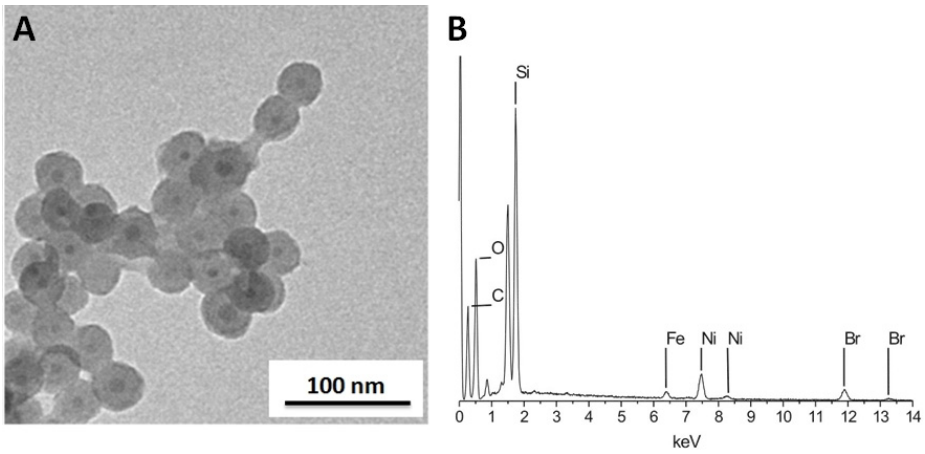

Figure 2-13. Representative TEM image of γ-Fe_2O_3/SiO_2/Complex 1 **(1-H)**. The surface is distinctly coarser compared to the blank particles. (B) EDX spectrum of the heterogeneous complex **1-H**.

In a second approach, the particles were attached to the complexes *via* click chemistry (Scheme 2-3). For this purpose the nickel complexes (Scheme 2-1 **2-4**) were substituted with an alkyne moiety. Here, the Huisgen 1,3-dipolar cycloaddition was used to bind azido-functionalized γ-Fe_2O_3/SiO_2 particles to the alkyne group of the complex. These particles were combined with azide functionalized propyl(triethoxy)silane *via* a condensation reaction.

Scheme 2-3. Synthetic procedure 2: Route of heterogenization for complexes **2-4**.

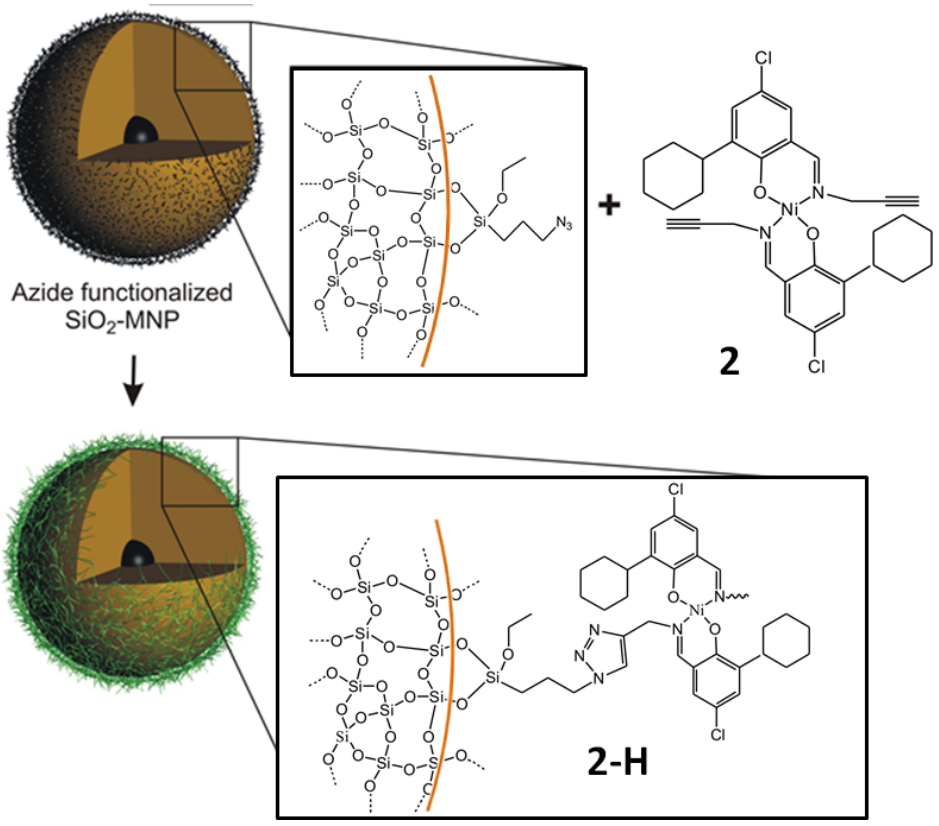

For the characterization of the modified core-shell particles TEM and FT-IR measurements were recorded (Figure 2-14). The surface of the heterogeneous core-shell-corona nanocatalysts is distinctly coarser than the pure γ-Fe_2O_3/SiO_2 particles. Characteristic peaks in FT-IR for the triazole group (1450 cm^{-1}) and for the C=N and C=C stretching bands (1620 cm^{-1} and 1730 cm^{-1}) confirmed a successful grafting of the nickel complex on the core-shell particles. All these aspects indicated that the heterogenization reaction was successful and the IR results are confirmed.

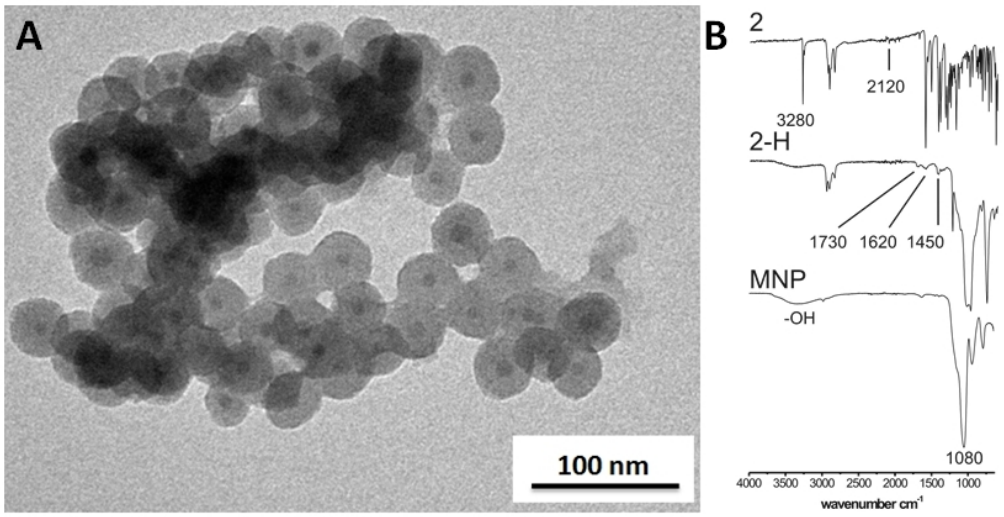

Figure 2-14. (A) TEM image of γ-Fe_2O_3/SiO_2/Complex 2 (**2-H**). The surface is distinctly coarser compared to the blank particles. (B) FT-IR spectrum of the pure nanoparticles, the supported complex (2-H), and the corresponding pure complex (2).

The catalytic performance of the heterogeneous catalysts **1-H**, **2-H**, **3-H** and **4-H** was investigated in the following experiments. The bisimino-nickel complex **1-H** was applied as catalyst for the catalytic polymerization of ethylene after activation with MAO. The polymerization resulted in Fe_2O_3/SiO_2 particles encapsulated within an polyethylene corona. SEM images of the product showed spherical particles with a rough polymer surface. Despite a broad polymer particle size distribution with particles sizes from 0.1 to 1.5 µm, the images proofed that the polymerization occurred at the catalysts on the particle surface and that the particles grew independently (Figure 2-15).

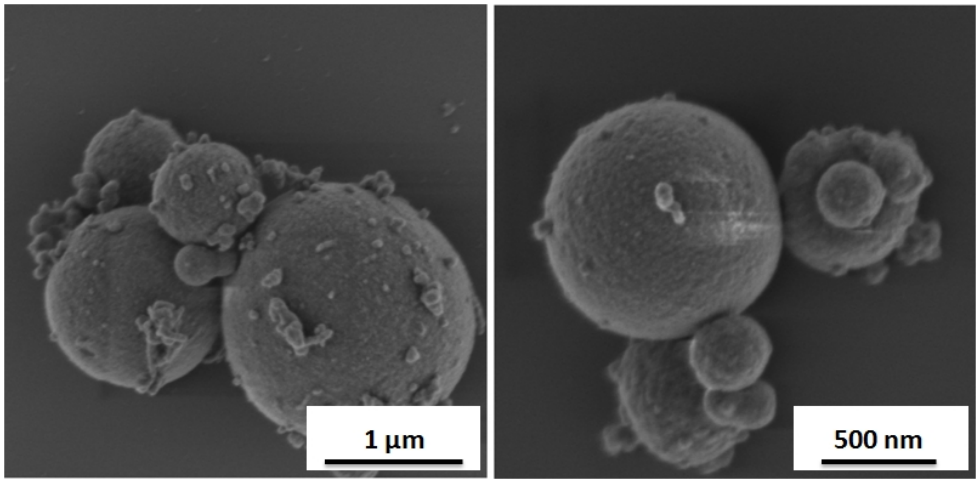

Figure 2-15. SEM images of the polyethylene particles polymerized by **1-H**.

Further performed dimerization experiments of propylene with the nanocatalysts **2-H**, **3-H** and **4-H** showed no change in the shape and size. During the catalytic tests, the center of focus was laid on the role of the support in order to ease the product separation. All synthesized phenoxyimine-nickel complexes were highly active for the dimerization of propylene after activation with MAO. All nanocatalysts showed high selectivities of up to 92 % for dimeric products. Besides some trimeric products nearly no higher oligomers were formed.

In conclusion, a facile preparation of functionalized nickel complexes on magnetic nano-particles incorporated in silica shells (γ-Fe_2O_3/SiO_2) was found with excellent catalytic behavior of these nanocatalysts during the catalyzed polymerization and dimerization of both ethylene and propylene. So, this type of heterogeneous nanocatalyst combines both homogeneous activities and selectivities and the separation of the product and the catalyst phase in one system.

2.5 Nanoscale hybrid Silica/Polymer Janus Particles with a double-responsive Hemicorona

Hybrid nanoparticles combining relevant materials properties from different material classes will be one of the most important building blocks for multifunctional materials in future technologies.[7]

In this project all knowledge from the previous projects about hybrid core-shell-corona particles and the modification of the intermediate silica shell was used to develop a versatile large-scale synthesis strategy for dual-responsive hybrid Janus nanoparticles with a silica core and a hemispherically attached PDMAEMA-corona in a size range of 100 nm.[9,10]

Scheme 2-4. Synthesis of SiO_2/PDMAEMA hybrid Janus nanoparticles.

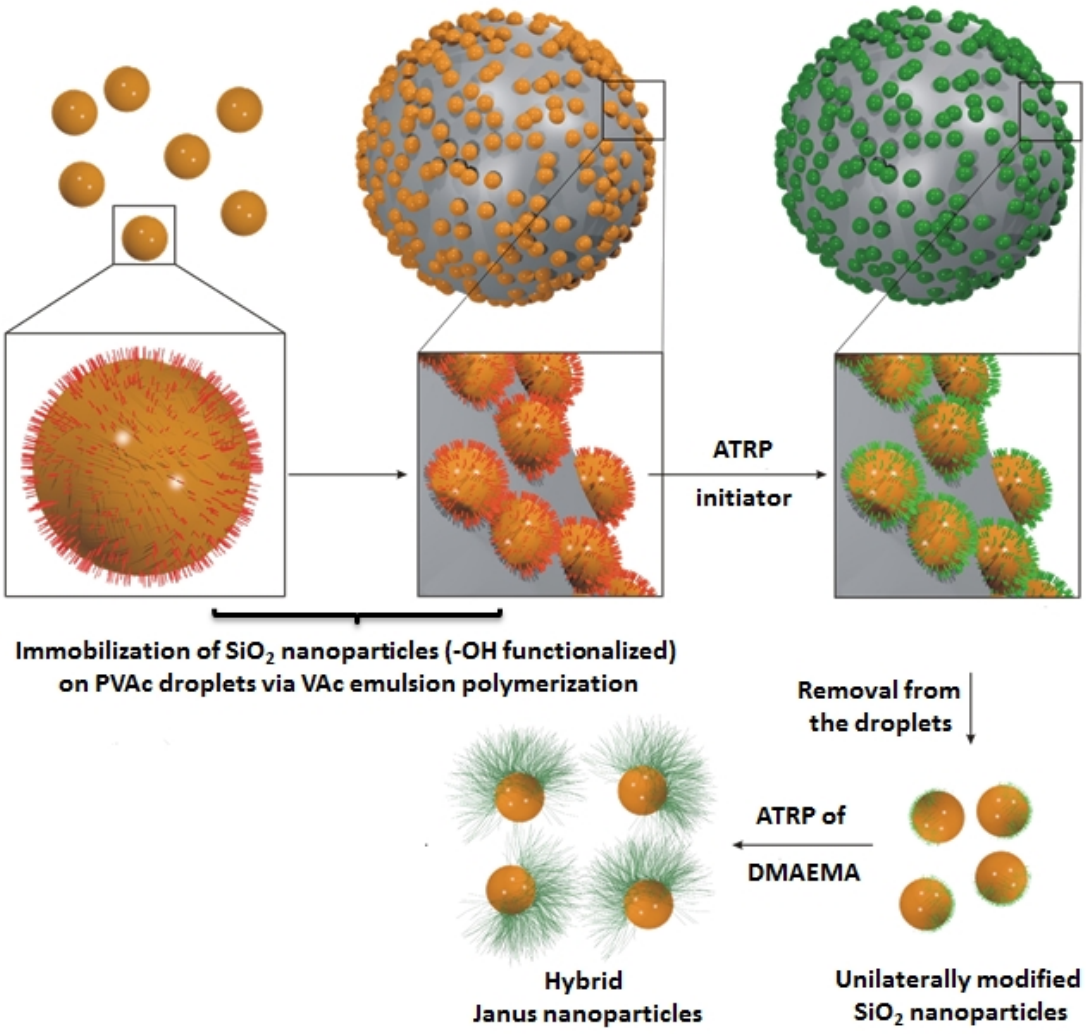

The synthesis was based on a modified version of the Pickering emulsion technique in combination with surface initiated atom transfer radical polymerization (ATRP) in a "grafting from" approach (Scheme 2-4). In a first step, colloidal stability was provided to latex particles prepared *via* emulsion polymerization using 30 nm silica nanoparticles that adhere to the surface of the growing poly(vinyl acetate) (PVAc) droplets. This resulted in polymer latexes which are armored with a layer of tightly immobilized nanoparticles. All silica particles were uniformly embedded in the surface of the PVAc phase. On basis of SEM pictures of the resulting Janus particles it can be estimated that ¾ of the particle surface is embedded and ¼ was unprotected and thus, free for modification (Figure 2-16).

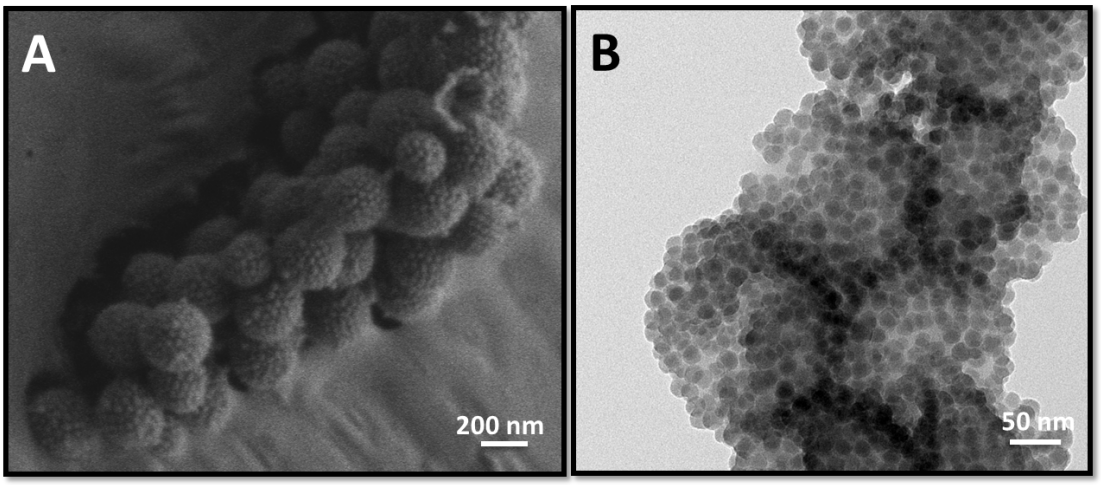

Figure 2-16. (A) cryo-SEM and (B) TEM images of PVAc latexes armored with SiO_2 nanoparticles obtained by Pickering emulsion polymerization.

To activate the surface of the silica particles for the growth of the final stimuli-responsive corona, the exposed side of the silica particles was modified with a silane-carrying ATRP initiator, (2-bromo-2-methyl)propionyloxyhexyltriethoxysilane. The structural changes during the experimental procedure were monitored *via* FT-IR and DLS.

After isolation of the hemispherically functionalized SiO_2 nanoparticles, ATRP was used to grow a PDMAEMA hemicorona by a "grafting from" polymerization of 2-(dimethylamino)ethyl methacrylate) (DMAEMA), yielding well-defined stimuli–responsive Janus nanoparticles. During this polymerization, the reaction can be conveniently quenched at different reaction times to furnish hemicoronas with different lengths of PDMAEMA chains (Figure 2-17 A). With increasing the molecular weight from 55 kg/mol to 108 kg/mol the hydrodynamic radii increased, too. Thus, the dimensions of our

hybrid particles can be controlled *via* the length of the PDMAEMA chains in the corona (Figure 2-17 B).

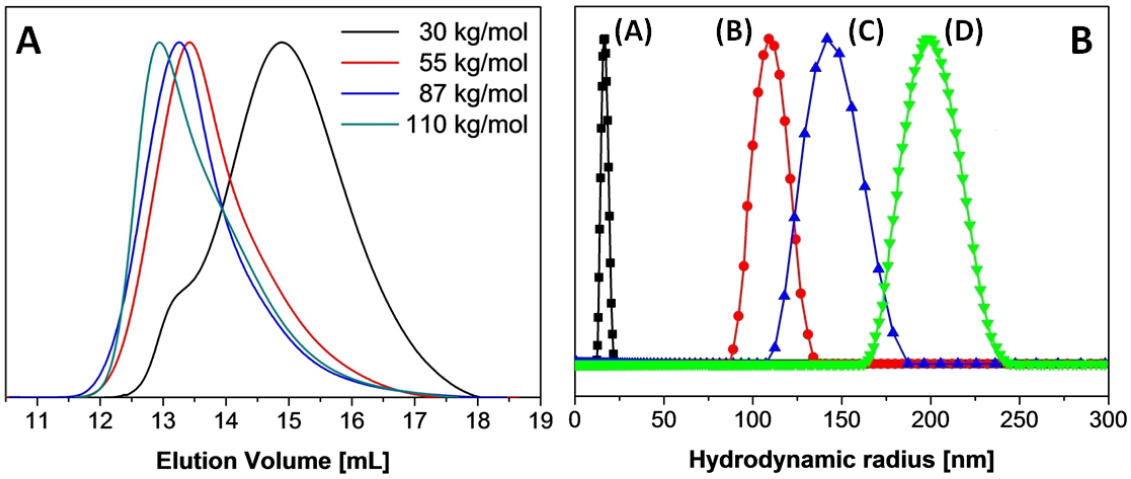

Figure 2-17. (A) GPC traces of cleaved PDMAEMA polymers with different molecular weights M_n. (B) Intensity-weighted hydrodynamic radii distribution (DLS) of (A) pristine silica particles and (B/C/D) Janus SiO_2/PDMAEMA nanoparticles with different molecular weights M_n (kg/mol) according to GPC: (B) 55, (C) 87, (D) 110. All samples are measured at pH 8 and RT.

Further, TEM and SEM images in Figure 2-18 allowed the detailed investigation of the Janus character of the obtained particles. The Janus nanoparticles are well-defined with the two components clearly separated with a sharp interface between the SiO_2 particles on one side and the grafted PDMAEMA on the other side.

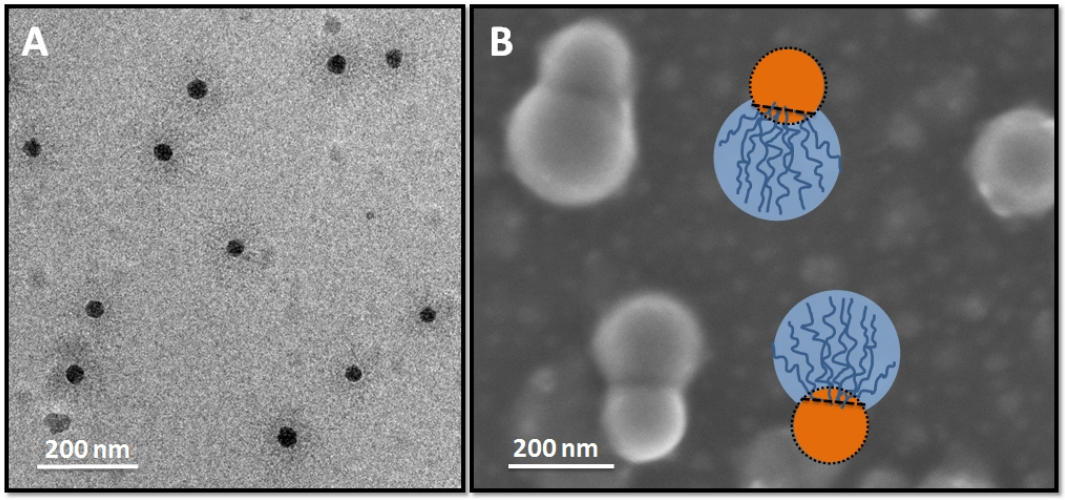

Figure 2-18. Janus SiO_2/PDMAEMA nanoparticles. (A) Representative TEM image of hybrid SiO_2/PDMAEMA Janus nanoparticles. (B) SEM images of Janus nanoparticles with clearly separated components (SiO_2 particle and PDMAEMA corona).

DLS and FT-IR demonstrated the successful polymerization of a PDMAEMA corona and in combination with TEM and SEM images a comprehensive proof was given for a successful immobilization of a PDMAEMA hemicorona on the activated SiO_2-particles and a successful synthesis of Janus nanoparticles.

In the last section, the pH- and temperature-responsive behavior of the Janus nanoparticles was highlighted *via* DLS and turbidimetry measurements (Figure 2-19). First, DLS was used to investigate the dual-responsive behavior of PDMAEMA at 20 °C (Figure 2-19 A). The hydrodynamic radius distributions of one sample were studied at different pH values. The particles displayed a clear increase of the radius with decreasing pH, due to the stretching of the polymer chains with increasing protonation.

Turbidity measurements were conducted to demonstrate the pH-dependent LCST behavior of the Janus NPs (Figure 2-19 B). The coil-to-globule transitions at the cloud point of the grafted particles are sharp and the clout points decrease from 85 °C at pH 7 to 30 °C at pH 10.

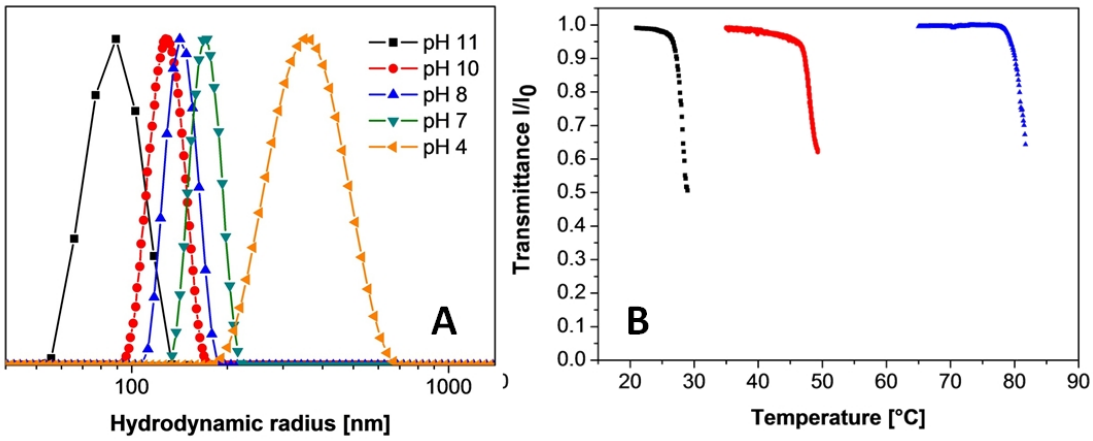

Figure 2-19. (A) Intensity-weighted hydrodynamic radii distribution (DLS) of Janus nanoparticles at pH 7, 8 and 10 at RT. (B) Turbidity measurements of the Janus SiO_2/PDMAEMA nanoparticles (c = 0.1 g/L) at different pH: pH 10 (black,■), pH 8 (red,●) and pH 7 (blue,Δ).

An unexpected, concentration dependent self-assembly and clustering of the Janus nanoparticles at low pH values (< 5) was observed in the TEM images in Figure 2-20. In more concentrated solutions we find a pH-dependent aggregation into linear strings. At low pH (pH 4) the PDMAEMA chains are charged and highly stretched. At low particle concentration only isolated particles can be observed, but increased concentrations lead to the formation of short worm-like assemblies. In contrast, at high pH (pH 11) the PDMAEMA

chains are collapsed. Then only isolated particles are found independent of the particle concentration. Further DLS measurements at different pH values from 0.1 g/L to 2 g/L confirmed the results obtained *via* TEM and the proposed mechanism of aggregate formation.

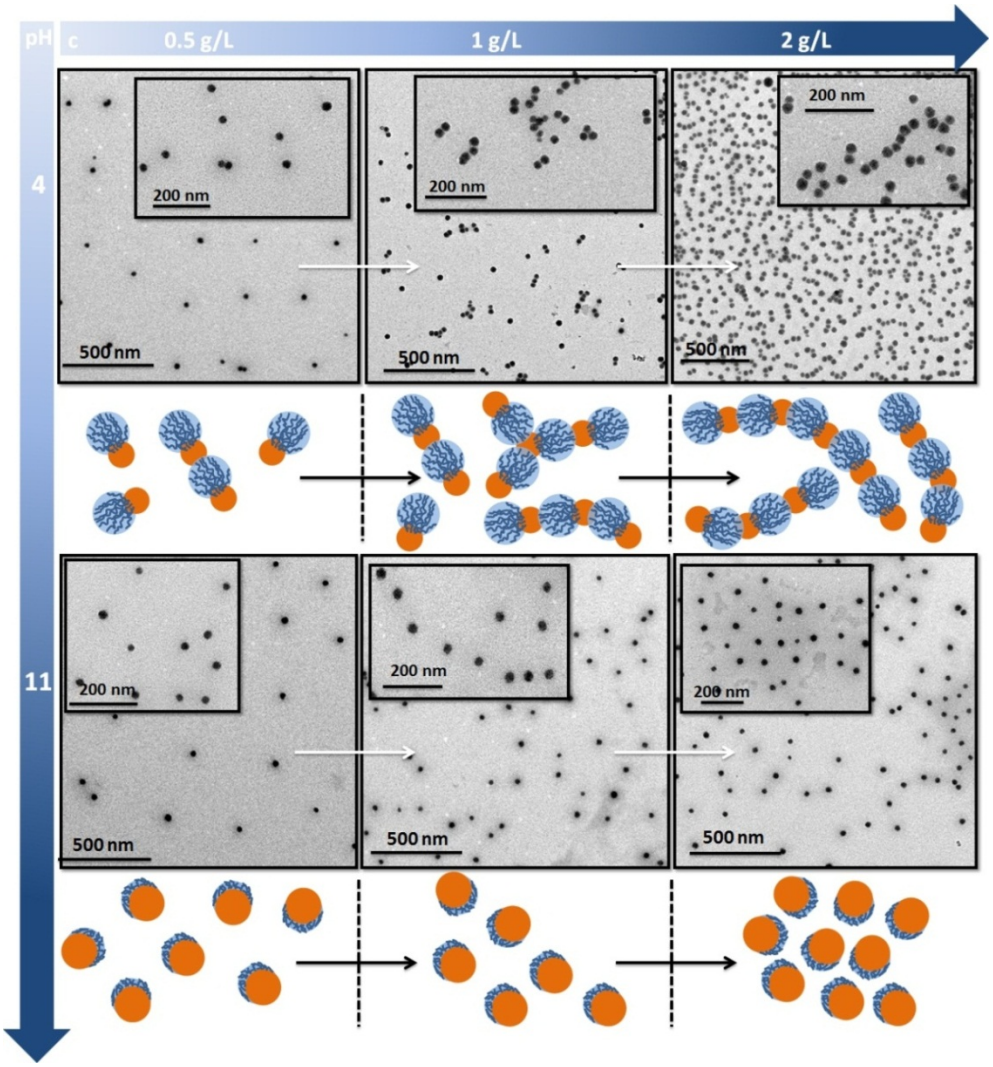

Figure 2-20. TEM images showing a concentration dependent clustering of the Janus SiO_2/PDMAEMA nanoparticles at pH 4 (top) and pH 11 (bottom) at different concentrations (0.5 g/L, 1 g/L, 2 g/L) and schematic representation of the Janus nanoparticles and their self-assembled structures.

In conclusion, an efficient and simple strategy based on a modified Pickering emulsion technique was developed for a large scale synthesis of well-defined and high-quality hybrid Janus nanoparticles with a 30 nm SiO_2 core and a temperature- and pH-responsive PDMAEMA hemicorona in the range of 100 nm. Most importantly, this synthetic approach is easily scalable and can be amended to furnish a wide range of nanoscale hybrid Janus particles with a wide variety of different stimuli-responsive polymers.

2.6 References

1. Binks, B. P.; Fletcher, P. D. I., *Langmuir* **2001**, 17, 4708.
2. Walther, A.; Müller, A. H. E., *Soft Matter* **2008**, 4, 663.
3. Nonomura, Y.; Komura, S.; Tsujii, K., *Langmuir* **2004**, 20, 11821.
4. Walther, A.; André, X.; Drechsler, M.; Abetz, V.; Müller, A. H. E., *J. Am. Chem. Soc.* **2007**, 129, 6187.
5. Ruhland, T. M.; Gröschel, A. H.; Walther, A.; Müller, A. H. E., *Langmuir* **2011**, 27, 9807.
6. Glaser, N.; Adams, D. J.; Böker, A.; Krausch, G., *Langmuir* **2006**, 22, 5227.
7. Sanchez, C.; Rozes, L.; Ribot, F.; Laberty-Robert, C.; Grosso, D.; Sassoye, C.; Boissiere, C.; Nicole, L., *C.R. Chim.* **2010**, 13, 3.
8. Karg, M.; Hellweg, T., *J. Mater. Chem.* **2009**, 19, 8714.
9. Ruhland, T. M.; Reichstein, P. M.; Majewski, A. P.; Walther, A.; Müller, A. H. E., *J. Colloid Interface Sci.* **2012**, 374, 45.
10. Pfaff, A.; Schallon, A.; Ruhland, T. M.; Majewski, A. P.; Schmalz, H.; Freitag, R.; Müller, A. H. E., *Biomacromolecules* **2011**, 12, 3805.

2.7 Individual Contributions to Joint Publications

The results presented in this thesis were obtained in collaboration with others and have been published or submitted to publication as indicated below. In the following, the contributions of all the co-authors to the different publications are specified. The asterisk denotes the corresponding author(s).

Chapter 3

This work is published in *Langmuir* **2011**, 27 (16), 9807–9814 under the title:

"Janus Cylinders at Liquid-Liquid Interfaces"

by Thomas M. Ruhland, André H. Gröschel, Andreas Walther* and Axel H. E. Müller*

I conducted all experiments and wrote the publication, except that:

- A. Gröschel was involved in discussions and designed the TOC image.
- A. Walther and A. H. E. Müller were involved in scientific discussions and correcting the manuscript.

Chapter 4

This work is published in *Langmuir* **2013**, 29 (5), 1388-1394 under the title:

"Influence of Janus Particle Shape on their Interfacial Behavior at Liquid-Liquid Interfaces"

by Thomas M. Ruhland, André H. Gröschel, Nicholas Ballard, Thomas S. Skehlon, Andreas Walther, Axel H. E. Müller and Stefan A. F. Bon*

I conducted all experiments and wrote the publication, except that:

- N. Ballard performed all simulations.
- T. Skehlon was involved in discussions and assisted the experimental procedure.
- A. Gröschel was in involved in discussions and the design of scheme 1 and 2.
- A. Walther was involved in discussions and synthesized the Janus discs used in this paper.
- A. H. E. Müller and S. A. F. Bon were involved in scientific discussions and correcting the manuscript.

Chapter 5

This work is published in the *Journal of Colloid and Interface Science* **2012**, 374, 45-53 under the title:

"Superparamagnetic and fluorescent thermo-responsive core-shell-corona hybrid nanogels with a protective silica shell"

by Thomas M. Ruhland, Paul M. Reichstein, Alexander P. Majewski, Andreas Walther* and Axel H. E. Müller*

I conducted all experiments and wrote the publication, except that:

- P. Reichstein was involved in all experiments and scientific discussions.
- A. Majewski synthesized the γ-Fe_2O_3 nanoparticles.
- A. Walther and A. H. E. Müller were involved in scientific discussions and correcting the manuscript.

Chapter 6

This work is published in *EUR. J. Inorg. Chem.* **2013**, 12, 2146-2153 under the title:

"Magnetic Core-Shell Nanoparticles as Carriers for Olefin Dimerization Catalysts"

by Thomas M. Ruhland, Julian R.V. Lang, Helmut G. Alt* and Axel H. E. Müller*

This is a joint project between the chairs of AC II and MC II.

I conducted all experiments concerning the preparation and the analysis of the Fe_2O_3/SiO_2 templates. I further assisted in the surface modification of the templates. I was involved in scientific discussions and wrote the manuscript.

J. Lang performed all experiments with respect to the modification of the core-shell particles, the catalytic behavior and the characterization of the hybrid materials. He was involved in discussions and correcting the manuscript.

Further:

- H. G. Alt and A. H. E. Müller were involved in scientific discussions and correcting the manuscript.

Chapter 7

This work has been submitted to *ACS Nano* under the title:

"Nanoscale hybrid silica/polymer Janus particles with a double-responsive hemicorona"

by Thomas M. Ruhland, Holly S. McKenzie, Thomas S. Skehlon, Stefan A. F. Bon, Andreas Walther* and Axel H. E. Müller*

I conducted all experiments and wrote the publication, except that:

- H. S. McKenzie and T. S. Skehlon supervised the synthesis of the PVAc/SiO_2 armored latex particles.
- S. A. F. Bon, A. Walther and A. H. E. Müller were involved in scientific discussions and correcting the manuscript.

Chapter 3

Janus Cylinders at Liquid-Liquid Interfaces

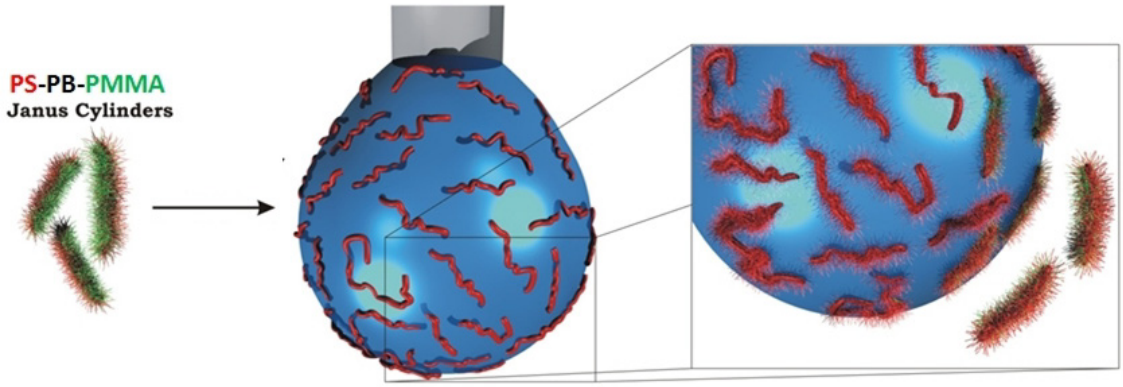

The results of this chapter have been published in *Langmuir* **2011**, 27 (16), 9807–9814 as:

"Janus Cylinders at Liquid-Liquid Interfaces"

by Thomas M. Ruhland, André H. Gröschel, Andreas Walther* and Axel H. E. Müller*

Janus Cylinders at Liquid-Liquid Interfaces

Thomas M. Ruhland[1], Andre Gröschel[1], Andreas Walther[2] and Axel H. E. Müller*[1]*

[1] Department of Macromolecular Chemistry II, University Bayreuth, Germany

[2] DWI at the RWTH Aachen, RWTH Aachen University, 52506 Aachen, Germany

walther@dwi.rwth-aachen.de;Axel.mueller@uni-bayreuth.de

Abstract

We herein describe the first study on the self-assembly behavior of Janus cylinders at liquid/liquid interfaces. The Janus cylinders are characterized by a phase-separation along the major axis into two hemicylinders of different wettability. The pendant drop technique and microscopic imaging were used to characterize the adsorption behavior and self-assembly of Janus cylinders at perfluorinated oil/dioxane and perfluorinated oil/dimethylsulfoxide interfaces. According to the evolution of the interfacial tension and a series of TEM images taken during the cylinder adsorption, we will specify the characteristics of early to late stages of the Janus cylinder adsorption at a liquid-liquid interface and discuss the effect of Janus cylinder length and their concentration. We also establish that the broken symmetry of the corona leads to significantly higher interfacial activity as compared to homogeneous core-shell cylinders. The adsorption is characterized by three different adsorption stages: First, free diffusion to the interface, followed by continuous adsorption of cylinders including ordering and domain formation and finally, additional packing with a rearrangement of domains and formation of a multilayer system.

KEYWORDS: Janus Cylinders, Janus Particle, Liquid-Liquid Interface, Self-Assembly, Adsorption, Interfacial Tension, Pickering Effect

Introduction

Colloidal particles in the nanometer range are a key ingredient for modern materials and life sciences. Their intrinsic properties can be harnessed to create new materials, carriers or devices with advanced properties. In this context, the self-assembly of nanoscale objects into ordered structures has attracted significant attention for generating new materials.[1-5] Because of the challenges of direct manipulation of nanoparticles, there is an increasing need of directing their structures and aggregates *via* self-assembly in a controlled manner. Thereby, the use of liquid interfaces as platforms to assemble nanoparticles has come into focus as it allows the generation of highly ordered materials.[6-41] At the beginning of the last century, Pickering and Ramsden discovered the stabilizing effect of particles in emulsions[7,41], which was followed by the theoretical description of this effect by Pieranski.[7,8] By now, the self-assembly of colloidal particles at fluid interfaces, driven by the reduction in interfacial energy, is well established for the case of spherical particles.[9-11] Using this approach a variety of supracolloidal structures have been reported and investigated, such as permeable hollow capsules made from partially fused polymer latexes (colloidosomes)[12], colloid-based foams[13], armored latex particles for enhanced dispersion in nanocomposite materials, crosslinked nanoparticle membranes[14] and well-defined monolayers which can be used as building blocks for nanoporous capsules.[15,16] The assembly of small nanoparticles at soft interfaces extends into many biological areas, for example, the fabrication of capsules *via* directed self-assembly and cross-linking of virus bionanoparticles[17] and the aggregation of crystalline arrays of proteins in bacterial layers[18]. Unlike spherically symmetric colloidal particles and disc-like particles,[19-26] anisotropic cylindrical nanoparticles have hardly been investigated although they can show interesting structures and orientation at interfaces due to their shape.[14,27,28,29] The key difference between spherical and anisotropic particles is the number of transitions in interfacial tension that can be encountered during concentration changes. He *et al.* investigated the interfacial assembly of stiff tobacco mosaic virus (TMV) nanorods. For instance, TMV nanorods orient first parallel and at higher concentrations an intuitively unexpected transition to an orientation normal to the interface occurs.[27]

Herein, we will demonstrate significant differences in the structures created at the interface by Janus cylinders. The broken symmetry into two sides (hemicylinders) of different physical properties is a decisive difference compared to uniform colloidal

particles. In the course of the last years Janus particles, named after the double-faced Roman god, have evolved as a very interesting class of colloidal structures among micron- or nanosized particles.[42-44] The terminology is based on the special architectural feature of having two sides or at least two surfaces of different chemistry or polarity. The lack of centrosymmetry in Janus systems has led to the discovery of new properties as well as unique hierarchical aggregation behavior into superstructures.[45-48] They can be divided into several classes according to their architecture and dimensionality. In particular much attention has been devoted to spherical Janus particles (3D). In contrast, the challenging synthesis of non-spherical Janus particles such as cylinders (1D) and disc-like particles (2D) (Scheme 3-1), has so far limited the possibilities for a comprehensive understanding of their properties.[42-44] Thus far, only the controlled crosslinking of microphase-segregated structures of block terpolymers is able to produce nano sized Janus cylinders and discs on the multigram scale.[42,46,47,49,50] This synthetic advantage allows to studying their properties in more detail.

Scheme 3-1. Overview of possible Janus particle architectures. (a) Sphere, (b + c) cylinders and (d + e) discs.[42] The cylinders utilized in this study are highlighted by the box.

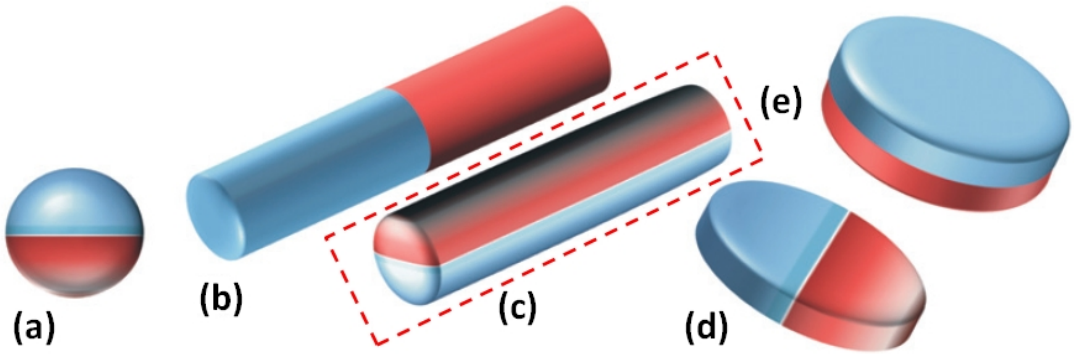

After being able to produce large amounts of different types of Janus particles, the question of understanding their solution and interfacial behavior needs to be answered to identify possibilities to produce new and more efficient materials. In contrast to a homogeneous particle with uniform wettability, the surface of Janus particles has two parts with different wetabilities. This results in an amphiphilic particle that combines the typical Pickering effect of the particles and the amphiphilicity of a classical surfactant. Therefore, the surface activity of Janus particles is of fundamental interest as they

represent a completely new class of Pickering surfactant. In recent years, several publications described the extraordinarily high adsorption strength of Janus particles at interfaces, originating from the corona segregation.[11,17] In the case of spherical particles, the adsorption energy at a liquid–liquid interface can be up to three times higher for Janus particles than for particles with a uniform surface.[51] In a similar context, Nonomura *et al.* published results of theoretical calculations about the influence of disc-shaped Janus beads on the oil/water interfacial tension.[52] The calculations demonstrated that the adsorption energy of Janus discs can be higher than that of classic surfactants by several orders of magnitude. In consequence, a considerable increase in surface activity is expected. These predictions render Janus structures an extremely interesting new class of future surfactants and for the nanostructuring of interfaces, both topics of great scientific and industrial interest. Earlier, Glaser *et al.* showed that bimetallic Janus particles lead to a significant reduction of the oil–water interfacial tension compared to uniform metallic nanoparticles of similar size.[53] In the following, other groups also reported the stabilization of liquid-liquid interfaces.[4,54,55] In terms of real prototype applications, Walther *et al.* could demonstrate a superior performance of Janus particles in case of emulsion polymerization and nanostructuring of polymer blend systems.[56,57] Therefore, the combination of amphiphilicity combined with the particle character and their strong adsorption and orientation at the interface makes them an attractive tool for the nanostructuring of blends, block copolymers[58] and liquid-liquid interfaces.

In the scope of this article, we describe adsorption studies of moderately amphiphilic Janus cylinders at liquid/liquid interfaces. We will deduce the effect of Janus cylinder length and the adsorption time on the structures formed at the interface and characterize the time-dependent evolution of the interfacial tensions.

Experimental Section

Materials. All chemicals (p.a. grade) were purchased from Aldrich.

Synthesis.

The polystyrene-*block*-polybutadiene-*block*-poly(methyl methacrylate) $S_{41}B_{14}M_{45}^{110}$ block terpolymer (PDI = 1.01) was synthesized *via* sequential anionic polymerization in tetrahydrofuran (THF). The subscripts denote the mass fraction in percent as calculated

from the ^{1}H-NMR spectrum, and the superscript gives the number-average molecular weight in kg/mol. The Janus cylinders are produced by the selective crosslinking of the lamella-cylinder morphology, formed by the SBM precursor in the bulk phase.[46,49] The crosslinking of the polybutadiene (PB) domains was performed *via* cold vulcanization using S_2Cl_2 in a well-ordered solvent-swollen bulk morphology. Ultrasound treatment is then used to produce dispersible cylinders from the crosslinked block terpolymer template and to adjust the length of the cylinders by the duration of the sonication treatment. Sonication treatment was performed with a Branson model-250 digital sonifier equipped with 1/8 in diameter tapered microtip (200 watt at 30% amplitude). TEM was used to characterize the size evolution of the Janus cylinders with time.

The polystyrene-*block*-polybutadiene $S_{72}B_{26}^{100}$ diblock copolymer (PDI = 1.1) was synthesized *via* sequential anionic polymerization in tetrahydrofuran (THF). The cylinders are produced from a cylindrical bulk morphology following the same pathway mentioned for the Janus cylinders.

Characterization.

Bright-field TEM was performed on Zeiss CEM 902 and LEO 922 OMEGA electron microscopes operated at 80 kV and 200 kV, respectively. Data evaluation and processing was carried out with Soft Imaging Viewer, Digital Micrograph 365 Demo software and Image Tool. *Cryo-TEM* samples on holey grids were frozen in liquid nitrogen.

Pendant Drop Tensiometer isotherms of the interfacial tension were measured on a Dataphysics OCA 20 tensiometer at room temperature. The cylinder concentrations were in the range of 0.5 g/L to 2.5 g/L. To image the Janus cylinder assembly at the perfluoroctane/dioxane interface as a function of time, a small drop of perfluoroctane was placed on a TEM grid and then immersed in a dioxane solution containing Janus cylinders, allowing the cylinder adsorption to proceed for a desired period of time that paralleled the tensiometer measurements. Subsequently, the grid was removed from the solution and the dioxane was extracted with dust free paper from below. The grid was then dried in air.

Results and Discussion

The synthetic pathway to obtain cylindrical Janus structures is based on a template-assisted synthesis, involving crosslinking of a microphase-segregated lamellar-cylinder morphology of a bulk film of a polystyrene-*block*-polybutadiene-*block*-poly(*methyl* methacrylate) (SBM) block terpolymer, followed by a sonication treatment as outlined in Figure 3-1 A.[49,59] This process results in the formation of core-crosslinked cylinders, possessing a PB core and two hemicylinders of PS and PMMA. Figure 3-1 C displays a typical cryogenic transmission electron microscopy (cryo-TEM) image of the Janus cylinders in THF solution. The individually dispersed, dark cylinders only correspond to the tightly crosslinked polybutadiene cylinders, which gain additional contrast from the crosslinking agent, S_2Cl_2. The highly swollen corona, composed of hemicylinders of PMMA and PS, remains invisible in this micrograph. The Janus cylinders are characterized by an extremely well-defined cross section, originating from the well-ordered block terpolymer bulk structure, but have a polydisperse length distribution. From earlier investigations[46] we know that the PB cylinder has an average diameter of ca. 23 nm with a surrounding corona, leading to a total diameter of the cross section of 80 nm. Since sonication is used to create soluble particles from the tightly crosslinked block terpolymer template, it is possible to control their length by variation of sonication times. Transmission electron microscopy (TEM) was used to characterize the size evolution of the Janus cylinders with time (Fig. 3-1 B, see Figure 3-S1 in the Supporting Information for the TEM images). A detailed look at the evolution of the length with sonication time shows a rapid decay with increasing sonication time. The curve follows an exponential decay, with asymptotical behavior and a plateau value of around 350 nm. Consequently, there is some higher resistance to the introduced sonication energy for shorter cylinders.[56,59,60]

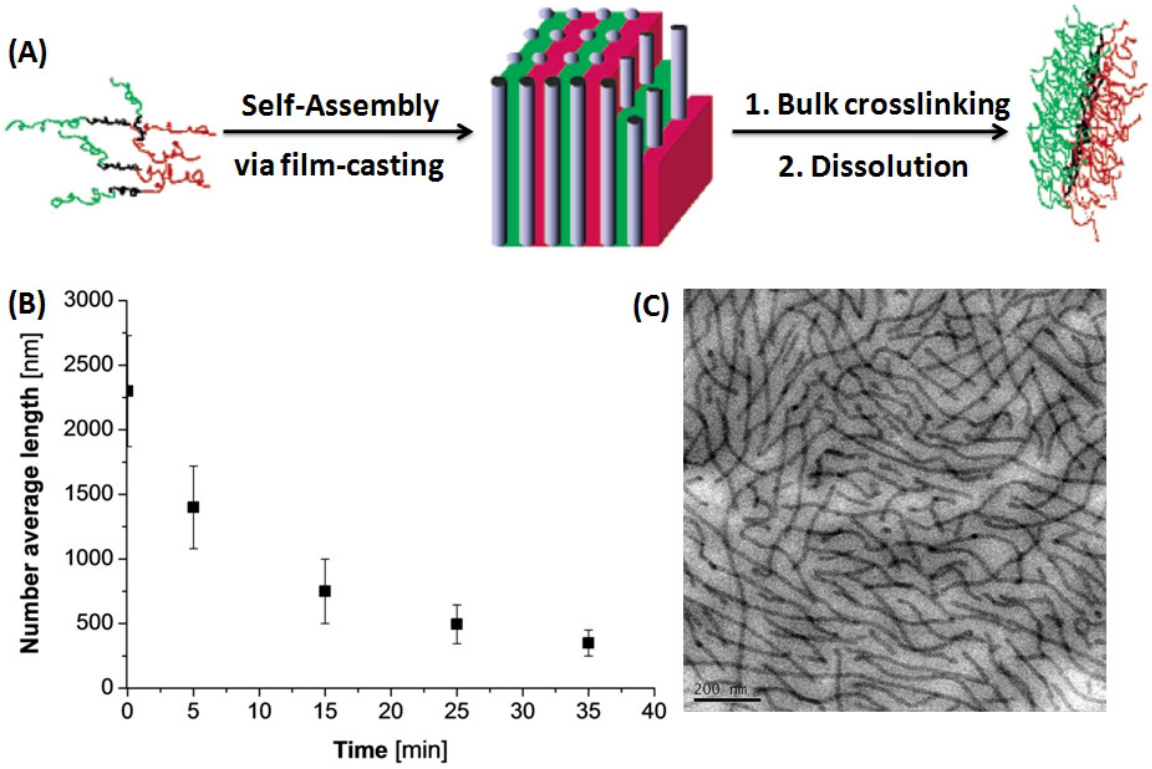

Figure 3-1. (A) Schematic synthesis of Janus cylinders.[49] (B) Time dependence of the number - average length for different sonication times at 30% amplitude. Error bars represent the standard deviations of the length distribution. (C) Cryo-TEM image of a Janus cylinder dispersion in THF with a number-average length of 2300 nm.

An elegant way of determining the influence of particles at liquid-liquid interfaces is to analyze the interfacial tension of a dispersion of the desired material *via* the pendant drop method. Computer automation allows rapid acquisition of the drop image, edge detection, and fitting of the Laplace–Young equation to determine the interfacial tension.[12,13,61-68] It is strongly required for the reference system of two fluids that the drop phase and the solution are immiscible. An initially relatively high interfacial tension is additionally beneficial to produce a large driving force for the cylinders to assemble at the interface. Furthermore, the density of the liquid forming the droplet needs to be higher than the surrounding dispersion liquid in order to ensure the development of a hanging drop at the end of the syringe needle. We chose perfluorooctane (PFO) as the drop phase. To find the right solvent combination for the experiment, the interfacial tensions γ of different solvent dimethylsulfoxide, dioxane, tetrahydrofuran and ethyl acetate with PFO were measured. The systems PFO/dimethylsulfoxide (DMSO) and PFO/dioxane show sufficiently high interfacial tensions with 21.7 and 10.7 mN/m, respectively, and thus fulfill the criteria mentioned above (Figure 3-S2, Supporting information).

In a first series of experiments, we assessed the influence of different length of the Janus cylinder on the interfacial tension of liquid-liquid interfaces for the two systems. Figure 3-2 A displays a series of pendant drop tensiometer measurements for cylinders with number-average lengths of 2300 nm, 1600 nm, 800 nm and 350 nm, dissolved in dioxane at a concentration of 1 g/L. The interfacial tension decreases with time and approaches quasi-equilibrium. At early stages of adsorption, the interfacial tension decreases rapidly. Subsequently, the decrease in interfacial tension slows down, and finally, it approaches a plateau, where the maximum coverage of the interface with cylinders is obtained. After reaching the plateau value, the Janus cylinders are located and arranged at the interface. An increase of the average length of the Janus cylinders leads to an enhanced adsorption at the interface and the plateau value is reached earlier. We will discuss a comparison of the interfacial tension isotherms of differently sized Janus cylinders at the same particle density (molar concentration) below.

The adsorption behavior is a clear and well developed feature of the system as it can be found independently of the solvent used dioxane (Figure 3-2 A) or DMSO (Figure 3-2 B). Figure 3-2 C summarizes the interfacial tensions for both systems as normalized by the value for the pure PFO/solvent interface. The relative change in interfacial tension obtained for DMSO and dioxane as initial dispersion phases for the Janus cylinders display similar characteristics. However, the PFO/dioxane system always exhibits a stronger relative decrease, which might be due to the lower viscosity of dioxane (1.37 cP) compared to DMSO (2.24 cP). Lower viscosity leads to higher diffusion coefficients of the dispersed materials and faster adsorption kinetics. A faster diffusion may also contribute to the lower values of the quasi-equilibrium state as the further minimization in this stage is collision-controlled in contrast to diffusion control in the early stages. Considering that higher diffusion coefficients in low viscosity medium impart the particles with a higher momentum, a larger pressure of the still dispersed Janus cylinders onto the interface may result.

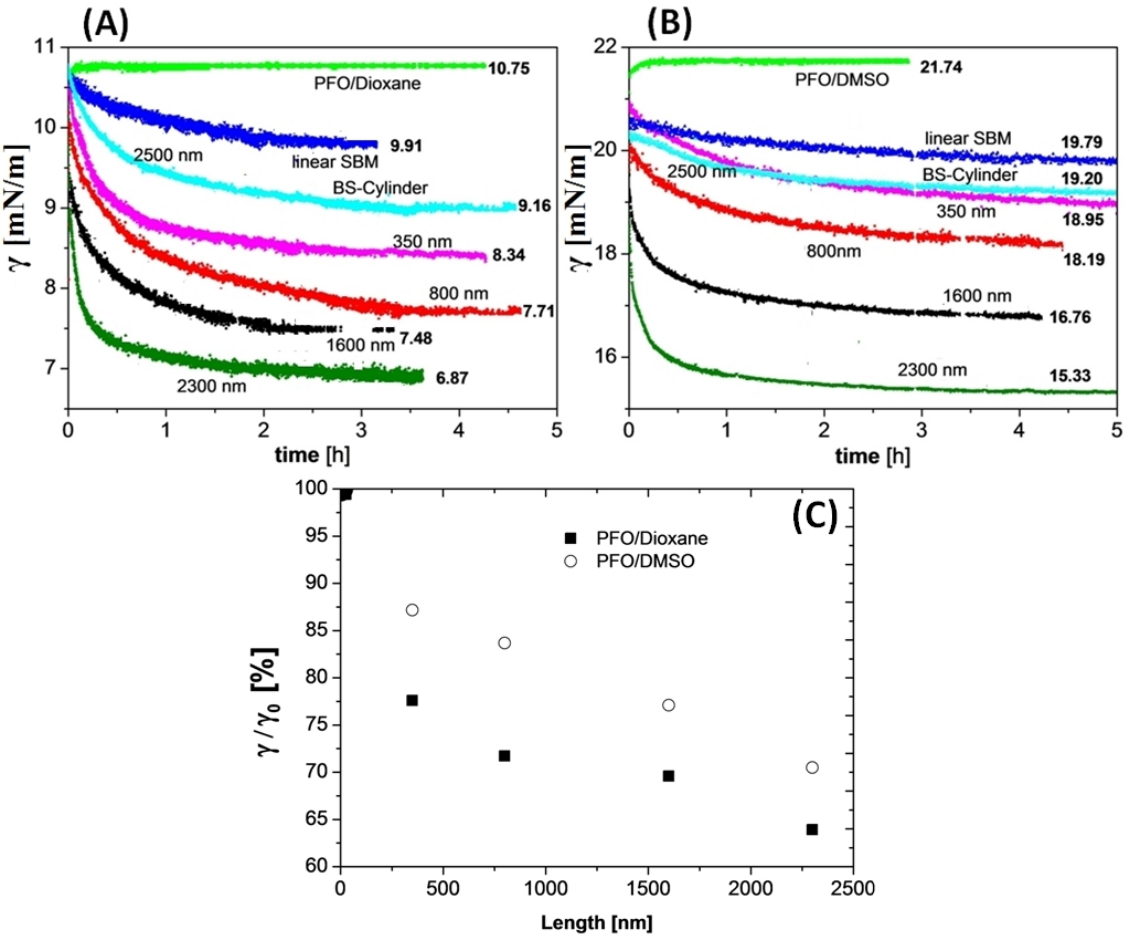

Figure 3-2. Influence of the length of Janus cylinders on the interfacial tension. (A) Interfacial tension isotherms of solutions of Janus cylinders in dioxane at the PFO/dioxane interface and (B) in DMSO at the PFO/DMSO interface (c = 1 g/L). Interfacial tension isotherms for uncrosslinked SBM and homogeneous BS core-shell cylinders are included. (C) Relative decrease if interfacial tensions vs. cylinder length for both solvent systems.

For the interpretation of the Janus cylinder adsorption, we take into consideration that the Janus cylinders are orientated parallel to the liquid-liquid interface and interfacial assembly of the cylinders is dictated by a minimization of the free energy. The initially high interfacial energy between PFO and the solvent can be reduced by ΔE *via* placing one cylinder with an effective length L at the interface. The stability of the particle assembly increases with L. For the microscopic Janus cylinders, the decrease in the energy per cylinder is much larger than the thermal energy, k_BT, so that the cylinders are strongly kept at the interface and the residence time at the interface is long. A desorption and occurring exchange with other Janus cylinders present in the surrounding dispersion occurs faster and more easily with decreasing length of the cylinders and, at the same particle concentration, the coverage of the interface will be ideally more complete with longer cylinders. Due to the polydispersity of each cylinder ensemble, the longer

cylinders preferentially assemble at the interface. Hence, the longest Janus cylinders have most influence on the interfacial tension and have the highest surface activity. Based on calculated solubility parameters of the various polymers, we deduced a favored orientation of PS to the PFO phase and the PMMA side chains to the dioxane phase.

Next, we compare the performance of our Janus cylinders to suitable benchmark materials. Figure 3-2 A and B additionally display the interfacial tension isotherms of the uncrosslinked polymer (SBM), used in the Janus particle synthesis. The block terpolymer precursor provides a minor reduction of around 10 % of the interfacial tension for both solvents. By comparison, the Janus cylinders show a significantly stronger decrease, i.e. an up to 5-fold better performance for the PFO/dioxane solvent system and up to 4–fold better performance for PFO/DMSO. Consequently, a synthetic transformation of the linear block terpolymer into Janus cylinders leads to superior interfacial activity and Janus cylinders emerge as clearly more efficient stabilizing agents for the nanostructuration of interfaces.

Finally, we present the important comparison to 2500 nm long core-shell BS-cylinders (B-core and S-shell, TEM image in Figure 3-S3) with very similar cross-sectional dimensions. These cylinders lack the compartmentalization into a biphasic hemicylinder corona. We specifically chose to study BS (and not BM) cylinders as calculations of the polymer/solvent interactions indicated that S preferentially adsorbs to the PFO phase, thus BS cylinders have a stronger tendency to migrate to the interface compared to BM ones. Despite the large length, the measured interfacial tension even remains above the value of the shortest Janus cylinders (350 nm) for both solvent systems. It is however slightly below the uncrosslinked SBM, as realized by the Pickering effect. Overall, the BS-cylinder show a much lower tendency to freely migrate to the interface and prefer the dioxane or dimethylsulfoxide phase due to their homogenous shell. These results clearly demonstrate, that breaking the corona symmetry into an even only slightly solvent-selective, amphiphilic Janus cylinder leads to a decisive increase in interfacial activity. The whole extent of this effect is surprisingly large.

Following the size dependent adsorption behavior and the comparison with reference materials, we analyzed the concentration dependence of the interfacial tension at two different cylinder lengths. Figure 3-S4 A-H (SI) illustrates all $\gamma(t)$-curves for 2300 nm and 350 nm long Janus cylinders at different cylinder concentrations in dioxane and DMSO.

A comprehensive summary is displayed in Figure 3-3 A which compares the quasi-equilibrium interfacial tension for both solvents, dioxane and DMSO, and for both cylinder lengths. The data allows concluding that a stronger decrease of the interfacial tension can be observed for higher concentrations. This is understandable considering the higher surface pressures and the partitioning between adsorbed and dispersed materials with increasing concentrations. This concentration series also allows comparing long (2300 nm) and short (350 nm) Janus cylinders at roughly the same molar concentration, i.e. particle density (Figure 3-3 B). Here, indeed we find a smaller reduction of the interfacial tension and a slower kinetic of adsorption for the shorter Janus cylinders, thus confirming stronger adsorption with increasing size. The slower kinetics is also displayed in Figure 3-S5 depicting the relative decay of the interfacial tension, where the smaller cylinders always show less relative decay until both materials reach their final quasi-equilibrium value.

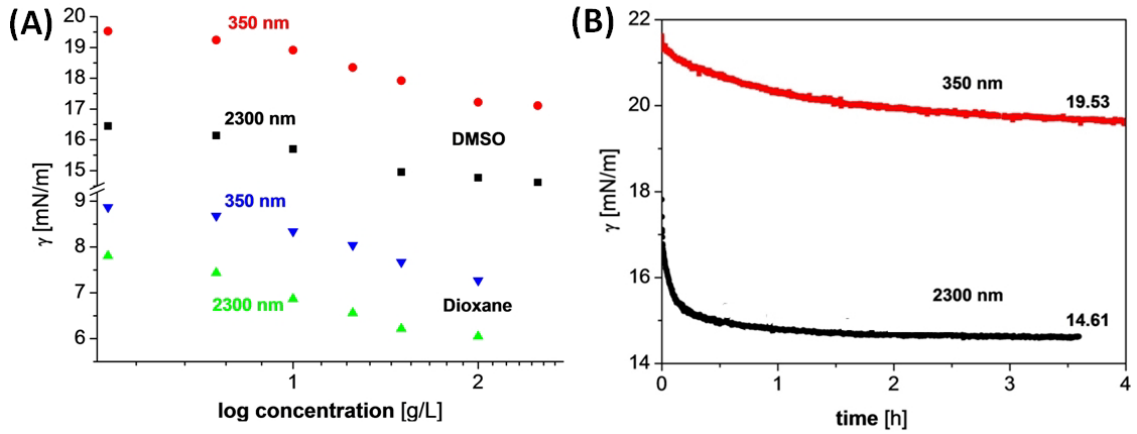

Figure 3-3. (A) Concentration dependence of the quasi-equilibrium interfacial tension for 2300 nm and 350 nm long Janus cylinders dissolved in dioxane and DMSO. (B) Interfacial tension isotherms of long (2.5 g/L) and short (0.5 g/L) cylinders at similar molar concentration (particle density) in DMSO, as calculated based on their length ratio.

Mechanism of cylinder adsorption.

The logarithmic representation of the interfacial tension values in Figure 3-4 points to three different stages of adsorption (see Scheme in Figure 3-4). First, there is a free cylinder diffusion to the interface (I). The number of particles at the interface increases rapidly, the cylinders pack closer and the decrease in interfacial tension slows down (II). Furthermore, similar to phase II a closer cylinder organization plays an important role in order to get more cylinders to the interface (III). Here, the adsorption of new Janus

cylinders comes along with a rearrangement and better ordering of already adsorbed cylinders at the interface. In order to gain more information of the microscopic arrangement of the Janus cylinders at the interface, we performed simultaneous ex-situ TEM measurements for a specific sample. We choose Janus cylinders with 2300 nm length as they lead to a well-developed and pronounced decrease of the interfacial tension. The adsorption isotherm (1 g/L) is shown together with the sample points and the corresponding TEM image series in Figure 3-4 A-H and a direct comparison of short (20s) and long (3h) adsorption time is displayed in the top right part of the figure. A small drop of perfluoroctane was placed on a TEM grid and then immersed into a Janus cylinder dispersion, allowing the cylinder adsorption to proceed for a desired period of time that paralleled the tensiometer measurements. Subsequently, the grid was removed from the solution and the solvent (dioxane or dimethylsulfoxide) was rapidly extracted with dust free paper from below. The grid was then dried in air. This methodology has proven useful for several other systems of interfacially assembled particles.[3,15,19,27] One has yet to bear in mind that the particles are transferred from a curved droplet interface to its projected area on the flat TEM grid during drying. Therefore, slight changes in the concentration regimes may occur which can at best be minimized by rapid blotting.

A careful observation of the TEM images confirms the stages of adsorption. First, a small amount of JC in the drop area (A) can be identified, corresponding to individual cylinder diffusion to the empty interface in the beginning of the adsorption process. The number of Janus cylinders is too small to form correlated structures at the interface. The number of particles at the interface increases rapidly thereafter, where randomly arranged (B) cylinders are followed by closer packed ones. After 1h, clusters are formed, which grow to form a closely packed cylinder array, lowering the interfacial tension. To immobilize further cylinders at the interface, the cylinders rearrange to form larger, more tightly packed aggregates (D-F), covering the full interface in the later stages. The Janus cylinders orient parallel to the liquid-liquid interface and show a type of organization that resembles isolated short-range liquid crystalline packing (E-G). Finally, even multilayers with only loosely attached outer cylinders can be observed (H). It is likely, that the outer layers are only loosely attached by a short part of the Janus cylinders to some remaining free areas. Nevertheless, a small attachment area is sufficient to anchor a second more fuzzy outer layer of adsorbing particles.

The observations of different adsorption regions are in line with results for the adsorption of spherical CdSe nanoparticles[26] and TMV nanorods.[27] However, one difference between the rod-like TMV and our Janus cylinders is the fact that the broken symmetry and amphiphilic character prevents a perpendicular orientation of the Janus cylinders at higher concentrations, unlike observed for TMV. Therefore, Janus cylinders remain oriented parallel to the interface and their flexibility allows to anchor a second loosely bound layer.

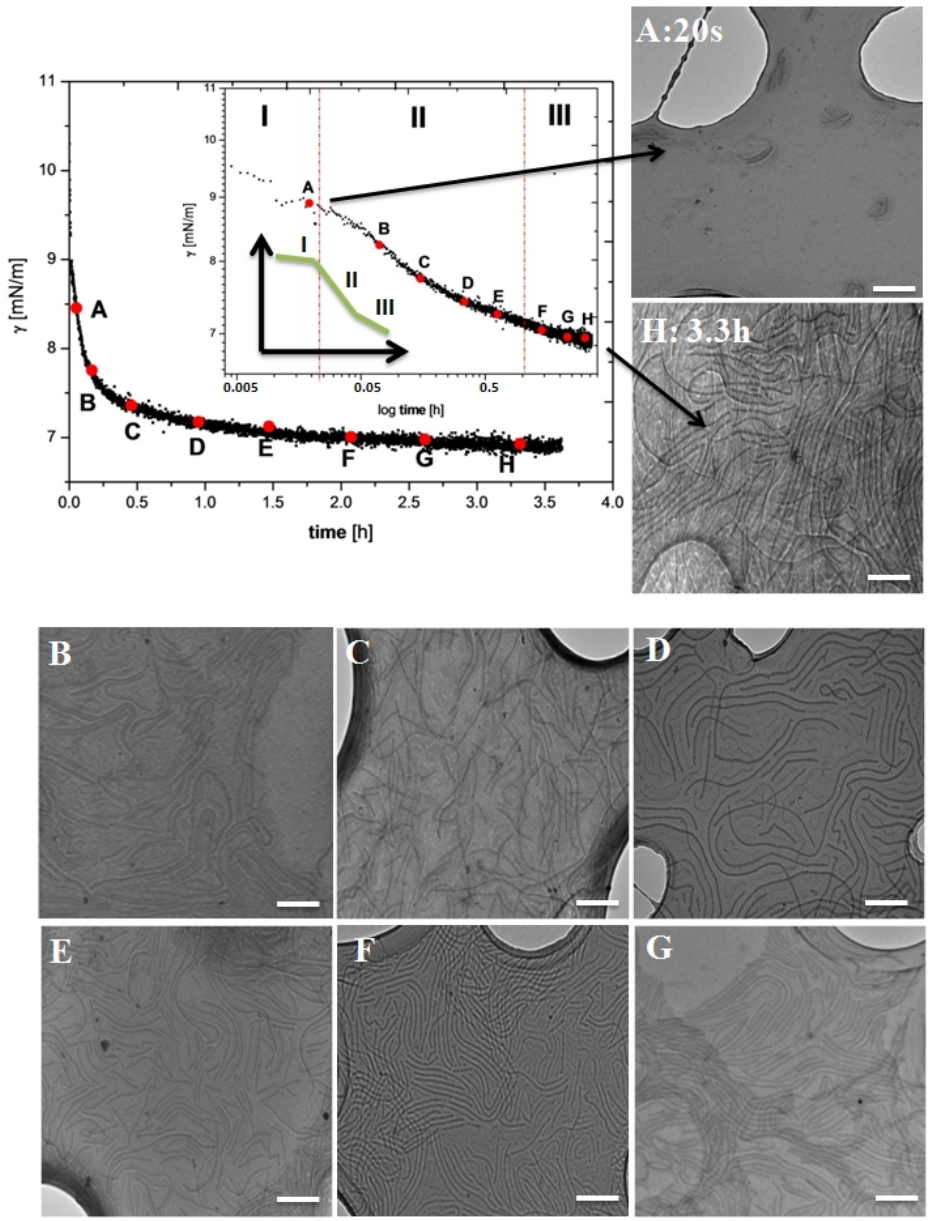

Figure 3-4. Left top: Adsorption curves in linear and logarithmic presentation. **A-H**: Series of TEM images (obtained from lacey grids) of 2300 nm Janus cylinders (1 g/L) adsorbing at the PFO/dioxane interface at different times as noted in the interfacial isotherms. (scale bars: 1 μm).

Conclusion

We presented detailed studies of the interfacial self-assembly of slightly amphiphilic Janus cylinders, a previously unexplored class of particle surfactants. Despite their only slightly amphiphilic character, Janus cylinders demonstrate significantly enhanced surface activity as compared to homogeneous cylindrical particles or the block terpolymer precursor SBM, consequently opening possibilities for a new class of superior surfactant. The interfacial tension decreases with increasing Janus cylinder length and concentration and the adsorption process is characterized by three different adsorption stages. In the beginning, free diffusion to the interface occurs, followed by continuous adsorption of cylinders including ordering and domain formation at the interface. Finally, additional packing leads to a rearrangement of the domains and to the formation of a multilayer system. The cylinders show a liquid crystalline like short-range correlation at the fluid interfaces, thus providing a novel tool for the nanostructuration of interfaces.

Acknowledgments

This work was supported by DFG within SFB 840 (project A1). We thank Prof. A. Böker for fruitful discussions. Thomas Ruhland thanks the Bavarian Elite Support Program for a scholarship.

Supporting Information

TEM images of Janus cylinders at different sonication times and pendant drop measurements of representing the concentration dependence of the Janus cylinders on the interfacial tension. This material is available free of charge *via* the Internet at http://pubs.acs.org.

References

1. Ozin, G. A.; Arsenault, A., *Nanochemistry: A Chemical Approach to Nanomaterials* (RSC, Cambridge, U.K., **2005**).
2. Kinge,S.; Crego-Calama, M.; Reinhoudt, D. N., *Chem. Phys. Chem.* 2008, 9, 20.
3. Böker, A.; He, J.; Emrick, T.; Russel, T.P., *Soft Matter* **2007**, 3, 1231.
4. Binder, W., *Angew. Chem. Int. Ed.* **2005**, 44, 5172.
5. Walther, A.; Bjurhager, I.; Malho, J.-M.; Ruokolainen, J.; Berglund, L.; Ikkala, O., *Angew. Chem. Int. Ed.* **2010**, 49, 6448.
6. Binks, B. P.; Horozov, T. S., *Cambridge University Press*, Cambridge, **2006.**
7. Pickering, S., *J. Chem. Soc.* **1907**, 91, 307.
8. Pieranski, P., *Phys. Rev. Lett*. **1980**, 45, 569-572.
9. Cheung, D.; Bon, S.A.F., Phys. *Rev. Lett.* **2009,** 102, 66103.
10. Cheung, D.; Bon, S.A.F., Soft *Matter* **2009**, 5, 3969.
11. Carrillo, J.-M. Y.; Raphael, E.; Dobrynin, A.V., *Langmuir* **2010**, 26, 12973.
12. Dinsmore, A.D.; Hsu, M.F.; Nikolaides, M.G.; Marquez, M.; Bausch, A.R.; Weitz, D.A., *Science* 2002, 298, 1006.
13. Binks, B. P.; Murakami, K., *Nature Mater.* **2006**, 5, 865.
14. Lin, Y.; Skaff, H.; Emrick, T.; Dinsmore, A. D.; Russell, T. P., *Science* **2003***, 299***,** 226.
15. Lin, Y.; Böker, A.; Skaff, H.; Cookson, D.; Dinsmore, A. D.; Emrick, T.; Russell, T.P., *Langmuir* **2005**, 21, 191.
16. Lin, Y.; Skaff, H.; Böker, A.; Dinsmore, A. D.; Emrick, T.; Russell, T. P., *J. Am. Chem. Soc.* **2003**, 125, 12690.
17. Russell, J. T.; Lin, Y.; Böker, A.; Su, L.; Carl, P.; Zettl, H.; He, J. B.; Sill, K.; Tangirala, R.; Emrick, T.; Littrell, K.; Thiyagarajan, P.; Cookson, D.; Fery, A.; Wang, Q.; Russell, T.P., *Angew. Chem. Int. Ed.* **2005**, 44, 2420.
18. Sleytr *et al. FEBS J.* **2007**, 274, 323.
19. Kutuzov, S.; He, J.; Tangirala, R.; Emrick,T.; Russell, T. P. ; Böker, A., *Phys. Chem. Chem. Phys*. **2007**, 9, 6351.
20. Voorn, D. J.; Ming, W.; van Herk, A. M., *Macromolecules* **2006**, 39, 2137.
21. Negrete-Herrera, N.; Putaux, J.L.; David, L.; Bourgeat-Lami, E., *Macromolecules* **2006**, 39*,* 9177.
22. Faucheu, J.; Gauthier, C.; Chazeau, L.; Cavaillea, J.Y.; Mellon ,V.; Bourgeat-Lami, E., *Polymer* **2010**, 51, 6.
23. Wang, T.; Colver, P.J.; Bon, S.A.F.; Keddie, J.L., *Soft Matter* **2009**, 5, 3842.
24. Cauvin,S.; Colver, P.J.; Bon, S.A.F., *Macromolecules* **2005**, 38*,* 7887.
25. Chen, T.; Bon, S.A.F., *Langmuir* **2007**, 23*,* 9527.
26. Colver, P.J., Bon, S.A.F., Langmuir **2007**, 23*,* 8316.

27. He, J; Niu, Z.; Tangirala, R.; Wang, J.Y.; Wei, X.; Kaur, G.; Wang, Q.; Jutz, G.; Böker, A.; Lee, B.; Pingali, S.-V.; Thiyagarajan, P.; Emrick, T.; Russel, T.P., *Langmuir* **2009**, 25, 4979.
28. Noble,P.F.; Cayre, O:J;, Alargova, R.G.; Velev, O.D.; Paunov, V.N., *J. Am. Chem. Soc.* **2004**, 126, 8092.
29. Madivala, B.; Vandebril, S.; Fransaer, J.; Vermant, J., *Soft Matter* **2009**, 5, 1717.
30. He, J.; Zhang, Q.; Gupta, S.; Thiyagarajan, P.; Emrick, T.; Russell, T. P. *Small* **2007**, 3, 1214.
31. Böker, A.; Lin, Y.; Chiapperini, K.; Horowitz, R.; Thompson, M.; Carreon, V.; Xu, T.;Abetz, V.; Skaff, H.; Dinsmore, A.D.; Emrick, T.; Russell, T. P., *Nat. Materials* **2004**, 3, 302.
32. Skaff, H.; Lin, Y.; Tangirala, R.; Breitenkamp, K.; Böker, A.; Russell, T. P.; Emrick, T., *Adv. Mater*. **2005**, 17, 2082.
33. Duan, H.; Wang, D.; Kurth, D.; Möhwald, H., *Angew. Chem Int. Ed*. **2005**, 43, 5639.
34. Duan, H.; Wang, D.; Sobal, N.; Giersig, M.; Kurth, D.; Möhwald, H., *Nano Lett.* **2005**, 5, 949.
35. Wang, D.; Duan, H.; Möhwald H., *Soft Matter* **2005**, 1, 412.
36. Reincke, F.; Hickey, S.G.; Kegel, W.K.; Vanmaekelbergh, D., *Angew. Chem. Int. Ed*. **2004**, 43, 458.
37. Aveyard, R.; Binks, B. P.; Clint, J. H., *Adv. Col. Int. Sci.* **2003**, 100, 503.
38. Carbone, L.; Nobile, C.; De Giorgi, M.; Sala, F. D.; Morello, G.; Pompa, P.; Hytch, M.; Snoeck, E.; Fiore, A.; Franchini, I. R.; Nadasan, M.; Silvestre, A. F.; Chiodo, L.; Kudera, S.; Cingolani, R.; Krahne, R.; Manna, L., *Nano Lett.* **2007,** 7, 2942.
39. Wang, R. K.; Reeves, R. D.; Ziegler, K. J., *J. Am. Chem. Soc.* **2007**, 129, 15124.
40. Bigioni, T. P.; Lin, X. M.; Nguyen, T. T.; Corwin, E. I.; Witten, T. A.; Jaeger, H.M., *Nat. Mater.* **2006**, 5, 265.
41. Ramsden, W., *Proc. R. Soc. London, Ser. A*, **1903**, 72, 156.
42. Walther, A.; Müller, A. H. E., *Soft Matter* **2008**, 4, 663.
43. Kilbinger, A.F.M., Wurm, F., *Angew. Chem. Int. Ed.* **2009**, 48, 8412.
44. Hong, L.; Jiang, S.; Granick, S., *Langmuir* **2006,** 22*,* 9495.
45. Hong, L.; Cacciuto, A.; Luijten, E.; Grannick, S., *Nano Lett.* **2006**, 6, 2510.
46. Walther, A.; Drechsler, M.; Rosenfeldt, S.; Harnau, L.; Ballauff, M.; Abetz, M.; Müller, A.H.E., *J. Am. Chem. Soc*. **2009**, 131, 4720.
47. Walther, A.; Drechsler, M.; Müller, A.H.E., *Soft Matter* **2009**, 5, 385.
48. Dendukuri, D.; Pregibon, D.; Collins, J.; Hatton, T.A.; Dolye, P.S., *Nat. Mater.* 2006, 5, 365.
49. Liu, Y.; Abetz, V; Müller, A. H. E, *Macromolecules* **2003**, 36, 7894.
50. Walther, A.; Göldel, A.; Müller, A. H. E., *Polymer* **2008**, 49, 3217.
51. Binks, B. P.; Fletcher, P. D. I., *Langmuir* **2001,** 17, 4708.
52. Nonomura, Y.; Komura, S.; Tsujii, K., *Langmuir* **2004,** 20, 11821.
53. Glaser, N.; Adams, D. J.; Böker, A.; Krausch, G., *Langmuir* **2006,** 22, 5227.

54. Kim, S.-H.; Lee, S. Y.; Yang, S.-M., *Angew. Chem. Int. Ed.* **2010**, 49, 2535.
55. Zheng, Z.; Nottbohm, C. T.; Turchanin, A.; Muzik, H.; Beyer, A.; Heilemann, M.; Sauer, M.; Gölzhäuser, A., *Angew. Chem. Int. Ed.* **2010**, 49, 8493 .
56. Walther, A.; André, X.; Drechsler, M.; Abetz, V.; Müller, A. H. E., *J. Am. Chem. Soc.* **2007,** 129,6187.
57. Walther, A.; Matussek, K.; Müller, A.H.E., *ACS Nano* **2008**, 2,1167.
58. Yan, L.-T.; Popp, N.;Ghosh, S.-K.; Böker, A., *ACS Nano* **2010**, 4,913.
59. Zhao, H.; Huang, B.; *J. Polym. Sci., Part B* **1998**, 36, 85.
60. Mackay, M. E.; Tuteja, A.; Duxbury, P. M.; Hawker, C. J.; Van Horn, B.; Guan, Z.; Chen, G., Krishnan, R. S., *Science* **2006**, 311, 1740.
61. Lewandowski, E. P.; Searson, P. C.; Stebe, K. J., *J. Phys. Chem. B* **2006**, 110, 4283.
62. He, J.; Zhang, Q.; Gupta, S.; Thiyagarajan, P.; Emrick, T.; Russell, T. P., *Small* **2007**, 3, 1214.
63. Binks, P. B., *Curr. Opin. Col. Int. Sci.* **2001**, 6, 17.
64. Xu, H.; Erhardt, R.; Abetz,V.; Müller, A.H.E.; Goedel, W. A., *Langmuir* **2001,** 17*,* 6787.
65. Chiranjeevi, P.; Graf, K.; Kressler, J., *Col. Polym. Sci.* **2006**, 285, 27.
66. Fainerman, V.B.; Makievski, A. V.; Miller, R., *Solids Surf. A* **1994**, 87, 61.
67. Basavaraj, M. G.; Fuller, G.G.; Fransaer, J.; Vermant, J., *Langmuir* **2006**, 22, 6605.
68. Dong, L.C.; Johnson, D.T., *Langmuir* **2005**, 21, 3838.

SUPPORTING INFORMATION
to

Janus Cylinders at Liquid-Liquid Interfaces

By Thomas M. Ruhland, André H. Gröschel, Andreas Walther and Axel H. E. Müller

1. TEM characterization of Janus cylinders at different sonication times.

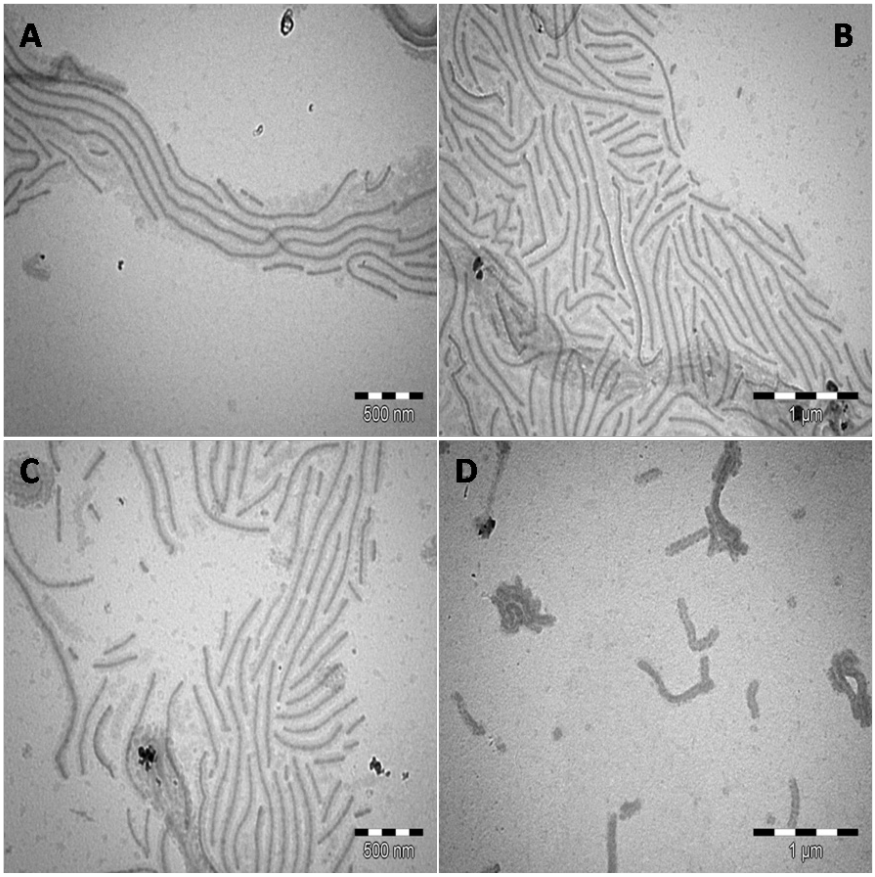

Figure 3-S1. Size evolution of Janus cylinder: TEM images obtained for different sonication times at 30% amplitude ((A) 0 min, (B) 5 min, (C) 15 min and (D) 35 min).

2. Reference system for pendant drop measurement

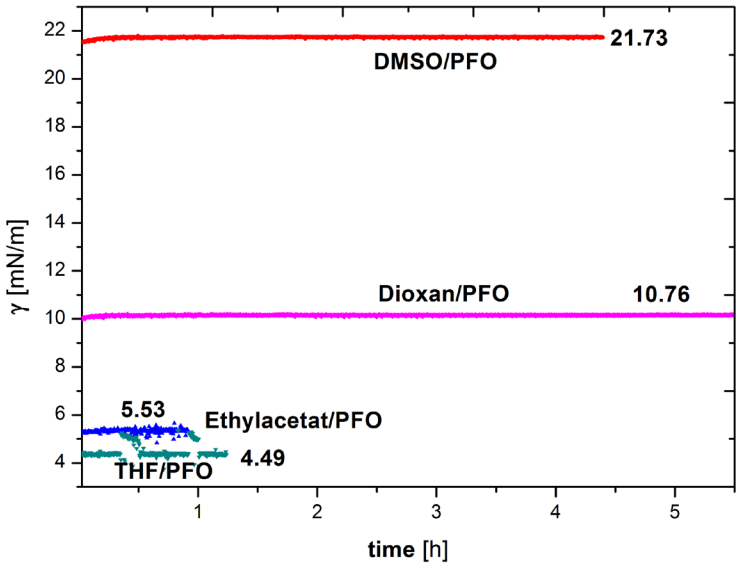

Figure 3-S2. Interfacial tension isotherms of four different systems.

3. TEM image of cylinders made from $S_{72}B_{26}^{100}$

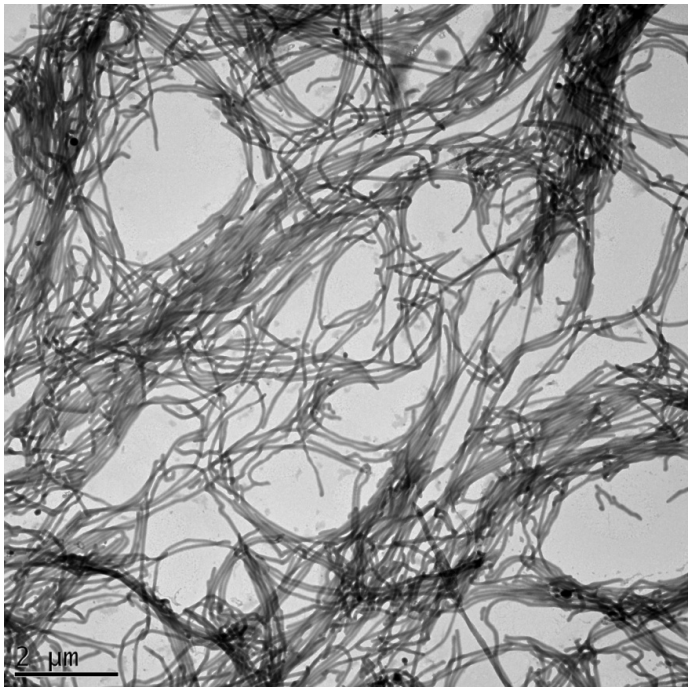

Figure 3-S3. 2500 nm long cylinders made from $S_{72}B_{26}^{100}$.

4. Concentration dependence of the adsorption behavior of differently-sized Janus cylinders at liquid/liquid interfaces in two different solvent systems.

Figure 4 A illustrates a decrease from 7.8 mN/m to 5.9 mN/m and from 8.9 mN/m to 7.2 mN/m for a concentration increase of long and short Janus cylinders (Fig. 4 B). The logarithmic plots in Figure 4 show the different stages of adsorption of the cylinders assembly as they manifest in regions of different slopes. For 2300 nm as well as for 350 nm cylinders, all concentrations investigated reached a plateau value in the final stage. For the short Janus cylinder more desorption than for the long Janus cylinders occurs, leading to a longer time necessary to reach the plateau value. To further verify the influence of the length, we also recorded the correlation between γ (t) and the concentration of Janus cylinders at the DMSO/PFO interface (Figure 4 E-H). The same tendency as for the PFO/dioxane system can be observed, thus corroborating the observations and demonstrating a robust behavior.

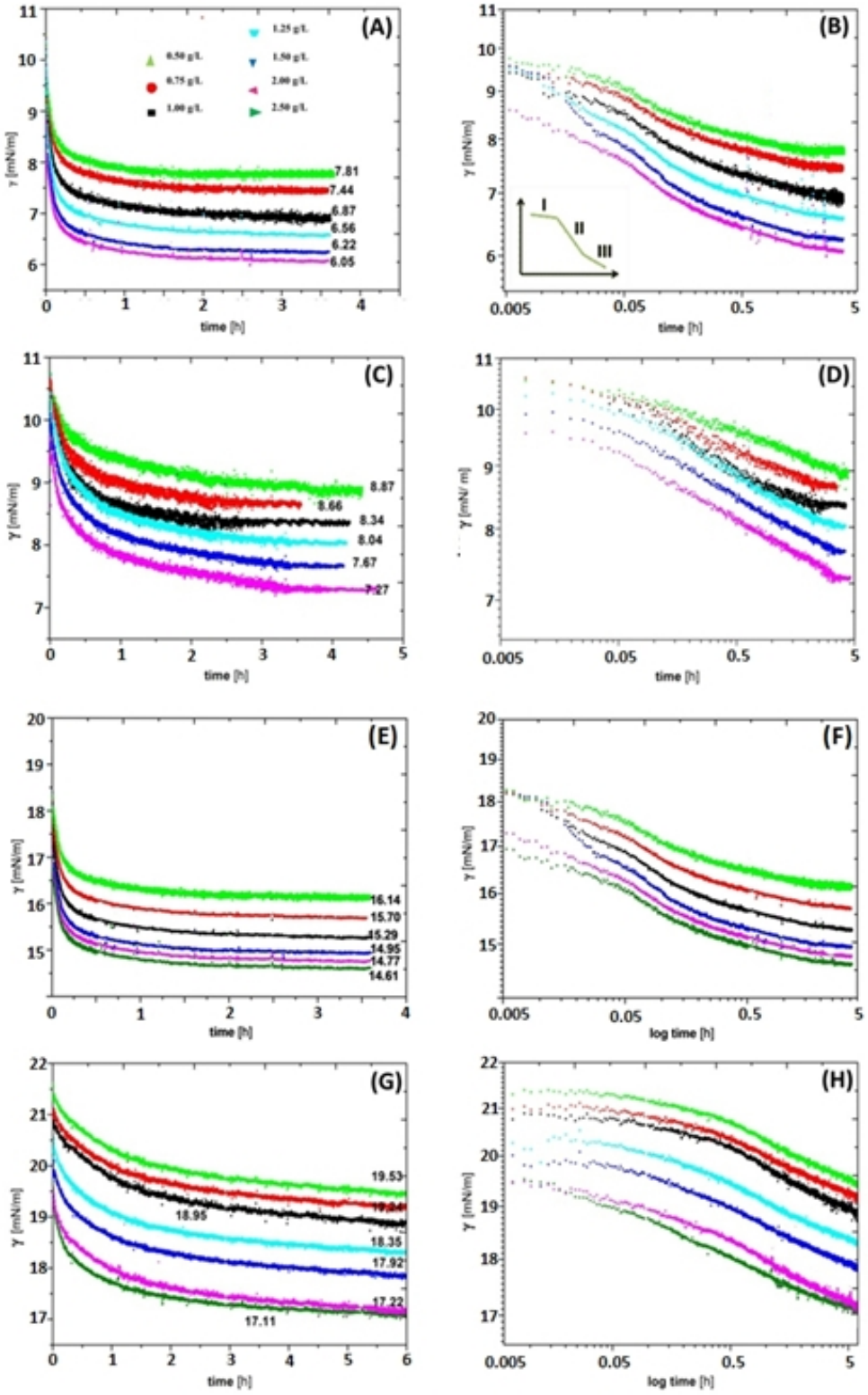

Figure 3-S4. Concentration dependence of the adsorption behavior of differently-sized Janus cylinders at liquid/liquid interfaces in two different solvent systems. Time dependence of γ (t) with (A, B) 2300 nm and (C, D) with 350 nm Janus cylinders in dioxane at various concentrations and the logarithm representation of data (B, D). Time dependence of γ (t) with (E, F) 2300 nm and (G, H) with 350 nm Janus cylinders in DMSO at various concentrations and the logarithmic representation of data (F, H).

Chapter 4

Influence of Janus Particle Shape on their Interfacial Behavior at Liquid-Liquid Interfaces

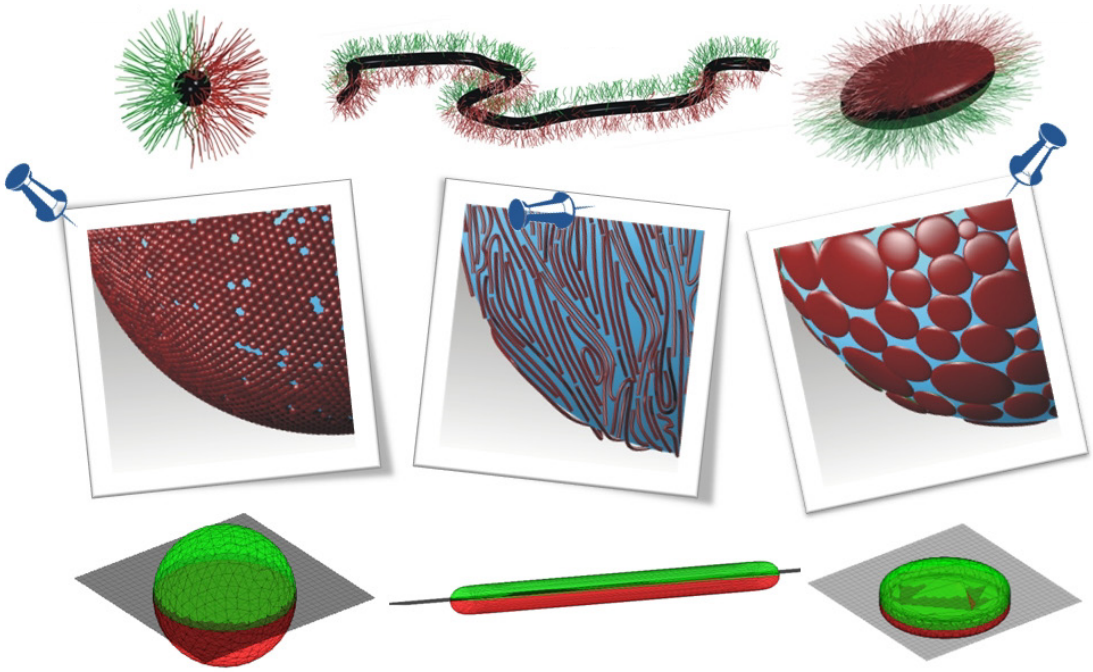

This work is published in *Langmuir* **2013**, 29 (5), 1388-1394 under the title:

"Influence of Janus Particle Shape on their Interfacial Behavior at Liquid-Liquid Interfaces"

by Thomas M. Ruhland, André H. Gröschel, Nicholas Ballard, Thomas S. Skehlon, , Andreas Walther, Axel H. E. Müller and Stefan A. F. Bon*

Influence of Janus Particle Shape on their Interfacial Behavior at Liquid-Liquid Interfaces

Thomas M. Ruhland[1], André H. Gröschel[1], Nicholas Ballard[2], Thomas S. Skelhon[2], Andreas Walther[3], Axel H. E. Müller[1] and Stefan A. F. Bon[2]*

[1] Department of Macromolecular Chemistry II, University Bayreuth, Germany

[2] Department of Chemistry, University of Warwick, Coventry CV4 7AL, United Kingdom

[3] DWI at the RWTH Aachen, RWTH Aachen University, 52506 Aachen, Germany

E: s.bon@warwick.ac.uk, W: www.bonlab.info

Abstract

We investigate the self-assembly behavior of Janus particles with different geometries at a liquid-liquid interface. The Janus particles we focus on are characterized by a phase-separation along their major axis into two hemicylinders of different wettability. We present a combination of experimental and simulation data together with detailed studies elucidating the mechanisms governing the adsorption process of Janus spheres, Janus cylinders and Janus discs. Using the pendant drop technique, we monitor the assembly kinetics following changes in the interfacial tension of nanoparticle adsorption. According to the evolution of the interfacial tension and simulation data we will specify the characteristics of early to late stages of the Janus particle adsorption and discuss the effect of Janus particle shape and geometry. The adsorption is characterized by three adsorption stages which are based on the different assembly kinetics and different adsorption mechanism depending on the particle shape.

KEYWORDS: Janus Particle, Janus Sphere, Janus Cylinder, Janus Disc, Liquid-Liquid Interface, Self-Assembly, Adsorption, Interfacial Tension, Pickering Stabilization

Introduction

One of the most promising research topics in nanotechnology is the bottom-up design of materials *via* spontaneous self-assembly of desired building blocks. Over the past decades, there have been reports on the self-assembly of a variety of nano-sized objects such as nanoparticles, nanorods, or nanosheets.[1] As a unique type of building block, anisotropic particles, such as patchy, multicompartment or Janus particles, have attracted significant interest.[2-5] Over the course of the last few years in particular Janus particles, named after the double-faced Roman god, have evolved as a very interesting class of very complex internal colloidal structures among micron- or nanosized particles[6,7] and therefore have attracted much attention from both industrial and academic areas due to their potential applications in emulsions[8,9], materials engineering[10-12], nanoscience[13], chemical and biological sensors[14-20], drug delivery and self-assembly[21-24]. To date, an exciting variety of synthesis methods, assembled structures and applications are under development with a special focus on polymeric Janus particles.[6,25-27]

Polymeric Janus particles can be divided into several classes according to their architecture and dimensionality. In particular much attention has been devoted to spherical Janus particles (3D). In contrast, the challenging synthesis of non-spherical Janus particles such as cylinders (1D) and disc-like particles (2D), has so far limited the possibilities for a comprehensive understanding of their properties. Thus far, only the controlled crosslinking of microphase-segregated structures of block terpolymers is able to produce nano-sized Janus spheres, Janus cylinders and discs on the multigram scale.[25,28-33] Due to this synthetic advantage the question of understanding their solution and interfacial behavior needs to be answered to find a way to produce new and more efficient materials.

As a result of their noncentrosymmetric architecture Janus particles can combine amphiphilicity known from classical surfactants with the Pickering character that strongly holds solid particles at interfaces. These synergetic properties are not accessible for their homogeneous analogues. Their superior affinity toward interfaces and their significantly enhanced reduction of interfacial tension as compared to particles with a isotopic chemical makeup[34-36] raises enormous interest for many technologically relevant real prototype applications as future surfactants and for nanostructuring of interfaces.[26,37,38]

At the beginning of the last century, Pickering and Ramsden discovered the stabilizing effect of particles in emulsions[39,40], which was followed by the theoretical description of this effect by Pieranski[41]. Nanoparticle adsorption to fluid interfaces has been studied from a fundamental standpoint and exploited in applications[42-48]. Consequently, there is an enormous potential to assemble anisotropic particles as well as Janus particles or anisotropic Janus particles at fluid interfaces. By now, intensive work has been carried out to observe and understand the extraordinarily high adsorption strength of Janus particles at fluid interfaces, driven by the reduction in interfacial energy and the stabilization of liquid-liquid interfaces. In the following, several theoretical and practical studies have been performed to predict Janus particle behavior at liquid–liquid interfaces after Binks and Fletcher's calculations of interfacial adsorption capabilities of biphasic Janus spheres predicted an up to three fold stronger adsorption as compared to particles of uniform wettability. [49-55] Additional studies have suggested that the geometry such as their size, aspect ratio, form and shape as well as the surface properties of Janus particles play a significant role to their surface activity, particle orientation and packing geometry.[34,35, ,56-61] Understanding the effect of Janus particles at fluid interfaces will be critical to find special design criteria for an efficient industrial use of Janus particles. Until now, the importance of controlling the particle shape and form is not so well understood. Non-spherical nanoparticles behave differently at the interfaces due to their shape and they can show interesting structures and orientation at interfaces[62-65]. The geometry of the particle is a very important factor which governs the adsorbed position. Apart from the interfacial energies, the role of particle size and form and the surface structure are paramount to the gain in the total interfacial energy of the system. Shape is an important parameter in controlling the maximum packing density and therefore, the surface properties of armored emulsion droplets. The geometry of particles strongly affects their physical properties. Unfortunately, most theoretical work has focused on understanding the behavior of spherical Janus particles, such as their equilibrium orientation, at fluid-fluid interfaces.[49,50,52-54,60,66]

In this article, we present a systematic study on the influence of geometry and shape of polymeric Janus particles on their surface activity and their orientation at a fluid-fluid interface. A combination of simulations and experiments is used to understand in more detail what happens at a toluene-water interface. The effect of Janus cylinders and Janus discs on the interfacial tension of liquid-liquid interfaces (oil/water) was already

highlighted before *via* the characterization of the time - time-dependent evolution of the interfacial tensions.[29,34] The Janus particles show a distinct and significant decrease of the interfacial tension as compared to their linear uncrosslinked block terpolymer precursors. But now we will deduce the effect of different geometries (spheres, cylinders and discs) on the structures formed at the interface in a direct comparison of these three particle shapes in the same experimental set up for a better understanding of the behavior of Janus particles at liquid-liquid interfaces in order to understand their behavior in more detail and to find the best fields of applications, e.g. as future surfactants. This investigation demonstrates the important role of the particle geometry in the interfacial assembly of the particles.

Experimental Section

Materials.

All chemicals (p.a. grade) were purchased from Aldrich.

Synthesis

Concerning a high control of the particle shape and size, an unique approach based on the self-organization of triblock terpolymers plays a significant role. The synthetic pathway to obtain Janus particles is based on a template-assisted synthesis, involving crosslinking of a bulk film of block terpolymers and a subsequent sonication treatment following the procedure described in the literature.[29,32,67]

Scheme 4-1. Overview of possible Janus particle architectures. (A) Spheres, (B) cylinders and (C) discs.

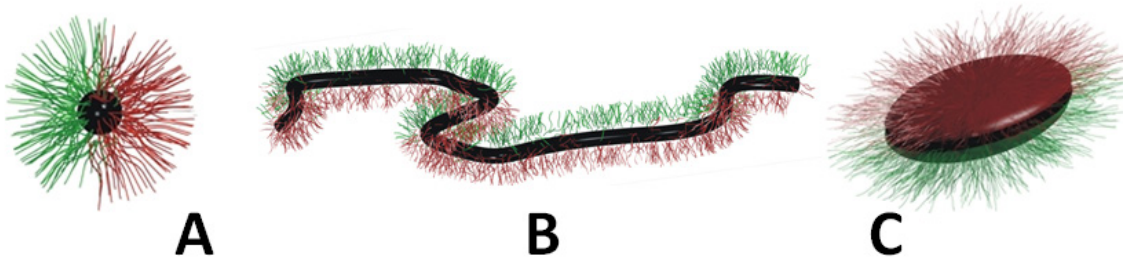

All polymers used in this paper were synthesized as well as completely characterized in former studies.[67,68,28,29,30,34] The subscripts denote the mass fraction in percent as calculated from the ^{1}H-NMR spectrum, and the superscript gives the number-average molecular weight in kg/mol. The two polystyrene-block-polybutadiene-block-poly(methyl methacrylate) block terpolymers $S_{41}B_{14}M_{45}^{110}$ (SBM-1, PDI = 1.01) and $S_{44}B_{8}M_{48}^{183}$ (SBM-2 PDI = 1.05) and the polystyrene-block-polybutadiene-block-poly(*tert*-butylacrylate) block terpolymer $S_{42}B_{10}T_{48}^{133}$ (SBT, PDI = 1.06) used in this study were synthesized *via* sequential anionic polymerization in tetrahydrofuran (THF) (Table 4-1).

Table 4-1. Correlation of the block terpolymer precursor and the resulting Janus particles (Scheme 4-1).

Block terpolymer precursor	Janus particle
$\mathbf{S_{41}B_{14}M_{45}^{110}}$	Janus cylinders
$\mathbf{S_{44}B_{8}M_{48}^{183}}$	Janus spheres
$\mathbf{S_{42}B_{10}T_{48}^{133}}$	Janus discs

Characterization.

Pendant Drop Tensiometer isotherms of the interfacial tension at the toluene/water interface were measured on a Krüss DSA100 tensiometer at room temperature. The setup of the pendant drop apparatus is shown elsewhere.[69] Computer automation allowed rapid acquisition of the drop image, edge detection, and fitting of the Laplace–Young equation to determine the interfacial tension. We performed the measurements with a degassed MilliQ-water droplet saturated with toluene immersed in a toluene solution of the Janus particles saturated with water.

Bright-field TEM was performed on Zeiss CEM 902 and LEO 922 OMEGA electron microscopes operated at 80 kV and 200 kV, respectively. Data evaluation and processing was carried out with Soft Imaging Viewer, Digital Micrograph 365 Demo software and ImageJ.

Free Energy Simulations of Janus particles at a toluene/water interface.

To have a closer look into the adsorption mechanism and particle orientations at the interface, we used a calculation of the free energy profile of a particle orientation in respect to the toluene/water interface in the same way as we already reported.[65] Briefly, we define mathematically the shape of a superellipsoid by

$$\left(\frac{x^{2/n_2}}{r_x}+\frac{y^{2/n_2}}{r_y}\right)^{n_2/n_1}+\frac{z^{2/n_1}}{r_z}=1$$

Where x, y, and z are Cartesian coordinates. r_x, r_y, and r_z are the particles x, y, and z radii respectively. n_1 and n_2 act as the "squareness" parameters in the z axis and the x-y plane respectively, with $0 < n_1, n_2 < \infty$. The particle is constructed from a series of point that satisfy the above equation using a triangular tessellation scheme that connects the points to create a surface. The free energy of adhesion (ΔG_{ad}) for the particle at the interface is calculated similarly to the method used by Pieranski at a series of rotations and translations through the interface from the equation

$$\Delta G_{ad}=\sum_P A_{P1}\gamma_{P1}+\sum_P A_{P2}\gamma_{P2}-A_{12}\gamma_{P12}$$

Where A represents area and γ the interfacial tension and the subscripts $P1$, $P2$ and $P12$ correspond to the polymer phases in liquid 1 the polymer phases in liquid 2 and the liquid liquid interface. The values of the areas are calculated by simply summing the area of triangles of the PMMA or PS phase in the corresponding liquid phase. We accurately describe the areas by subdividing any triangles that lie at the interface as described in Dijkstra *et al.*.[70] The axis of rotation is along the z axis and is performed in the xy-plane. The translation through the interface is described by a parameter Z that is given by z_{int}/R_{bound} where z_{int} is the distance from the centre of the particle to the liquid liquid interface and R_{bound} is the minimum radius of a sphere that contains all the points given by the equation for a superellipsoid (where Z=1 the particle resides in the upper liquid phase, where Z = -1 the particle resides in the lower liquid phase). For our simulations we use the data presented in the supporting information Table 4-S1/2.

Results and discussion

We synthesized three Janus particles with different geometries to isolate the role of shape in the interfacial assembly process. To establish the effect of the Janus character together with the effect of particle shape on the interfacial activity and orientation of the Janus particles at an oil-water interface, we study the influence of Janus spheres, Janus cylinders and Janus discs, trapped at a toluene/water interface, on the interfacial tension of the system. The geometries of Janus particles used in this study are shown in scheme 4-1. Additionally, to understand in more detail what happens at the interface we present simulations about the orientation of the different shaped particles at the liquid-liquid interface to show how geometry influences the strength of the particle adsorption. In order to compare the influence of the geometry all types of Janus particles were investigated in the same solvent system and under the same conditions.

In pendant drop tensiometry the interfacial tension γ between two immiscible fluids is measured by imaging a pendant droplet of one fluid phase immersed in the second one. The drop profile is automatically detected and fitted with the Young-Laplace equation, extracting the value of γ. An initially relatively high interfacial tension between to completely immiscible fluids is additionally beneficial to produce a large driving force for the particles to assemble at the interface. In our case water droplets are formed in toluene which contains the dissolved Janus particles and the interfacial tension is measured as a function of time. Adsorption of particles at the liquid–liquid interface lowers the system free energy which translates into an effective interfacial tension reduction, therefore by monitoring γ as a function of time we can obtain information about the adsorption kinetics. For the chosen toluene/water interface the determined interfacial tension of the pristine system (34 mN/m) agrees well with the literature value (Supporting Information, Figure 4-S1).[71]

We first studied time-dependent measurements at the toluene/water interface for Janus spheres, Janus discs and Janus cylinder dissolved in toluene at a concentration of 1 g/L. Figure 4-1 presents the dynamic surface tension plots and the logarithmic representation of these values, where the interfacial tension decreases with time, approaching an quasi - equilibrium value.

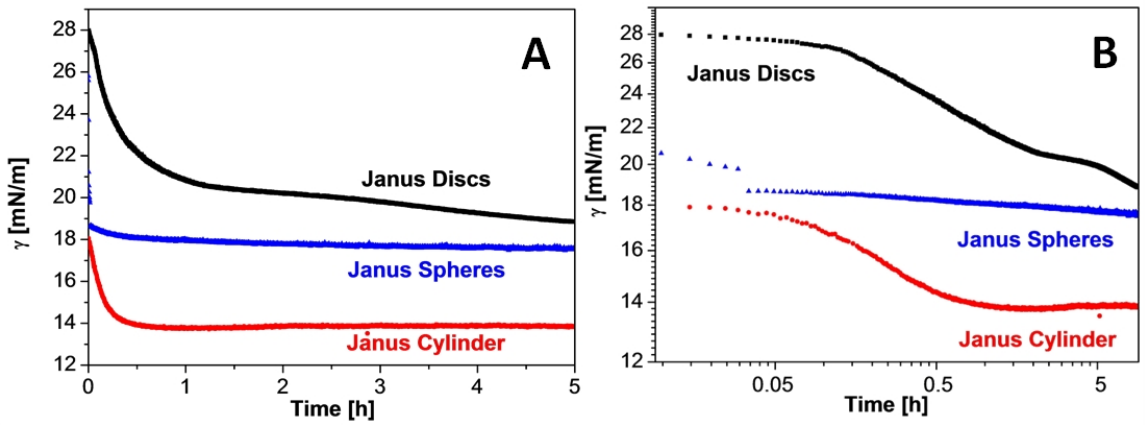

Figure 4-1. Influence of the Janus particle shape on the interfacial tension. (A) Interfacial tension isotherms of solutions of Janus particles in toluene at a water/toluene interface. (B) Logarithmic representation of the data in (A).

For all particles in the early stages, the interfacial tension drops rapidly because of instantaneous assembly of the particles at the interface, then the decrease in interfacial tension slows down and once the droplet is mostly covered, the decrease in interfacial tension reaches a quasi - equilibrium. After reaching the plateau value, the Janus particles are located and arranged at the interface. A change in shape of the Janus particles leads to a different adsorption behavior at the interface. We observe different adsorption dynamics for spheres, cylinders and discs.

The addition of Janus cylinder results in the maximum reduction in the equilibrium interfacial tension. After the addition the interfacial tension between toluene and water is decreased from 34 mN/m to ca. 14 mN/m. In comparison, Janus spheres show a moderately lower surface activity with an intermediate γ_∞ value of ca. 17.5 mN/m. Janus discs provide the smallest amount of effective interfacial tension reduction. The interfacial tensions decreases from 34 mN/m to ca. 19 mN/m. In the case of Janus discs, in addition to a similar trend of adsorption, we observed an additional behavior. The interfacial tension first decreased rapidly, but not so fast as for Janus spheres or Janus cylinders, but slowed down for an extended period of time and finally slowly decreased again until the interfacial tension reached an equilibrium value. After 2h the interfacial tension reached a plateau around 20.5 mN/m. The next transition occurred after 2 ½ h, whereupon the interfacial tension further decreased to an equilibrium interfacial tension (~19 mN/m). This behavior was only observed for the disc-shaped Janus particles, which clearly points towards a change in the packing of the Janus discs at the interface with time due to the anisotropic shape. Furthermore, this indicates that the concentration of particles

trapped at the interface influences the packing of Janus discs in a way that is different from Janus spheres, where only a simple decay was observed.

Comparison and explanation of different adsorption behavior

One reason for the different adsorption kinetics is the size of the Janus particles. The Janus spheres are 50 nm in diameter, whereas the cylinders have a length of 2300 nm and the discs are around 300 nm (supporting information, Figure 4-S1). Smaller sizes lead to higher diffusion coefficients (Brownian behavior) and thus faster adsorption kinetics. A faster diffusion may also contribute to the lower values of the quasi-equilibrium state as the further minimization in this stage is collision-controlled in contrast to diffusion control in the early stages. Thus, the Janus spheres show a very fast adsorption behavior in the early stages of the process which is completely different to the ones for discs and cylinders. Janus cylinders and Janus discs show slower adsorption kinetics, but show a similar initial drop in interfacial tension. Both are highly anisotropic particles and have two length scales, thickness h and lateral size. A cluster of amphiphilic discs trapped at the interface is equivalent to a closed packing of amphiphilic spheres but without the interstitial space between the different domains filled. Furthermore, domains built up with larger and smaller discs in diameter result in larger interstitial spaces compared with domains with monodisperse spheres. Upon adsorption, Janus cylinders show differences in their structure when compared with those of spherical ones. Probably, this is due to the fact that cylindrical particles can easily slide along their long axis and built up more dense domains. All results confirm our experimental observation that all Janus particles demonstrate significantly enhanced surface activity but possess different adsorption kinetics resulting from differences in interface stabilization. The ability for stabilization slightly decreases from Janus cylinders to Janus spheres to Janus discs. In order to further understand the absorption behavior and kinetics of Janus particles at liquid-liquid interfaces we simulated the free energy change upon adsorption of the various types of Janus particles used in this work.

Simulations

Based on the energy profiles it can generally be seen that Janus particle adsorption is effectively irreversible (Figure 4-2 A). All calculation are based on the particle dimensions mentioned in Table 4-S1 and 4-S2 representing values determined *via* TEM, DLS and AFM. Measurements with the pendant drop tensiometer result in a global

interfacial tension which is a function of the packing of the particles and the energy calculated here. In principal, large lateral sized particles offer strong adsorption towards the interface, preventing its removal. Thus, particles with a large cross-sectional area can be strongly adsorbed to the interface. That is the reason for the different energy landscapes of Janus spheres, Janus cylinders, and Janus discs. Based on calculated data, we find a favored orientation of polystyrene (PS) to the toluene phase and the poly(methyl methacrylate) (PMMA) side chains to the water phase (Figure 4-2 B).

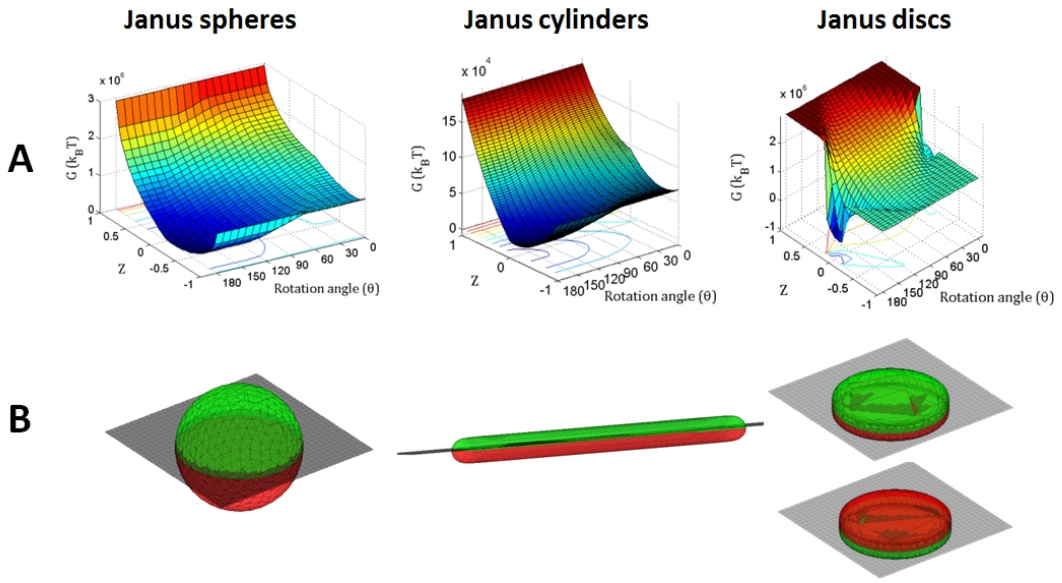

Figure 4-2. (A) Energy profiles for Janus spheres, Janus cylinders and Janus discs at toluene/water interface. **(B)** Shape dependent equilibrium position of Janus particles at toluene (bottom phase) and water (top phase) interface. PS is red labelled and PMMA is green labeled.

The energy profile of an isolated Janus sphere at the toluene/water interface indicates one energy minimum with the PS in the toluene phase and the PMMA sitting predominantly in the aqueous phase. The energy barrier for the removal from the interface is ~5×10^4 kT. In comparison, the energy profile of Janus discs indicates two energy minima and therefore predicts the existence of two different orientations of the Janus discs at the toluene/water interface. In the first orientation, the global minimum, the discs are immersed in the toluene phase with their PMMA side just protruding into the aqueous phase and in the other they are lying in a upside down with respect to the global minimum, that is with the PS phase just protruding into the aqueous phase. The energy barrier for removal from the global minimum is ~1.5×10^6 kT whereas the energy barrier for removal of the second local energy minimum is 5×10^5 kT. Janus cylinders have one energy global minimum. The energy necessary to remove a cylindrical shaped Janus

particle from its equilibrium position at the oil-water interface along is defined as 1×10^6 kT. Janus cylinders are expected to lie with the PS in the toluene phase and the PMMA in the aqueous part and remain oriented parallel to the interface.

Based on the experimental data and these simulation results we can describe the fundamental aspects of Janus particle adsorption and kinetics at liquid - liquid interfaces.

Mechanism of Janus particle adsorption

As previously mentioned, all particles exhibit different kinetic behaviors due to a different adsorption and packing behavior. Minimal changes in the geometry directly influence the interfacial behavior. The variation in interfacial tension with different particles can be explained by the effect of their geometry on their assembly at the oil/water interface. We now will discuss the fundamental mechanism for each particle geometry in more detail. Additionally, for simplicity we try to come up with a schematically presentation of the different adsorption stages during the adsorption process explaining the adsorption mechanism described below (Scheme 4-2).

Janus spheres

The Janus spheres show a homogenous size distribution with 50 nm in diameter (Figure 4-S1 A). First, the interfacial tension rapidly decreases due to fast Brownian diffusion and adhesion of isolated spheres to the interface (Scheme 4-2 A-I). Subsequently, the decrease in interfacial tension slows down dramatically, as the fraction of unoccupied toluene-water interface is becomes limited preventing successful adhesion upon collision. The particles at the interface pack closer into ordered domains, the domains consist of well-separated and highly ordered individual spheres (Scheme 4-2 A-II), and, finally, minimal packing issues start to dominate and a small decrease in interfacial tension occurs until the assembly attains a quasi – equilibrium. Under these conditions the maximum coverage of the interface with spheres is reached (Scheme 4-2 A-III). The packing of the spheres at the interface is nearly perfect and in the end, only minimal changes and rearrangements of single spheres take place in order to get the maximal possible packing. As a result of this the logarithmic presentation of the interfacial values over time (Figure 4-1 B and Figure 4-S3 C) show two stages, a fast decrease in the interfacial tension as a result of diffusion controlled collision of the particles to the interface and a second slow decrease due to increased packing density and collision controlled adsorption.

Scheme 4-2. Schematic representation of the packing behavior of the Janus particles at the toluene/water interface during the adsorption process. The most typical adsorption stages pointed out for (A) Janus spheres, (B) Janus discs and (C) Janus cylinders. The Janus particles are simplified for a better illustration of their position at the liquid - liquid interface (Scheme 4-S1).

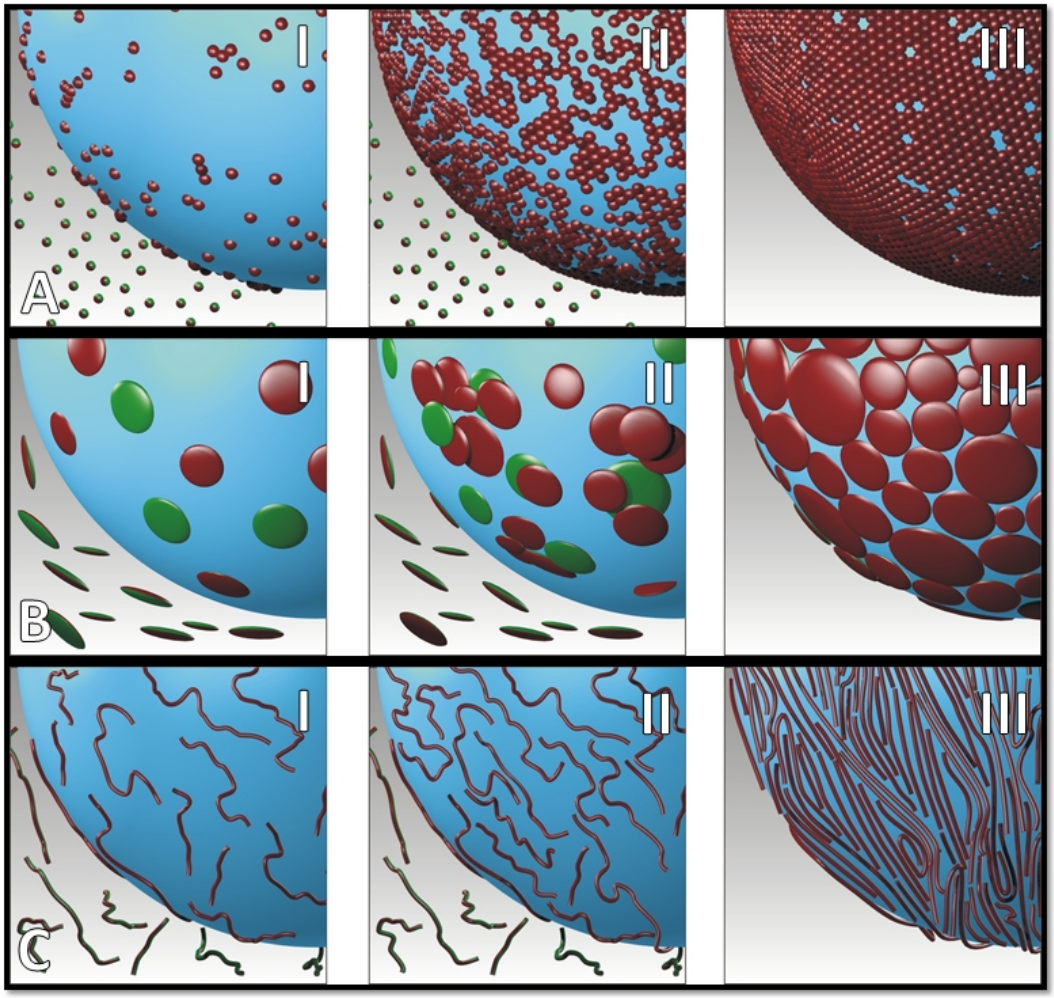

Janus discs

The Janus discs possess a broad size distribution, which is typically obtained at short sonication times. It contains a fraction of relatively large Janus discs with a diameter of 350 nm and fraction of smaller ones with a diameter around 250 nm (Figure 4-S1 B). Scheme 4-2 B illustrates the adsorption process for the Janus discs which shows significant differences in comparison to the adsorption of Janus spheres and discs.

Simulation results have suggested that Janus discs of the type used experimentally here have two energy minima at liquid - liquid interfaces. In the early stages of adsorption the adhesion of the Janus discs to the interface is diffusion controlled and the orientation of the Janus discs upon approach is likely to be random resulting in a roughly bimodal distribution of the two orientations of the particles at the interface (Scheme 4-2 B-I).

Exchange between the two orientations and/or removal of the particles in the secondary energy minimum from the interface is unlikely at short timescales because of the large energy involved in the transition. Therefore there will exist a large proportion of the less energetically favourable orientation in the initial stages and the global interfacial tension value is likely to decrease to a lesser extent that in the cases of Janus spheres or cylinders. This indeed is clearly observed in Figure 4-1.

As the packing density increases, leading to monolayer rafts of aggregated and packed discs and reaches a maximum the value of $\gamma(t)$ reaches a plateau after 2.0 h (Scheme 4-2 B-II). These dense aggregates collide at their edges and "touch" each other. The collision of the edges can lead to a partial overlap. As thinking analogy compare these rafts with the earths tectonic plates. Movement can cause ridges and trenches which potentially can lead to the formation of a bilayer of discs and/or desorption of discs. Discs with their orientation corresponding to the secondary minimum are more likely to desorb. In contrast to the case of a particle with a single energy minima re-adsorption of particles into the lower global energy minima results in a net lowering of the global interfacial tension and hence a period of slow decline in the global interfacial tension occurs corresponding to the slow re-orientation of particles into the more favored orientation assuming an optimal packing at the interface to avoid edge to edge overlapping or tilted orientations. As a second possibility, discs with the polystyrene phase exposed to the water phase can be covered up through adhesion of a particle on top in the correct conformation. This is an additional point explaining slow dynamics as adhesion of the second must be kinetically slower as collision needs to find a disc with the wrong side up already.

At a given point, particle rearrangements are no longer possible, no free space is left at the interface and a monolayer system is build up (Scheme 4-2 B-III). Additionally, it is known according to the theory of Nonomura *et al.*[53] that the largest discs adsorb most strongly. Thus, the polydispersity can be another issue in the adsorption process.

Janus cylinders

Ruhland *et al.* already presented detailed studies of the interfacial self-assembly of slightly amphiphilic 2300 nm long Janus cylinders (Figure 4-S1 C) in a recent work.[34] All results found for particles at a PFO/Dioxane and a PFO/DMSO interface can be transferred and confirmed using a toluene/water interface. The interfacial tension

decreases with time and the adsorption process is characterized by three different adsorption stages. In the beginning, free diffusion to the interface occurs (Scheme 4-2 C-I), followed by continuous adsorption of cylinders including ordering and domain formation at the interface (Scheme 4-2 C-II). Finally, additional packing leads to a rearrangement of the domains and to the formation of a multilayer system. The cylinders show a liquid crystalline like short-range correlation at the fluid interfaces (Scheme 4-2 C-III). The logarithmic data points towards a more gradual transition from stage I to II as it can be seen for spheres (Figure 4-S3 D). This suggests that the structural rearrangements in the monolayers containing cylindrical particles differ from the case of spheres. In the second stage of adsorption domains with both tip-tip and side-side contacts can be found. Upon adsorption, monolayers show differences in their structure when compared with those of spherical ones. Probably, this is due to the fact that cylindrical particles can easily slide along their long axis, whereas translation in the perpendicular direction and rotation are restricted. The Janus cylinders remain oriented parallel to the interface and their flexibility allows anchoring of a second, loosely bound Janus cylinder. Furthermore, the particles pack more densely due to in-plane and out-of-plane rearrangements. The local ordering leads to a better packing because of excluded volume interactions, which will increase with increasing aspect ratio.

Conclusion

We have studied the behavior of slightly amphiphilic Janus particles at a liquid-liquid toluene/water interface. The mechanism of particle adsorption was investigated in detail using time dependent measurements of the interfacial tension *via* a pendant drop tensiometer. The differences in the reduction of interfacial tension were attributed to enhanced adsorption of Janus particles at the oil–water interface under the influence of different geometries of the Janus particles. Janus spheres, Janus cylinders and Janus discs show significantly enhanced surface activity as compared to homogeneous particles as shown in previous studies. One interesting point is if the particle geometry and shape plays a crucial role in the interfacial behavior or not. These studies demonstrate based on experiments and simulations that changes in the geometry of the particles strongly influence the stabilizing of the liquid - liquid interface. As the shape changes from spheres to discs and cylinders, you can find different adsorption kinetics, different packing behaviors, different energy barriers and finally different equilibrium values for

the interfacial tension. Notably, the dynamic interfacial behaviors of the particles are governed by the packing behavior at the interface, which set the energy barrier for their adsorption. The interfacial tension depends not only on length, concentration of the particles, but also on their form and shape and on the packing behavior of the Janus particles. Based on that, the adsorption behavior is characterized by different adsorption steps, which show similar trends but differ in detail. The combination of experimental data and modeling results lends itself to the discussion of several interesting issues. It is a noteworthy fact that our very simple simulation approach explains several qualitative features of our experiments. Given the important role that the interfacial assembly of particles plays in the formation and stability of droplets, these studies provide useful guidelines for designing particles for interfacial stabilization.

Acknowledgment

This work was supported by DFG within SFB 840 (project A1). The authors thank André H. Gröschel for his help with the schemes and Dr. Andreas Walther for providing the Janus discs and for fruitful discussions. Thomas Ruhland thanks the Bavarian Elite Support Program (ENB) for a scholarship.

Author information

Corresponding author: Dr. ir. Stefan Bon
*E-mail: S.Bon@warwick.ac.uk

Supporting Information

Figures 4-S1-S3, Scheme 4-S1 and Tables 4S1-S2. This material is available free of charge *via* the Internet at http://pubs.acs.org.

References

1. Glotzer, S. C.; Solomon, M. J., *Nat. Mater.* **2007,** 6, 557.
2. Loget, G.; Kuhn, A., *J. Mater. Chem.* **2012**, 22, 15457.
3. Chen, Q.; Yan, J.; Zhang, J.; Bae, S. C.; Granick, S., *Langmuir* **2012,** 28, 13555.
4. Du, J.; O'Reilly, R. K., *Chem. Soc. Rev.* **2011**, 40, 2402.
5. Hu, J.; Zhou, S.; Sun, Y.; Fang, X.; Wu, L., *Chem. Soc. Rev.* **2012**, 41, 4356.
6. Walther, A.; Müller, A. H. E., *Soft Matter* **2008,** 4, 663.
7. Hong, L.; Jiang, S.; Granick, S., *Langmuir* **2006,** 22, 9495.
8. Walther, A.; Hoffmann, M.; Müller, A. H. E., *Angew. Chem. Int. Ed.* **2008,** 47, 711.
9. Kim, J.-W.; Lee, D.; Shum, H. C.; Weitz, D. A., *Adv.Mater.* **2008,** 20, 3239.
10. Perro, A.; Reculusa, S.; Ravaine, S.; Bourgeat-Lami, E.; Duguet, E., *J. Mater. Chem.* **2005,** 15, 3745.
11. Vanakaras, A. G., *Langmuir* **2005,** 22, 88.
12. Erb, R. M.; Jenness, N. J.; Clark, R. L.; Yellen, B. B., *Adv. Mater.* **2009,** 21, 4825.
13. de Gennes, P.-G., *Angew. Chem. Inter. Ed.* **1992,** 31, 842.
14. Faria, J.; Ruiz, M. P.; Resasco, D. E., *Adv. Synth. Catal.* **2010** *352*, 2359.
15. Yin, S.-N.; Wang, C.-F.; Yu, Z.-Y.; Wang, J.; Liu, S.-S.; Chen, S., *Adv. Mater.* **2011**, 23, 2915.
16. Behrend, C. J.; Anker, J. N.; Kopelman, R., *Appl. Physi. Lett.* **2004,** 84, 154.
17. Behrend, C. J.; Anker, J. N.; McNaughton, B. H.; Brasuel, M.; Philbert, M. A.; Kopelman, R., *J. Phys. Chem. B* **2004,** 108, 10408.
18. Kaufmann, T.; Gokmen, M. T.; Wendeln, C.; Schneiders, M.; Rinnen, S.; Arlinghaus, H. F.; Bon, S. A. F.; Du Prez, F. E.; Ravoo, B. J., *Adv. Mater.* **2011**, 23, 79.
19. Kretzschmar, I.; Song, J. H., *Curr. Opin. Colloid Interface Sci.* 2011, 16, 84.
20. Nisisako, T.; Torii, T.; Takahashi, T.; Takizawa, Y., *Adv. Mater.* **2006,** 18, 1152.
21. Jiang, S.; Chen, Q.; Tripathy, M.; Luijten, E.; Schweizer, K. S.; Granick, S., *Adv. Mater.* **2010** ,22, 1060.
22. Whitelam, S.; Bon, S. A. F., *J. Chem. Phys.* **2010**, 132, 074901.
23. Smoukov, S. K.; Gangwal, S.; Marquez, M.; Velev, O. D., *Soft Matter* **2009,** 5, 1285.
24. Hong, L.; Cacciuto, A.; Luijten, E.; Granick, S., *Nano Letters* **2006,** 6, 2510.
25. Walther, A.; Drechsler, M.; Rosenfeldt, S.; Harnau, L.; Ballauff, M.; Abetz, V.; Müller, A. H. E., *J. Am. Chem. Soc.* **2009,** 131, 4720.
26. Wurm, F.; Kilbinger, A. F. M., *Angew. Chem. Int. Ed.* **2009,** 48, 8412.
27. Gröschel, A. H.; Walther, A.; Löbling, T. I.; Schmelz, J.; Hanisch, A.; Schmalz, H.; Müller, A. H. E., *J. Am. Chem. Soc.* **2012,** 134, 13850.
28. Walther, A.; Drechsler, M.; Rosenfeldt, S.; Harnau, L.; Ballauff, M.; Abetz, V.; Müller, A. H. E., *J. Am. Chem. Soc.* **2009,** 131, 4720.
29. Walther, A.; Andre, X.; Drechsler, M.; Abetz, V.; Müller, A. H. E., *J. Am. Chem. Soc.* **2007,** 129, 6187.

30. Walther, A.; Drechsler, M.; Mülller, A. H. E., *Soft Matter* **2009,** 5, 385.
31. Walther, A.; Gödel, A.; Müller, A. H. E., *Polymer* **2008,** 49, 3217.
32. Liu; Abetz, V.; Müller, A. H. E., *Macromolecules* **2003,** 36, 7894.
33. Wolf, A.; Walther, A.; Müller, A. H. E., *Macromolecules* **2011**, 44, 9221.
34. Ruhland, T. M.; Gröschel, A. H.; Walther, A.; Müller, A. H. E., *Langmuir* **2011,** 27, 9807.
35. Glaser, N.; Adams, D. J.; Böker, A.; Krausch, G., *Langmuir* **2006,** 22, 5227.
36. Walther, A.; Matussek, K.; Müller, A. H. E., *ACS Nano* **2008,** 2, 1167.
37. Pawar, A. B.; Kretzschmar, I., *Macromol. Rapid Commun.* **2010**, 31, 150.
38. Kim, S.-H.; Lee, S. Y.; Yang, S.-M., *Angew. Chem. Int. Ed.* **2010,** 49, 2535.
39. Pickering, S. U., *J. Chem. Soc., Trans.* **1907,** 91, 2001.
40. Ramsden, W., *Proc. R.l Soc. London* **1903,** 72, 156.
41. Pieranski, P., *Phys. Rev. Lett.* **1980,** 45, 569.
42. Popp, N.; Kutuzov, S.; Böker, A.; Müller, A. H. E.; Schmidt, H.-W., Various Aspects of the Interfacial Self-Assembly of Nanoparticles Complex Macromolecular Systems II. Springer Berlin / Heidelberg: 228, 39.
43. Niu, Z.; He, J.; Russell, T. P.; Wang, Q., *Angew. Chem. Int. Ed.* **2010,** 49, 10052.
44. Garbin, V.; Crocker, J. C.; Stebe, K. J., *J. Colloid Interface Sci.* **2012,** 387, 1.
45. Lewandowski, E. P.; Bernate, J. A.; Searson, P. C.; Stebe, K. J., *Langmuir* **2008,** 24, 9302.
46. Lewandowski, E. P.; Bernate, J. A.; Tseng, A.; Searson, P. C.; Stebe, K. J., *Soft Matter* **2009,** 5, 886.
47. Lewandowski, E. P.; Cavallaro, M.; Botto, L.; Bernate, J. C.; Garbin, V.; Stebe, K. J., *Langmuir* **2010,** 26, 15142.
48. Lin, Y.; Skaff, H.; Emrick, T.; Dinsmore, A. D.; Russell, T. P., *Science* **2003,** 299, 226.
49. Binks, B. P.; Fletcher, P. D. I., *Langmuir* **2001,** 17, 4708.
50. Cheung, D. L.; Bon, S. A. F., *Soft Matter* **2009,** 5, 3969.
51. Ondarçuhu, T.; Fabre, P.; Raphaël, E.; Veyssié, M., *J. Phys. France* **1990,** 51, 1527.
52. Jiang, S.; Granick, S., *J. Chem. Phys.* **2007,** 127, 161102.
53. Hirose, Y.; Komura, S.; Nonomura, Y., *J. Chem. Phys.* **2007,** 127, 054707.
54. Fan, H.; Resasco, D. E.; Striolo, A., *Langmuir* **2011**, 27, 5264.
55. Cheung, D. L.; Bon, S. A. F., *Phys. Rev. Lett.* **2009,** 102, 066103.
56. Park, B. J.; Brugarolas, T.; Lee, D., *Soft Matter* **2011,** 7, 6413.
57. Park, B. J.; Furst, E. M., *Langmuir* **2010,** 26, 10406.
58. Park, B. J.; Lee, D., *ACS Nano* **2011,** 6, 782.
59. Park, B. J.; Lee, D., *Soft Matter* **2012,** 8, 7690.
60. Casagrande, C.; Fabre, P.; Raphaël, E.; Veyssié, M., *EPL* **1989,** *9*, 251.
61. Jiang, S.; Granick, S., *Langmuir* **2008,** 24, 2438.

62. Zhang, Z.; Pfleiderer, P.; Schofield, A. B.; Clasen, C.; Vermant, J., *J. Am. Chem. Soc.* **2011**, 133, 392.

63. Choi, C.-H.; Lee, J.; Yoon, K.; Tripathi, A.; Stone, H. A.; Weitz, D. A.; Lee, C.-S., *Angew. Chem. Int. Ed.* **2010** ,49, 7748.

64. Grzelczak, M.; Vermant, J.; Furst, E. M.; Liz-Marzán, L. M., *ACS Nano* **2010,** 4, 3591.

65. Morgan, A. R.; Ballard, N.; Rochford, L. A.; Nurumbetov, G.; Skelhon, T. S.; Bon, S. A. F., *Soft Matter* **2013**, 9, 487.

66. Ayward, R., *Soft Matter* **2012,** 8, 5233.

67. Erhardt, R.; Böker, A.; Zettl, H.; Kaya, H.; Pyckhout-Hintzen, W.; Krausch, G.; Abetz, V.; Müller, A. H. E., *Macromolecules* **2001,** 34, 1069.

68. Erhardt, R.; Zhang, M.; Böker, A.; Zettl, H.; Abetz, C.; Frederik, P.; Krausch, G.; Abetz, V.; Müller, A. H. E., *J. Am. Chem. Soc.* **2003,** 125, 3260.

69. Kutuzov, S.; He, J.; Tangirala, R.; Emrick, T.; Russell, T. P.; Boker, A., *PCCP* **2007,** 9, 6351.

70. de Graaf, J.; Dijkstra, M.; van Roij, R., *Phys. Rev. E* **2009,** 80, 051405.

71. Andala, D. M.; Shin, S. H. R.; Lee, H.-Y.; Bishop, K. J. M., *ACS Nano* **2012,** 6, 1044.

SUPPORTING INFORMATION

to

Influence of Janus Particle Shape on their Interfacial Behavior at Liquid-Liquid Interfaces

By Thomas M. Ruhland, André H. Gröschel, Nicholas Ballard, Thomas S. Skelhon, Andreas Walther, Axel H. E. Müller and Stefan A. F. Bon

1. TEM characterization of Janus particles.

The synthetic pathway to obtain Janus structures is based on a template-assisted synthesis, involving crosslinking of the microphase-segregated morphologies of a bulk film of the respective triblock block terpolymer, followed by a sonication treatment as outlined in previous work.[1] This process results in the formation of core-crosslinked Janus particles, possessing a PB core and two hemicylinders of PS and PMMA. Figure 4-S1 displays a typical transmission electron microscopy (TEM) micrographs of Janus sphere (S1 A), Janus cylinders (S1 B) and Janus discs (S1 C). The Janus particles are characterized by an extremely well-defined cross section, originating from the well-ordered block terpolymer bulk structure. Figure 4-S1 D-E points out the size and diameter distribution of the Janus particles used in the experiments. The Janus spheres are monodisperse in form and shape with a diameter of ca. 50 nm. A polydisperse length distribution can be found for the Janus cylinders with the main peak at ~ 2300 nm. From earlier investigations we know that the PB cylinder has an average diameter of ca. 23 nm with a surrounding corona, leading to a total diameter of the cross section of 80 nm.[2] The Janus discs show a bimodal size distribution with a fraction of relatively large Janus discs (ca. 350 nm in diameter) and a fraction of smaller ones with a diameter of around 250 nm.

The height of the discs, investigated in prior studies of our group, approaches values between 30 nm and 40 nm, respectively.[3]

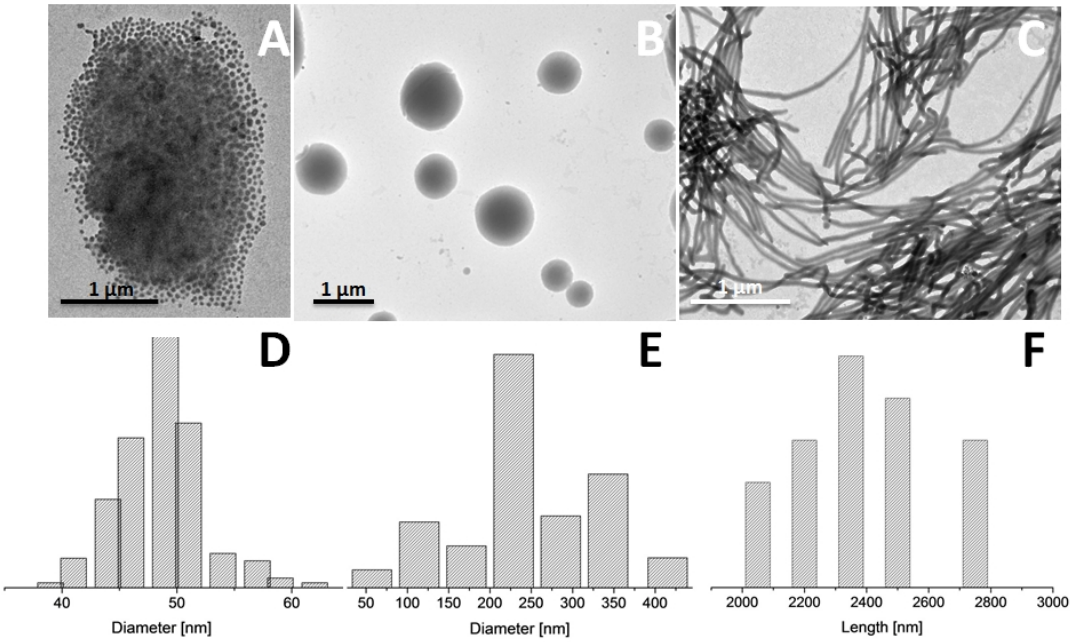

Figure 4-S1. TEM micrographs of (A) Janus spheres, (B) Janus discs and (C) Janus cylinders. Length and diameter distribution of (D) Janus spheres, (E) Janus discs and (F) Janus cylinders.

2. Reference system for pendant drop measurement.

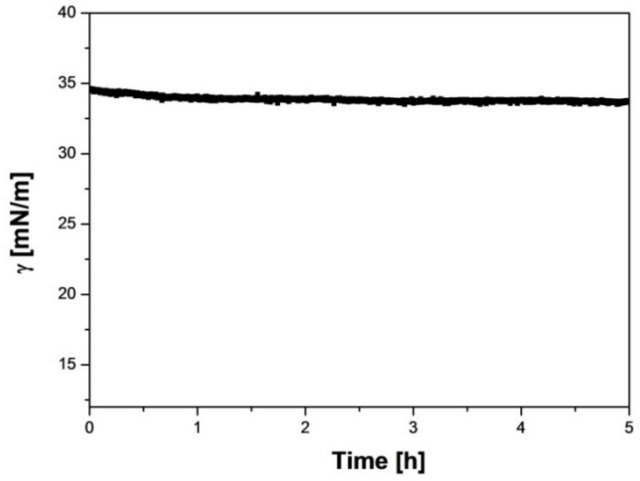

Figure 4-S2. Interfacial tension isotherm of the pristine toluene/water interface.

3. Interpretation of the different adsorption stages in the adsorption process of the Janus particles at the toluene/water interface.

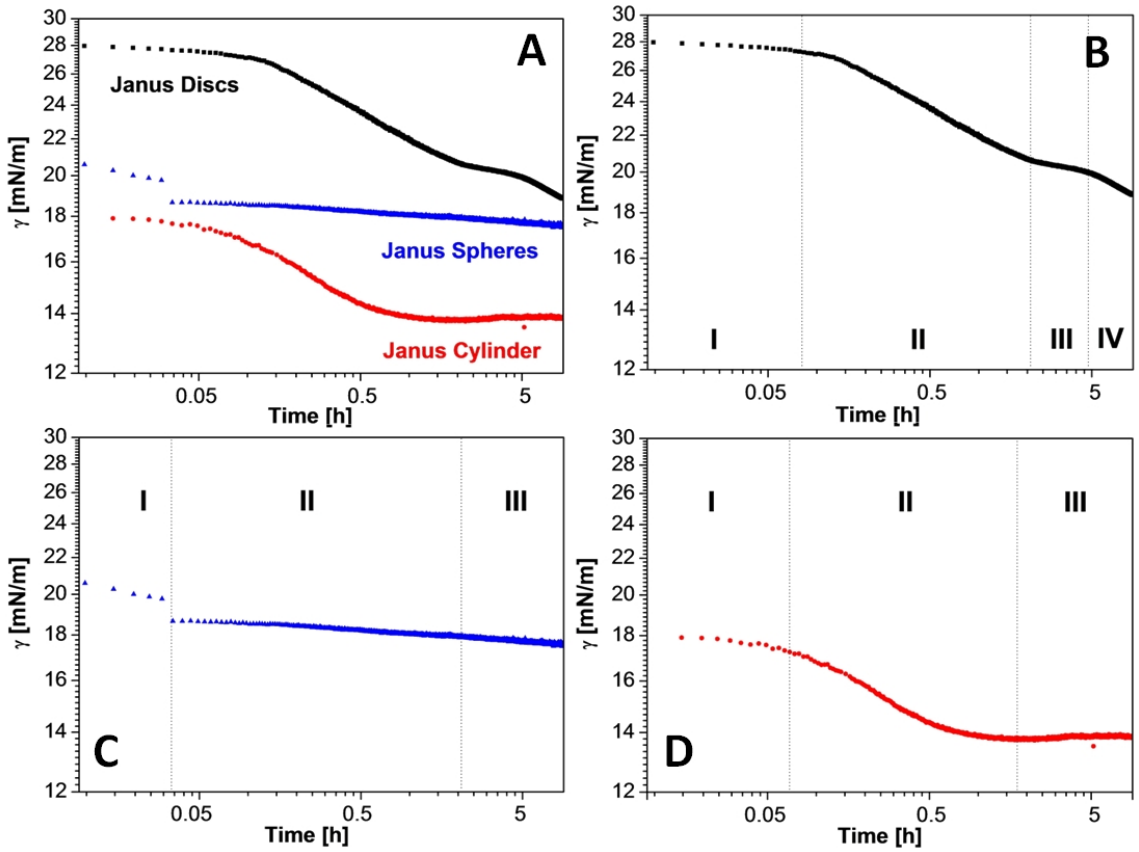

Figure 4-S3. Interpretation of the different adsorption stages in the adsorption process of the Janus particles at the toluene/water interface. (A) Adsorption curves of Figure 4-1 in logarithmic presentation for all Janus particles. Logarithmic presentation of the interfacial values for (B) Janus discs, (C) Janus spheres and (D) Janus cylinder

The logarithmic plots in Figure 4-S3 show the different stages of adsorption of the Janus particle assembly at the toluene/water interface as they manifest in regions of different slopes. All shapes of Janus particles reached a plateau value in the final stage. For all types of Janus particles almost the same adsorption process can be observed except of slightly different adsorption mechanism due to the different shapes. The interfacial tension decreases with time and approaches different quasi-equilibrium values due to different particle shapes. The adsorption process is characterized by different adsorption stages. At early stages of adsorption, the interfacial tension decreases rapidly. Subsequently, the decrease in interfacial tension slows down, and finally, it approaches a plateau, where the maximum coverage of the interface with particles is obtained. After reaching the plateau value, the Janus particles are located and arranged at the interface.

Different particle geometries lead to minimal different adsorption mechanism and kinetics, and the plateau value is reached earlier.

In the beginning, free diffusion to the interface occurs (I), followed by continuous adsorption of Janus particles including ordering and domain formation at the interface and the decrease in interfacial tension slows down (II). Finally, similar to stage II additional packing leads to a rearrangement of the domains in order to get more particles to the interface. The adsorption of new Janus particles comes along with a rearrangement and better ordering of already adsorbed particles at the interface and to the formation of a multilayer system (III).

In case of the Janus discs the adsorption process is based on a slightly different adsorption mechanism so that an additional adsorption step takes places (IV).

4. Free energy simulation of Janus particles at a toluene/water interface.

The simulation method is the same Bon *et al.* used for their calculations of orientation of hematite particles at a liquid-liquid interface.[4] First, it is important to define the form of the particles in a mathematic way. X, y, z are cartesian coordinates. r_x, r_y, r_z are the radii of the particles. n_1 and n_2 act as parameter in the z-axis and the x-y plane respectively. The values in Table 4-S1 are in agreement with the shape of the Janus particles used in the measurements, already characterized in former studies and in Figure 4-S1. Table 4-S2 describes the interfacial tension values we used as assumptions for our calculations.

Table 4-S1. Geometrical data for the different shapes of the Janus particles.

	x [nm]	y [nm]	z [nm]	n_1	n_2
Janus spheres	50	50	50	1	1
Janus discs	250	250	40	0.1	1
Janus cylinders	20	20	2000	0.1	1

Table 4-S2. Interfacial tension values used in the calculations.[5]

γ [mN/m]	**Toluene**	**Water**	**PS**	**PMMA**
Toluene	-	34	6.5	11.4
Water	34	-	32	16

Keep in mind that this model neglects some factors which may contribute to the complete adsorption energy. The influence of gravity, interfacial deforming and line tension is also ignored as the influence of capillary bridging described by Stebe *et al.*[6,7] due to the fact that we are calculating with isolated particles. We believe that these assumptions are acceptable for this kind of simulations.

5. Shape simplifications of the Janus particles for scheme 2.

Scheme 4-S1. Overview of possible Janus particle architectures and their simplifications for the description of their adsorption process in scheme 2. (A) Spheres, (B) cylinders and (C) discs.

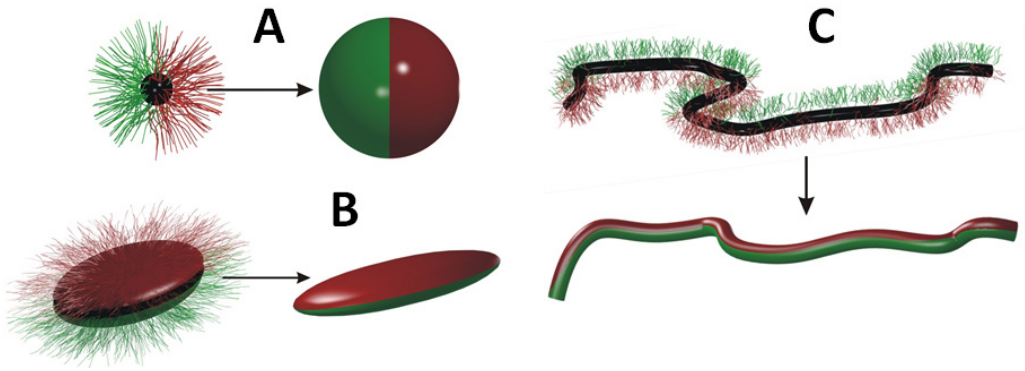

References

1. Walther, A.; Müller, A. H. E., *Soft Matter* **2008,** 4, 663.
2. Ruhland, T. M.; Gröschel, A. H.; Walther, A.; Müller, A. H. E., *Langmuir* **2011,** 27, 9807.
3. Walther, A.; André, X.; Drechsler, M.; Abetz, V.; Müller, A. H. E., *J. Am. Chem. Soc.* **2007,** 129 , 6187.
4. Morgan, A. R.; Ballard, N.; Rochford, L. A.; Nurumbetov, G.; Skelhon, T. S.; Bon, S. A. F., *Soft Matter* **2013**, 9, 487.
5. Binks, B. P.; Clint, J. H., *Langmuir* **2002,** 18, 1270.
6. Lewandowski, E. P.; Bernate, J. A.; Tseng, A.; Searson, P. C.; Stebe, K. J., *Soft Matter* **2009,** 5, 886.
7. Lewandowski, E. P.; Cavallaro, M.; Botto, L.; Bernate, J. C.; Garbin, V.; Stebe, K. J., *Langmuir* **2010,** 26, 15142.

Chapter 5

Superparamagnetic and fluorescent thermo-responsive Core-Shell-Corona hybrid Nanogels with a protective Silica Shell

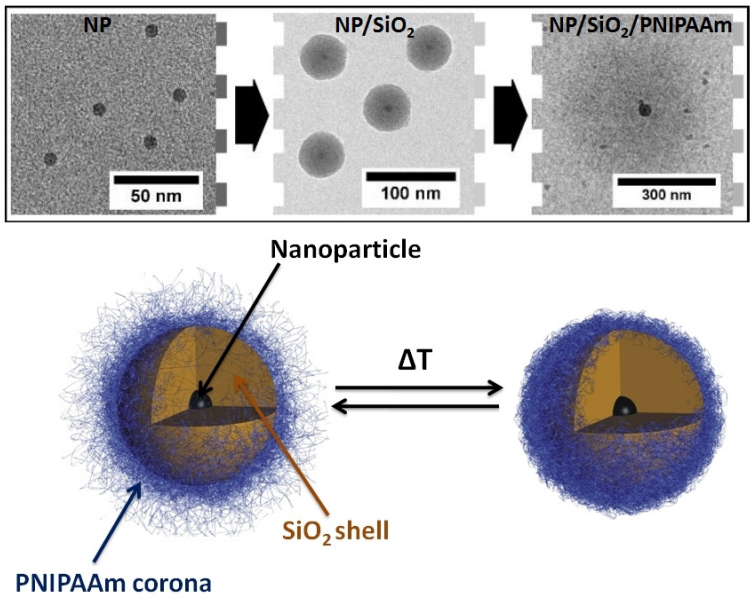

This work is published in the *Journal of Colloid and Interface Science* **2012**, 374 (1), 45-53:

"Superparamagnetic and fluorescent thermo-responsive Core–Shell–Corona hybrid Nanogels with a protective Silica Shell"

by Thomas M. Ruhland, Paul M. Reichstein, Alexander P. Majewski, Andreas Walther* and Axel H. E. Müller*

Superparamagnetic and fluorescent thermo-responsive Core-Shell-Corona hybrid Nanogels with a protective Silica Shell

Thomas M. Ruhland[1], Paul M. Reichstein[1], Alexander P. Majewski[1], Andreas Walther[2], Axel H. E. Müller[2*]*

[1] Department of Macromolecular Chemistry II, University Bayreuth, Germany

[2] DWI at the RWTH Aachen, 52506 Aachen

walther@dwi.rwth-aachen.de; Axel.mueller@uni-bayreuth.de

ABSTRACT

We present the preparation and the characterization of the solution behavior and functional properties of superparamagnetic and/or fluorescent, thermo-responsive inorganic/organic hybrid particles with an intermediate protective silica shell and a smart polymer corona. These well-defined multifunctional nanogels were prepared *via* two consecutive encapsulation processes of superparamagnetic Fe_2O_3 nanoparticles (NPs) and/or fluorescent CdSe(ZnS) semiconductor nanocrystals with a silica layer and a crosslinked poly(N-isopropylacrylamide) (PNIPAAm) polymer shell. First, the different NPs were entrapped into a silica shell using a microemulsion process. Therein, the precise adjustment of the conditions allows to either entrap several particles or single ones and to tailor the thickness of the silica shell in the range of 20 – 60 nm. In a second step, a polymer coating, i.e. thermosensitive PNIPAAm, was attached onto the surface of the multifunctional core-shell particles *via* free radical precipitation polymerization, furnishing multifunctional core-shell-corona hybrid nanogels. Analyses of the functional properties, i.e. optical brightness and magnetic moments, along with transmission electron microscopy reveal near monodisperse hybrid nanoparticles that retain the intrinsic properties of the original nanocrystals. Additionally, we demonstrate the drastically increased chemical stability due to the barrier properties of the intermediate silica layer that protects and shields the inner functional nanocrystals and the responsive character of the smart PNIPAAm shell.

KEYWORDS: Core-shell-corona Particles, Nanogels, Hybrid Particles, Stimuli-responsive Particles.

Introduction

Colloidal hybrid nanostructures target multifunctional materials for future technologies, in which the most interesting functionalities of different material classes are combined in a single entity.[1] Inorganic Nanoparticles (NPs) of controlled size and shape, made from semiconductor nanocrystals (quantum dots), metals and metal oxides, demonstrate unique and advanced size-dependent optical, electronic and magnetic properties, and as such have a high potential for a number of possible applications ranging from drug delivery[2-4], biological sensing and imaging[5,6], biomaterials[7] to catalysis[8,9], therapy and diagnostics[10,11] and materials engineering[12-15]. Semiconductor nanocrystals (quantum dots) have been extensively studied due to their excellent optical and electronic properties, size-tunable photophysics with broad excitation and narrow emission spectra and high photochemical stability. This renders them viable tools for biosensing, as cellular markers or for optoelectronic devices.[16-21] A second most important class of functional NPs are magnetic materials, in particular based on iron oxide. Iron oxide NPs with variable surface chemistry and size dependent properties consisting of maghemite (γ-Fe_2O_3) or magnetite (Fe_3O_4) are not only of great interest for the study of their magnetic properties, but can be used for a variety of *in-vivo* applications, such as MRI contrast enhancement, magnetic immobilization, and drug targeting. [22-27]

Importantly, the central key to develop quantum dots or iron oxide particles as a tool in future applications is to control their surface structure and chemistry *via* simple and robust synthetic functionalization schemes.[28-35] The main goals are to achieve water solubility, biocompatibility, low cytotoxicity, good stability and flexible surface chemistry/functionality that will enable efficient coupling of these NPs with polymers or active compounds. Silica shells are one of the possibilities to generate core-shell inorganic-organic hybrid materials with increased wettability and / or improved biocompatibility. However, polymers are the key surface functionality with which a NP communicates with complex biological environments or experiences affinity/compatibility/repulsion with other materials in device applications. The controlled and easy attachment of polymers onto different NP surfaces still requires tailored ligands to initiate polymerizations and at the same time provide tight adhesion to the NP surface.

Stimuli-responsive multifunctional inorganic/organic hybrid materials find widespread applications, due to the intriguing properties associated with the core (optical, magnetic, mechanical properties) and the desired (inter)active properties of the soft matter components.[36,37] The organic part of the hybrids is made of so-called smart polymers, which undergo structural changes in response to external stimuli such as temperature[38,39], pH[40,41], light[42], solvent[43] and ionic strength[44]. The functionality can be enhanced further by breaking the symmetry and splitting up the corona into Janus configuration.[45-47] The preparation of polymer chains with different sensitivities on two opposite sides can still diversify the properties of Janus particles.

Poly(N-isopropyl acrylamide), PNIPAAm, is a well - known model material exhibiting a lower critical solution temperature (LCST). Below the critical transition at 32 °C, the polymer is hydrophilic, above the LCST the polymer becomes hydrophobic and the polymer chains collapse. Suitable precipitation polymerization methods can be used to prepare spherical thermoresponsive microgels and nanogels.[48] Combining the soft-matter responsiveness with the advanced functionality, magnetism and fluorescence, can therefore result in very attractive multifunctional hybrids.

Herein, we are interested in combining optical and magnetic properties of inorganic NPs with the stimuli-responsive behavior of polymers in hybrid inorganic/inorganic/organic core-shell-corona nanogels and developing reliable experimental procedures to later-on apply our knowledge in the preparation of inorganic/organic core-shell-corona hybrid Janus particles. In more detail, multifunctional hybrids are realized by entrapping magnetic and/or semiconductor NPs within the same silica spheres and a following encapsulation with thermo-responsive polymer shells using a flexible and facile synthesis of well-defined PNIPAAm coronas. We chose the intermediate silica shell not only as a synthetic intermediate and to improve biocompatibility, but wanted to impart the final nanocomposite particles with a beneficial barrier layer that also protects the nanocrystals against harmful chemicals degrading the functionality of the core nanocrystals. Although a polymer shell provides steric repulsion against larger entities, it cannot hinder diffusion of ions or small proteins to the center of the material. The final particles consist of silica-coated maghemite and/or CdSe(ZnS) cores and thermo-responsive and lightly crosslinked PNIPAAm nanogel corona. We demonstrate highly monodisperse hybrid particles that possess a high magnetization and/or bright luminescence as well as uniform temperature sensitivity and enhanced chemical protection of the functional core. Although earlier

work discusses silica encapsulation and/or polymer functionalization of quantum dots or magnetic nanoparticles,[49,50-52] we herein describe a comprehensive approach covering all aspects from the synthesis of the multilayered systems to the elucidation of the functional and responsive property profile of well-defined stimuli-responsive hybrid nanogels.

Experimental Section

Materials

Cadmium oxide (CdO; >99.99%), stearic acid (>99%), trioctylphosphine oxide (TOPO; >99%), hexadecylamine (HDA; >99 %), selenium pellets (Se; >99.999%), trioctylphosphine (TOP; 90%), sulphur (S;>99.5%), Polyoxyethylene(5)nonylphenylether (Igepal ® CO 520), 3-(trimethoxysilyl) propylmethacrylate (MPTS; >98%) ammonium hydroxide (NH_4OH; 28 % in H_2O), Tetraethylorthosilicate (TEOS; >98%), 3-(methacryloyloxy)propyl trimethoxysilane (MPTS; 98%), N-N'-methylenebisacrylamide (BIS; >98 %), potassium peroxodisulfate (KPS; >99%), dioctyl ether (99%), oleic acid (90%), Iron(0)pentacarbonyl (99.9%) were purchased from Sigma Aldrich and zinc stearate (purum) was obtained by Riedel-de-Häen. All chemicals and solvents were used without further purification. N-Isopropylacrylamide (NIPAAm, Sigma Aldrich) was recrystallized from hexane. Deionized water was generated by a MilliQ system (Millipore).

Synthesis of CdSe(ZnS) quantum dots

All synthetic steps were performed under inert atmosphere. For the synthesis of quantum dots, 0.45 g CdO (3.5 mmol) were dissolved in 8 g stearic acid (28.1 mmol) and the solution was heated in a 250 ml three-necked flask to 180°C for nearly 20 min and then cooled to room temperature. During heating the mixture was degassed. 8 g TOPO (20.7 mmol) and 12 g HDA (49.7 mmol) were added to this mixture, which was then heated to 280 °C. 0.78 g selenium pellets (9.9 mmol) dissolved in trioctylphosphine (TOP) were quickly injected into this mixture with a syringe when the temperature stayed constant and the resulting CdSe quantum dots were allowed to grow for different time periods (1-10 min), resulting in different sizes of the QDs. To dissolve the selenium pellets in TOP the mixture had to be gently heated and additionally the mixture was degassed before being injected. Afterwards the red-colored mixture was given to methanol at 60 °C and centrifuged at 4000 rpm for 30 min. In the next step the precipitate was dispersed in

chloroform, again precipitated in methanol and centrifuged. The slightly red precipitate was dried overnight in the vacuum oven. Furthermore, the dry CdSe NPs were dissolved again in chloroform and dialyzed against chloroform, followed by precipitation in methanol. The synthesis of the ZnS shell was carried out using 0.2 g Zn-stearate (0.32 mmol) dissolved in 2 g TOP (5.4 mmol) and 2 g HDA (8.3 mmol), 0.1 g elementar sulphur (3.1 mmol) melted in 2 g DDA (10 mmol) as precursors and 50 mg CdSe (0.26 mmol). Under argon atmosphere the synthesis was conducted during 70 min at 150 °C.[53]

Synthesis of γ-Fe_2O_3 NPs

The synthesis of the γ-Fe_2O_3 NPs was adopted by the publication of Hyeon *et al.*.[26] A 250 mL two-neck round-bottom flask, connected to a reflux condenser, was charged with 120 mL dioctyl ether and 29.0 mL oleic acid (25.76 g, 91.2 mmol) and degassed with N_2 for 15 min. The reaction mixture was heated to 100 °C under N_2 atmosphere before adding 4 mL $Fe(CO)_5$ (30.4 mmol). Subsequently, the resulting mixture was heated to reflux and kept for 1.5 h until the solution colour turned to black. After cooling down to room temperature the reaction mixture was stirred under air to initiate the oxidation process of iron to achieve γ-Fe_2O_3 NPs. The yielded particles were precipitated with ethanol and separated by means of a NbFeB-magnet. The particles were immediately redispersed in toluene, THF or *n*-hexane. For further purification the precipitation and separation process was repeated.

Experimental procedure for the preparation of Fe_2O_3/SiO_2, CdSe(ZnS)/SiO_2 and Fe_2O_3/CdSe(ZnS)/SiO_2 core-shell particles

The synthesis was adapted from an experimental procedure published earlier.[54,55] Herein, we present detailed experimental conditions. Polyoxyethylene(5)nonylphenyl ether (0.23 g, 0.54 mmol, Igepal CO-520) was dispersed in a 10 ml small flask containing 4.5 mL cyclohexane in a ultrasound bath for 10 minutes. Next, 400 µL of γ-Fe_2O_3 nanoparticles dispersed in cyclohexane (0.5 mg/mL), 160 µL of CdSe(ZnS) quantum dots dispersed in cyclohexane (1 mg/mL)] were added to the flask and vortexed for 5 minutes at 200 min^{-1}. The rapid addition of ammonium hydroxide (29.4%, 40 µL) formed a reverse brownish microemulsion and the subsequent addition of tetraethylorthosilicate (30 µL, TEOS) started the growth of the silica shell. The nanocomposite particles were aged for 48 hours using a shaking incubator at RT and 100 rpm as oscillation rate (soft agitation!) and purified by several cycles of centrifugation with 4500 rpm for 10 minutes and cautious

redispersion in ethanol. The magnetic core shell particles could also be magnetically collected. The final product was redispersed in millipore water. The simultaneous addition of both types of particles with the same volumes and concentrations mentioned above leads to for Fe_2O_3/CdSe(ZnS)/SiO_2 core-shell particles.

Modification of NP/SiO_2 core shell particles

The surface of the core-shell NP/SiO_2 nanospheres were endowed with reactive double bonds *via* modification with 3-(methacryloyloxy)propyl trimethoxysilane (MPTS). Briefly, 0.050 g of NP/SiO_2 core shell particles were mixed with 1.0 mL of MPTS and 25 mL of ethanol at 40 °C for 12 h. The MPTS-modified NP/SiO_2 colloids were then separated and washed repeatedly with ethanol and water to remove excess MPTS. Afterwards the modified core shell particles were redispersed in water.

Synthesis of NP/SiO_2/PNIPAAm hybrid core-shell-corona material

The synthesis of the NP/SiO_2/PNIPAAm was accomplished by precipitation polymerization. Typically, 0.010 g of MPTS-modified NP/SiO_2 core-shell particles was mixed with 30 mL of aqueous solution containing 0.050 g of N-isopropylacrylamide (NIPAM, 0.44 mmol)) and 0.005 g of N,N-methylenebisacrylamide (BIS, 0.032 mmol) for crosslinking *via* moderate stirring at 100 rpm. After being degassed with nitrogen for 30 min, the solution was heated up to 70 °C, and 0.5 mL of 4 mg/mL potassium sulfate (KPS) solution was injected to initiate the polymerization. After 4 h of reaction, the final products were collected by centrifugation at 4000 rpm for 10 minutes or magnetic separation and washed with water and finally redispersed in milipore water.

Characterization

Bright-field Transmission electron microscopy (TEM) was performed on Zeiss CEM 902 and LEO 922 OMEGA electron microscopes operated at 80 kV and 200 kV, respectively. Data evaluation and processing was carried out with Soft Imaging Viewer and Image Tool. For ***cryogenic transmission electron microscopy (cryo-TEM)*** studies, a drop of the sample dissolved in water was put on a lacey transmission electron microscopy (TEM) grid, where most of the liquid was removed with blotting paper, leaving a thin film stretched over the lace. The specimens were instantly vitrified by rapid immersion into liquid ethane and cooled to approximately 90 K by liquid nitrogen in a temperature controlled freezing unit (Zeiss *Cryo*box, Zeiss NTS GmbH, Oberkochen,

Germany). The temperature was monitored and kept constant in the chamber during all of the sample preparation steps. After freezing the specimens, the specimen was inserted into a *cryo*-transfer holder (CT3500, Gatan, München, Germany) and transferred to a Zeiss EM922 EF-TEM instrument. Examinations were carried out at temperatures around 90 K. The transmission electron microscope was operated at an acceleration voltage of 200 kV. Zero-loss filtered images were registered digitally by a bottom mounted CCD camera system (Ultrascan 1000, Gatan) combined and processed with a digital imaging processing system (Gatan Digital Micrograph 3.9 for GMS 1.4).

Scanning electron microscopy (SEM) was performed using a LEO 1530 Gemini instrument equipped with a field emission cathode with a lateral resolution of approximately 2 nm. The acceleration voltage was chosen between 0.5 kV, and 30 kV for element dispersive x-ray analysis (EDX).

Dynamic light scattering (DLS) was performed on an ALV DLS/SLS-SP 5022F compact goniometer system with an ALV 5000/E cross-correlator and a He–Ne laser (λ_0 = 632.8 nm). Prior to the light scattering measurements the sample solutions were filtered using Roth filters (housing: polypropylene, membrane: polytetrafluoroethylene) with corresponding pore sizes. All samples were analyzed at high dilution. The data evaluation of the dynamic light scattering measurements was performed with the CONTIN algorithm.

X-ray powder diffraction (XRD) measurements were performed on a X'Pert Pro Powder diffractometer from PANalytical ($Cu_{k\alpha}$ radiation, 40 kV, 40 mA). For detection a X'Celerator Scientific RTMS detection unit was used. The dried samples were pestled and measured after 24 h.

Fourier-Transform Infrared Spectroscopy (FT-IR) was carried out on a Spectrum 100 FT-IR spectrometer from Perkin Elmer. For measurements the U-ATR unit was used. The dried samples were directly placed on top of the U-ATR unit for measurements.

Vibrating Sample Magnetometer (VSM) monitors the magnetization curves at room temperature with an Lake Shore Vibrating Sample Magnetometer Model7404 up to maximum field strength of 1.4 T. Samples were measured in sealed Kel-F vessels, placed on a fiber glass sample holder between two poles of an electromagnet, and vibrated at a frequency of 82 Hz.

UV-Vis excitation and fluorescence emission spectra were recorded on a Hitachi U-300 and a Shimadzu RF-5301 instrument, respectively. The excitation wavelength for the fluorescence spectra was at 645 nm.

Results and Discussion

The synthetic strategy towards monodisperse thermo-sensitive hybrid materials with core-shell-corona architecture is schematically illustrated in Scheme 5-1. In a first step, we synthesized monodisperse and hydrophobically functionalized superparamagnetic (γ-Fe_2O_3) or fluorescent (CdSe(ZnS)) NPs, which serve as functional cores for the final hybrid nanogels. This is followed by the encapsulation of single or multiples NPs with a silica layer (depending on the conditions as we will show below) by a dedicated microemulsion procedure, yielding monodisperse core-shell γ-Fe_2O_3/SiO_2, CdSe(ZnS)/SiO_2 or γ-Fe_2O_3/CdSe(ZnS)/SiO_2 particles. To attach the final thermo-responsive polymer corona, the surface of the core-shell NP is then activated by a silane-carrying methacrylate, 3-(methacryloyloxy)propyl trimethoxysilane (**MPTS**), which leads to the formation of double-bonds on the surface. In the end, a lightly crosslinked PNIPAAm shell is immobilized by a "grafting through/onto" polymerization of N-isopropylacrylamide (**NIPAAm**) in the presence of a bifunctional crosslinker, N,N`-methylenediacrylamide (**BIS**).

Scheme 5-1. Synthesis of NP/SiO_2/PNIPAAm core-shell-corona hybrid nanogels.

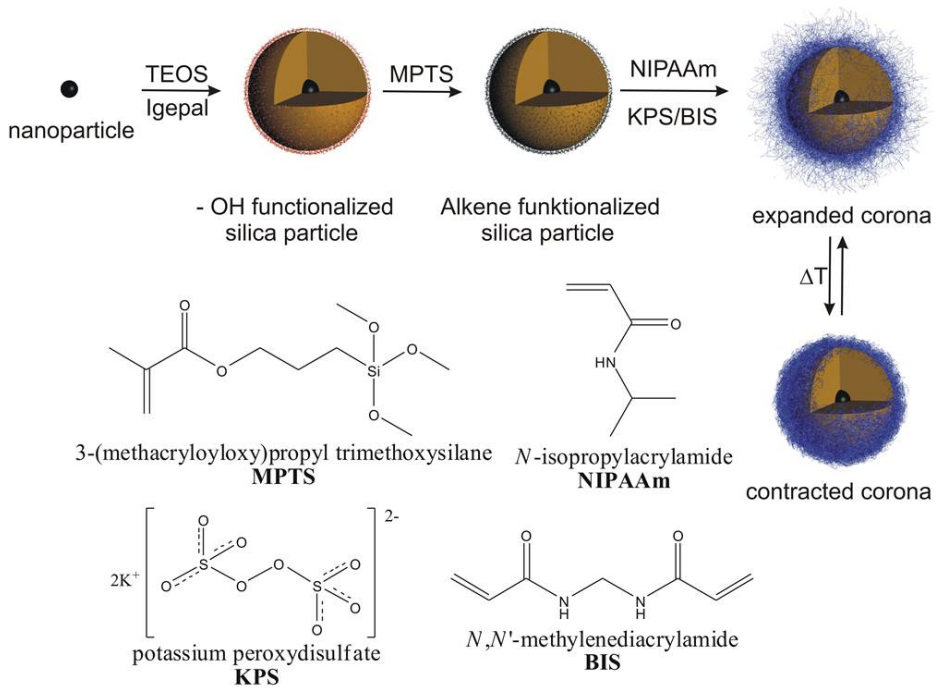

The monodisperse superparamagnetic γ-Fe_2O_3 NPs were synthesized *via* thermal decomposition of $Fe(CO)_5$ using a procedure developed by Hyeon *et al.*.[26] Therein, the size is well controlled by the amount of oleic acid that is used in relation to the $Fe(CO)_5$ amount. TEM characterization (Figure 5-1 A) reveals a number-average radius of 5.5 ± 0.15 nm, which is corroborated by dynamic light scattering (DLS) with a z-average hydrodynamic radius of 6.5 nm and a PDI of 1.03 (see also Figure 5-6 and Figure 5-S1 in the supporting information). Obviously, the oleic acid ligand shell is invisible in the TEM, but is resolved in the hydrodynamic distribution function obtained by DLS, resulting in a higher value.

X-ray diffraction (XRD) confirms that the superparamagnetic NPs are composed of γ-Fe_2O_3 crystallites (Figure 5-1 D). The measured diffractogram can be indexed using the cubic cell of a maghemite structure (PCPDF 00-039-1346). An access to brightly luminescent particles for optical detection possibilities is provided *via* semiconductor CdSe(ZnS) nanocrystals (so-called quantum dots). To improve the optical and electronic properties of the quantum dots a thin ZnS layer was added onto the pure CdSe quantum dot cores.

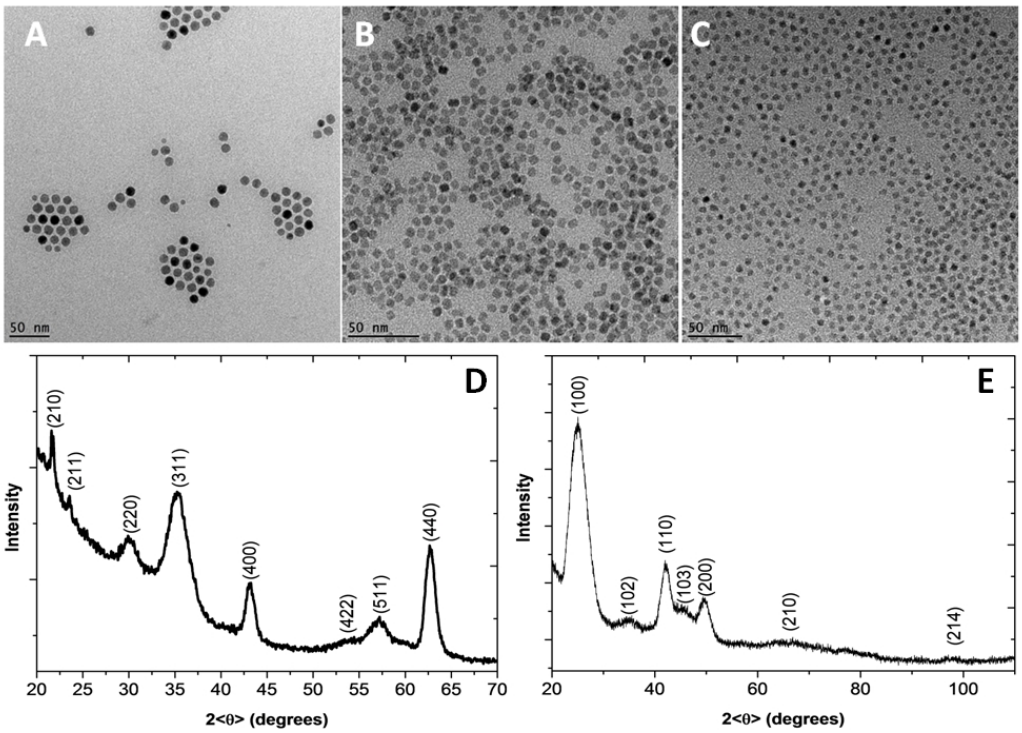

Figure 5-1. TEM images for (A) γ-Fe_2O_3-NP, (B) CdSe-NP and (C) CdSe(ZnS)-NP. XRD measurements for (D) γ-Fe_2O_3-NP and for (E) CdSe-NP.

The brightly fluorescent CdSe (Figure 5-1 B) as well as CdSe(ZnS) (Figure 5-1 C) NPs are of uniform size and shape with number average radii of 2.6 ± 0.1 nm and 3.1 ± 0.15 nm (TEM) before and after the thin ZnS coating, respectively. The optical absorption and the small size hamper an unambiguous characterization with DLS. The CdSe NPs are clearly identified as hexagonal CdSe (Figure 5-1 E, PCPDF 01-077-2307). The UV-Vis and photoluminescence spectra of CdSe and CdSe(ZnS) nanocrystals are provided in the Supporting Information (Figure 5-S1). The emission peaks are centred around 646 nm for CdSe and 654 nm for CdSe(ZnS). The sharp emissions suggest highly monodisperse samples. Calculating the radii of both types of quantum dots from the adsorption maxima of the UV-Vis spectra[56] results in CdSe NPs of 2.7 nm and CdSe(ZnS) NPs of 2.9 nm in radius. These values coincide nicely with the dimensions obtained *via* TEM.

To achieve a thorough barrier layer as chemical protection, to gain wettability and biocompatibility and to enable a flexible surface chemistry, we coated these nanocrystals in a next step with a silica shell using a microemulsion process. Therein, surfactants allow the hydrophobic NPs to be encapsulated within a reverse microemulsion. Then tetraethoxysilane (TEOS) is introduced to condense a tight silica shell around the droplets.[57] The condensation of the silica layer is achieved by hydrolyzing TEOS in a mixture of NPs, cyclohexane, polyoxyethylene(5)nonylphenyl ether (Igepal CO-520) and ammonium hydroxide.

Although there are several different synthesis procedures described in the literature, it was a true challenge to fully reproduce their experiments and achieve a reliable encapsulation. Therefore, we looked in detail on the influence of the amount of TEOS on the product homogeneity and evolution of the thickness of the silica shell. We also provide in-depth details of the procedure in the experimental section. Figure 5-2 summarizes the change in average radius of the silica-encapsulated particles formed in presence of CdSe(ZnS) cores, as determined *via* TEM.

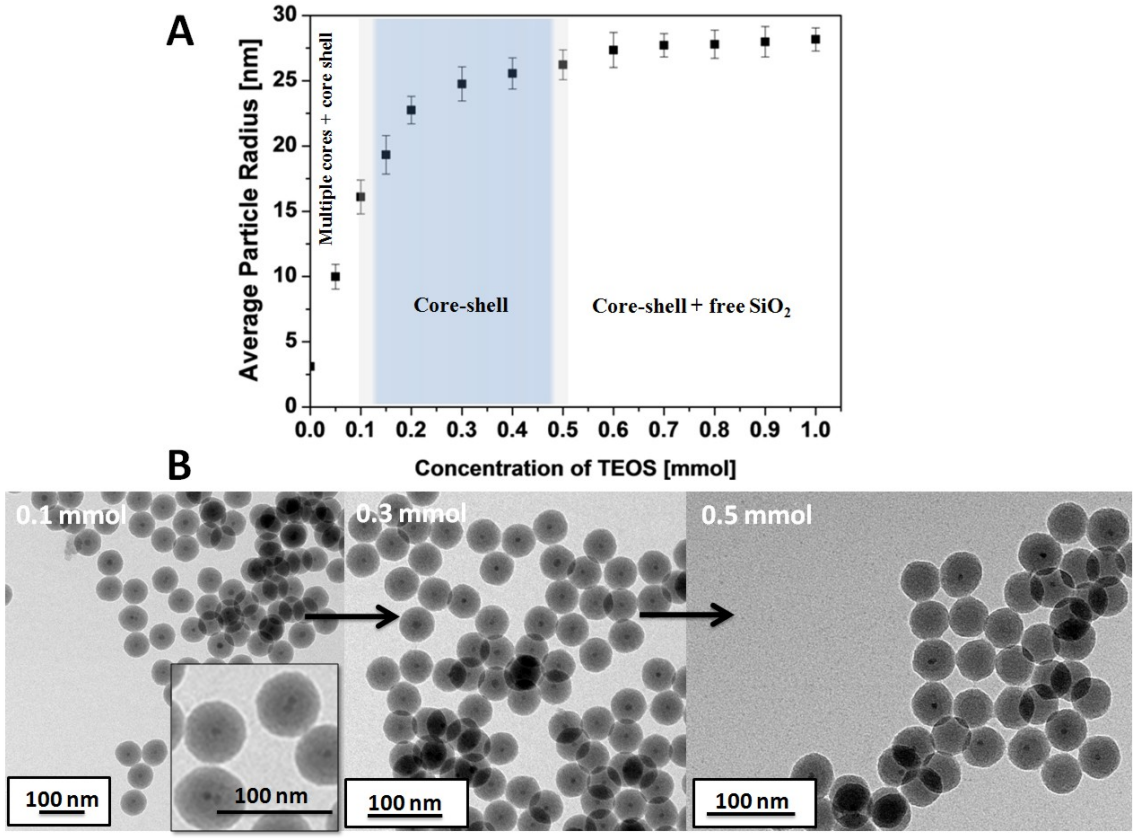

Figure 5-2. (A) Dependence of the particle radius and product homogeneity of CdSe(ZnS)/SiO_2 core-shell particles as a function of the TEOS concentration and constant NP concentration. (B) TEM images of CdSe(ZnS)/SiO_2 core shell particles prepared using different TEOS amounts.

The total particle radius including the silica shell rises from 10 nm to 28 nm upon increasing the concentration of TEOS from 0.05 to 1 mmol. This corresponds to a maximum SiO_2 shell thickness of ca. 26 nm, considering the encapsulation of a single CdSe(ZnS) nanoparticle. Interestingly, the dimensions of the core-shell particles rapidly increase at first and then level off upon reaching a certain concentration of 0.5 mmol. Careful TEM imaging of various samples reveals a competition between NP-induced nucleation of silica growth and secondary, free nucleation in solution. When the TEOS amount is less than 0.5 mmol, the deposition of the silica on the surface of the NP is dominant over the secondary nucleation in solution and the silica shell thickness is sensitive to the amount of TEOS. In the range of 0.1 - 0.5 mmol, only core-shell particles with nearly perfect architectures are formed. Interestingly, multiple NPs are encapsulated if the TEOS concentration is decreased below 0.1 mmol. On the contrary, if the added amount of TEOS in the reaction system is increased above 0.5 mmol, free SiO_2 particles are generated *via* secondary nucleation in solution in addition to core-shell NPs. Further

addition of TEOS leads to an increasingly large amount of free particles and the shell thickness/particle radius remains roughly unchanged in the observed window. In summary, the total diameter can be reliably controlled between 20 nm to 60 nm for both types of NPs. Fe_2O_3 and CdSe(ZnS) behave similar in the coating process as demonstrated in Figure 5-3 A-B. Therefore, we believe that the procedure can be extended to other types of nanoparticles dispersed in organic solvents. Elemental analysis *via* energy-dispersive x-ray analysis (EDX) confirms the different kinds of NP cores surrounded by a silica shell (Figure 5-3 D-F).

The strong dependence of the homogeneity (Figure 5-3 A-C), that is multiple core vs. single core, of the product at low TEOS concentrations is somewhat unexpected. Intuitively, we would have anticipated a stronger dependence of the encapsulation of multiple NPs vs. single NPs on the NP concentration and the amount of surfactant used for the microemulsion. Herein we however demonstrate that at a given concentration of NPs and surfactant, the homogeneity depends on the TEOS concentration. The concentrations of TEOS does not only regulate the shell thickness, but surprisingly also influences the nucleation and the amount of encapsulated NP within one silica particle. Defined uniform core-shell particles with very thin silica shells are not accessible as multiple NPs are entrapped within one silica shell under these conditions. This initially undesired encapsulation of multiple NPs into a single silica shell can yet be turned into an advantage for the preparation of mixed Fe_2O_3/CdSe(ZnS)/SiO_2 composite particles. A silica coating of a mixture of both NP leads to the statistic entrapment of various NPs in one shell and thus to the formation of silica particles with magnetic and photoluminescent cores as displayed in Figure 5-3 C. We believe that the detailed investigation shown here and the precise details in the experimental section will help to reliably apply the silica coating procedure to other nanoparticle systems in the future.

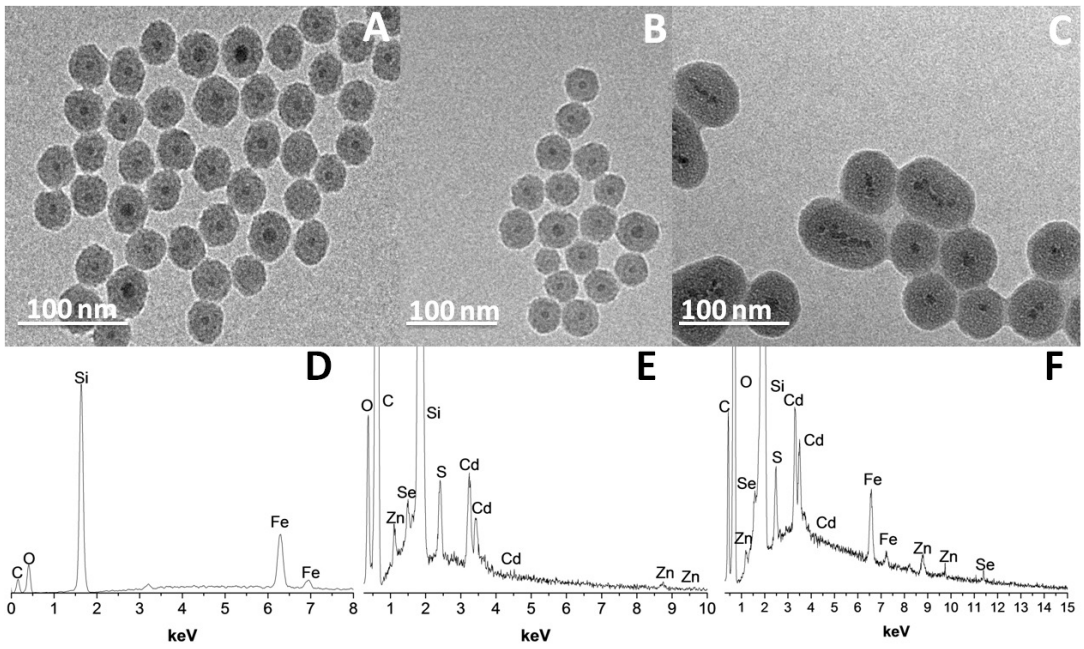

Figure 5-3. TEM images of (A) Fe_2O_3/SiO_2, (B) CdSe(ZnS)/SiO_2 and (C) Fe_2O_3/CdSe(ZnS)/SiO_2, prepared at different concentrations of TEOS, favoring either single NP entrapment (A-B) or encapsulation of multiple cores (C). EDX spectra of (D) Fe_2O_3/SiO_2, (E) CdSe(ZnS)/SiO_2 and (F) Fe_2O_3/CdSe(ZnS)/SiO_2 core-shell particles with a diameter of around 50 nm.

The resulting silica-coated quantum dots and/or superparamagnetic NPs exhibit water solubility and colloidal stability, as well as magnetic and photoluminescent properties as further quantified below. Among the many benefits, such as increased biocompatibility and wettability, the gained flexibility for simple and well-developed chemical modifications of the silica surface is tremendous. A simple platform technology evolves. The tedious and demanding synthesis of tailored ligands for immobilization of functional biomolecules or polymers can be overcome.[58,59] In fact, the silica surfaces can easily be functionalized to undergo surface-initiated controlled radical polymerizations (ATRP, RAFT), or free radical "grafting onto" polymerizations can be used modify the silica surface. Herein, we achieved a straight-forward modification of the silica-coated NPs (typical radius 25 nm) with double bonds using a methacrylate-carrying trimethoxysilane, MPTS. The immobilized, terminal double bonds serve as the linkage between the inorganic and the organic polymer part of the final hybrids. Subsequently, NIPAAm was polymerized with an additional bifunctional crosslinking agent, BIS (ca. 10 %). The MPTS-modified silica-coated core-shell particles act as seeds to immobilize the polymer layer in this precipitation polymerization. During the synthesis, the polymer chains collapse onto the silica surface due to the polymerization temperature of 70 °C, which is drastically above the LCST of PNIPAAm, leading to a self-limiting growth of the

polymer shell. Minimization of the surface free energy forms regular spherical shapes. After purification, the highly water-soluble PNIPAAm corona enables a complete dissolution into core-shell-corona hybrid nanogel-type particles.

The hydrodynamic radius distributions of all materials were studied by DLS at 20 °C (Figure 5-4 A/B and 5-S2). The γ-Fe_2O_3, γ-Fe_2O_3/SiO_2 particles and γ-Fe_2O_3/SiO_2/PNIPAAm hybrid nanogels with a 10% crosslinking density have z-average hydrodynamic radii of 6.5 nm, 25 nm and 200 nm, respectively (Figure 5-4 A). Similarly, CdSe(ZnS), CdSe(ZnS)/SiO_2 and CdSe(ZnS)/SiO_2/PNIPAAm show hydrodynamic radii of 3.1 nm (*via* TEM), 26 nm and 180 nm. Both samples display a consistent increase throughout the various steps and the obtained distribution functions are remarkably narrow. The PDI values for both PNIPAAm hybrid nanogels are in the range of 1.04, thus near monodisperse. These values demonstrate an access to very well-defined and homogeneous hybrid core-shell-corona materials.

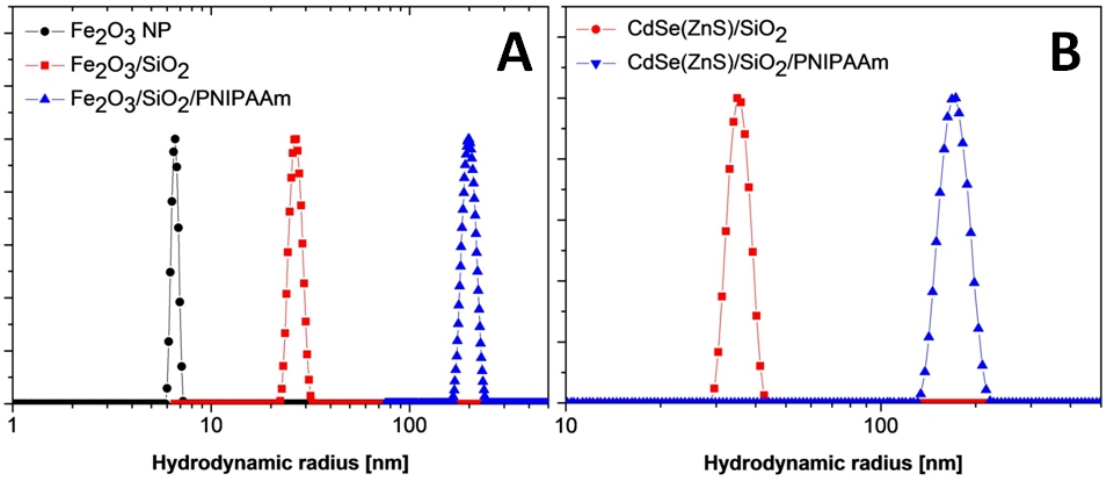

Figure 5-4. Intensity-weighted hydrodynamic radii distribution (DLS) of (A) γ-Fe_2O_3, γ-Fe_2O_3/SiO_2 and γ-Fe_2O_3/SiO_2/PNIPAAm and (B) CdSe(ZnS)/SiO_2 and CdSe(ZnS)/SiO_2/PNIPAAm hybrid nanoparticles at 10% cross-linking density and 20° C.

To confirm the structures of the materials, we show TEM and cryo-TEM images of the fluorescent CdSe(ZnS)/SiO_2/PNIPAAm hybrids in Figure 5-5. The lightly crosslinked PNIPAAm shell can be clearly seen in the TEM micrograph as a greyish homogeneous layer surrounding the central core. Similar images can be obtained for the γ-Fe_2O_3 and CdSe(ZnS)/γ-Fe_2O_3 containing particles (not shown). All resulting hybrids are very uniform in size and shape and exhibit a narrow size distribution. In some cases two silica-coated core-shell particles are encapsulated within one PNIPAAm corona, but there is no drastic influence on the PDI in TEM or DLS. The radius of the core-shell-corona

materials obtained *via* TEM is 110 ± 15 nm for both types of hybrid materials. This radius is lower than the dimensions from DLS, which measures the fully extended particle size in solution, whereas the TEM values correspond to sizes in dried state. Additionally, a number-average value from imaging is compared to an intensity-weighted value from DLS, also leading to slight differences despite the near monodisperse distribution. Therefore, we also recorded cryo-TEM images. The micrograph of CdSe(ZnS)/SiO_2/PNIPAAm display a fuzzy corona, highlighted by the encircled areas (Figure 5-5 B) and the greyscale analysis (Figure 5-5 C). Due to the highly swollen character of the corona and the thereof originating low contrast, it is not possible to visualize the full extension of the corona with cryo-TEM. The imaging data however nicely confirms the successful formation of the hybrid core-shell-corona nanoparticles.
Figure 5-S3 shows the changes in FT-IR spectra during the experimental procedure. In combination with the TEM images the appearing absorption peaks are positive proofs of a successful immobilization of a PNIPAAm gel-like corona on the activated core – shell particles.

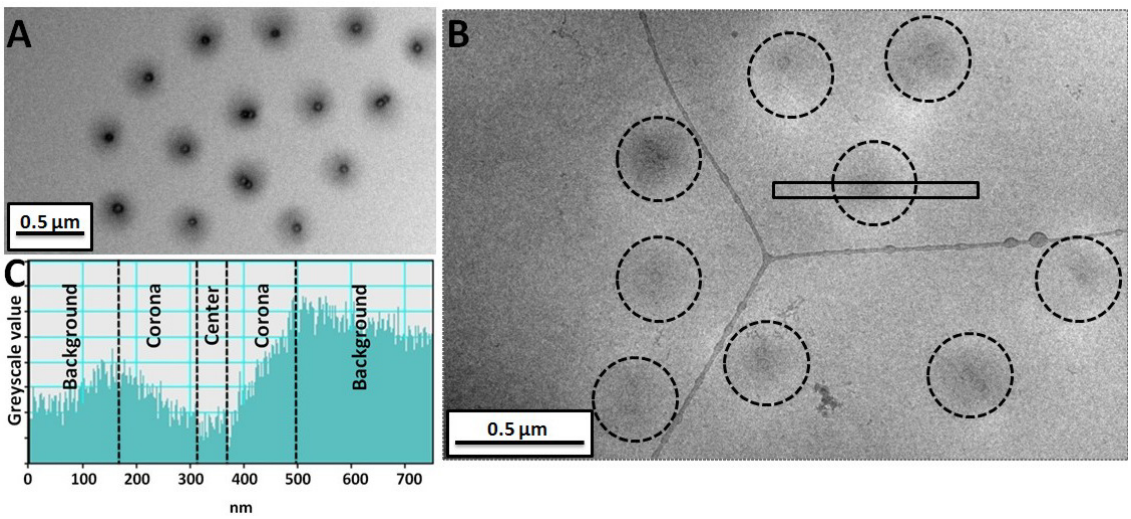

Figure 5-5. (A) Representative TEM image of CdSe(ZnS)/SiO_2/PNIPAAm and (B) cryo-TEM images of CdSe(ZnS)/SiO_2/PNIPAAm core-shell-corona hybrid nanogels. The circles correspond to the DLS radius. (C) Greyscale analysis of the cross section indicated in micrograph B.

In a next step we investigated whether the functional properties of the underlying nanocrystals were retained upon embedding them into a silica shell and polymer corona. The magnetic properties were investigated *via* quasi-static magnetization experiments using a Vibrating Sample Magnetometer (Figure 5-6 A). After normalizing with the saturation magnetization, the three graphs of γ-Fe_2O_3, γ-Fe_2O_3/SiO_2 and γ-

Fe_2O_3/SiO_2/PNIPAAm only show slight differences, proving that neither the incorporation into the core-shell nor core-shell-corona deteriorates the superparamagnetism and the magnetic moment distribution. The same effect can be seen analyzing the magnetization of the γ-Fe_2O_3/CdSe(ZnS)/SiO_2 and γ-Fe_2O_3/CdSe(ZnS)/SiO_2/PNIPAAm (Figure 5-S4). The macroscopic magnetic behaviour of all hybrid materials can be confirmed by magnetic separation of the various structures with a weak finger-tip sized magnet as demonstrated in Figure 5-S5.

Fluorescence spectroscopy of the core-shell-corona CdSe(ZnS)/SiO_2/PNIPAAm particles demonstrates a preserved photoluminescence during the various encapsulation steps (Figure 5-6 B). The decrease of QY is a common phenomenon because quantum yield is highly sensitive to the surface and the chemical surrounding of the QDs, especially with respect to ligand chemistry. A slight shift can be observed during the reaction steps, which may evolve from the changes in local refractive index of the surrounding shells. Fluorescence experiments with both types of particles as cores show the same results as mentioned above and can be seen in the Supporting information (Figure 5-S6).

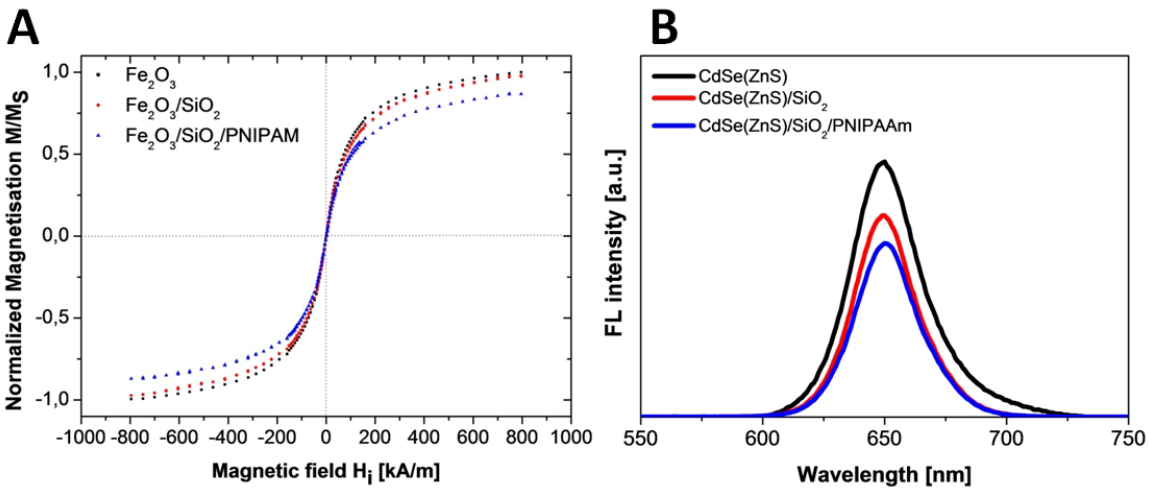

Figure 5-6. (A) Magnetic hysteresis curves of γ-Fe_2O_3 NPs, γ-Fe_2O_3/SiO_2 core shell particles and γ-Fe_2O_3/SiO_2/PNIPAAm hybrid material with a 10% crosslinking density at RT. (B) Fluorescence spectra for CdSe(ZnS), CdSe(ZnS)/SiO_2 and CdSe(ZnS)/SiO_2/PNIPAAm.

In the last section, we highlight the well-defined smart thermo-responsive character of the hybrids and the barrier properties of the silica shell. A simple experiment to demonstrate the chemical protection of core nanocrystals of the silica-encapsulated hybrid particles versus the pristine nanoparticles can be accomplished by attempted acidic dissolution of γ-Fe_2O_3 nanoparticles (Figure 5-7). Within one day in 1 M HCl, the pure γ-Fe_2O_3 are

completely decomposed into $FeCl_3$ as indicated by the yellowish-green color. The superparamagnetic behavior is lost. On the contrary, the silica-encapsulated γ-Fe_2O_3 hybrids are stable for weeks and retain their magnetic behavior. Consequently, we can prepare long-term stable hybrid particles, which can even survive in the harshest body fluid environments in the stomach and are as such ready for oral delivery.

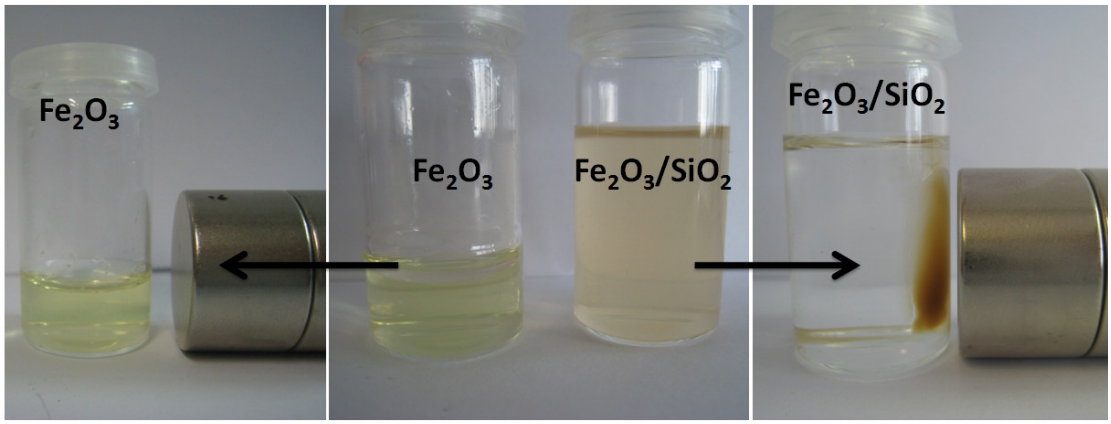

Figure 5-7. Analysis of the nanoparticle stability of the pure particles and Fe_2O_3/SiO_2 core-shell particles *via* the addition of 1 M HCl after 1 week. All photos were made after 30 min.

Furthermore, the thermo-responsive character of the core-shell-corona PNIPAAm hybrid material was investigated by DLS. Figure 5-8 displays the dependence of the z-average hydrodynamic radius as a function of temperature. The samples exhibit a thermo-responsive volume phase-transition centered around 33 - 34 °C, originating from the smart PNIPAAm corona around the core-shell particles. The dimensions of the hybrids decrease drastically as temperature rises. According to the DLS, the structures experience a collapse to ca. 55% of the original size. They remain however soluble as individual particles due to the presence of sulphate groups on the particle exterior generated during the precipitation polymerization. The shrinking and swelling cycle of the CdSe(ZnS)/SiO_2/PNIPAAm particles is reproducible many times as depicted in the inset. This behavior is reminiscent of spherical PNIPAAm micro/nanogels. But herein, the overall property profile is amplified by the presence of functional components inside the core and all of it is conserved in a well-defined hybrid architecture.

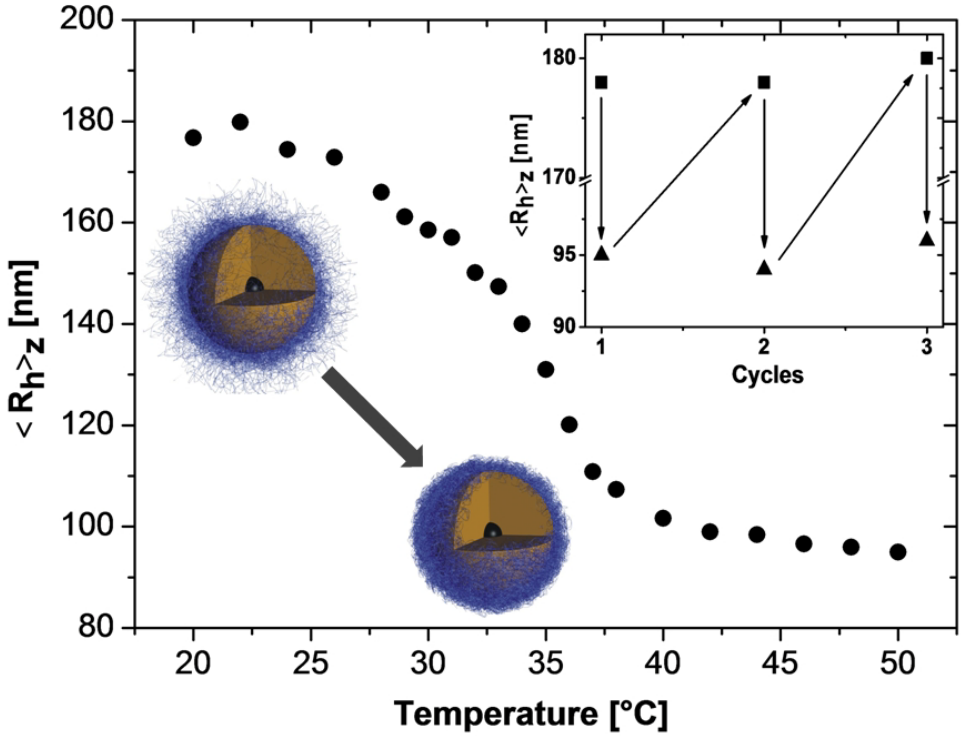

Figure 5-8. Dependence of the z-average hydrodynamic radius of CdSe(ZnS)/SiO_2/PNIPAAm nanogel particles upon temperature with a crosslinking density of 10%. The inset depicts the changes in the z-average hydrodynamic radius for various temperature cycles below and above the volume transition temperature, respectively.

Conclusion

In conclusion, we have developed an efficient and reproducible method for the synthesis of monodisperse core-shell-corona hybrid nanomaterials with a γ-Fe_2O_3/SiO_2, CdSe(ZnS)/SiO_2 and γ-Fe_2O_3/CdSe(ZnS)/SiO_2 core-shell structure and a thermosensitive PNIPAAm corona. The thickness of the SiO_2 shell can be controlled and the composition of the NPs within the silica particle can be manipulated according to the needs of a given application. The final particles retain full functionality of the superparamagnetic and fluorescent core materials and combine it with the barrier properties and ease of chemical functionalization of the silica shell. The responsive and interactive properties of the polymer corona, which can be easily attached, impart advanced functionality of soft matter materials, similar to the known property spectrum of nano/microgels. The reported multifunctional hybrid core-shell-corona nanogels could be applied for possible applications in cell and tissue imaging, oral delivery of acid-sensitive imaging probes and clinical diagnosis. In the next steps we want to use our new knowledge about the synthesis of core-shell-corona particles and their stimuli-responsive properties to create

hybrid core-shell-corona Janus particles with two polymers immobilized to the opposite sides of the core-shell particles on the basis of our particles. The flexible surface chemistry due to the silica intermediate offers a wide range of different functionalization and polymerization types (RAFT-, ATRP-, Free Radical-Polymerisation or Click-chemistry). With a view to the long way towards hybrid Janus particles we decided to use the "grafting through/from" - approach for the polymerisation which can be considered the easiest polymerization technique, but nevertheless, leading to good control. Useful strategies to prepare inorganic/organic core-shell-corona Janus particles with unique and novel architectures are the use of special templates for a temporary immobilization and desymmetrization. Such systems and the herein developed flexible synthetic platform provide many different set screws and a wide range of possibilities to successfully target biphasic patchy and highly functional Janus particles in the future.

Acknowledgement

We thank André Gröschel for his help with the schemes, Thomas Lunkenbein for measuring the XRD spectra, Thomas Friedrich for performing the VSM measurements and Dr. Yvonne Hertle for helpful discussions. This work was supported by the DFG within SFB 840 program (TP A1). Thomas Ruhland thanks the Bavarian Graduate Support Program for a scholarship.

Notes and References

†Electronic Supplementary Information (ESI) available: DLS data of Fe_2O_3 and UV-Vis and photoluminescence spectra for CdSe and CdSe(ZnS)-NP in toluene at RT. Intensity-weighted hydrodynamic radii distribution (DLS) of CdSe(ZnS)/γ-Fe_2O_3/SiO_2/PNIPAAm at 10% cross-linking density and 20°C. Fourier transform infrared (FT-IR) spectra of Fe_2O_3 NPs, Fe_2O_3/SiO_2 core shell particles and Fe_2O_3/SiO_2/PNIPAAm hybrid material with a 10% crosslinking density at RT. Magnetic hysteresis curves of γ-Fe_2O_3 NPs, γ-Fe_2O_3/CdSe(ZnS)/SiO_2 and core shell particles and γ-Fe_2O_3/CdSe(ZnS)/SiO_2/PNIPAAm hybrid material with a 10% crosslinking density at RT. Photographs of the macroscopic magnetic behavior of the hybrid materials and UV-Vis and fluorescence data concerning the particles which have CdSe as core.

References

1. Costi, R.; Saunders, A. E.; Banin, U., *Angew. Chem. Int. Ed.* **2010**, 49, 4878.
2. Kim, D. K.; Dobson, J., *J. Mater. Chem.* **2009**, 19, 6294.
3. Lee, J. E.; Lee, N.; Kim, H.; Kim, J.; Choi, S. H.; Kim, J. H.; Kim, T.; Song, I. C.; Park, S. P.; Moon, W. K.; Hyeon, T., *JACS* **2009**, 132, 552.
4. Hu, L.; Mao, Z.; Gao, C., *J. Mater. Chem.* **2009**, 19, 3108.
5. Selvan, S. T.; Tan, T. T.; Yi, D. K.; Jana, N. R., *Langmuir* **2009**, 26, 1163.
6. Müllner, M.; Schallon, A.; Walther, A.; Freitag, R.; Müller, A. H. E., *Biomacromolecules* **2009**, 11, 390.
7. De, M.; Ghosh, P. S.; Rotello, V. M., *Adv. Mater.* **2008**, 20, 4225.
8. Mori, K.; Yamashita, H., *Phys. Chem. Chem. Phys.* **2010**, 12, 14420.
9. Lu, Y.; Mei, Y.; Drechsler, M.; Ballauff, M., *Angew. Chem. Int. Ed.* **2006**, 45, 813.
10. Kim, J.; Piao, Y.; Hyeon, T., *Chem. Soc. Rev.* **2009**, 38, 372.
11. Das, G. K.; Heng, B. C.; Ng, S.-C.; White, T.; Loo, J. S. C.; D'Silva, L.; Padmanabhan, P.; Bhakoo, K. K.; Selvan, S. T.; Tan, T. T., *Langmuir* **2010**, 26, 8959.
12. Minnich, A J.; Dresselhaus, M. S.; Ren, Z. F.; Chen, G., *Energy Environ. Sci.* **2009**, 2, 466.
13. Walther, A.; Matussek, K.; Müller, A. H. E., *ACS Nano* **2008**, 2, 1167.
14. Walther, A.; Hoffmann, M.; Müller, A. H. E., *Angew. Chem. Int. Ed.* 2008), 120, 723.
15. Kotov, N. A., *Science* **2010**, 330, 188.
16. Alivisatos, A. P., *J. Phys. Chem.* **1996**, 100, 13226.
17. Medintz, I. L.; Uyeda, H. T.; Goldman, E. R.; Mattoussi, H., *Nat. Mater.* **2005**, 4, 435.
18. Liu, J.-H.; Fan, J.-B.; Gu, Z.; Cui, J.; Xu, X.-B.; Liang, Z.-W.; Luo, S.-L.; Zhu, M.-Q., *Langmuir* **2008**, 24, 5241.
19. Yu, W. W.; Wang, Y. A.; Peng, X., *Chem. Mater.* **2003**, 15, 4300.
20. Peng, Z. A.; Peng, X., *J. Am. Chem. Soc.* **2000**, 123, 183.
21. Jamieson, T.; Bakhshi, R.; Petrova, D.; Pocock, R.; Imani, M.; Seifalian, A. M., *Biomaterials* **2007**, 28, 4717.
22. Gupta, A. K. ; Gupta, M. ; *Biomaterials* **2005**, 26, 3995.
23. Lu, A. H.; Salabas, E.; Schüth, F , *Angew. Chem. Int. Ed.* **2007**, 46, 1222.
24. Laurent, S.; Forge, D.; Port, M.; Roch, A.; Robic, C.; Vander Elst, L.; Muller, R. N.,*Chem. Rev.* **2008**, 108, 2064.
25. Kwon, S. G.; Hyeon, T., *Acc. Chem. Res.* **2008**, 41, 1696.
26. Hyeon, T.; Lee, S. S.; Park, J.; Chung, Y.; Na, H. B., *J. Am. Chem. Soc.* **2001**, 123, 12798.
27. Goldmann, A. S.; Schödel, C.; Walther, A.; Yuan, J.; Loos, K.; Müller, A. H. E., *Macromol. Rapid Comm.* **2010**, 31, 1608.
28. Schärtl, W., *Adv. Mater.* **2000**, 12, 1899.
29. Schärtl, W., *Nanoscale* **2010**, 2, 829.
30. Sanchez, C.; Rozes, L.; Ribot, F.; Laberty-Robert, C.; Grosso, D.; Sassoye, C.; Boissiere, C.; Nicole, L., *C. R. Chim.* **2010**, 13, 3.

31. Sanchez, C.; Soler-Illia, G. J. D. A. A.; Ribot, F.; Grosso, D., *C. R. Chim.* **2003**, 6, 1131.
32. Fahmi, A.; Pietsch, T.; Mendoza, C.; Cheval, N., Mater. *Today* **2009,** 12, 44.
33. Caruso, F., *Adv. Mater.* **2001**, 13, 11.
34. Caruso, F.; Caruso, R. A.; Möhwald, H., *Science* **1998**, 282, 1111.
35. Salgueiriño-Maceira, V.; Correa-Duarte, M.; Spasova, M., Liz-Marzán, L.; Farle, M., *Adv. Funct. Mater.* **2006**, 16, 509.
36. Pyun, J.; Matyjaszewski, K., *Chem. Mater.* **2001**, 13, 3436.
37. Tagit, O.; Janczewski, D.; Tomczak, N.; Han, M. Y.; Herek, J. L.; Vancso, G. J., *J. Europ. Polym.* **2010**, 46, 1397.
38. Pelton, R., *Adv. Colloid Interface Sci.* **2000**, 85, 1.
39. Tagit, O.; Tomczak, N.; Benetti, E. M.; Cesa, Y.; Blum, C.; Subramaniam, V.; Herek, J. L.; Vancso, G. J., *Nanotechnology* **2009**, 20, 185501.
40. Jone, C. D.; Lyon, L. A., *Macromolecules* **2003**, 36, 1988.
41. Gan, D.; Lyon, L. A., *J. Am. Chem. Soc.* **2001**, 123, 7511.
42. Nayak, S.; Lyon, L. A., *Chem. Mater.* **2004**, 16, 2623.
43. Ionov, L.; Sapra, S.; Synytska, A.; Rogach, A.; Stamm, M.; Diez, S., *Adv. Mater.* **2006**, 18, 1453.
44. McPhee, W.; Tam, K. C.; Pelton, R., *J. Colloid Interface Sci.* **1993**, 156, 24.
45. Walther, A.; Müller, A. H. E., *Soft Matter* **2008**, 4 , 663.
46. Wurm, F.; Kilbinger, A. F. M., A*ngew Chem Int Ed* **2009**, 48, 8412.
47. Jiang, S.; Chen, Q.; Tripathy, M.; Luijten, E.; Schweizer, K. S.; Granick, S., *Adv. Materials* **2010**, 22 , 1060.
48. Pich, A.; Richtering, W., *Adv. Polym. Sci.* **2011**, 234, 1.
49. Laurenti, M.; Guardia, P.; Contreras-Cáceres, R.; Pérez-Juste, J.; Fernandez-Barbero, A.; Lopez-Cabarcos, E.; Rubio-Retama, J., *Langmuir* **2011**, 27, 10484.
50. Li, Q.; Zhang, L.; Bai, L.; Zhang, Z.; Zhu, J.; Zhou, N.; Cheng, Z.; Zhu, X., *Soft Matter* **2011**, 7, 6958.
51. Deng, Y. H.; Yang, W. L.; Wang, C. C.; Fu, S. K., *Adv. Mater*. **2003**, 15 , 1729.
52. Cai, J.; Guo, J.; Ji, M.; Yang, W.; Wang, C. C.; Fu, S. K., *Colloid Polym. Sci.* **2007**, 285, 1607.
53. Zhelev, Z.; Ohba, H.; Bakalova, R., *J. Am. Chem. Soc.* **2006**, 128, 6324.
54. Yi, D. K.; Selvan, S. T.; Lee, S. S.; Papaefthymiou, G. C.; Kundaliya, D.; Ying, J. Y., *J. Am. Chem. Soc.* **2005**, 127, 4990.
55. Yi, D. K.; Lee, S. S.; Papaefthymiou, G. C.; Ying. J. Y., *Chem. Mater.* **2006**, 18, 614.
56. Qu, L.; Peng, X.; *J. Am. Chem. Soc.* **2002**, 124, 2049.
57. Selvan, S. T.; Tan T.; Ying, J.Y., *Adv. Mater.* **2005**, 17, 1620.
58. Sudeep, P. K.; Early, K. T.; McCarthy, K. D.; Odoi, M. Y.; Barnes, M. D.; Emrick, T., *J. Am. Chem Soc.* **2008**, 130, 2384.
59. Skaff, H.; Sill, K.; Emrick, T., *J. Am. Chem. Soc.* **2004**, 126, 11322.

SUPPORTING INFORMATION

to

Superparamagnetic and fluorescent thermo-responsive Core-Shell-Corona hybrid Nanogels with a protective Silica Shell

By Thomas M. Ruhland, Paul M. Reichstein, Alexander P. Majewski, Andreas Walther, Axel H. E. Müller

1. Characterization of the pristine nanoparticles

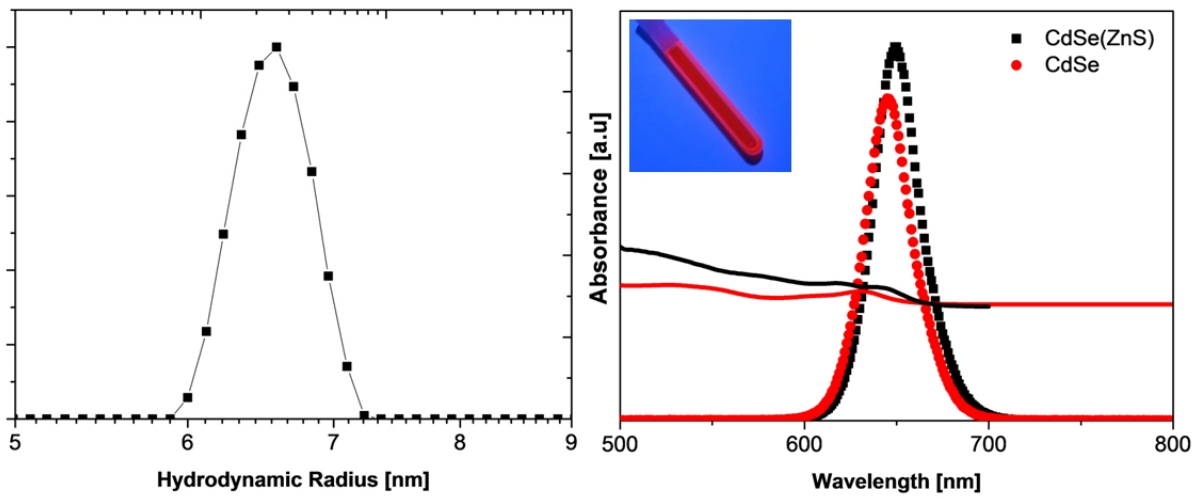

Figure 5-S1. DLS data of Fe_2O_3 and UV-Vis and photoluminescence spectra for CdSe and CdSe(ZnS)-NP in toluene at RT.

2. Structural analysis

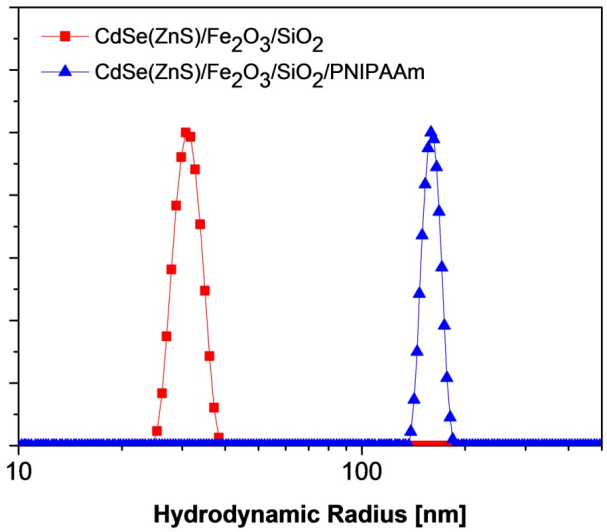

Figure 5-S2. Intensity-weighted hydrodynamic radii distribution (DLS) of CdSe(ZnS)/γ-Fe_2O_3/SiO_2/PNIPAAm and hybrid nanogels at 10% cross-linking density and 20° C.

CdSe(ZnS)/γ-Fe_2O_3/SiO_2 and CdSe(ZnS)/γ-Fe_2O_3/SiO_2/PNIPAAm show hydrodynamic radii of 32 nm and 170 nm.

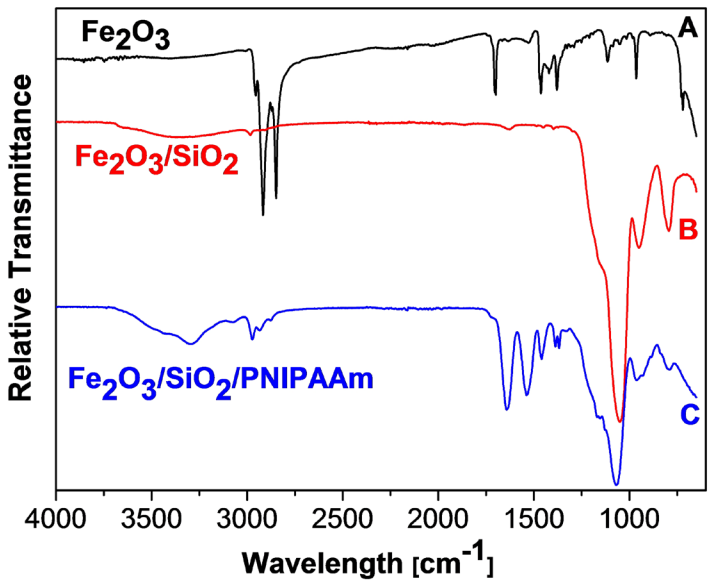

Figure 5-S3. Fourier transform infrared (FT-IR) spectra of Fe_2O_3 NPs, Fe_2O_3/SiO_2 core shell particles and Fe_2O_3/SiO_2/PNIPAAm hybrid material with a 10% crosslinking density at RT.

The polymerization process can be monitored by infrared spectroscopy (FT-IR) as shown in Figure 5-S3.

Figure 5-S3 A corresponds to the pure Fe_2O_3 nanoparticles and depicts the characteristic signal of the carbonyl groups of the oleic acid covered NPs at approximately 1700 cm^{-1} and additionally the signal for (CH_2-CH_3) - bonding at 2800-2900 cm^{-1}. The condensation of TEOS on the Fe_2O_3 surface (Figure 5-S3 B) was confirmed by the presence of the following absorption bands: 2970 cm^{-1} (aliphatic CH stretching vibrations), 1634 cm^{-1} (C=C stretching), 1160 cm-1 (Fe-O-Si), 1063 cm^{-1} + 804 cm^{-1} (Si-O-Si bonds) and 956 cm^{-1} (Si-O(H)). Figure 5-S3 C depicts the IR spectrum of the core-shell-corona particles, where the following bands should be noted: 3450 cm^{-1} (N-H stretching of PNIPAAm amide), 1645 cm^{-1} and 1550 cm^{-1} (secondary amide C=O stretching and N-H stretching of the CONH groups of the NIPAAm polymer chains, respectively), 1410 cm^{-1} and 1390 cm^{-1} (C-H bending of isopropyl groups).

2. Functional properties

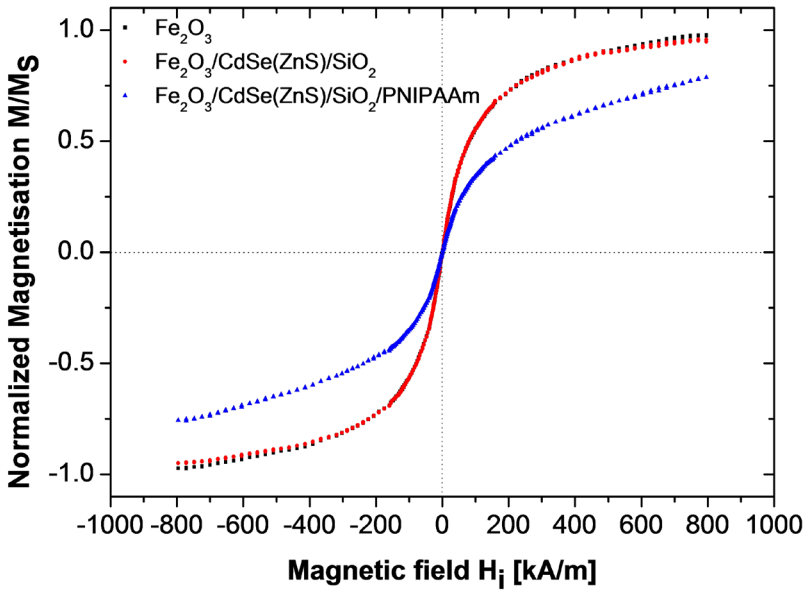

Figure 5-S4. Magnetic hysteresis curves of γ-Fe_2O_3 NPs, γ-Fe_2O_3/CdSe(ZnS)/SiO_2 and core shell particles and γ-Fe_2O_3/CdSe(ZnS)/SiO_2/PNIPAAm hybrid material with a 10% crosslinking density at RT.

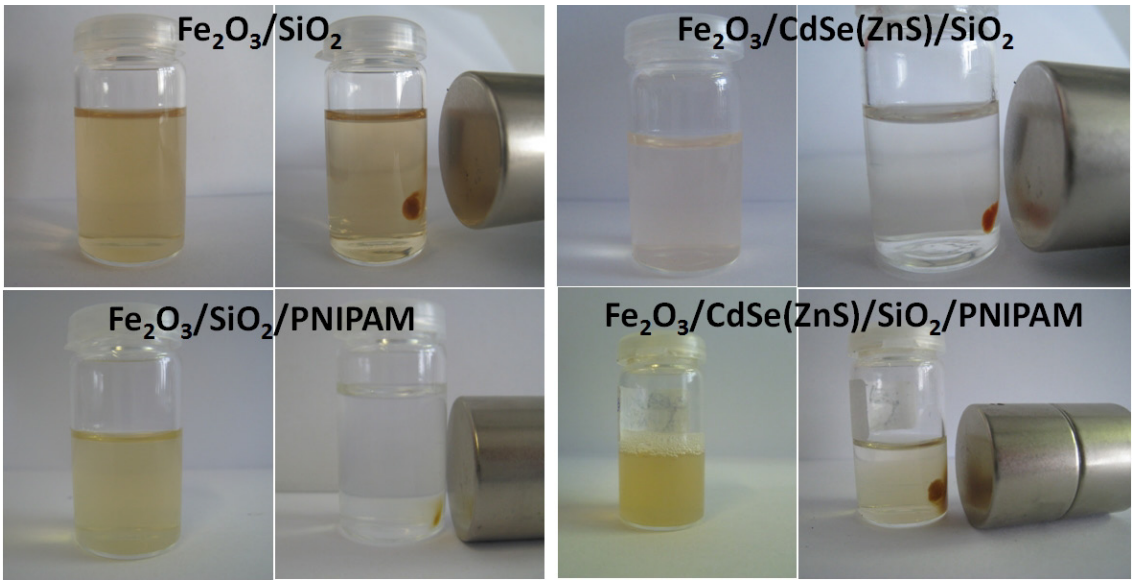

Figure 5-S5. Photographs of (left side) γ-Fe_2O_3/SiO_2 and γ-Fe_2O_3/SiO_2/PNIPAAm and (right side) γ-Fe_2O_3/CdSe(ZnS)/SiO_2 and γ-Fe_2O_3/CdSe(ZnS)/SiO_2/PNIPAAm hybrid materials. (10% cross-linking density at 20° C). All photos were taken after 30min.

2. Optical properties

Fluorescence spectroscopy of the core–shell–corona particles demonstrates a preserved photoluminescence during the various encapsulation steps, as already mentioned in Figure 5- 8 B. To discuss in detail, the optical properties of the samples were investigated using the photoluminescence spectra and UV–Vis absorption. In comparison of the adsorption spectra of the CdSe(ZnS) quantum dots, CdSe(ZnS)/SiO_2 core–shell particles and CdSe(ZnS)/SiO_2/PNIPAAm core–shell–corona particles, the absorbtion peaks of the core–shell and core–shell–corona particles are in good agreement with the maximum absorption peak of QD´s (Figure 5-S6 A). A slight red shift can be observed during the reaction steps, which may evolve from the changes in local refractive index of the surrounding shells. The PL spectra in Figure 5-S6 B shows a minimal shift in the photoluminescence peak position, demonstrating preservation of photophysical properties. Figures 5-S6 C and D present the absorbance and photoluminescence spectra of CdSe(ZnS)/Fe_2O_3/SiO_2 core–shell particles and CdSe(ZnS)/Fe_2O_3/SiO_2/PNIPAAm core-shell-corona particles. The statistical distribution of QD`s and $Fe_2O_3$ NP`s within one silica shell does also not induce any negative effect on the optical properties, as the absorbance and photoluminescence peaks of CdSe(ZnS)/Fe_2O_3/SiO_2 and CdSe(ZnS)/Fe_2O_3/SiO_2/PNIPAAm particles are similar to the homogeneous CdSe(ZnS)/SiO_2 particles.

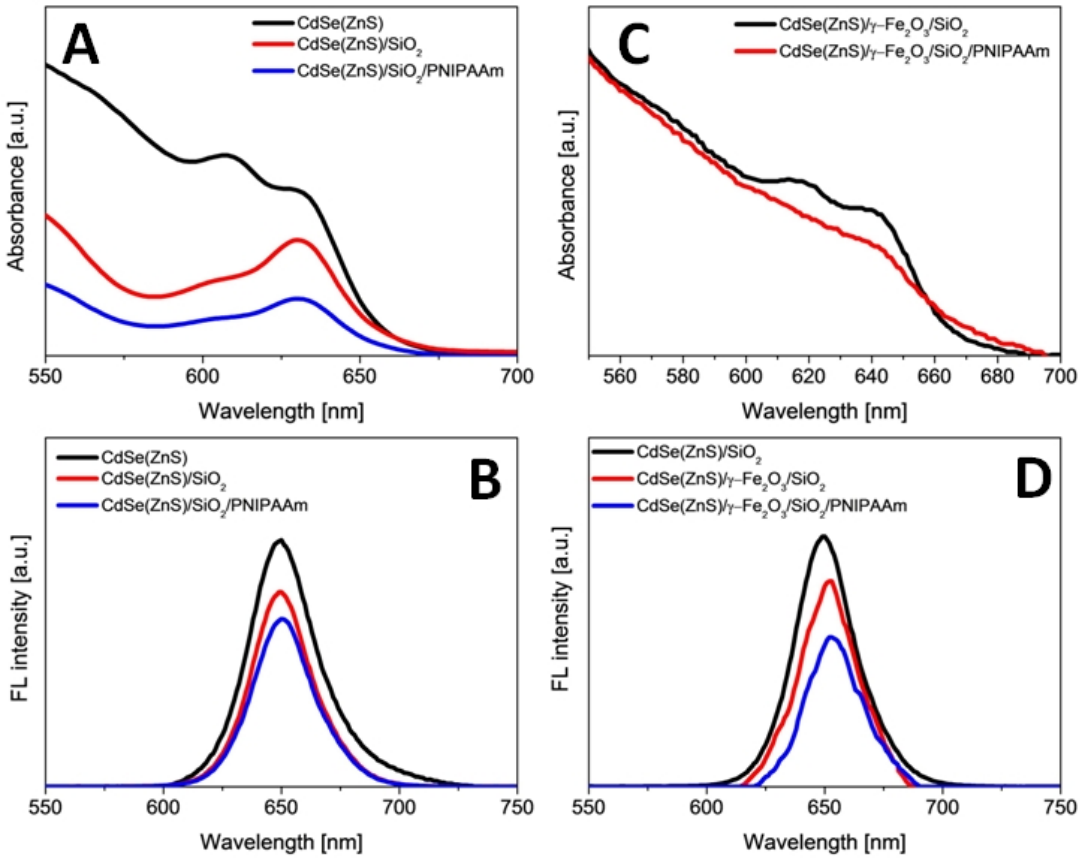

Figure 5-S6. Optical properties of hybrid core – shell – corona hybrid particles. (A+B) Fluorescence and Photoluminescence spectra for hybrid particles with a CdSe(ZnS) core. (C+D) Fluorescence and Photoluminescence spectra for hybrid particles with a statistical distribution of CdSe(ZnS) NP`s and $Fe_2O_3$ NP`s cores.

Chapter 6

Magnetic Core-Shell Nanoparticles as Carriers for Olefin Dimerization Catalysts

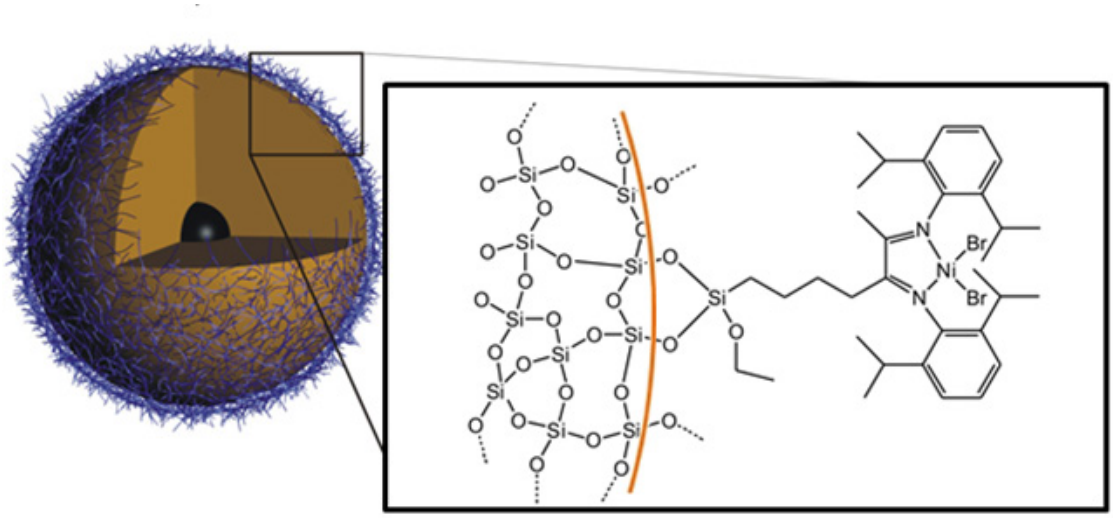

This work has been published in *Eur. J. Inorg. Chem.* **2013**, 12, 2146-2153
as a joint project
between the departments *Inorganic Chemistry II* and *Macromolecular Chemistry II*
under the title:

"Magnetic Core-Shell Nanoparticles as Carriers for Olefin Dimerization Catalysts"

by Thomas M. Ruhland, Julian R.V. Lang, Helmut G. Alt* and Axel H. E. Müller*

Magnetic Core-Shell Nanoparticles as Carriers for Olefin Dimerization Catalysts

Thomas M. Ruhland[1], Julian R.V. Lang[2], Helmut G. Alt[2], Axel H. E. Müller[1]**

[1] Department of Macromolecular Chemistry II, Universität Bayreuth, Universitätsstraße 30, 95440 Bayreuth, Germany, E-Mail: axel.mueller@uni-bayreuth.de

[2] Department of Inorganic Chemistry II, Universität Bayreuth, Universitätsstraße 30, 95440 Bayreuth, Germany, E-mail: helmut.alt@uni-bayreuth.de

Thomas M. Ruhland and Julian R.V. Lang contributed equally to this work.

Abstract

We report the covalent support of functionalized nickel complexes on magnetic core-shell hybrid particles γ-Fe_2O_3/SiO_2. Two completely different ways of connecting the particle with these nickel complexes were carried out. The first approach used the hydrosilylation method between the alkene substituted nickel-complex and a silane. In a second approach, the particles were connected with the complexes via click chemistry (copper catalyzed Huisgen 1,3-dipolar cycloaddition). For this purpose the nickel complexes were substituted with an alkyne moiety. The characterization methods transmission and scanning electron microscopies, energy dispersive X-ray diffraction, and FT-IR spectroscopy were employed to characterize the successful heterogenization of the nickel complexes.

Keywords: Hybrid Core-Shell Particle, Iron Oxide, Silica, Phenoxyimin Nickel, Catalyst

Introduction

Nanotechnology is a multidisciplinary platform to target materials for a wide field of applications. Magnetic nanoparticles and hybrid core-shell particles of well-defined size and shape with unique and advanced properties for a large field of possible applications have received a great deal of attention ranging from biomedical applications, magnetic separation media and other high-functional devices[1-5] to materials engineering[6-10] and catalysis[11-17]. A spherical nanoparticle with a core–shell architecture is a viable way to combine multiple functionalities on a nanoscopic length scale.[18-20]

Catalysis is becoming a strategic field of science because it represents a new way to meet the challenges in a lot of different fields of daily life. The concept of green chemistry, which makes catalysis science even more important, has become an daily present part of sustainable chemistry and life. Nanocatalysts with tunable size, shape, and composition drew tremendous interest in both theoretical and technological fields in recent years.[21,22] Although heterogeneous catalysts are widely used in a variety of industries, it is often difficult to isolate and separate the final product after the reaction has completed. Homogeneous catalysis suffers from the problematic separation of the catalysts and products, and the re-use of the catalyst. These problems are of environmental and economic interest in large scale synthesis. A possible heterogenization of the existing catalysts could help to design nanocatalysts with excellent activity, greater selectivity, higher stability and could be an attractive solution to this problem. These characteristics can easily be achieved via tailoring the size, shape, morphology, composition, thermal and chemical stability. The pioneers of magnetochemistry are superparamagnetic iron oxid particles, such as magnetite (Fe_3O_4) and maghemite (γ-Fe_2O_3). Besides these oxide materials, pure metal nano-magnets made out of iron or cobalt are produceable in relevant scales.[23-26] Both blank particles are vulnerable towards chemical reactions to lose magnetism. For further applications, the particles need to be protected against chemical, thermal or mechanical influences. In general, there are three ways of stabilization: 1) addition of monomers such as carboxylates or phosphates,[27-30] 2) coating with inorganic materials such as silica or gold metal,[31-36] 3) coating with organic matrices, as surfactants and polymers.[37-42] Silica plays an important role in the preparation of core–shell nanoparticle systems due to its excellent physical and chemical properties, the varable surface chemistry and the drastically increased chemical stability: it is optically transparent, easily functionalized, and the simple and robust synthesis of silica particles

from the monomer tetraethoxysilane (TEOS) has been established for many decades. Silica-coated γ-Fe_2O_3 magnetic nanoparticles (MNPs) combine the advantages of magnetic cores and functionalizeable silica surfaces. While classic heterogeneous catalysts are widely used in industry, lower activities compared to homogeneous systems are commonly detected.[42] A great proportion of these catalysts is deep inside the supporting material and thus reactants have limited access to the catalytic sites.[43] Decreasing the size of the support down to the nanometer scale, the surface area is increased and the support can be evenly dispersed in solution, forming a homogeneous emulsion.[13] In recent years, much attention has been focused on catalysis research and magnetic nanoparticles have been employed in important reactions as hydrogenation, hydroformylation, Suzuki-Miyaura and Heck couplings, and olefin metathesis.[44-46]

Herein, we combine the properties of core-shell nanoparticles with the catalytic character of certain complexes in hybrid core-shell-corona nanoparticles. The idea was to create a heterogeneous catalyst for facile product separation for the catalytic conversion of olefins. An external magnet can remove the magnetic particles out of the solution, or generate two phases for following product separation. We report the application of nickel complexes supported on magnetic nanoparticles incorporated in silica shells during the catalyzed polymerization and dimerization of both ethylene and propylene.

Experimental Section

General considerations

Air- and moisture sensitive reactions were carried out under an atmosphere of purified argon using conventional Schlenk or glove box techniques. The dimerization reactions were performed with pressure Schlenk tubes.

Materials

All solvents were purchased as technical grade and purified by distillation over Na/K alloy under an argon atmosphere. Iron(0)pentacarbonyl ($Fe(CO)_5$; 99.9 %), oleic acid (90 %), dioctyl ether (> 99 %), poly[oxyethylene(5)]nonylphenylether (Igepal ® CO 520), ammonium hydroxide (NH_4OH; 28 % in H_2O), tetraethylorthosilicate (TEOS; > 98 %), were purchased from Sigma Aldrich. All other chemicals were purchased commercially from Aldrich or Acros or were synthesized according to literature procedures. The

methylaluminoxane solution (MAO, 30wt% in toluene) was obtained from Albemarle, USA.

Procedure for the synthesis of γ-Fe_2O_3 nanoparticles

The synthesis of γ-Fe_2O_3 nanoparticles was adopted from literature.[5,10] A 250 ml two-neck round-bottom flask, connected to a reflux condenser, was charged with 120 ml dioctyl ether and 29.0 ml oleic acid (25.76 g, 91.2 mmol) and degassed with N_2 for 15 min. The reaction mixture was heated to 100 °C under N_2 atmosphere before adding 4ml $Fe(CO)_5$ (30.4 mmol). Subsequently, the resulting mixture was heated to reflux and kept for 1.5 h until the solution colour turned to black. After cooling down to room temperature the reaction mixture was stirred under air to initiate the oxidation process of iron to achieve γ-Fe_2O_3 nanoparticles. The yielded particles were precipitated with ethanol and separated by means of a NbFeB-magnet. The particles were immediately redispersed in toluene, THF or *n*-hexane. For further purification the precipitation and separation process was repeated.

Procedure for the synthesis of γ-Fe_2O_3/SiO_2 core shell particles

The synthesis is based on the experimental procedure mentioned in the literature.[10] Herein, we present detailed experimental conditions. Polyoxyethylene(5)nonylphenyl ether (0.23 g, 0.54 mmol, Igepal CO-520) was dispersed in a 10 ml small flask containing 4.5 mL cyclohexane in a ultrasound bath for 10 minutes. Next, 400 µL of γ-Fe_2O_3 nanoparticles dispersed in cyclohexane (0.5 mg/mL) were added to the flask and vortexed for 5 minutes at 200 min^{-1}. The rapid addition of ammonium hydroxide (29.4%, 40 µL) formed a reverse brownish microemulsion and the subsequent addition of tetraethylorthosilicate (30 µL, TEOS) started the growth of the silica shell. The nanocomposite particles were aged for 48 hours using a shaking incubator at RT and 100 rpm as oscillation rate (soft agitation!) and purified by several cycles of centrifugation with 4500 rpm for 10 minutes and cautious redispersion in ethanol. The magnetic core shell particles could also be magnetically collected. The final product was redispersed in millipore water.

Procedure for the synthesis of the complexes

Complex **1** was prepared and characterized elsewhere.[47]

2, 3, 4: 10 mmol of the respective ligand precursor in 100 ml ethanol were mixed with 5 mmol $Ni(OAc)_2$ * x H_2O. The solution was stirred under reflux for 24 h. The volume was reduced and the complexes precipitated by the addition of pentane. The products were filtered through a glas frit and washed with pentane. The complexes were obtained as green solids with yields in the range of 73 – 82%.

Scheme 6-1. Prepared complexes **2-4** containing an alkyne moiety.

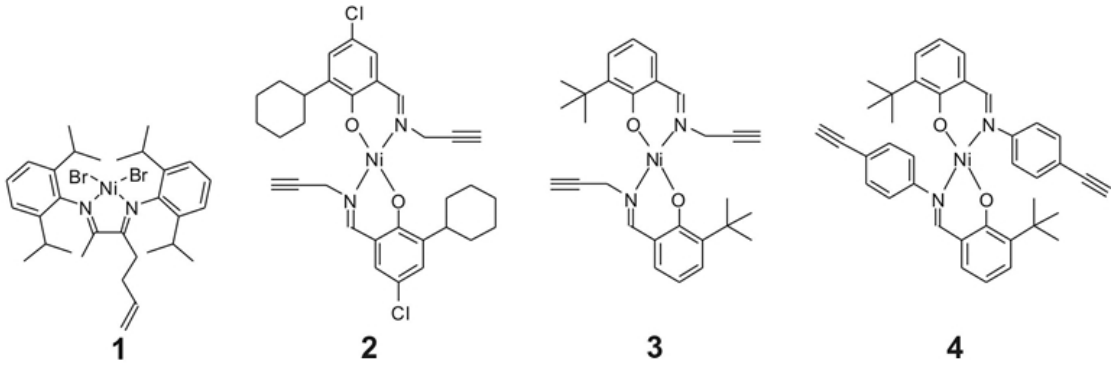

2: MS data: 608 ($M^{\bullet+}$) (68), 357 (9), 333 (72), 236 (100). $C_{32}H_{34}Cl_2N_2O_2Ni$: calcd. C 63.19, H 5.63, N 4.61. Found C 63.08 H 5.52 N 4.53%.

3: MS data: 485 ($M^{\bullet+}$) (37), 214 (100). $C_{28}H_{31}N_2O_2Ni$: calcd. C 69.16, H 6.43, N 5.76. Found C 69.64.08 H 6.31 N 5.47%.

4: MS data: 610 ($M^{\bullet+}$) (41), 510 (41), 335 (27), 276 (100). $C_{38}H_{36}N_2O_2Ni$: calcd. C 74.65, H5.93, N 4.58. Found C 74.17, H 5.34, N 4.81%.

Synthesis of the supported complexes

These core-shell particles contain a γ-Fe_2O_3 core coated with a silica layer. The silica shell has plenty of hydroxyl groups for potential derivatization, on which the catalysts can be successfully immobilized. The series of catalysts was designed to include two ways of linkage with the core-shell support material. Both methods contain simple reaction steps and uncomplicated handling and anchoring of a triethoxysilane group. The first approach (Scheme 6-2 and 6-3) uses hydrosilylation to combine the bis(imin)nickel complex with the supporting material. The second approach (Scheme 6-4) describes the combination of the magnetic particles and the alkyne end-functionalized phenoxyimine-nickel complexes using the copper catalyzed azide alkyne Huisgen 1,3-dipolar cycloaddition (CuAAC).

Approach 1:

Scheme 6-2. Hydrosilylation reaction of the diimine nickel complex and triethoxysilane.

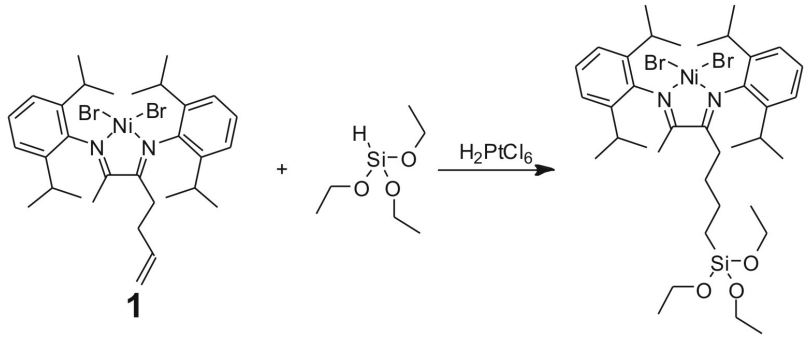

1-H An amount of 630 mg (1.28 mmol) of the complex **1** was dissolved in a minimum amount of toluene. 5 mg (12 µmol) of Speier´s catalyst (H_2PtCl_6) was added. Triethoxysilane (233 mg, 1.42 mmol) was added dropwise over a period of 30 minutes. After 24 hours of stirring, the complex precipitated by the addition of pentane (Scheme 6-2). The solution was removed and 100 mg of the magnetic core-shell nanoparticles in 25 ml toluene were added. The suspension was stirred for 3 d at 85°C. The slight blue solution was separated from the brown-green solid and the particles were thoroughly washed with toluene, THF and DCM (Scheme 6-3).

Scheme 6-3. Route of heterogenization for complex **1**.

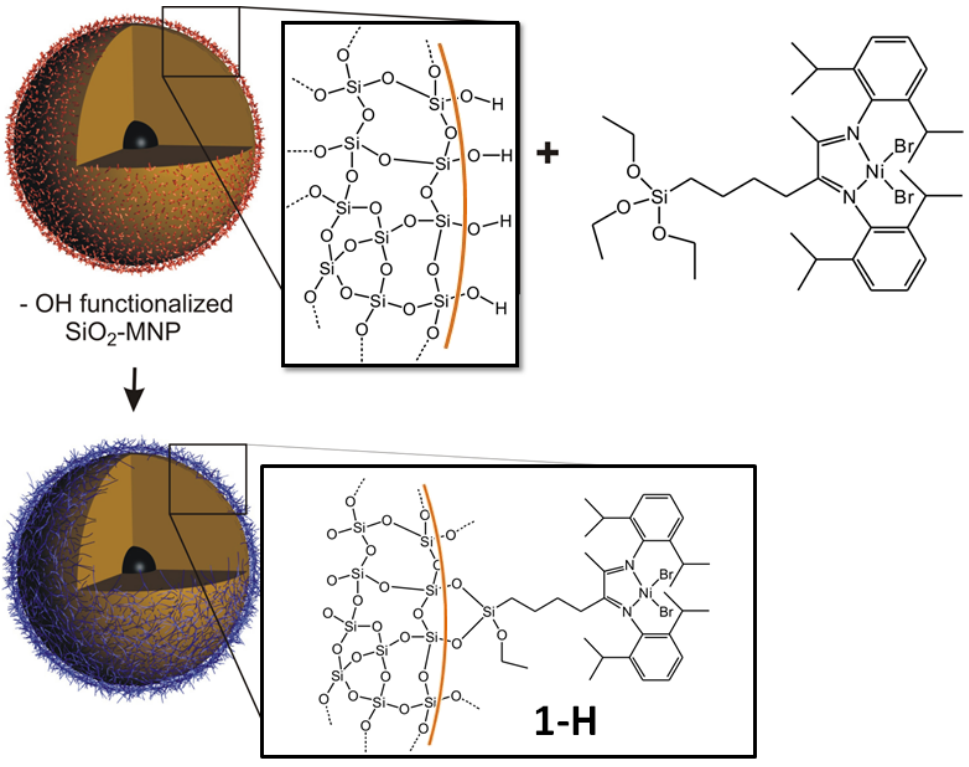

Approach 2: [48-51]

2-H, 3-H, 4-H: An amount of 8.8 g chloropropyl(triethoxy)silan and 2.4 g sodiumazid were stirred in 100 ml DMSO for 4 d. A white solid precipitated and was filtered off. 200 mg of the magnetic particles were added to third of the solution and stirred for 4 days at 80°C.

Scheme 6-4. Route of heterogenization for complexes **2-4**.

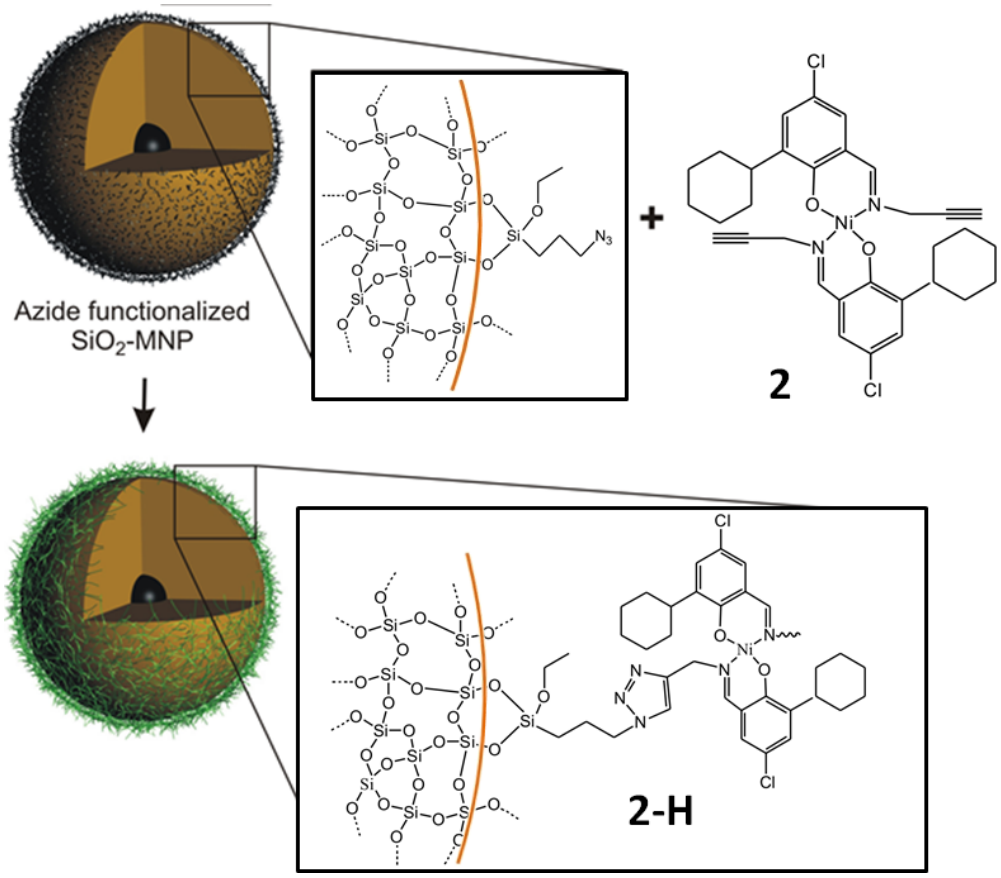

The particles were separated and suspended in toluene with an excess of the respective catalysts (1 g). Copper chloride (2 mg) and sodium ascorbate (4 mg) were dissolved in 5 ml distilled water and added to the stirred mixture. After a reaction time of 4 days, the particles were separated *via* centrifugation and washed thoroughly with toluene, ethanol and pentane.

Polymerization of ethylene

An amount of 25 mg of the supported catalyst was placed in a pressure Schlenk tube with 10 ml toluene and 12 ml MAO solution (10%wt.). Ethylene was added under pressure (2

bars) for 20 min at room temperature. The particles were carefully washed with isopropanol and toluene and separated from the solution and dried under vacuum.

Dimerization of propylene

An amount of 25 mg of the supported catalyst was placed in a 400 ml pressure Schlenk tube with 5 ml of toluene and activated with 10 ml MAO solution (Ni:Al = 1:500). The pressure Schlenk tube was filled with 50 ml liquid propylene and closed, warmed to room temperature with an external water bath and stirred. After the reaction time of 1 hour, the Schlenk tube was opened and the solution was analyzed by GC.

Characterization

The products of the dimerization experiments were characterized with a ***gas chromatograph*** (Agilent 6890) and ***GC/MS*** (FOCUS DSQ^{TM} Thermo Scientific).

Mass spectra were recorded on a Varian MAT CH7 instrument (direct inlet system, electron impact ionization 70 eV). Elemental analyses were performed with a VarioEl III CHN instrument. Acetanilide was used as standard.

Bright-field Transmission electron microscopy (TEM) was performed on Zeiss CEM 902 and LEO 922 OMEGA electron microscopes operated at 80 kV and 200 kV, respectively. Data evaluation and processing was carried out with Soft Imaging Viewer and Image Tool.

Scanning electron microscopy (SEM) was performed using a LEO 1530 Gemini instrument equipped with a field emission cathode with a lateral resolution of approximately 2 nm. The acceleration voltage was chosen between 0.5 kV, and 30 kV for element dispersive x-ray analysis (EDX).

Energy Dispersive X-Ray Scattering (EDX) spectra were measured with a LEO 1530 Gemini instrument using an Oxford EDX INCA 400 device. The obtained spectra were analysed with the microscope software and the present elements in the sample were detected by their corresponding X-ray absorption peaks.

Fourier-Transform Infrared Spectroscopy (FT-IR) was carried out on a Spectrum 100 FT-IR spectrometer from Perkin Elmer. For measurements the U-ATR unit was used. The dried samples were directly placed on top of the U-ATR unit for measurements.

Results and Discussion

Here we describe in detail the synthesis, characterization and catalytic behavior of the synthesized catalysts on magnetic core-shell nanoparticles. Therefore, the synthetic strategy towards monodisperse hybrid catalysts with core-shell architecture consists of the following steps. In a first step, we synthesized monodisperse and hydrophobically functionalized superparamagnetic γ-Fe_2O_3 NPs *via* thermal decomposition of $Fe(CO)_5$ in the presence of oleic acid, which serve as cores for the final hybrid particles (Figure 6-1A). Afterwards single NPs are encapsulated with a silica layer by a dedicated microemulsion procedure, yielding monodisperse core-shell γ-Fe_2O_3/SiO_2 particles. The precise adjustment of the conditions allows to achieve a reliable encapsulation and to either entrap several particles or single ones and to precisely tailor the thickness of the silica shell.[10] The size of the γ-Fe_2O_3 particles is well controlled by the amount of oleic acid that is used in relation to the $Fe(CO)_5$ amount. Transmission electron microscopy (TEM) images in Figure 6-1 A show the γ-Fe_2O_3 cores with an average diameter of 9.9 nm ± 1.8 nm, which is corroborated by dynamic light scattering (DLS) with a z-average hydrodynamic radius of 6.6 nm and a PDI of 1.04 (Figure 6-1 C). Obviously, the oleic acid ligand shell is invisible in the TEM, but contributes to in the hydrodynamic distribution function obtained by DLS, resulting in a higher value.[5] A thin 20 nm layer of silica was coated on this core, *via* a sol-gel process to give silica-coated γ-Fe_2O_3 magnetic nanoparticles with an average diameter of 52 nm (Figure 6-1 B and C).

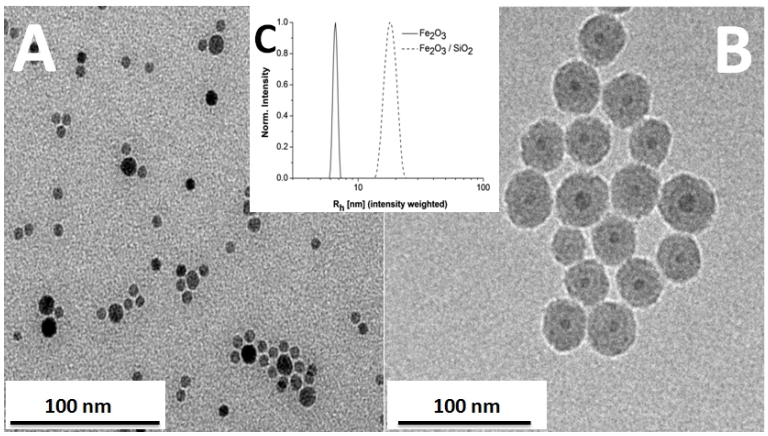

Figure 6-1. TEM images of (A) the iron oxide cores and (B) the magnetic nanoparticles with silica shell. (C) Intensity-weighted hydrodynamic radii distribution (DLS) of γ-Fe_2O_3 and γ-Fe_2O_3/SiO_2.

The series of catalysts (Scheme 6-1) was designed to include two ways of linkage with the core-shell support material. Both methods contain simple reaction steps and

uncomplicated handling and anchoring of a triethoxysilane group. As already mentioned in the experimental section, the first approach (Scheme 3) uses hydrosilylation to combine the bis(imin)nickel complex with the supporting material. The second approach (Scheme 4) describes the combination of the azido-functionalized magnetic particles and the alkyne end-functionalized phenoxyimine-nickel complexes using the copper catalyzed azide alkyne Huisgen 1,3-dipolar cycloaddition (CuAAC).[48,49] For both approaches, the same magnetic core-shell particles containing a γ-Fe_2O_3 core coated with a silica layer were used.

The first synthetic strategy involves a precursor consisting of an ω-alkenyl diimine moiety coordinated to nickel(II)bromide and a silane that can react with the silica particles (Scheme 6-2). After the silane-ene reaction the complex with the triethoxysilane moiety can be coupled directly to the support material (Scheme 6-3). This hydrosilylation reaction is simple and quick. After heating in toluene, the complex **1** is immobilized covalently on the silica support (**1-H**). Following the product removal by centrifugation, the particles were washed with toluene, THF and DCM. TEM images in Figure 6-2 show the core-shell structure with the modified surface of the particles. The surface of the particles with connected complexes is distinctly coarser than the blank Fe_2O_3/SiO_2 nanoparticles. This indicates that a thin layer of supported catalyst is surrounding the silica particles.

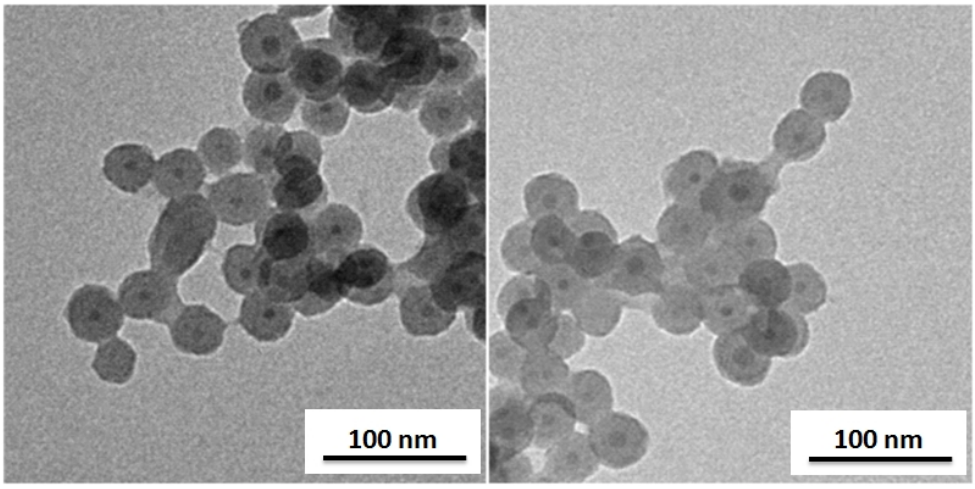

Figure 6-2. TEM image of **1-H**. The surface is distinctly coarser compared to the blank particles.

Energy dispersive x-ray diffraction (EDX) was used to identify the chemical composition at the surface and of the particles. The EDX spectrum in Figure 6-3 clearly shows the typical peaks. A small peak from the iron core is obvious. Silicon (shell) and oxygen

(core and shell) are the dominant peaks. can be confirmed by peak integration of the typical nickel and bromine peaks shows a 4.2% and 7.9% fraction, respectively, which represents an atomic ratio of 1:1.9 confirming the composition $NiBr_2$. These results are in good agreement with the proposed structure and the conclusion drawn from the TEM image.

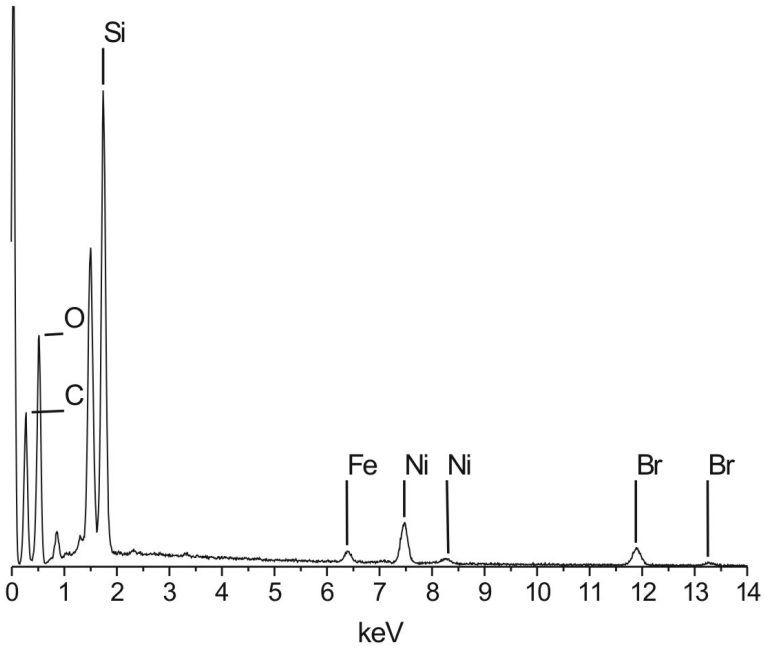

Figure 6-3. EDX spectrum of the heterogeneous complex **1-H**.

In the second approach (Scheme 6-4), we discuss the heterogenization of phenoxyimine nickel complexes. Here, the Huisgen 1,3-dipolar cycloaddition is used to attach azido-functionalized γ-Fe_2O_3/SiO_2 particles to the alkyne group of the complex. This is a very adaptable and orthogonal method to attach any compound carrying an alkyne group to a desired surface. Therefore, three different nickel complexes bearing an alkyne group (Scheme 6-2) were synthesized and connected to the azido-functionalized support following the procedure shown in scheme 6-4. The respective ligands were synthesized according to the literature[50] and the complexes were obtained *via* a known process.[51] The magnetic particles Fe_2O_3/SiO_2 were combined with azide functionalized propyl(triethoxy)silan-moiety *via* condensation. The Huisgen 1,3-dipolar cycloaddition is used to attach azido-functionalized γ-Fe_2O_3/SiO_2 particles to the alkyne group of the complex. Figure 6-4 shows the FT-IR spectra of the pure γ-Fe_2O_3/SiO_2 particles, the nickel-phenoxyimine connected γ-Fe_2O_3/SiO_2 (**2-H**) and the pure complex **2**. The silica surface is characterized by two dominant peaks, the nonbonded surface Si-OH groups

with the band in the range of 3300-3700 cm^{-1} and the characteristic Si-O-Si vibration (1080 cm^{-1}).

The supported complex shows two peaks at 1620 cm^{-1} and 1730 cm^{-1}, typical for the C=N and C=C stretching bands. The created triazole group shows a typical peak at 1450 cm^{-1}, dominated by the peaks of the support. This resonance is not very intense, but it is the only characteristic resonance of the triazole group and confirms a successful grafting. The phenoxyimine complex unit itself shows no strong IR stretching frequency and it is likely masked by the silica bands of the support. The pure complex shows the very intense band of the C-H vibration of the alkyne group (3280 cm^{-1}).

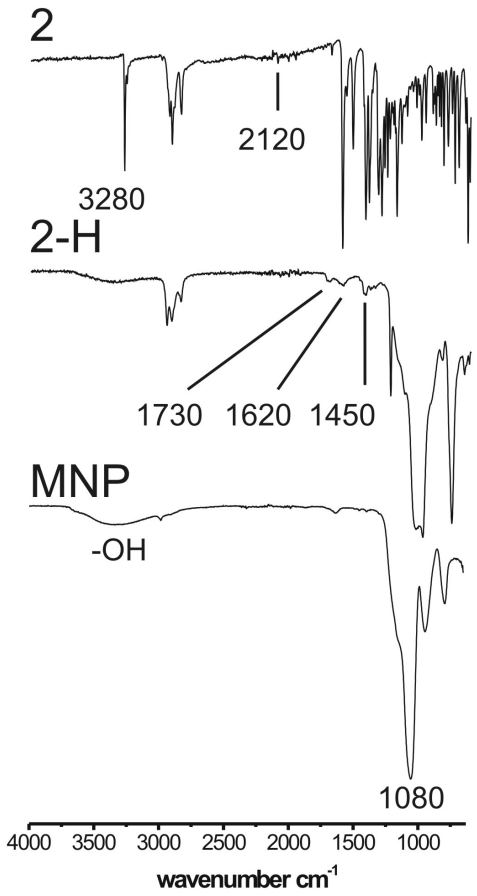

Figure 6-4. FT-IR spectra of the pure nanoparticles (MNP), the supported complex (**2-H**), and the corresponding pure complex (**2**).

After the click reaction with the alkyne-complexes, the particles were imaged by TEM. Figure 6-5 shows the core-shell structure with the modified surface of the particles. The surface of the heterogeneous complexes is distinctly coarser than the blank γ-Fe_2O_3/SiO_2

particles. All these aspects indicate that the heterogenization reaction was successful and the IR-results are confirmed.

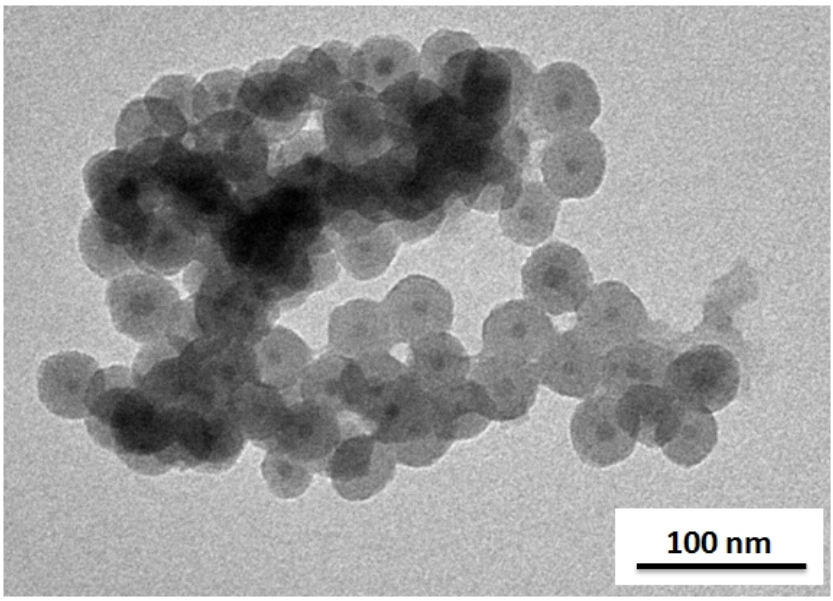

Figure 6-5. TEM image of **2-H**, The surface is distinctly coarser compared to the blank particles.

Catalytic properties

The catalytic performance of the heterogeneous catalysts **1-H**, **2-H**, **3-H** and **4-H** is described in the following section. The bisimino-nickel complex **1-H** was applied as catalyst for the catalytic polymerization of ethylene. Recent works described the homogeneous polymerization of ethylene with bisimino-nickel complexes after activation with MAO.[39] In our experiments, the immobilized catalyst was stirred in toluene, and ethylene was added under low pressure for 20 minutes to the solution. After quenching with isopropanol, the polymer particles were washed and separated *via* centrifugation. The particles were visualized by scanning electron microsopy (SEM) in Figure 6-6. The images show spherical particles with a rough polymer surface. A broad polymer particle size distribution with particles sizes from 0.1 to 1.5 µm was observed. The images show that polymerization happens at the catalysts on the particle surface and that particles grow independently.

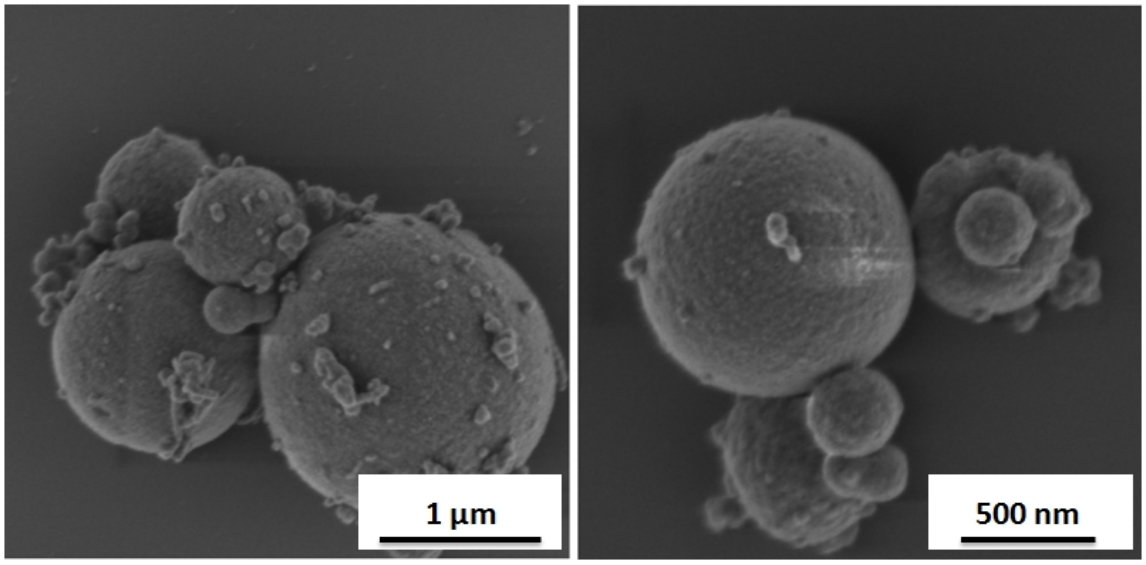

Figure 6-6. SEM images of the polyethylene particles polymerized by **1-H**.

The polymerization test proves that covalently immobilized complexes on γ-Fe_2O_3/SiO_2 particles are catalytically active and that catalysis happens at these functionalized particles. The polymerization experiments were carried out as control experiments for the following dimerization experiments, where no change in the shape and size of the catalytic active particles can be observed. During the catalytic test, we mainly focused on the role of the support in order to ease the product separation. Thus, all catalytic tests were carried out using a heterogeneous catalyst in a closed system (pressure Schlenk tube). Here, we used phenoxyimine-nickel complexes (**2-H**), which are normally highly active for the dimerization of propylene after activation with MAO.

Scheme 6-5. Phenoxyimine nickel complexes before and after activation with MAO. The square represents the free coordination site.[52]

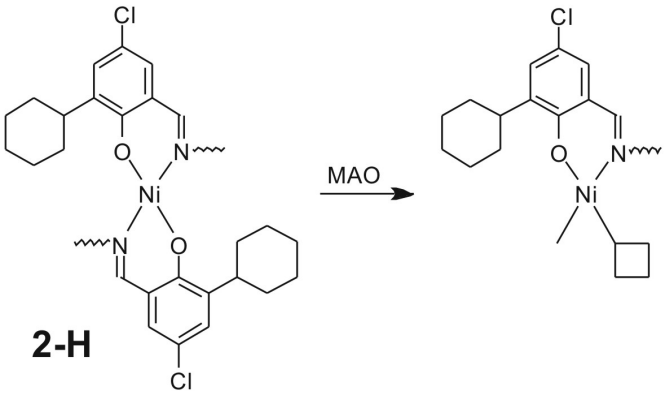

With two ligands coordinating the central metal, the phenoxyimine complexes have two sides for heterogenization (scheme 6-5). After activation with MAO, one ligand leaves the complex and leaves a free coordination side. After activation, a single complex is

fixed on a single side to a particle. With all three immobilized catalysts the catalytic dimerization of propylene was performed. While bisimine nickel catalysts are known for their catalytic polymerization of ethylene[39], phenoxyimine nickel complexes are highly active for the dimerization of propylene.[41]

Table 6-1. Results of the catalytic dimerization of propylene with the heterogeneous complexes **2-H**, **3-H** and **4-H**.

	C 6 [%]	C 9 [%]	C 12 [%]	Activity of the Heterogeneous Catalyst [kg(product)/mol h]
2-H	75	25	-	264
3-H	92	6	2	405
4-H	87	7	6	380

The results in Table 6-1 show products of the dimerization reactions of the supported catalysts **2-H**, **3-H** and **4-H** after activation with MAO. All three heterogeneous catalysts show high selectivities of up to 92 % for dimeric products. Besides some trimeric products nearly no higher oligomers are formed. Aside from all already mentioned general advantages of heterogeneous catalysts, the activity of our heterogeneous catalysts is comparable to its homogenous analogues.[51] Table 6-1 shows the dimerization results of the heterogeneous catalysts. The catalytic activities are in the range of 264 to 405 which represents the "Turn over Numbers" (TONs) of 3150 (**2**), 4520 (**4**) and 4820 (**3**). The gas chromatograms of the dimerization experiments show the typical distribution. The branched methylpentenes t-4-MP-2 (trans-4-methyl pent-2-en) and 2-MP-2 (2-methylpent-2-en) are the main products, with 4-MP-1(4.methylpent-1-en), c-4-MP-2 (cis-4-methylpent-2-en), t-2-Hex (trans-2-hexen) and c-2-Hex (cis-2-hexen) as byproducts.

All three heterogeneous catalysts are highly efficient for the catalytic dimerization of propylene (table 1). The catalytic activities and the product distribution are in a range according to the literature.[41] The reaction products were decanted after separating the particles using a strong magnet to hold the catalyst in the Schlenk tube.

Conclusions

We demonstrated both the successful heterogenization of phenoxyimine nickel and bis(imine) nickel complexes *via* the azide-alkyne click-reaction and hydrosilylation reaction. Uniformly nano-sized silica-coated magnetic nanoparticles were synthesized and used as support material. The complexes were covalently bound to the silica shell, according to EDX, TEM and FT-IR observations. Polymerization of ethylene after activation with MAO was successful and SEM images clearly show spherical particles with a rough polymer surface. Dimerization of propylene showed the excellent catalytic properties of the heterogenizated phenoxyimine nickel complexes. The compared use under homogeneous "free" conditions resulted in the same product distribution. The facile preparation and the catalytic properties show the high potential of this heterogeneous system. Catalysts can be separated by the means of a strong magnet, and ease the problematic product separation. The application of this catalytic system combines homogeneous activities and selectivities, and the separation of the product and the catalyst phase in heterogeneous systems.

Acknowledgement

The authors acknowledge financial support from ConocoPhillips, Bartlesville, USA. We thank André H. Gröschel for his help with schemes **3** and **4**, Alexander Majewski for providing the γ-Fe_2O_3 nanoparticles. This work was supported by the DFG within SFB 840 program (TP A1). Thomas Ruhland thanks the Bavarian Graduate Support Program for a scholarship.

References

1. Lee, J. ; Lee,Y.; Youn,, J. K. ; Na, H. B.; Yu, T. ; Kim, H.; Lee, S.M.; Koo, Y. M.; Kwak, J. H.; Park, H. G. ; Chang, H. N.; Hwang, M.; Park, J. G.; Kim, J.; Hyeon, T., *Small* **2008**, 4, 143.
2. Klein, D. L.; Roth, R.; Lim, A. K. L.; Alivisatos, A. P.; McEuen, P. L., *Nature* **1997**, 389, 699.
3. Soci, C.; Zhang, A.; Xiang, B.; Dayeh, S. A.; Aplin, D. P. R.; Park, J.; Bao, X. Y.; Lo, Y. H.; Wang, D., *Nano Lett*. **2007**, 7, 1003.
4. Pfaff, A.; Schallon, A.; Ruhland, T. M.; Majewski, A. P.; Schmalz, H.; Freitag, R.; Müller, A. H. E., *Biomacromolecules* **2011**, 12, 3805.
5. Majewski, A. P.; Schallon, A.; Jérôme, V.; Freitag, R.; Müller, A. H. E.; Schmalz, H., *Biomacromolecules* **2012,** 13,857-866.
6. Minnich, A. J.; Dresselhaus, M. S.; Ren, Z. F.; Chen, G., *Energy Environ. Sci.* **2009**, 2, 466.
7. Kaur, A.; Gupta, U., *J. Mater. Chem.* **2009**, 19, 8279.
8. Walther, A.; Matussek, K.; Müller, A. H. E., *ACS Nano* **2008**, 2**,** 1167.
9. Walther, A.; Hoffmann, M.; Müller, A. H. E., *Angew. Chem. Int. Ed.* **2008,** 47**,** 711.
10. Ruhland, T. M.; Reichstein, P. M.; Majewski, A. P.; Walther, A.; Müller, A. H. E., *J. Colloid Interface Sci.* 2012, 374, 45.
11. Mori, K.; Yamashita, H., *Phys. Chem. Chem. Phys.* **2010**, 12, 14420.
12. Sethi, M.; Pacardo, D. B.; Knecht, M. R., *Langmuir* **2010**, 26, 15121.
13. Li, Y.; Somorjai, G. A., *Nano Lett.* **2010**, 10, 2289.
14. Bergbreiter, D. E.; Osburn, P. L.; Li, C., *Org. Lett.* **2002**, 4, 737.
15. Biffis, A.; Orlandi, N.; Corain, B., *Adv. Mater.* **2003**, 15, 1551.
16. Lu, Y.; Mei, Y.; Drechsler, M.; Ballauff, M., *Angew. Chem. Int. Ed* **2006**, 45, 813.
17. Lu, Y.; Mei, Y.; Drechsler, M.; Ballauff, M., *J. Phys. Chem. B*, 110 **2006**, 110, 3930.
18. Schärtl, W., *Nanoscale* **2010**, 2, 829.
19. Chaudhuri, R. G.; Paria, S., *Chem. Rev.* **2012**, 112, 2373.
20. Costi, R.; Saunders, A.; Banin, U., *Angew. Chem. Int. Ed.* 2010, 49, 4878.
21. Polshettiwar, V.; Luque, R.; Fihri, A.; Zhu, H.; Bouhrara, M.; Basset, J.–M., *Chem. Rev.* **2011**, 111, 3036.
22. K. An, S. Alayoglu, T. Ewers, A. G. Somorjai, *J. Colloid Interface Sci.* **201**2, 373, 1.
23. Grass, A. N.; Athanassiou, E. K.; Stark, W. J., *Angew. Chem.* **2007**, 119, 4996.
24. Herrmann, I. K.; Grass, R. N.; Mazunin, D.; Stark, W. J., *Chem. Mater.* **2009**, 21, 3275.
25. Grass, R. N.; Stark, W. J., *J. Mater. Chem.* **2006**, 16, 1825.
26. Stark, W. J.; Mädler, L.; Maciejewski, M.; Pratsinis, S. E.; Baiker, A., *Chem. Comm.* (**2003**) 588.
27. Sahoo, Y.; Pizem, H.; Fried, T.; Golodnitsky, D.; Burstein, L.; Sukenik, C. N.; Markovich, G., *Langmuir* **2001**, 17, 7907.

28. Sahoo, Y.; Goodarzi, A.;. Swihart, M. T.; Ohulchanskyy, T. Y.; Kaur, N.; Furlani, E. P.; Prasad, P. N., *J. Phys. Chem. B* **2005**, 109, 3879.
29. Fauconnier, N. N.; Pons, J. N.; Roger, J.; Bee, A., *J. Colloid Interface Sci.* **1997**, 194, 427.
30. Fauconnier, N. N.; Bee, A.; Roger, J.; Pons, J. N., Prog. *Colloid Polym. Sci.* **1996**, 100, 212.
31. Lu, A. H.; Salabas, E. L.; Schüth, F., *Angew. Chem. Int. Ed.* **2007**, 46, 1222.
32. Alcala, M. D.; Real, C., Solid *State Ionics* **2006**, 177, 955.
33. Woo, K.; Hong, J.; Ahn, J. P., *J. Magn. Magn. Mater* **2005**, 293, 177.
34. Ulman, A., *Chem. Rev.* **1996**, 96, 1533.
35. Lin, J.; Zhou, W.; Kumbhar, A., Fang, J., Carpenter, E. E.; O´Connor, C. J., *J. Solid State Chem.* **2001**, 159, 26.
36. Colvin, V. L.; Goldstein, A. N ; Alivisatos, A. P., *J. Am. Chem. Soc.* **1992**, 114, 5221.
37. Gamarra, L. F.; Brito, G. E. S.; Pontschka, W. M.; Amaro, E.; Parma, A. H. C.; Goya, G. F., *J. Magn. Magn. Mater.* **2005**, 289, 439.
38. Schöpf, B.; Neuberger, T.; Schulze, K.; Petri, A.; Chastellain, M.; Hofmann, M.; von Rechenberg, B., *J. Magn. Magn. Mater.* **2005**, 293, 419.
39. Schultz, M. D.; Calvin, S.; Fatouros, P. P.; Morrison, S. A.; Carpenter, E. E., *J. Magn.Magn. Mater.* **2007**, 311, 464.
40. Kohler, N.; Fryxell, G. E.; Zhang, M., *J. Am. Chem. Soc.* 126 **2004**, 126, 7206.
41. Gomez-Lopera, S. A.; Arias, J. L.; Gallardo, V.; Delgado, A. V., *Langmuir* **2006**, 22, 2816.
42. Rase, H. F., *Handbook of commericial catalysts: Heterogeneous catalysts, CRC Press*, New York (**2000**).
43. Zhu, Y.; Stubbs, L. P.; Ho, F.; Liu, R.; Ship, C. P.; Maguire, J. A.;. Hosmane, N. S., *ChemCatChem* **2010**, 2, 365.
44. Yoon, T. J.; Lee, W.; Oh, Y. S.; Lee, J. K., New. *J. Chem.* **2003**, 27, 227.
45. Zhu, Y. H.; Lee, C. N.; Kemp, R. A.; Hosmane, N. S.; Maguire, J. A., *Chem. Asian J.* **2008**, 3, 650.
46. Asteruc, D.; Lu, F.; Aranzaes, J. R., *Angew. Chem. Int. Ed.* **2005**, 117, 8062.
47. Al Shammari, H., *Dissertation thesis*, University Bayreuth (**2009**).
48. Kolb, H. C.; Finn, M. G.; Sharpless, K. B., *Angew. Chem. Int. Ed.* **2001**, 40, 2004.
49. Binder, W. H.; Sachsenhofer, R., *Macromol. Rapid Commun.* **2007**, 28, 15.
50. Görl, C.; Alt, H. G., *JJC* **2008**, 3, 245.
51. Alt, H. G.; Schneider, K., *JJC* **2008, 1,** 11.
52. Carlini, C., *Appl. Catal* **2002, 231,** 307.

Chapter 7

Nanoscale hybrid Silica/Polymer Janus Particles with a double-responsive Hemicorona

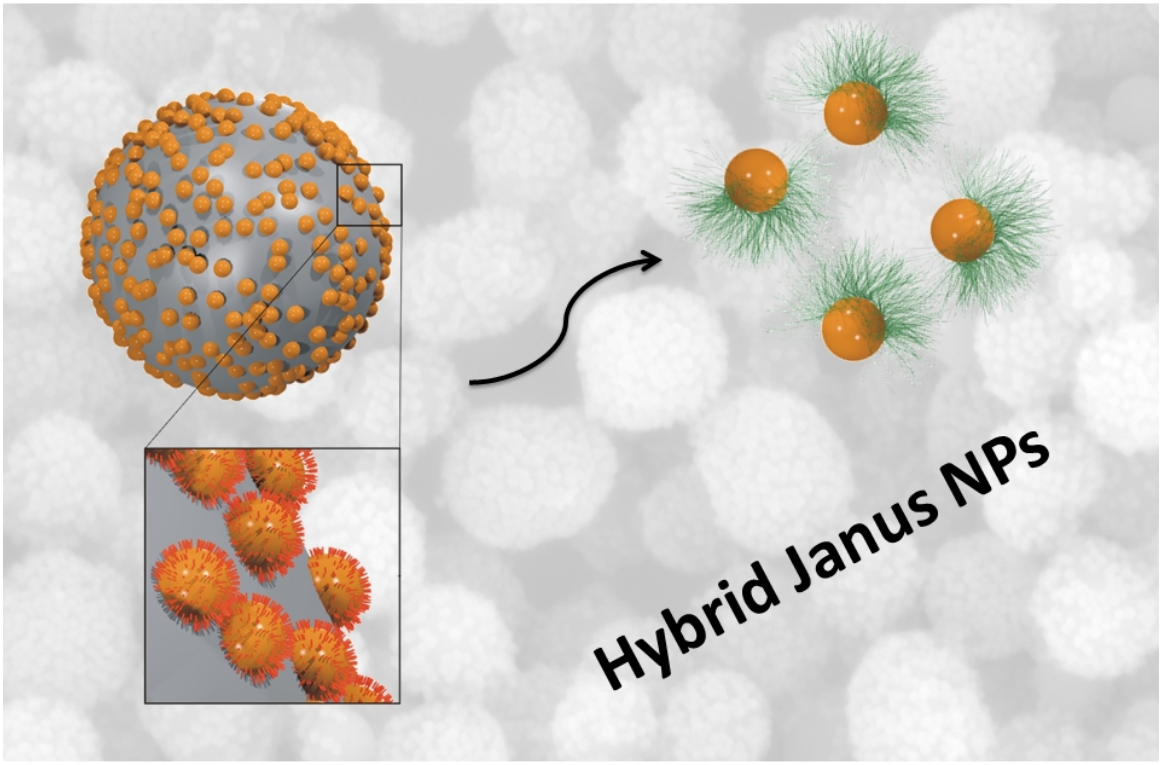

This work has been submitted to *ACS Nano* under the title:

"Nanoscale hybrid Silica/Polymer Janus Particles with a double-responsive Hemicorona"

by Thomas M. Ruhland, Holly S. McKenzie, Thomas S. Skehlon, Stefan A. F. Bon, Andreas Walther and Axel H. E. Müller*

Nanoscale hybrid silica/polymer Janus particles with a double-responsive hemicorona

Thomas M. Ruhland[1], Holly S. McKenzie[2], Thomas S. Skelhon[2], Stefan A. F. Bon[2], Andreas Walther[3] and Axel H. E. Müller[1,4]**

[1] Department of Macromolecular Chemistry II, University Bayreuth, 95444 Bayreuth, Germany

[2] Department of Chemistry, University of Warwick, Coventry CV4 7AL, United Kingdom

[3] DWI at RWTH Aachen University, 52506 Aachen, Germany

[4] new address: Institute of Organic Chemistry, Johannes Gutenberg University Mainz, 55099 Mainz, Germany

walther@dwi.rwth-aachen.de; axel.mueller@uni-mainz.de

Abstract

We report a versatile large-scale synthesis strategy for hybrid Janus nanoparticles with a silica core and a unilaterally attached polymer corona in a size range below 100 nm. The stimuli-responsive behavior of these nanoparticles with a poly(2-(dimethylamino)ethyl methacrylate) hemicorona is investigated. The synthesis is based on a modified version of the Pickering emulsion technique in combination with surface-initiated atom transfer radical polymerization (ATRP) in a "grafting from" approach. In a first step, poly(vinyl acetate) (PVAc) latex particles are prepared *via* emulsion polymerization. Colloidal stability is provided by 30 nm silica nanoparticles that adhere to the surface of the growing polymer droplets. This results in polymer latexes which are armored with a layer of tightly immobilized nanoparticles, one side of which is immersed in the latex and thus protected. After modification of the exposed side of the particles with an ATRP-initiator and the removal of the particles from the interface, PDMAEMA chains are grown from the unprotected side of the silica particles, yielding well-defined Janus nanoparticles with

a stimuli–responsive PDMAEMA hemicorona. Transmission and scanning electron microscopy, dynamic light scattering, thermogravimetric analysis and turbidity measurements were used to characterize the Janus particles. Most importantly, this synthetic approach is easily scalable and can be amended to furnish a wide range of nanoscale hybrid Janus particles. Furthermore, we demonstrate reversible switching behavior upon pH and temperature changes and find a peculiar aggregation behavior into linear strings at low pH and high concentration.

KEYWORDS: Janus Particles, Hybrid Particles, Pickering Emulsion, Stimuli-Responsive Nanoparticles

Introduction

Hybrid nanoparticles combining relevant properties from different material classes will be one of the fundamentally important building blocks for multifunctional materials in future technologies. As a unique type of building block, anisotropic particles, such as patchy, multicompartment, or Janus particles, have attracted much interest.[1-5] The anisotropy in structure, shape, chemical and morphological patchiness generates defined self-assembly behavior and advanced functionalities and thus, has great potential in the scientific field as well as in industry. Besides being used as building blocks for the study of hierarchical self-assembly processes, Janus particles have in fact demonstrated a considerable potential in a number of fields such as drug carriers[6], stabilizers in emulsion polymerizations[7] and blends[8], surfactants[9- 11], switchable devices[12] and optical probes[13,14]. Suitable Janus particles can be synthesized *via* several synthetic pathways including microfluidic techniques[6,15], lithography[16], controlled phase separation phenomena[17,18], template-directed self-assembly[19-21], controlled surface nucleation[22-24] and partial masking.[25,26] Despite advances in the synthesis routes mentioned above, major limitations prevail for the synthesis of nanoscale and highly functional Janus particles with facile and scalable procedures.

A promising route towards a large number of complex anisotropic Janus nanoparticles is based on the Pickering emulsion method.[27-36] Pickering emulsions are stabilized by particles instead of surfactant molecules. A kinetically stable emulsion is achieved when particles in the range of nanometers to micrometers are located stably at the interface between oil and water. One hemisphere of a particle is located in the oil phase, such as a latex or wax, whereas the other hemisphere is exposed and susceptible to chemical reactions. After the chemical modification amphiphilic Janus particles can be obtained upon release from the intermediate desymmetrizing template. This synthesis was originally proposed by Granick and co-workers, who immobilized silica particles (> 100 nm) at oil/wax interfaces.[27-29] The Pickering particles were frozen at the interface of water and wax upon cooling of the system. On the basis of this method, Stamm *et al.* prepared large stimuli-responsive bicomponent polymeric Janus particles with diameters larger than 800 nm.[32] Other groups used this method, too, to create a particularly interesting group of Janus colloidal particles which have asymmetric surface structures and specifically responding to external stimuli.[32-36.] Research so far has focused on rather

large Pickering particles (much larger than 100 nm), which are easier to immobilize at interfaces. When approaching nanoscale Pickering particles, their rotation needs to be arrested to furnish high-quality Janus nanoparticles.[35] This has been a major problem, so far.

In this work, we propose a versatile and simple synthetic route towards hybrid core-shell-corona Janus nanoparticles with a core size well below 100 nm. In comparison to other methods based on Pickering emulsion we can work with particles, which are much smaller than those used in previous research and simultaneously reduce the experimental efforts. First, silica nanoparticles (30 nm in diameter) are immobilized at the interface of sub-micrometer sized droplets of poly(vinyl acetate) (PVAc) using a Pickering emulsion polymerization protocol developed by Bon *et al.*.[37-42] The nanoparticles are partially embedded in the resulting latex and thus protected on one hemisphere. Subsequently, after removing the particles from the latex we graft poly(2-dimethylamino)ethyl methacrylate (PDMAEMA) chains from the formerly unprotected side of the silica particles using surface-initiated atom transfer radical polymerization (ATRP). Thus, we present the first detailed study on a synthesis route to obtain nanoscale amphiphilic Janus silica nanoparticles decorated with pH- and thermo-responsive PDMAEMA chains. We describe their double-stimuli responsive properties at high dilution and highlight their self-assembly behavior in more concentrated solutions, for which we find a pH-dependent aggregation into linear strings.

Experimental Section

Materials

AVS buffer solutions (Titrinorm, VWR), Ammonium hydroxide (NH_4OH; 28% in H_2O), potassium peroxodisulfate (KPS; >99%, Sigma Aldrich), Styrene (≥99%, Sigma Aldrich), AIBN (2,2′-Azobis(2-methylpropionitrile; 98%, Sigma Aldrich), 2-Bromo-2-methylpropionyl bromide (98%, Sigma-Aldrich), 2-(dimethylamino)-ethyl methacrylate (DMAEMA; 99%, Sigma-Aldrich), vinyl acetate (VAc; 99%, Sigma Aldrich), 1,1,4,7,10,10-hexamethyl triethylenetetramine (HMTETA; 97%, Sigma-Aldrich), Karstedt`s catalyst (Platinum(0)-1,3-divinyl-1,1,3,3-tetramethyldisiloxane complex solution; platinum content ~3 %, Sigma Aldrich), Triethoxysilane (95%, Sigma Aldrich), Triethylamine (>99 %, Sigma Aldrich), 5-Hexen-1-ol (98%, Sigma Aldrich), Ludox TM-

40 sol (30 nm colloidal silica ; 40 wt% in water) and HF (48 wt%, Sigma Aldrich) were used as received. Copper(I) chloride (99.99%, Sigma Aldrich) was purified according to the literature[43] and the monomer DMAEMA was destabilized by passing through a basic aluminum oxide column. For dialysis, a regenerated cellulose tube (ZelluTrans, Roth) with a MWCO of 6−8 kDa was used. All chemicals and solvents (ethanol; methanol, acetone) were used without further purification. Deionized water was generated by a MilliQ system (Millipore) and was used in all experiments.

Silica-armoured poly(vinyl acetate) latexes made using Pickering emulsion polymerization

The emulsion polymerization was carried out in round bottom flasks or in a double-walled cylindrical glass reactor (250 mL, Asynt Ltd.) equipped with an external circulating heating bath (Julabo F-25 unit), a condenser, and a four-bladed metal overhead turbine stirrer fitted at approximately 2 cm from the bottom of the reactor vessel (Cowie Ltd.) typically running at 300 rpm. The pH measurements were performed on a pH-Meter (765 calimatic, Knick).

A 40.0 wt% solution of Ludox TM-40 silica sol (33.0 g, 5.7 wt% overall, or 44.0 wt% based on monomer) was diluted and dispersed in 167.0 g of deionised water. The pH of the dispersion was adjusted with concentrated HCl (aq) to pH ~ 4.5 and was placed under a nitrogen atmosphere in a 250 mL double-walled glass reactor by purging. Monomer, 30.0 g, was added and the reaction mixture was heated to 65 ºC, whilst stirring at 300 rpm. The emulsion polymerisation was started upon addition of 0.13 g KPS dissolved in 3.0 g of water. The reaction time was 6 h.[37] Contents and ratios of the experiment can be summarized as follows: The monomer content is 7.6 wt%, the silica content 4.2 wt%, the ratio of silica to monomer 0.56 and the ratio KPS to monomer is 0.0055.

Synthesis of the ATRP initiator (2-bromo-2-ethyl)propionyloxyhexyltriethoxysilane

The experimental procedure is illustrated in Scheme 7-S1 (Supporting Information). The corresponding ^{1}H NMR spectra are shown in Figure 7-S1.

Pent-4′-enyl 2-bromo-2-methylpropionate

The synthesis follows a procedure mentioned in the literature.[44] 2-Bromo-2-methylpropionyl bromide (34.5 g, 150 mmol) was added in a dropwise fashion to a stirred

solution of 5-hexen-1-ol (15.0 g, 150 mmol) and triethylamine (18.1 g, 179 mmol) in dry dichloromethane (80 mL). After stirring at 0 °C under argon for 1 h, the reaction mixture was allowed to warm to room temperature where it was stirred for an additional 2.5 h. The precipitated triethylamine hydrochloride was removed by filtration, and the solution was washed with aqueous ammonium chloride (saturated) and water. The dichloromethane was then removed, and the crude product was purified by vacuum distillation (85 °C/200 mbar) to give Pent-4′-enyl 2-bromo-2-methylpropionate as a colourless oily liquid.

^{1}H NMR ($CDCl_3$) δ 1.44 (quintet, 2H, CH_2), 1.65 (quartet, 2H, CH2), 1.93 (s, 3H, CH_3), 2.08 (q, 2H, CH_2), 4.16 (t, 2H, CH_2), 4.91-5.04 (complex m, 2H, alkene =CH_2), and 5.70-5.85 (complex m, 1H, alkene =CH)

Synthesis of the ATRP initiator, (2-bromo-2-ethyl)propionyloxyhexyltriethoxysilane (Scheme S1-2)

Pent-4′-enyl 2-bromo-2-methylpropionate (0.75 g, 3.20 mmol) and dry toluene (10 mL) were charged into a two-neck round-bottom flask equipped with a magnetic stir bar and a rubber septum, and the system was purged with argon. Triethoxysilane (15 mL) purged with argon was added dropwise into the flask through a cannula, and subsequently Karstedt's catalyst solution (8.5 μl) was added into the system by a syringe. The reaction mixture was magnetically stirred overnight under an argon atmosphere. Unreacted triethoxysilane and toluene were completely removed under vacuum by raising the temperature to 60 °C to yield the initiator as a slightly yellow liquid in a quantitative yield.[44,45]

^{1}H NMR ($CDCl_3$): δ 0.63 (t, 2H, $SiCH_2$), 1.22 (t, 9H, CH_3CH_2OSi), 1.32-1.50 and 1.60-1.75 (Br, 8H, CH_2), 1.93 (s, 6H, CCH_3), 3.83 (q, 6H, CH_3CH_2OSi), 4.16 (t, 2H, CH_2O).

Unilateral attachment of ATRP initiators at the silica nanoparticles

The silica armoured PVAc latex suspension (PVAc/SiO_2) in water was solvent exchanged to ethanol *via* successive centrifugal separation. The collected PVAc/SiO_2 was redispersed in ethanol followed by centrifugation. This cycle was repeated five times and the armoured latex particles were suspended in ethanol. A mixture of ammonia solution (28% NH_3 aqueous solution, 4.6 g) and ethanol (15 mL) was added dropwise into the

suspension in ethanol (7.7 wt %, 2 mL) under magnetic stirring, and the system was stirred for 2 h at 40 °C. The ATRP initiator (100 mg, 0.15 mmol) dissolved in ethanol (1.5 mL) was added dropwise into the system, and the reaction mixture was continuously stirred for another 24 h at 40 °C. The modified silica particles were cleaned by consecutive centrifugation and redispersion in ethanol.

Removal of the ATRP initiator-modified silica nanoparticles and their characterization.

To remove the Pickering particles from the interface the silica-armored latex was suspended in toluene (2-5% solid content) and a mixture of styrene (99%) and AIBN (1%) was added in a ratio of 1:1 with respect to the latex. This mixture was stirred overnight at RT to allow the silica armored PVAc latex to swell, degassed with nitrogen for 15 minutes and then heated up to 70 °C for 8 hours. During the last step, the Pickering effect is neutralized and the unilaterally modified silica particles are removed from the swollen latex. While the detailed origin of this stress-induced expulsion of the Pickering particles is not fully understood, the procedure proved to be highly reproducible to remove the particles from the interface. Afterwards, the silica particles can be easily separated *via* centrifugation. Finally, the unilaterally initiator-coated silica particles were subjected to another solvent exchange treatment to obtain an acetone suspension for the following polymerization.

Synthesis of PDMAEMA-grafted silica Janus nanoparticles *via* ATRP

In a typical surface-initiated ATRP reaction, a 25 mL screw cap glass equipped with a septum was charged with 100 mg of initiator-modified Janus silica nanoparticles dispersed in 10 mL of acetone, 10 mL of DMAEMA (0.059 mol) and 3 mg CuCl (0.03 mmol). The mixture was purged with nitrogen for 30 min before adding 0.1 ml of degassed HMTETA (0.36 mmol) dissolved in 2.5 mL of acetone *via* syringe sequentially. The flask was then transferred to an oil bath at 45 °C. The polymerization was stopped after 1 h to 5 h by opening the flask and exposing the reaction mixture to air. After 10 min the reaction mixture is cooled down and can be used for further purification steps. The crude product was purified by centrifugation at 8000 rpm for 1 h to remove the copper catalyst. Subsequently, the half-grafted NPs were washed several times *via* centrifugation and redispersion using methanol and freeze-dried.

Cleavage of PDMAEMA chains from the Janus nanoparticles

A 48% HF (aq) solution (1 mL) was added to 1 mL of a particle suspension in water (H_2O) (~10 mg/mL), and the reaction was allowed to stir at room temperature for 4 h. Afterwards, the resulting white solution was dialyzed for 2 days against deionized water to neutral pH. The detached polymer chains were characterized by H_2O-SEC using a PEG_PEO calibration.

Characterization Methods

^{1}H Nuclear magnetic resonance (NMR) spectroscopy. ^{1}H-NMR spectra were recorded on a Bruker Ultrashield 300 spectrometer at an operating frequency of 300 MHz with deuterated chloroform ($CDCl_3$) as solvent. For the characterization of the water soluble polymers D_2O was used.

Bright-field Transmission electron microscopy (TEM) was performed on Zeiss CEM 902 and LEO 922 OMEGA electron microscopes operated at 80 kV and 200 kV, respectively. Data evaluation and processing was carried out with Soft Imaging Viewer and Image Tool. For ***cryogenic transmission electron microscopy (cryo-TEM)*** studies, a drop of the sample dissolved in water was put on a lacey transmission electron microscopy (TEM) grid, where most of the liquid was removed with blotting paper, leaving a thin film stretched over the lace. The specimens were instantly vitrified by rapid immersion into liquid ethane and cooled to approximately 90 K by liquid nitrogen in a temperature controlled freezing unit (Zeiss *Cryo*box, Zeiss NTS GmbH, Oberkochen, Germany). The temperature was monitored and kept constant in the chamber during all of the sample preparation steps. After freezing the specimens, the specimen was inserted into a *cryo*-transfer holder (CT3500, Gatan, München, Germany) and transferred to a Zeiss EM922 EF-TEM instrument. Examinations were carried out at temperatures around 90 K. The transmission electron microscope was operated at an acceleration voltage of 200 kV. Zero-loss filtered images were registered digitally by a bottom mounted CCD camera system (Ultrascan 1000, Gatan) combined and processed with a digital imaging processing system (Gatan Digital Micrograph 3.9 for GMS 1.4).

Scanning electron microscopy (SEM) **images** were taken using a LEO 1530 Gemini instrument equipped with a field emission cathode with a lateral resolution of approximately 2 nm. The acceleration voltage was chosen between 0.5 kV- 5kV. The

specimen were prepared by drying one drop of a highly diluted suspension on a clean silicon wafer at room temperature and coating with a platinum layer of 2 nm thickness using a sputter coater (Cressington 208HR) to make the specimen conductive. For ***cryogenic scanning electron microscopy (cryo-SEM)*** studies, a Zeiss Ultra plus FE-SEM equipped with Gatan Alto 2500 Cryo-stage was used. In a cryo-preparation the sample was freeze-fractured, lightly etched for 60 s at −112 ◦C, and sputtered with platinum. The specimen was transferred by a cryo-shuttle to the cold stage of the microscope.

Dynamic light scattering (DLS) was performed on an ALV DLS/SLS-SP 5022F compact goniometer system with an ALV 5000/E cross-correlator and a He–Ne laser (λ_0 = 632.8 nm). Prior to the light scattering measurements the sample solutions were filtered using Nylon filters with corresponding pore sizes. All samples were analyzed at high dilution. The data evaluation of the dynamic light scattering measurements was performed with the CONTIN algorithm.

Fourier-Transform Infrared Spectroscopy (FT-IR) was carried out on a Spectrum 100 FT-IR spectrometer from Perkin Elmer. For measurements the U-ATR unit was used. The dried samples were directly placed on top of the U-ATR unit for measurements.

Size Exclusion Chromatography (SEC) was performed on a system based on PL-aquagel-OH and PL-aquagel-OH-30 columns (8 µm particle diameter, Varian) equipped with an RI-detector. A mixture of 0.1M NaN_3 + 0.01M NaH_2PO_4 in water at pH = 2.5 was used as eluent at a flow rate of 1.0 mL/min. The measurements were conducted at 20 °C. For data evaluation, a calibration with linear PEG_PEO standards was applied.

Thermogravimetric Analysis (TGA). TGA measurements were carried out using a Mettler Toledo TGA/SDTA 85 at a heating rate of 10 K/min between 30 and 1000°C under an air-flow of 60 mL/min. The typical sample weight was 10 mg. For determining the grafting densities the weight loss of the Janus nanoparticles determined by TGA was used to calculate the amount of molecules per nm^2 according to equation 1.

$$\rho_{graft} = \frac{\Delta m/M}{Q \cdot A_{NP}} \cdot N_A \qquad (1)$$

$$Q = \frac{(m_0 - \Delta m)}{m_{NP}} \qquad (2)$$

Here, m_0, Δm and m_{NP} correspond to the initial sample weight, the weight of the grafted molecules or polymer determined by TGA, and the mass of a single silica particle, respectively. M is the molecular weight of the ATRP-Initiator or M_n of the grafted polymer. N_A is the Avogadro's number and A_{NP} corresponds to the surface of one nanoparticle. For the calculation the particles were assumed to be monodisperse in size with a spherical shape and an average diameter of 30 nm as determined by TEM and DLS. Further, on the basis of SEM images of the particle armored PVAC latexes in Figure 1 and the janus nanoparticles in Figure 6 we estimate that 1/4 of the particle surface can be modified and 3/4 is protected. This results in an average surface area of $A_{NP} = 2120$ nm^2 for a single silica nanoparticle. The mass of a single NP ($m_{NP} = 5.9 \cdot 10^{-14}$ g) was obtained by considering the density of the silica particles ($\rho = 2.3$ g/ml).

Turbidity Measurements. Turbidity measurements were performed using a titrator (Titrando 809, Metrohm, Herisau, Switzerland) equipped with a turbidity probe ($\lambda_0 = 523$ nm, Spectrosense, Metrohm) and a temperature sensor (Pt 1000, Metrohm). The temperature program (1 K/min) was run by a thermostat (LAUDA RE 306 and Wintherm_Plus software), using a homemade thermo-stable vessel. The cloud points were determined from the intersection of the two tangents applied to the two linear regimes of the transmittance curve at the onset of turbidity.

Results and Discussion

The synthetic strategy towards well-defined stimuli-sensitive hybrid Janus nanoparticles is illustrated in Scheme 1.

In a first step, we conduct a simple emulsion polymerization of vinyl acetate (VAc) in the presence of a commercial silica sol (Ludox TM-40). The silica particles used as Pickering stabilizers allow the fabrication of silica-armored polymer latexes. For the pristine silica particles, transmission and scanning electron microscopies (TEM, SEM; Figure 7-S2 A/B; Supporting Information) reveal a number-average radius of 14.5 ± 2 nm, which is corroborated by dynamic light scattering (DLS) resulting a z-average hydrodynamic radius of 15 ± 3 nm (Figure 7-S2 C).

Scheme 7-1. Synthesis of SiO_2/PDMAEMA hybrid Janus nanoparticles.

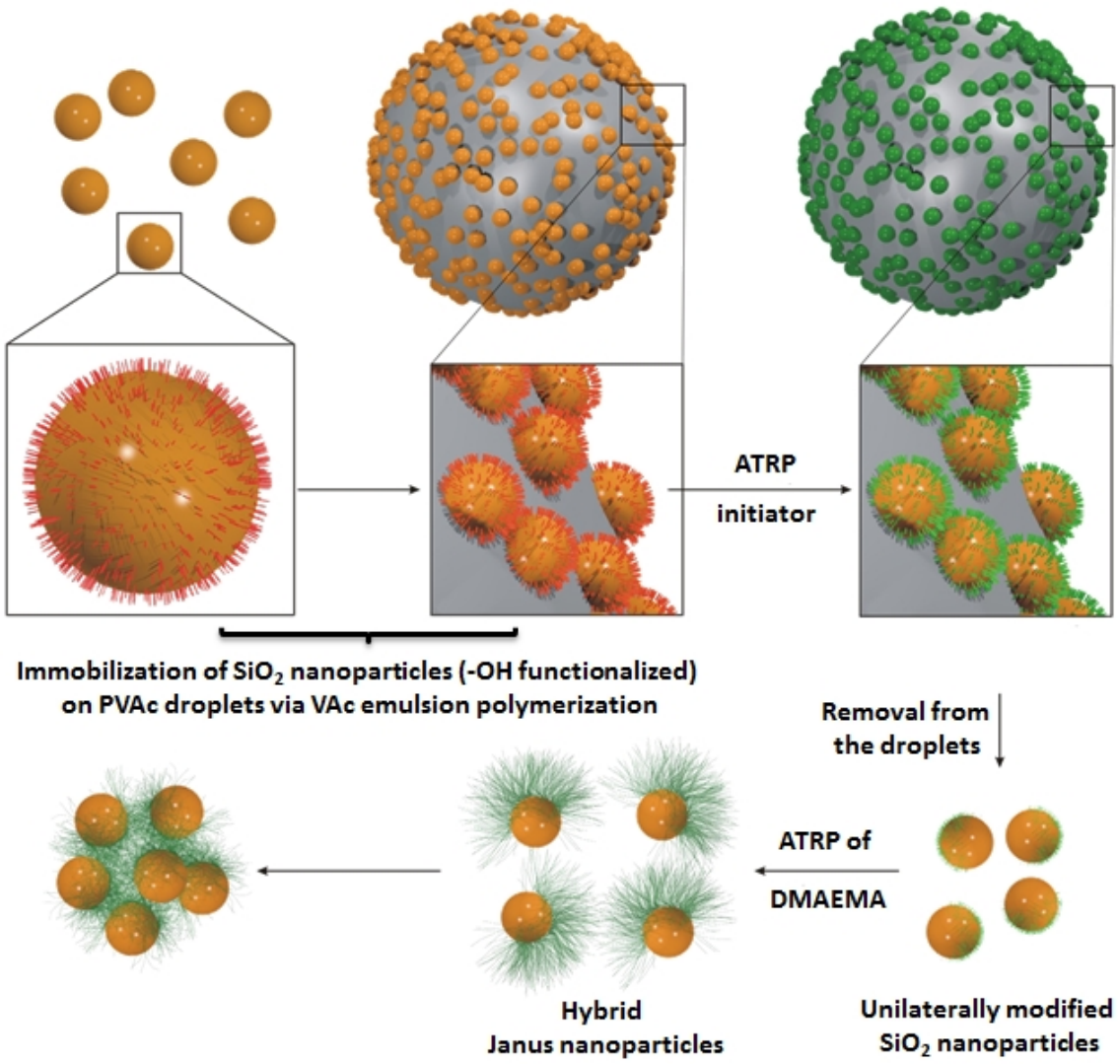

After the emulsion polymerization process, electron microscopy analysis shows a closely packed layer of silica particles present on the polymer latex particles (Figure 1). The SiO_2 armored polymer latexes exhibit a size distribution in the diameter range from 300 to 400 nm. All silica are uniformly embedded at the PVAc interface. They are slightly separated as a direct result of electrostatic repulsion, due to their overall negative zeta-potential. This particle separation is a positive feature helping with the modification of the silica particle surface exposed to water. The protected area is determined by the respective surface tensions of the three components silica, polymer, and water.[10] PVAc was chosen as the polymer phase because the surface tensions are suitable for a sufficiently strong embedding of the silica particle into the PVAc latex.

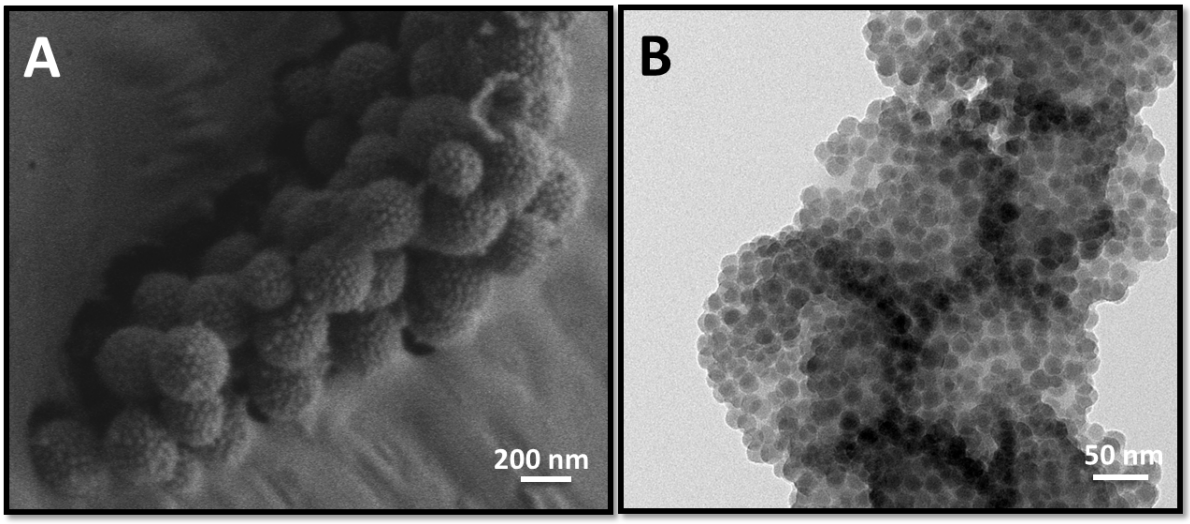

Figure 1. (A) cryo-SEM and (B) TEM images of PVAc latexes armored with SiO_2 nanoparticles obtained by Pickering emulsion polymerization.

To activate the unprotected surface of the silica particles for the growth of a stimuli-responsive corona, the exposed side of the silica particles was modified with a silane-functional ATRP initiator, (2-bromo-2-methyl)propionyloxyhexyltriethoxysilane. Figure 2 shows the infrared spectra of the pristine silica nanoparticles and those modified with our ATRP initiator. In the spectrum of the SiO_2 particles, the broad band at ~3440 cm^{-1} is associated with silanol and adsorbed water. Si–OH vibrations at 958 cm^{-1} show hydroxyl groups in the surface of silica. Further characteristic adsorption bands can be found at 1634 cm^{-1} (H–O–H stretching) and 1084 cm^{-1} + 804 cm^{-1} (Si-O-Si bonds). After the surface modification with the ATRP initiator, this band becomes weaker and at the same time, a stretching vibration absorption of carbonyl group C=O of ester group appears at 1712 cm^{-1}, showing that the ATRP initiator is bound to the surface of silica particles. For the next step, the polymerization of DMAEMA, we separated the silica particles from the latexes *via* a swelling procedure (see Experimental Section). Since, the characteristic bands of the ATRP initiator (C=O of ester group) appears for the pure PVAc latexes, too (Figure 7-S3), it is only possible to control the successful modification of the silica particles after their removal from the PVAc droplets (Figure 7-S4).

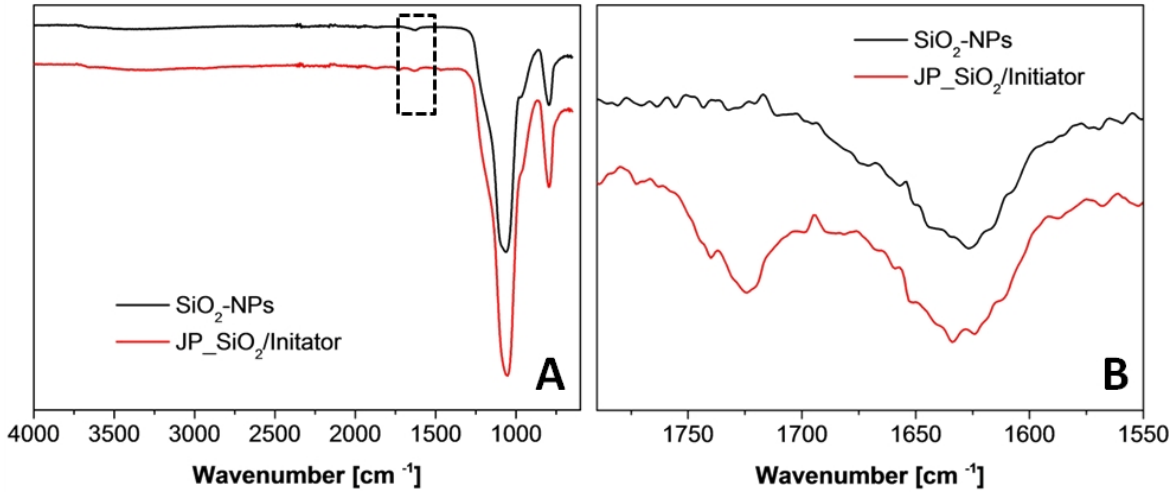

Figure 2. Fourier transform infrared (FT-IR) spectra of SiO_2 NPs (black) and SiO_2/initiator NPs with half of the surface modified with initiator (red).

After isolation of the hemispherically functionalized SiO_2 nanoparticles, we used ATRP to grow a PDMAEMA hemicorona by a "grafting from" polymerization of 2-(dimethylamino) ethyl methacrylate (DMAEMA). The Lower Critical Solution Temperature (LCST) of PDMAEMA depends on both pH and temperature.[46-51] The grafted silica particles were purified by several centrifugation steps removing the residual monomer, catalyst and free polymer.

FT-IR was also used to confirm the successful polymerization of the PDMAEMA corona (Figure 3A). In the spectrum of the Janus SiO_2/PDMAEMA particles, the stretching vibration absorption of the carbonyl group C=O of ester group has shifted from 1712 cm^{-1} (α-bromo ester) to 1740 cm^{-1} (ester). The absorption of the C–N bond appears at 1392 cm^{-1} and at the same time, the stretching vibrations of $–CH_3–$ and $–CH_2–$ groups in the main chain of the grafted PDMAEMA occur at 2925 cm^{-1} and 2850 cm^{-1}. The changes in the spectra clearly demonstrate that the monomer was successfully polymerized on the surface of the silica particles and grafted SiO_2/PDMAEMA nanoparticles were formed. Additionally, thermogravimetric analysis (TGA) also confirm the existence of an organic corona. The TGA trace of the purified Janus nanoparticles shows a weight loss of about 86 %, indicating the successful grafting of PDMAEMA (Figure 3B). In the following, this data can be used for an evaluation of the grafting density.

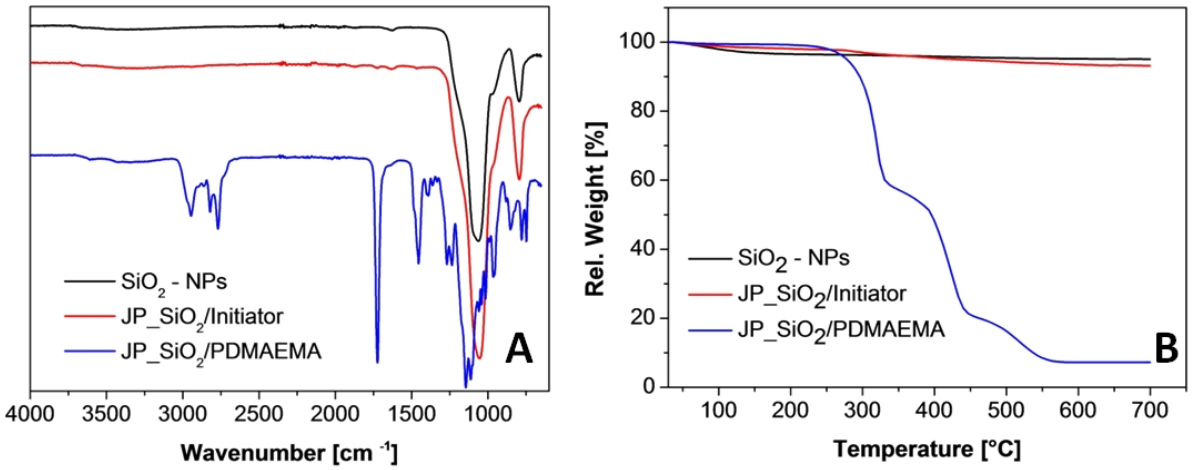

Figure 3. (A) FT-IR spectra of SiO_2-NPs, SiO_2/Initiator-NPs with half of the surface modified with initiator (JP_SiO_2/Initiator) and the Janus nanoparticles SiO_2/PDMAEMA after a reaction time of 5 h (JP_SiO_2/PDMAEMA) at RT. (B) TGA traces of pristine SiO_2-NPs, SiO_2-NPs modified with initiator and SiO_2/PDMAEMA NPs.

During this polymerization, the reaction was quenched at various reaction times to furnish hemicoronas with different lengths of PDMAEMA chains. To determine the molecular weights and polydispersity indices *via* SEC, we cleaved the grafted polymer chains from the silica surface by dissolution of the silica cores with HF.

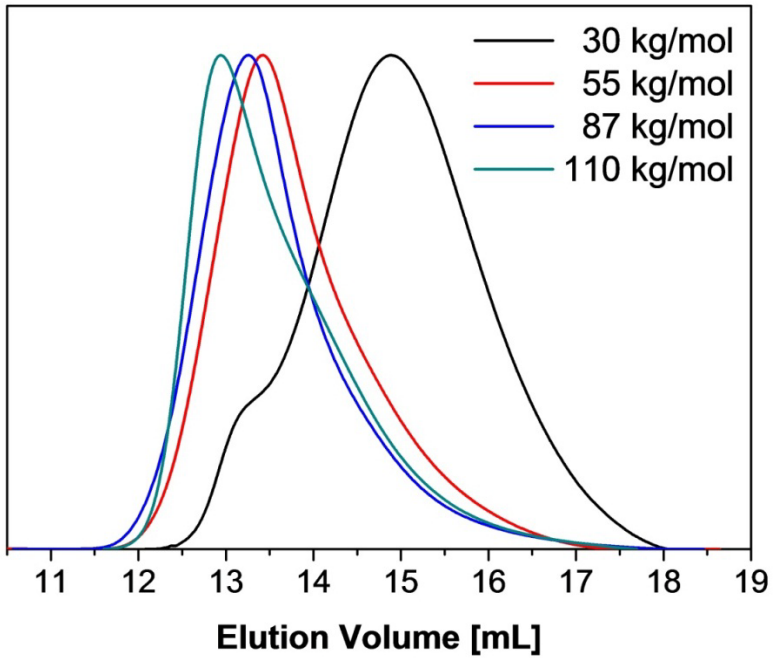

Figure 4. SEC traces of cleaved PDMAEMA polymers with different number-average molecular weights.

Table S1 shows an overview of all SiO_2/PMAEMA nanoparticles synthesized in this study. For the following investigations we focus on the sample with the number-average molecular weight M_n =87 kg/mol (M_w = 148 kg/mol; entry 3 in table S1).

For an evaluation of the grafting density we performed TGA measurements. The data obtained from TGA together with the molecular weight can be used now to calculate the grafting density. Using the method described by Schmalz *et al.*[43] and equation (1) and assuming that ca. 25% of the surface is grafted (see SEM images below), the resulting grafting density for the PDMAEMA chains tethered to the surface of the NPs is about 1.7 chains/nm^2 or 1.5 x 10^3 chains/particle). Dynamic light scattering (DLS) measurements of the nanoparticles throughout the synthetic steps were performed in water at 20 °C and pH 8 (Figure 5) and display a consistent increase in size. The hydrodynamic radii can be controlled *via* the variation of the molecular weight of the PDMAEMA hemicorona. With increasing the molecular weight from 55 to 110 the hydrodynamic radii are increased too. The dispersity index values for all samples of Janus nanoparticles are in the range of 0.2.

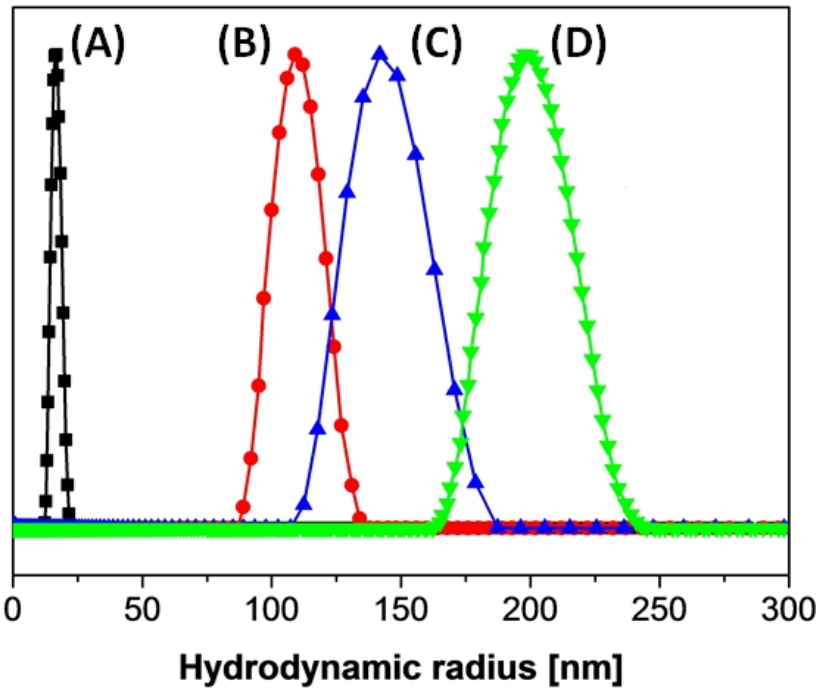

Figure 5. Intensity-weighted hydrodynamic radius distributions (from DLS, measured at pH 8 and RT) of (A) pristine silica particles and Janus SiO_2/PDMAEMA nanoparticles with different M_n (kg/mol) according to SEC: (B) 55, (C) 87, (D) 110.

Next, we performed TEM and SEM measurements of the hybrid particles with PDMAEMA chains of 87 kg/mol to demonstrate their Janus character (Figure 6). The

core-corona structure can be clearly observed in the TEM micrographs as a greyish polymer layer surrounding a darker silica core (Figure 6 A). The number-average radius of the Janus particles obtained *via* TEM is 121 ± 17 nm. This value is lower than the z-average value from DLS (145 ± 22 nm), due to contraction upon drying. We also measured cryogenic TEM (Figure 6 B). The micrograph of the nanoparticles displays a fuzzy corona, highlighted by the encircled areas. A closer inspection allows identifying the different orientations of the Janus nanoparticles relative to the surface. Particles marked with half-circles correspond to Janus particles lying on the side, particles marked with a circle correspond to those where one hemisphere is facing the surface of the vitrified film. Due to the swollen character of the corona and the thereof originating low contrast, it is not possible to visualize the absolute dimensions of the corona by cryo-TEM.

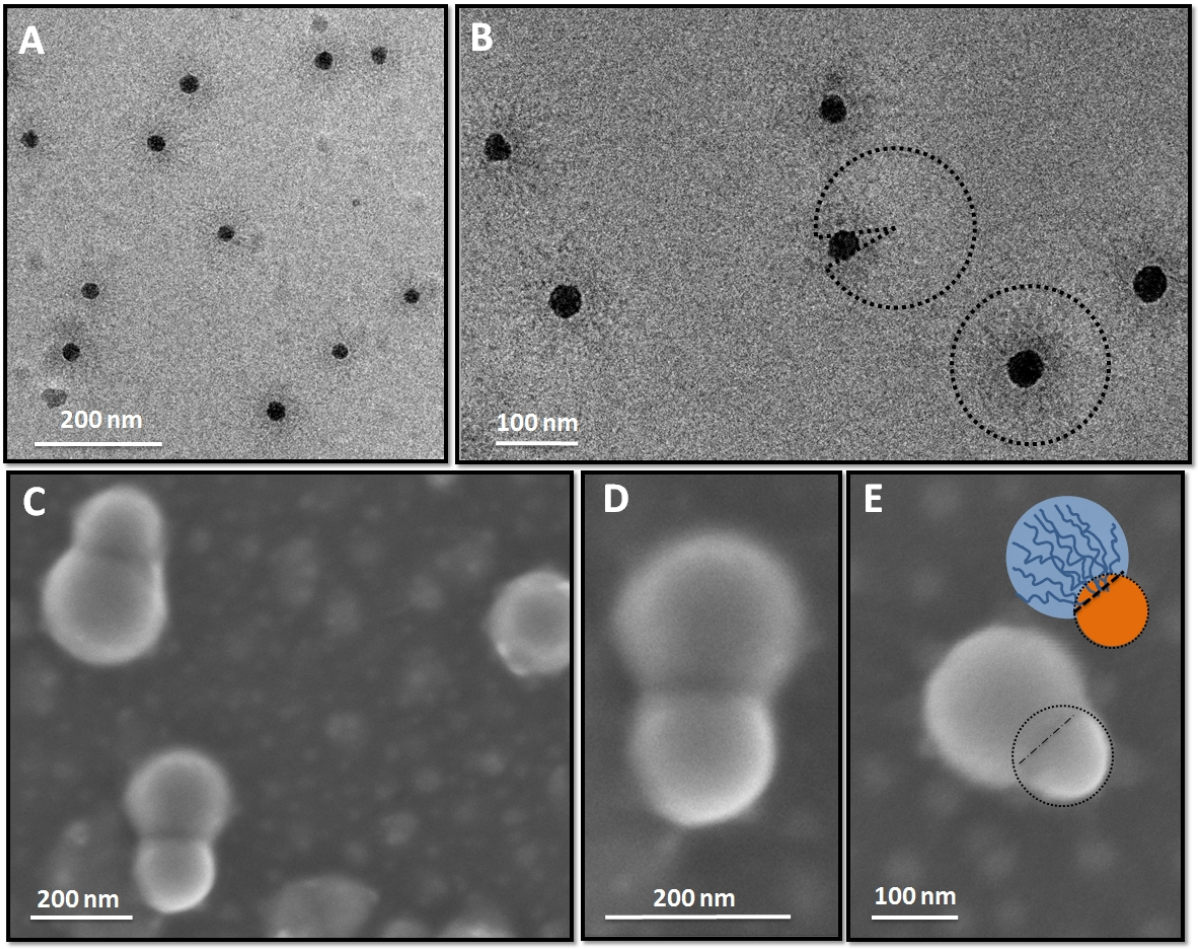

Figure 6. Janus SiO_2/PDMAEMA nanoparticles (pH 7-8). (A) Representative TEM image of hybrid SiO_2/PDMAEMA Janus nanoparticles. (B) cryo-TEM image with a representation of the different orientation of the hemicoronas relative to the surface. (C-E) SEM images of Janus nanoparticles with clearly separated silica NP and PDMAEMA hemicorona. The SiO_2-NP is enclosed by a dashed line in E.

SEM images (Figure 6 C-E) show the Janus character of the obtained nanoparticles much more clearly. The silica NPs and the polymer hemicorona are clearly separated by a sharp interface. In Figure 6E the dashed circle schematically illustrates the silica particle with approximately 1/4 of the surface covered with PDMAEMA. In all SEM images different orientations of the Janus nanoparticles can be found in the same way as observed in the TEM images. The number-average radius obtained *via* SEM is 135 ± 40 nm. To explain the large polydispersity of these particles in SEM and the increased radius of the silica particles, one has to consider the sample deposition process and the used substrate. During the deposition of the Janus nanoparticles, drying takes place and in the end the object is trapped in the droplet-like shape. Further, for the SEM investigations solutions of Janus particles at pH 8 were used. At this pH value the corona is slightly positive charged, but due to the lower isoelectric point of silica the silica surface is still negatively charged. Hence, since the polymer chains are relatively long, some chains may surround the silica particles. Further, as a substrate a silicon wafer was used so that interactions between the slightly positively charged PDMAEMA corona and the substrate may arise, too, leading to a spreading of the Janus particles on the wafer. Moreover, up to 30 nm of the additional particle diameter can be caused by the necessary sputtering process, which is part of the SEM sample preparation procedure.

We conclude that electron microscopy in combination with DLS and FT-IR convincingly confirms the successful formation of the hybrid Janus nanoparticles.

In the last section, we demonstrate the pH- and temperature-responsive behavior of the Janus nanoparticles with a PDMAEMA hemicorona. We first investigate the pH-responsive behavior *via* DLS measurements at 20 °C (Figure 7A). The hydrodynamic radius distributions were studied at different pH values. The Janus nanoparticles have z-average hydrodynamic radii of 88 nm (pH 11), 128 nm (pH 10), 143 nm (pH 8) and 175 nm (pH 6) and 354 nm (pH 4). This reflects the stretching of the corona with increasing protonation.

Turbidity measurements were conducted to demonstrate the pH-dependent LCST behavior of the Janus NPs (Figure 7B). The coil-to-globule transitions at the cloud point of the grafted particles are sharp an the clout points decrease from 85 °C at pH 7 to 30 °C at pH 10, showing similar values to those found for DPMAEMA stars and sphere-symmetric nanoparticles.[43,47]

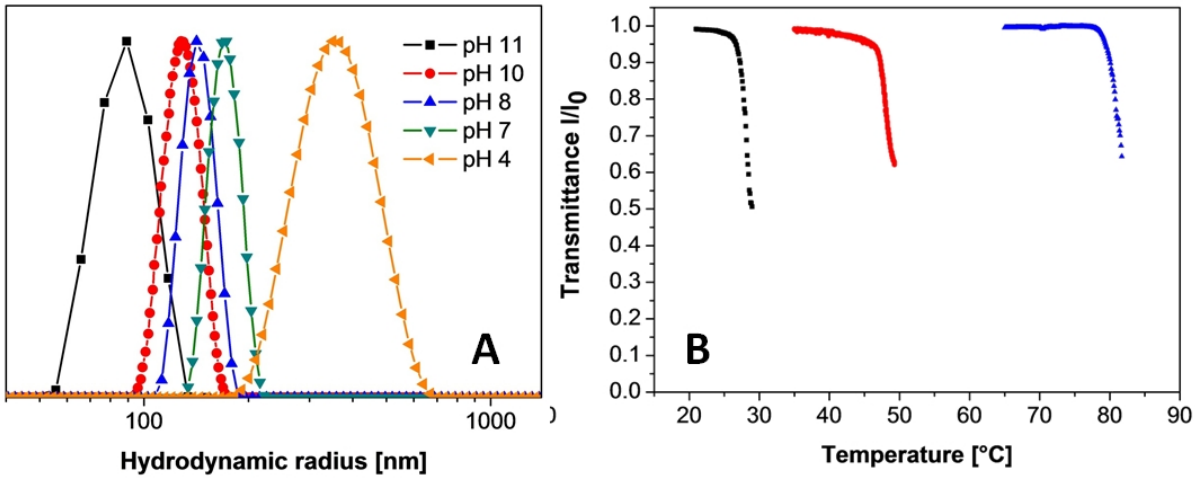

Figure 7. (A) Intensity-weighted hydrodynamic radius distributions of Janus nanoparticles at RT. (B) Turbidity measurements of the Janus SiO_2/PDMAEMA nanoparticles (c = 0.1 g/L) at different pH: pH 10 (black,■), pH 8 (red,●) and pH 7 (blue,Δ).

An unexpected, concentration dependent self-assembly and clustering of the Janus nanoparticles at low pH values (< 5) was observed in the TEM images in Figure 8. In general, at low pH (pH 4) the PDMAEMA chains are completely charged and highly stretched. At low particle concentration only isolated particles can be observed, but increased concentrations lead to the formation of short worm-like assemblies. The isoelectric point of silica is in the range between 2 and 3. As a consequence, at pH 4 the silica particles are still negatively charged which leads to an interaction between the unmodified side of the silica particles and the positively charged PDMAEMA corona. Thus, a worm-like clustering can be observed where the Janus nanoparticles are connected in a head-to-tail fashion of long PDMAEMA chains attaching to the unprotected face of the silica particle. In contrast, at high pH (pH 11) the PDMAEMA chains are contracted and only isolated particles are found, independent of the particle concentration.

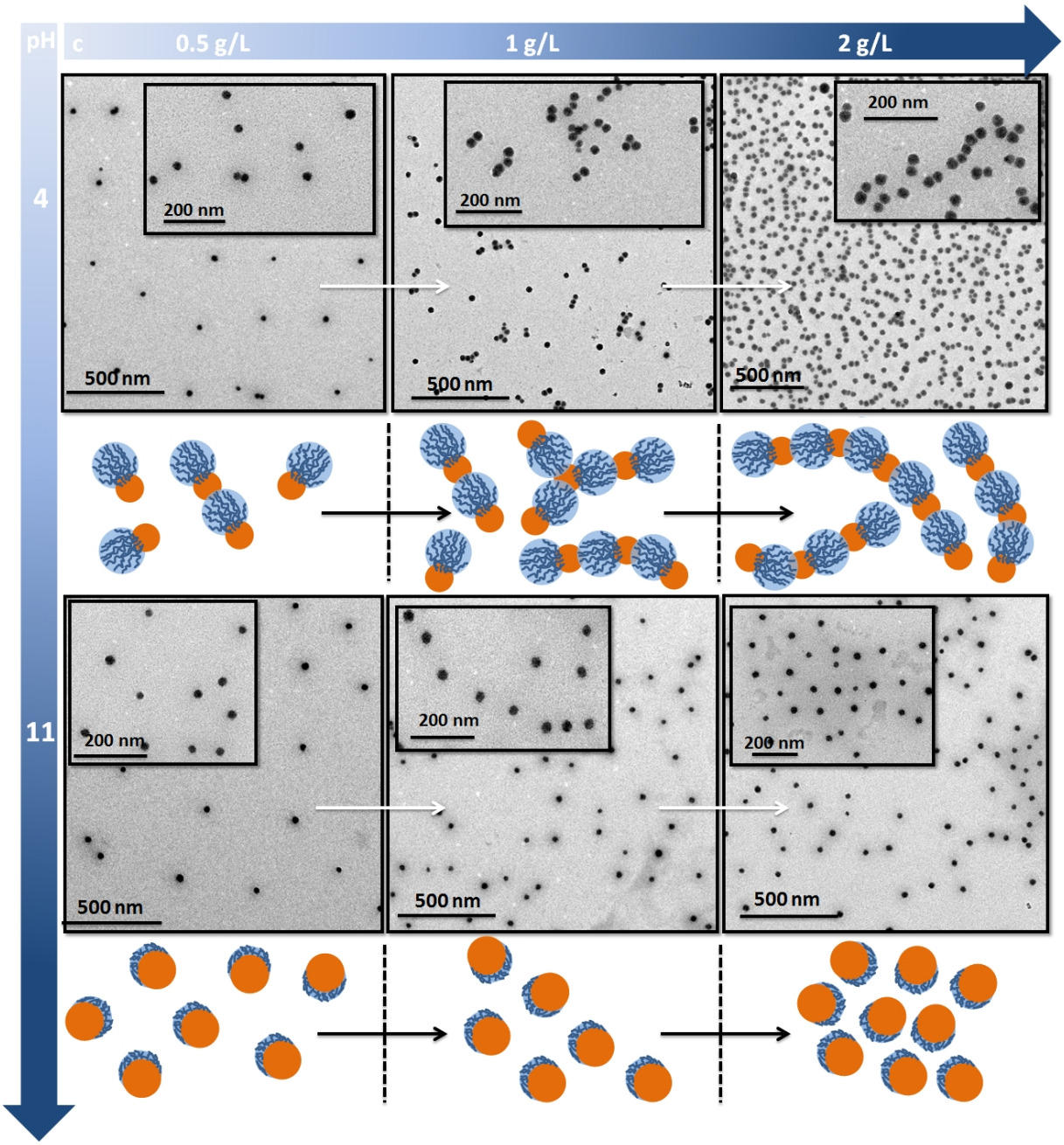

Figure 8. TEM images showing a concentration dependent clustering of the Janus SiO_2/PDMAEMA nanoparticles at pH 4 (top) and pH 11 (bottom) at different concentrations (0.5 g/L, 1 g/L, 2 g/L) and schematic representation of the Janus nanoparticles and their self-assembled structures.

DLS measurements at three different concentration (0.1 g/L, 1g/L and 2 g/L; Figure 9) show a clear shift of 100 nm in size from 354 ± 21 nm to 463 ± 28 nm with increasing the concentration at pH 4, confirming specific aggregation. For Janus nanoparticles at pH 11 the same increase in concentration leads to an only minor change in size from 88 ± 9 nm to 121 ± 29 nm, but to a large increase of the dispersity index. The relatively broad peak around 500 nm points towards an unspecific aggregation due to the fact that the polymer

corona is uncharged. With an increase in concentration the number of unspecific aggregates is increased too, resulting in a large dispersity. These results confirm the results obtained *via* TEM and the proposed mechanism of aggregate formation.

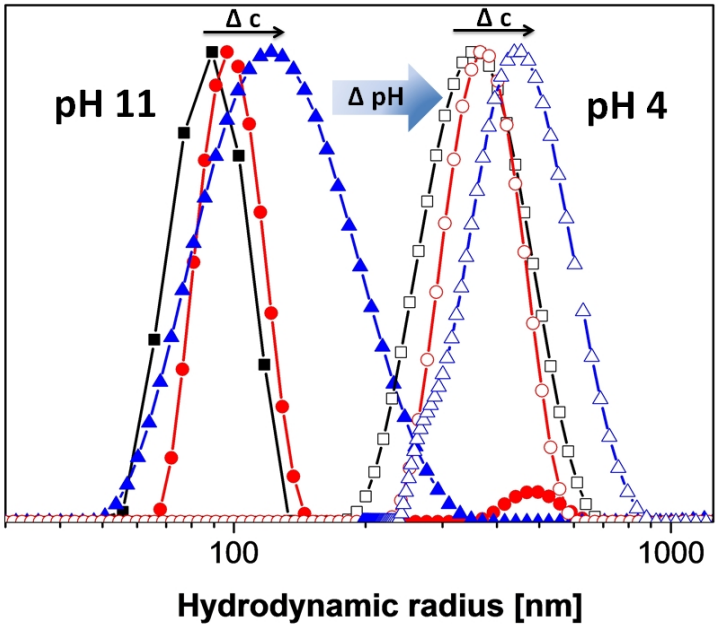

Figure 9. Intensity-weighted hydrodynamic radius distributions of Janus nanoparticles at pH 4 (□, ○, Δ) and pH 11 (■, ●, ▲) at RT with three concentrations (0.1 g/L (black;■,□), 1g/L (red;●,○), and 2 g/L (blue;▲,Δ)) for each pH value.

Conclusions

Our modified Pickering emulsion technique has proven to be an efficient and simple strategy for the large-scale synthesis of well-defined hybrid Janus nanoparticles with a silica core of only 30 nm and a stimuli-responsive PDMAEMA hemicorona. This core size is about one order of magnitude smaller than those reported in the literature. The obtained Janus nanoparticles are well defined in size and shape, can be easily separated and show stimuli-responsive structural changes depending on the pH and temperature. This approach still needs more optimization but can be surely extended to the synthesis of different types of highly functional Janus nanoparticles in further studies based on the experience of our preceding work on surface modification of hybrid silica particles.[52-54] In the next steps we will create hybrid core-shell-corona Janus particles with two stimuli-responsive polymers immobilized at the opposite sides of core-shell particles. Inorganic cores can contain superparamagnetic γ-Fe_2O_3 or fluorescent CdSe(ZnS)-NPs embedded in a silica shell. The flexible surface chemistry of silica offers a wide range of additional

functionalization and polymerization types like RAFT or click chemistry and thus, our approach can be extended to a wide range of different Janus structures.

Acknowledgments

This work was supported by DFG within SFB 840 (project A1). The authors thank André H. Gröschel for his help with Scheme 1, Alexander Majewski for helpful discussions and Warwick chemistry for great support during a scientific exchange. Thomas Ruhland thanks the Bavarian Elite Support Program (ENB) for a scholarship.

Author information

Corresponding authors: Dr. Andreas Walther; Prof. Axel H.E. Müller
*E-mail: walther@dwi.rwth-aachen.de; axel.mueller@uni-mainz.de

Electronic Supplementary Information (ESI)

Scheme 7-S1, Table 7-S1 and Figures 7-S1-S4 presenting synthetic strategies, ^{1}H-NMR spectra, TEM and SEM images, FT-IR spectra and DLS measurements for a further characterization of the hybrid Janus SiO_2/PDMAEMA nanoparticles. This information is available free of charge at http://pubs.acs.org.

References

1. Du, J.; O'Reilly, R. K., *Chem. Soc. Rev.* **2011**, 40, 2402.
2. Loget, G.; Kuhn, A., *J. Mater. Chem.* **2012**, 22, 15457.
3. Hu, J.; Zhou, S.; Sun, Y.; Fang, X.; Wu, L., *Chem. Soc. Rev.* **2012**, 41, 4356.
4. Chen, Q.; Yan, J.; Zhang, J.; Bae, S. C.; Granick, S., *Langmuir* **2012**, 28, 13555.
5. Walther, A.; Müller, A. H. E., In: *Janus particle synthesis, self-assembly and applications*, Jiang, S.; Granick, S., Eds. The Royal Society of Chemistry: Cambridge, 2012; p 1.
6. Roh, K. H.; Yoshida, M.; Lahann, J., *Materialwiss. Werkstofftech.* **2007**, 38, 1008.
7. Walther, A.; Hoffmann, M.; Müller, A. H. E., *Angew. Chem. Int. Ed.* **2008**, 47, 711.
8. Walther, A.; Matussek, K.; Müller, A. H. E., *ACS Nano* **2008**, 2, 1167.
9. Ruhland, T. M.; Gröschel, A. H.; Walther, A.; Müller, A. H. E., *Langmuir* **2011**, 27, 9807.
10. Binks, B. P.; Fletcher, P. D. I., *Langmuir* **2001**, 17, 4708.
11. Glaser, N.; Adams, D. J.; Böker, A.; Krausch, G., *Langmuir* **2006**, 22, 5227.
12. Nisisako, T.; Torii, T.; Takahashi, T.; Takizawa, Y., *Adv. Mater.* **2006**, 18, 1152.
13. Behrend, C. J.; Anker, J. N.; Kopelman, R., *Appl. Phys. Lett.* **2004**, 84, 154.
14. Behrend, C. J.; Anker, J. N.; McNaughton, B. H.; Brasuel, M.; Philbert, M. A.; Kopelman, R., *J. Phys. Chem. B* **2004**, 108, 10408.
15. Roh, K.-H.; Martin, D. C.; Lahann, J., *Nat. Mater.* **2005**, 4, 759.
16. Dendukuri, D.; Gu, S. S.; Pregibon, D. C.; Hatton, T. A.; Doyle, P. S., *Lab Chip* **2007**, 7, 818.
17. Vilain, C.; Goettmann, F.; Moores, A.; Le Floch, P.; Sanchez, C., *J. Mater. Chem.* **2007**, 17, 3509.
18. Gu, H.; Zheng, R.; Zhang, X.; Xu, B., *J. Am. Chem. Soc.* **2004**, 126, 5664.
19. Nagle, L.; Fitzmaurice, D., *Adv. Mater.* **2003**, 15, 933.
20. Yin, Y.; Lu, Y.; Xia, Y., *J. Am. Chem. Soc.* **2001**, 123, 771.
21. Walther, A.; Müller, A. H. E., *Soft Matter* **2008**, 4, 663.
22. Gao, X.; Yu, L.; MacCuspie, R.; Matsui, H., *Adv. Mater.* **2005**, 17, 426.
23. Teranishi, T.; Inoue, Y.; Nakaya, M.; Oumi, Y.; Sano, T., *J. Am. Chem. Soc.* **2004**, 126, 9914.
24. Yu, H.; Chen, M.; Rice, P. M.; Wang, S. X.; White, R. L.; Sun, S., *Nano Lett.* **2005**, 5, 379.
25. Bao, Z.; Chen, L.; Weldon, M.; Chandross, E.; Cherniavskaya, O.; Dai, Y.; Tok, J. B. H., *Chem. Mater.* **2001**, 14, 24.
26. Paunov, V. N.; Cayre, O. J., *Adv. Mater.* **2004**, 16, 788.
27. Hong, L.; Jiang, S.; Granick, S., *Langmuir* **2006**, 22, 9495.
28. Jiang, S.; Granick, S., *J. Chem. Phys.* **2007**, 127, 161102.

29. Jiang, S.; Granick, S., *Langmuir* **2008**, 24, 2438.
30. Suzuki, D.; Tsuji, S.; Kawaguchi, H., *J. Am. Chem. Soc.* **2007**, 129, 8088.
31. Jiang, S.; Schultz, M. J.; Chen, Q.; Moore, J. S.; Granick, S., *Langmuir* **2008**, 24, 10073.
32. Berger, S.; Synytska, A.; Ionov, L.; Eichhorn, K.-J.; Stamm, M., *Macromolecules* **2008**, 41, 9669.
33. Zhang, J.; Jin, J.; Zhao, H., *Langmuir* **2009**, 25, 6431.
34. Nie, L.; Liu, S.; Shen, W.; Chen, D.; Jiang, M., *Angew. Chem. Int. Ed.* **2007**, 46, 6321.
35. Liu, B.; Wei, W.; Qu, X.; Yang, Z., *Angew. Chem. Int. Ed.* **2008**, 47, 3973.
36. Wang, B.; Li, B.; Zhao, B.; Li, C. Y., *J. Am. Chem. Soc.* **2008**, 130, 11594.
37. Colard, C. A. L.; Teixeira, R. F. A.; Bon, S. A. F., *Langmuir* **2010**, 26, 7915.
38. Teixeira, R. F. A.; McKenzie, H. S.; Boyd, A. A.; Bon, S. A. F., *Macromolecules* **2011**, 44, 7415.
39. Bon, S. A. F.; Chen, T., *Langmuir* **2007**, 23, 9527.
40. Bon, S. A. F.; Colver, P. J., *Langmuir* **2007**, 23, 8316.
41. Cauvin, S.; Colver, P. J.; Bon, S. A. F., *Macromolecules* **2005**, 38, 7887; Fortuna, S.; Colard, C. A. L.; Troisi, A.; Bon, S. A. F., *Langmuir* **2009**, 25, 12399.
42. Colver, P. J.; Chen, T.; Bon, S. A. F., *Makromol. Chem. Macromol. Symp.* **2006**, 245-246, 34.
43. Majewski, A. P.; Schallon, A.; Jérôme, V.; Freitag, R.; Müller, A. H. E.; Schmalz, H., *Biomacromolecules* **2012**, 13, 857.
44. Husseman, M.; Malmström, E. E.; McNamara, M.; Mate, M.; Mecerreyes, D.; Benoit, D. G.; Hedrick, J. L.; Mansky, P.; Huang, E.; Russell, T. P.; Hawker, C. J., *Macromolecules* **1999**, 32, 1424.
45. Ohno, K.; Morinaga, T.; Koh, K.; Tsujii, Y.; Fukuda, T., *Macromolecules* **2005**, 38, 2137.
46. Schmalz, A.; Hanisch, M.; Schmalz, H.; Müller, A. H. E., *Polymer* **2010**, 51, 1213.
47. Plamper, F. A.; Ruppel, M.; Schmalz, A.; Borisov, O.; Ballauff, M.; Müller, A. H. E., *Macromolecules* **2007**, 40, 8361.
48. Plamper, F. A.; Schmalz, A.; Müller, A. H. E., *J. Am. Chem. Soc.* **2007**, 129, 14538.
49. Plamper, F. A.; Schmalz, A.; Penott-Chang, E.; Drechsler, M.; Jusufi, A.; Ballauff, M.; Müller, A. H. E., *Macromolecules* **2007**, 40, 5689.
50. Schmaljohann, D., *Adv. Drug Delivery Rev.* **2006**, 58, 1655.
51. Dimitrov, I.; Trzebicka, B.; Müller, A. H. E.; Dworak, A.; Tsvetanov, C. B., *Prog. Polym. Sci.* **2007**, 32, 1275.
52. Pfaff, A.; Schallon, A.; Ruhland, T. M.; Majewski, A. P.; Schmalz, H.; Freitag, R.; Müller, A. H. E., *Biomacromolecules* **2011**, 12, 3805.
53. Ruhland, T. M.; Reichstein, P. M.; Majewski, A. P.; Walther, A.; Müller, A. H. E., *J. Colloid Interface Sci.* **2012**, 374, 45.

SUPPORTING INFORMATION
to

Nanoscale hybrid Silica/Polymer Janus Particles with a double-responsive Hemicorona

By Thomas M. Ruhland, Holly S. McKenzie, Thomas S. Skehlon, Stefan A. Bon,

Andreas Walther and Axel H. E. Müller

Scheme 7-S1. Synthetic route for the silane-functional ATRP-initiator (2-bromo-2-methyl) propionyloxyhexyltriethoxysilane.

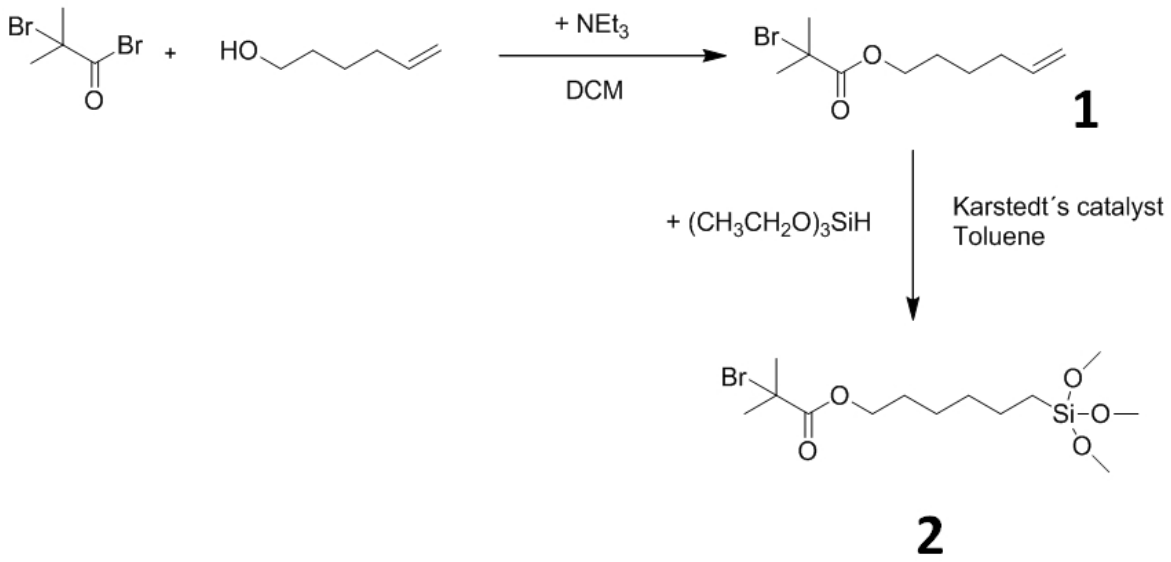

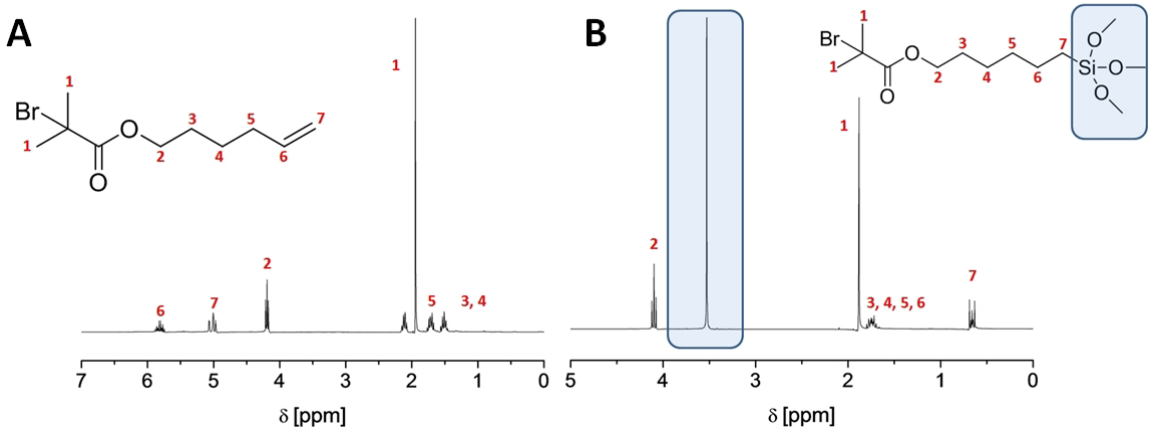

Figure 7-S1. [1]H NMR analysis spectra of (A) *Pent-4'-enyl 2-bromo-2-methylpropionate* and (B) *(2-Bromo-2-methyl) propionyloxyhexyltriethoxysilane.*

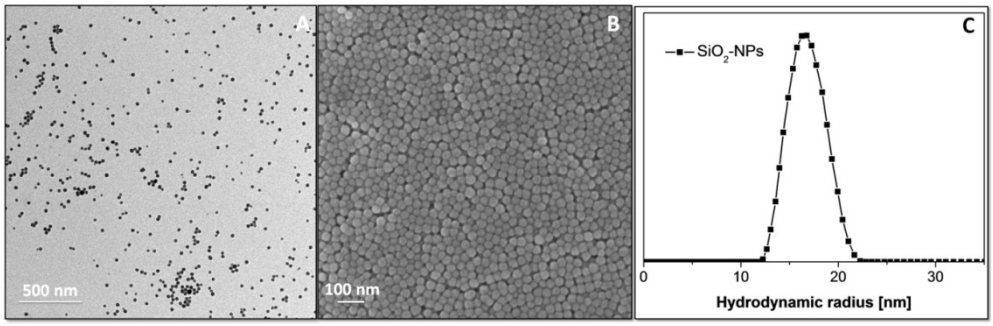

Figure 7-S2 (A) TEM image, (B) SEM image and (C) DLS measurement of the pristine 30 nm silica particles

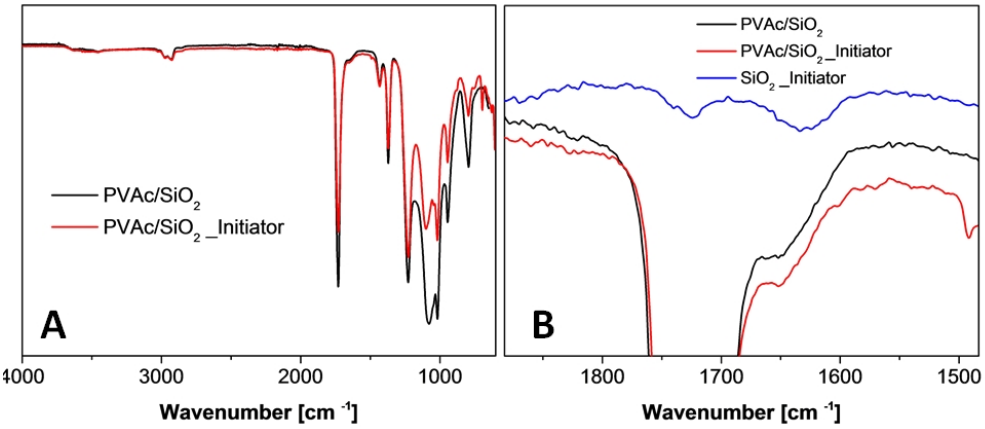

Figure 7-S3. Fourier transform infrared (FT-IR) spectra of (A) pure PVAc droplets with unmodified silica particles (PVAc/SiO_2) and of the ATRP modified silica particles which are still immobilized at the surface of the PVAc droplets (PVAc/SiO_2_Initiator). (B) Zoom-in to demonstrate to problematic characterization of a successful modification of the silica particles with ATRP-Initiator when the silica particles are still immobilized in the PVAc droplets.

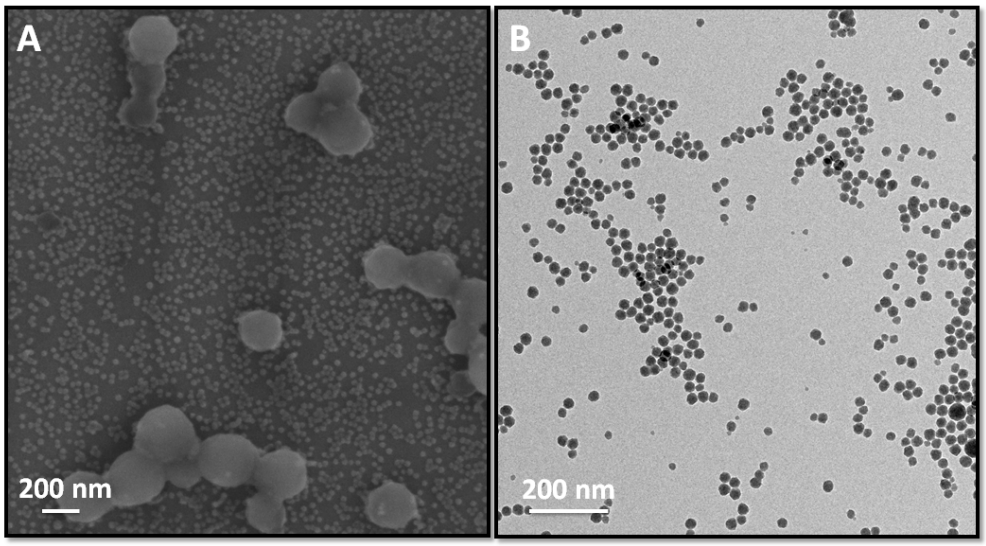

Figure S4. (A) SEM image of the silica particles modified with the ATRP-Initiator after the removal from the PVAc droplets and before purification for the analysis of a successful modification with the ATRP-Initiator *via* FT-IR spectroscopy (B) TEM image of the unilaterally modified silica particles after several centrifugation steps for the removal of the latex particles.

Table 7-S1. Overview of all synthesized Janus SiO_2/PDMAEMA nanoparticles including number-average molecular weight, polydispersity index (PDI) of PDMAEMA chains and radii obtained *via* TEM, SEM and DLS at RT and pH 8.

Janus-NPs	Mn [kg/mol]	PDI	$\langle R \rangle_n$ [nm] TEM	$\langle R \rangle_n$ [nm] SEM	$\langle R \rangle_z$ [nm] DLS
1	30	1.4			
2	55	1.5			128 ± 12
3	87	1.7	121 ± 17	135 ± 40	145 ± 23
4	110	2.0			172 ± 28

List of Publications

1. **Ruhland, T. M.**; McKenzie H. S.; Skehlon T. S.; Bon S. A. F.; Walther A.; Müller, A. H. E.: Nanoscale hybrid silica/polymer Janus particles with a double-responsive hemicorona, **2013**, submitted to *ACS Nano*.
2. Schmelz, J.; Pirner, D.; Krekhova, M.; **Ruhland, T. M.**; Schmalz, H.: Interfacial activity of patchy worm-like micelles, **2013**, *Soft Matter* **2013**, accepted, **DOI**: 10.1039/C3SM51914G.
3. Hanisch, A.; Gröschel, A. H.; Förtsch, M.; Drechsler, M.; Jinnai, H.; **Ruhland, T. M**.; Schacher, F. H.; Müller, A. H. E.: Counterion.Mediated Hierachial Self-Assembly of an ABC Miktoarm Star Terpolymer, **2013**, *ACS Nano* **2013**, 7, 4030.
4. **Ruhland, T. M.**; Gröschel, A. H.; Ballard, N.; Skehlon, T. S.; Walther A.; Müller, A. H. E.; Bon, S. A. F.: Influence of Janus particle shape on their interfacial behavior at liquid - liquid interfaces, *Langmuir* **2013**, 29, 1388.
5. **Ruhland, T. M.**; Lang, J. R. V.; Alt, H. G.; Müller, A. H. E.: Magnetic Core-Shell Nanoparticles as Carriers for Olefin Dimerization Catalysts, *Eur. J. Inorg. Chem.* **2013**, 12, 2146.
6. **Ruhland, T. M.**; Reichstein, P. M.; Walther, A.; Müller, A. H. E.: Superparamagnetic and fluorescent thermo-responsive core-shell-corona hybrid nanogels with a protective silica shell*, Pol. Mater. Sci. Technol.* **2012**, 95.
7. **Ruhland, T. M.**; Reichstein, P. M.; Majewski, A. P.; Walther, A.; Müller, A. H. E.: Superparamagnetic and fluorescent thermo-responsive core-shell-corona hybrid nanogels with a protective silica shell, *J. Colloid Interface Sci.* **2012**, 374, 45.
8. Pfaff, A.; Schallon, A.; **Ruhland, T. M.**; Majewski, A. P.; Schmalz, H.; Freitag, R.; Müller, A. H. E.: Magnetic and Fluorescent Glycopolymer Hybrid Nanoparticles for Intranuclear Optical Imaging, *Biomacromolecules* **2011**, 12, 3805.
9. **Ruhland, T. M.**; Gröschel, A. H.; Walther, A.; Müller, A. H. E.: Janus Cylinders at Liquid-Liquid Interfaces, *Langmuir* **2011**, 27, 9807.

Acknowledgements & Danksagung

"..Sharing (information) leads to connections, connection leads to collaborations, collaboration leads to creativity and innovation, creativity and innovation are what changes the world!.."

(Marisa Mayer)

Bevor ich anfange „ Danke" zu sagen, möchte ich vorausschicken, dass die Bayreuther „Chemie - Community" für mich etwas ganz Besonderes auf dieser Welt ist und ich sehr stolz darauf bin, ein Teil davon zu sein!!

Zuallererst will ich mich bei Herrn Prof. Dr. A.H.E. Müller aufs herzlichste bedanken. Er hat mir nicht nur die Möglichkeit gegeben in seinem Arbeitskreis an einem äußerst interessanten Thema zu arbeiten, sondern auch immer genügend Freiraum gelassen, um eigenen Ideen nachzugehen, neue Dinge auszuprobieren und sich dabei weiterzuentwickeln. Als Mentor in der Graduiertenschule und als Doktorvater stand er aber dennoch immer mit Rat und Tat zur Seite, um in Gesprächen und Diskussionen die bestmöglichste Hilfestellung zu geben! Im Besonderen ist zu erwähnen, dass er mir die einzigartige Möglichkeit gegeben hat, die eigene Arbeit auf nationalen wie internationalen Konferenzen vorzustellen, Forscherinnen und Forscher vieler verschiedener Länder kennenzulernen und nicht zu vergessen, mich ermuntert hat, während meiner Doktorarbeit, 5 Monate im Ausland zu verbringen und an der Universität Warwick meinen Horizont zu erweitern! All das ist nicht selbstverständlich und zeichnet Herrn Prof. Müller als Mensch, Mentor und Doktorvater in hohem Maße aus.

Des Weiteren möchte ich mich auch bei Herrn Prof. Hellweg, Herrn Prof. Alt und Herrn Dr. Andreas Walther ganz herzlich für alle Gespräche, Anregungen, Korrekturen und eine angenehme Zusammenarbeit bedanken.

Meine Anerkennung gilt auch Herrn Dr. Andreas Walther für seine Hilfe. Zu jeder Zeit erreichbar, hatte er immer ein offenes Ohr, hörte sich geduldig alle Probleme an und hatte immer Rat, Tipps, Tricks, neue Ideen und Anregungen zur Hand. Und all das obwohl selbst immer im Stress und auf dem Sprung! Dafür wirklich besten Dank!!

Wie an den zahlreichen Co-Autoren zu erkennen ist, beruht diese Arbeit nicht nur auf meiner Leistung, sondern ist auch Resultat der Anstrengungen und Hilfe vieler meiner Kolleginnen, Kollegen und Freunde, wofür ich äußerst dankbar bin.

Am allerwichtigsten ist es mir, ein Dankeswort an die gesamte **MC II** zu richten. Die Mitglieder der **MC II**, Aktuelle wie Ehemalige, sind und waren nicht nur Arbeitskollegen/innen für mich, sondern eine Art zweite Familie. Eine Familie mit engen Zusammenhalt, großer Hilfsbereitschaft und wahnsinnig guter Atmosphäre. Die Vielzahl der unterschiedlichen Charaktere und Persönlichkeiten machen den besonderen Charme unseres Lehrstuhles aus. Ich denke, was Marissa Mayer im oben gezeigten Zitat sagt, trifft hier bei uns gut zu: „Wer etwas teilt, baut ein Netzwerk auf. Ein Netzwerk führt zu Zusammenarbeit, Zusammenarbeit führt zu Kreativität und Innovation - und diese verändern die Welt.“ Wir waren immer alle füreinander da, haben uns in einer super angenehmen Atmosphäre gegenseitig geholfen, unterstützt und eng zusammengearbeitet. Motiviert aus diesem Zusammenhalt haben wir alle unseres Bestes gegeben und das Maximale für uns und die Gruppe erreicht. Und das nicht nur auf der wissenschaftlichen sondern auch auf privater Ebene! Die Zeit bleibt einfach unvergesslich und ich werde mich gerne daran zurückerinnern. Dafür möchte ich mich von ganzen Herzen bedanken bei Andreas Hanisch, André Gröschel, André Pfaff, Alexander Majewski, Alexander Schmalz, Sandrine Tea, Christopher Synatschke, Joachim Schmelz, Stephan Weiß, Anja Goldmann, Gaby Rösner-Oliver, Andreas Walther, Felix Schacher, Melanie Förtsch, Annika Pfaffenberger, Marietta Böhm, Annette Krökel, Kerstin Küspert, Markus Drechsler, Eva Betthausen, Francesca Bennet, Marina Krekhova, Carmen Kunert, Kerstin Küspert, Tina Löbling, Ramón Novoa-Carballal, Lourdes Pastor-Pérez, Holger Schmalz, Andrea Wolf, Zhicheng Zheng, Sergey Nosov, Felix Plamper, Stefan Reinicke, Markus Retsch, Manuela Schumacher, Ainhoa Tolentino Chivite, Hans-Joachim Voigtländer, Michael Witt, Jiayin Yuan, Sohei Ida, Pierre-Eric Millard, Alexander (Sascha) Yakimansky, Jie Kong, Anthony Granville und viele mehr.

Nichtsdestotrotz möchte ich explizit den drei weiteren Exil-Doktoranden Andrea, Andreas und Stephan danken, die mit mir die Fahne der MC II im „Asylantenraum“ der MC I hochgehalten und den „zahlreichen“ Anfeindungen erfolgreich getrotzt haben! Was wären die letzten Monate und der Aufenthalt in den USA nur ohne die täglichen gegenseitigen Sticheleien mit Andreas „Miagauisch“ Hanisch gewesen.

Dabei will ich auch alle Master-, Bachelorstudenten und Praktikanten erwähnen, die mit ihrer Arbeit zum Erfolg meiner Arbeit beigetragen haben. Deshalb geht ein großes Dankeschön an Paul Reichstein, Fabian Nutz, Annika Eckardt, Christian Hübner, Toni Hille und Tobias Rudolph.

Vor allem bedanken will ich mich nochmals bei Melanie, Annika, Marietta, Carmen und beim ganzen TEM und SEM-Team, die immer mit großer Ausdauer, viel Können und großer Bereitschaft eine ungeheure Hilfe bei TEM, SEM oder GPC Messungen waren. Vielen Dank!!

Nicht zu vergessen natürlich Gaby, die immer ein offenes Ohr für alle Probleme hatte, jederzeit aufopferungsvoll bei diesen geholfen hat und die gute Seele unseres „verrückten Haufens“ war, auch wenn sie mit uns einiges aushalten musste.

Ein großes Dankeschön geht an die gesamte MC I und auch an die Experimentalphysik IV, die uns sehr herzlich aufgenommen haben!!

Natürlich will ich auch allen meinen Freunden meinen Dank aussprechen für die angenehme und kameradschaftliche Stimmung, den außerordentlichen Zusammenhalt, für viele lustige und spontane gemeinsame Unternehmungen, sehr viel Spaß und auch für eine Menge Quatsch, Tollerei und Unsinn. Ich hoffe keiner ist mir böse falls ich ihn oder sie vergessen sollte: Johannes Brendel, Sebastian With, Andreas Hanisch, Andreas Ringk, Alexander Majewski, Isabelle Haas, Katja von Nessen, Christian Hannappel, Yvonne Hertle, Marko Schmidt, Denise Barelmann-Kahlbohm, Sascha Ehlert, Sara Mehdizadeh Taheri, Jan Schröder, Daniel Kunz, Thomas Lunkenbein, Florian Richter, Christian Bartz, Florian Wieberger, Dominik Erhardt, Johannes Heigl, Christian Probst, Nonio Wolter, Julian Lang, Mathias Hanisch, Tobias Bauer, Christoph Angermann, Bastian Wedel, Nadine Popp, Markus Retsch, Mathias Karg, …….

Nicht zuletzt basierend auf diesem besonderen Zusammenhalt ist es uns gelungen in Bayreuth mit unserem Alumniverein CSG e.V. ein Netzwerk aufzubauen, das uns alle ein Leben lang miteinander verbindet. Hier möchte ich mich nochmals herzlich bei Marko Schmidt, Christian Bartz, Johannes Obenauf, Markus Herling, Johannes Heigl, Sina Rösler und Mareen Müller bedanken für ihrem Eifer und Einsatz für unseren Verein! Es war eine tolle Zeit, in der wir einiges auf die Beine gestellt haben!

Immer wenn es hieß: „Zwei Minuten gespielt und noch immer hohes Tempo“ oder „Entlaubinger“ war es in den letzten 8 Jahren Dienstagabend und die Chemiker versuchten verzweifelt Fußball zu spielen! Und um ehrlich zu sein, eins um andere Mal wurde auf dem Feld der Ehre ganz schön aufgezaubert! Es war immer eine tolle Zeit, die eine Menge Spaß brachte!

Ich hatte die einzigartige Gelegenheit während meiner Doktorarbeit fünf Monate an der Universität WARWICK in der Arbeitsgruppe von Herrn Dr. ir. Stefan Bon zu verbringen. Diese fünf Monate haben mich nicht nur in meiner Doktorarbeit weitergebracht, sondern ich habe auch viele neue Dinge, wissenschaftliche genauso wie nichtwissenschaftliche, kennen und schätzen gelernt. Es war eine wundervolle Zeit in der ich viele nette, freundliche und äußerst hilfsbereite Menschen getroffen habe und viele Freundschaften entstanden sind. Ein ganz großes Dankeschön verdienen deshalb Stefan, Nick, Tom, Andy, Adam, Holly, Yunhua, Rong, Maddy und nicht zu vergessen Luke R. und Stefan S..

Natürlich danke ich auch der Bayreuther Graduiertenschule für Mathematik und Naturwissenschaften für die Unterstützung innerhalb des Promotionsprogrammes „Polymer Science“ genauso wie der Deutschen Forschungsgemeinschaft (DFG) im Rahmen des SFB 840. Dem Staat Bayern gebührt ebenfalls Dank für die große Hilfestellung im Rahmen des Elitenetzwerkes Bayerns und dem Studiengang „Macromolecular Science“ und für die Förderung meiner Forschung über ein Stipendium (BayEFG).

Zuletzt, will ich mich besonders bei meinen Eltern bedanken, die es mir ermöglicht haben zu studieren, die mit mir durch alle Höhen und Tiefen gegangen sind, die mich immer unterstützt und neu motiviert haben und die trotz aller meiner Launen immer für mich da waren und bei allen Problemen aufopferungsvoll versucht haben in jeglicher Weise zu helfen.

Erklärung

Die vorliegende Arbeit wurde von mir selbstständig verfasst und ich habe dabei keine anderen als die angegebenen Hilfsmittel und Quellen benutzt.

Ferner habe ich nicht versucht, anderweitig mit oder ohne Erfolg eine Dissertation einzureichen oder mich einer Doktorprüfung zu unterziehen.

Bayreuth, den 31.12.2012

Thomas M. Ruhland